LIGHT INDUCED A.C. LOSS IN AMORPHOUS SEMICONDUCTORS

MARTIN CHRISTOPHER HOLLAND

Ph.D.

THE UNIVERSITY OF GLASGOW

DEPARTMENT OF PHYSICS AND ASTRONOMY

DECEMBER 1987

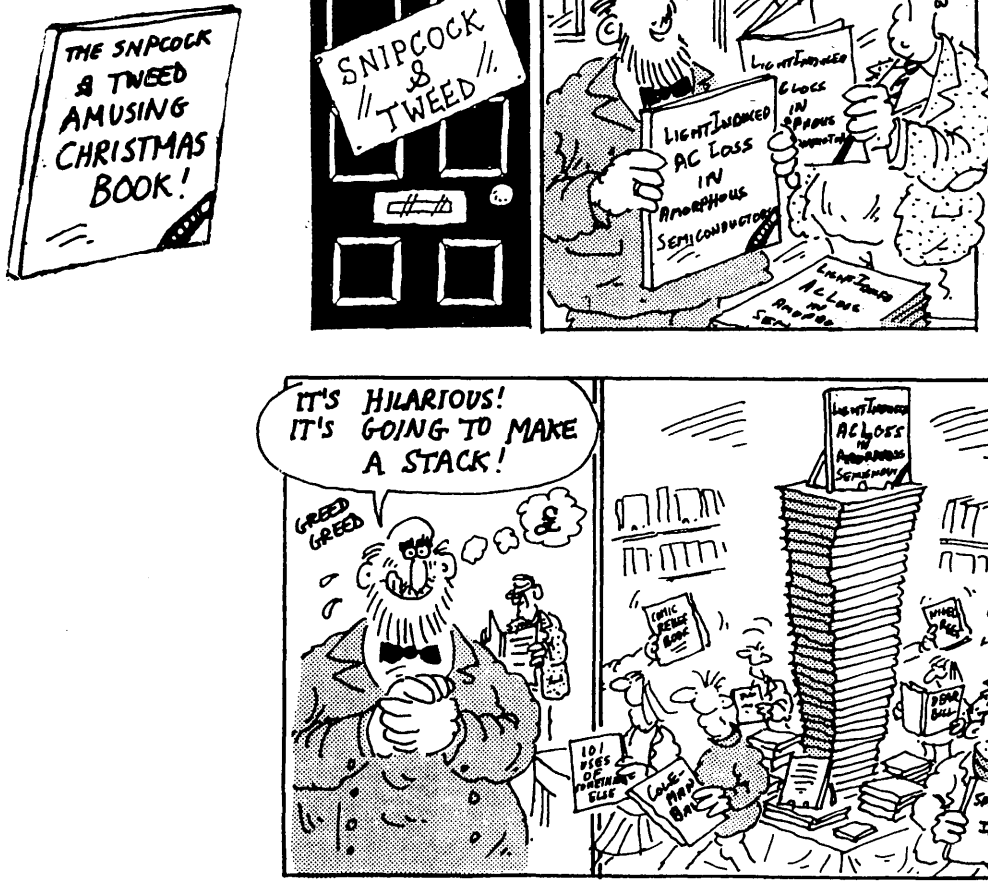
THE SNIPCOCK & TWEED AMUSING CHRISTMAS BOOK!
SNIPCOCK & TWEED
AT LAST WE'VE GOT OUR CHRISTMAS BOOK OUT!
LIGHT INDUCED AC LOSS IN AMORPHOUS SEMICONDUCTORS
IT'S HILARIOUS! IT'S GOING TO MAKE A STACK!
GREED GREED
£
LIGHT INDUCED AC LOSS IN AMORPHOUS SEMICONDUCTORS
EPITAXIC RELEASE BOOK
WHEEL BOOK
DEAD BULL
101 USES OF SOMETHING ELSE
CAVE-MAN BALL
SPITTING IMAGE

Declaration

The work presented in this thesis is by the author except where explicitly mentioned in the text where an appropriate reference is given.

Some of the results in this thesis have already been published (A.R. Long, W.R. Hogg, M.C. Holland, N. Balkan and R.P. Ferrier (1985) Phil. Mag. B, 51, 39 and A.R. Long and M.C. Holland (1985) J. Non-Cryst. Solids, 77 & 78, 471) but no part has been submitted previously for a degree at this or any other university.

Acknowledgements

It is a pleasure to thank everyone who has helped me during the four years of this project. In particular, thanks go to my supervisor, Dr. A.R. Long, for his help and encouragement throughout the period of this work. I would also like to thank the members of the Solid State Physics Group for many helpful discussions.

I am also grateful to the technicians of the Solid State Physics Group, especially Mr. D. MacDonald, Mr. A. Young. and Mr. D. Blackwell.

Finally I would thank the S.E.R.C. for provision of a research studentship.

Table of Contents

ABSTRACT

Enhanced a.c. losses have been observed in thin films of a-Ge and a-Si exposed to low intensity light, of wavelength 633nm, derived from a He-Ne laser. The samples were prepared in sandwich configuration by R.F. sputtering in argon or argon-hydrogen atmospheres. Illumination intensities of $1uWcm^{-2}$ or less were applied through a semi-transparent gold top electrode. Changes in a.c. conductivity and capacitance of up to 10% were measured at helium temperatures.

The optical response at helium temperatures is non-linear. At high intensities, the permittivity increases as $I^{1/4}$, but at low intensities the response is closer to $I^{1/2}$. The temperature dependence of the response is small up to 20K. The recovery to the dark state is non-exponential and usually many hours elapse before no further change can be detected.

When 500nm and 800nm light is used, no difference in response can be seen after the different absorption factors of the semiconductor film at these wavelengths have been accounted for. The loss changes induced in the $I^{1/4}$ region are similar in pure a-Si and pure a-Ge films but decrease as the hydrogen content of films increases. At low intensities heavily hydrogenated material shows a greater response than pure material.

The following model is used to explain the data. Incident photons generate free carriers which are rapidly trapped by deep, clustered defects. The trapped electrons (or holes) are able to respond to the applied a.c. field and contribute an additional loss. The only escape for the

trapped electrons at low temperatures is by tunnelling to a neighbouring excess hole. An simple analysis of the appropriate rate equations leads to carrier densities which compare well to the e.s.r. signal in sputtered material. The above model predicts the $I^{1/2}$ behaviour at low intensities.

During the decay to dark equilibrium, the induced loss is proportional to -log(time). To account for the form of the decay the model is modified to include the fact that, in the dark, the average excited pair separation will increase with time. By postulating a minimum pair separation it is possible to explain the inconsistency of the slow decays to equilibrium and the recombination times estimated from the high temperature loss. However this model fails in that the predicted maximum pair separation is less than the minimum pair separation. This can only be explained by strong carrier self-trapping at the defect site.

The reduced response at higher intensities is ascribed to reduced self-trapping for states excited far from the fermi level. The increased self-trapping in hydrogenated material is also reflected in a slower free decay to equilibrium.

The active defect is estimated to be approximately 10Å in extent which is consistent with the results of the low temperature a.c. field effect. It is suggested that the optically induced loss is derived from a population of correlated pairs of dangling bond states which exist on the internal surfaces of voids.

CHAPTER 1 : Introduction

The a.c. loss in amorphous materials, particularly a-Si and a-Ge, has been studied for a number of years. There has been considerable progress in our understanding of the mechanisms responsible for the loss in these materials. The conductivity is derived from electron tunnelling between localized states in the region of the fermi level. This was established by Mott (1969) who first derived the $T^{1/4}$ law for d.c. conduction and by Austin & Mott (1969) who considered the a.c. conductivity within the pair approximation. For many years it was assumed that the total conductivity could be represented as the sum of the d.c. contribution and the a.c. term derived from the pair approximation. This ignores the contribution of extended clusters of states to the a.c. loss. The models based on this assumption proved to be unsatisfactory (Long, 1982).

Butcher & Summerfield (1982,1984) developed the extended pair approximation (EPA) to take into account the interactions between isolated pairs of states and its surroundings. This model has been highly successful in explaining many aspects of the a.c. loss in sputtered a-Si and a-Ge. (Balkan et al., 1985, Long et al., to be published).

The Glasgow group has also investigated the effect of magnetic fields on the loss (J. McMillan, PhD Thesis, to be published) and the effect of optical illumination. The latter is the subject of this thesis. A number of different light induced phenomena have been reported in the literature over a wide range of temperatures and light intensities. The

Staebler-Wronski effect, the introduction of deep states in the gap by exposure to high intensity light (>1mWcm^{-2}), is generally studied at room temperature. At low temperatures light induced electron spin resonance, luminescence and infared-induced transients are observed. No previous report has been made of an attempt to quantify the light induced a.c loss in tetrahedral amorphous semiconductors.

In the following chapter we give a review of the present understanding of hopping conductivity in amorphous materials. Chapter 3 outlines some of the work on optically and electrically induced long-lived states that have been reported in recent years. Chapter 4 is devoted the development of experimental techniques carried out in order to investigate optically induced a.c. losses. In Chapter 5 we summarize the d.c. and a.c. conductivity measurements taken in the dark. Chapter 6 presents the light-induced loss results. The results are analysed in chapter 7 and a model to explain them is introduced. In chapter 8 a summary of the work is given.

CHAPTER 2 : Hopping Conductivity in Amorphous Semiconductors

In this chapter a summary of the present understanding of hopping conductivity in amorphous semiconductors is given.

2.1 : D.C. Conductivity

In the states above the localization limit, E_c, extended state conduction occurs. Below E_c the Anderson localization criterion is satisfied and carriers move between localized states by exchanging energy with the lattice, by thermally activated hopping (Mott, 1969).

If one considers two sites, A & B, separated by a distance R and by an energy difference W, there are two possibilities to consider. If W is less than $\hbar\omega_0$, where ω_0 is the highest phonon frequency in the lattice, then the hopping process involves a single phonon. If W is greater than $\hbar\omega_0$ then several phonons assist the carrier to hop.

Mott calculated the transition rate for a single phonon process and found it to be of the form

$$\nu = \nu_0 e^{-2\alpha R_0} e^{-W/kT} \qquad (2.1)$$

α^{-1} is a measure of the spatial extent of the localized electron wavefunction and the factor $e^{-2\alpha R_0}$ is the probability of electron transfer by tunnelling. The Boltzmann factor $e^{-W/kT}$ is the probability of the existence of a phonon of energy W. ν_0 is defined as the characteristic frequency and depends on the phonon density of states and the electron -phonon coupling.

At high temperatures electrons are excited to localized

states at energy E in the band edges and the main contribution to the conductivity is from hopping within kT of E to unoccupied nearest neighbour centres. As the temperature drops the hopping path will sink to lower energies and the most important conduction mechanism becomes the hopping of electrons within a few kT of the fermi level, provided that there is a sufficiently high density of states in this region. When the temperature is lowered still further the number and energy of the available phonons decreases and hopping becomes restricted not to the nearest neighbour centres in space,but to those states that are energetically closer, (Mott 1969,1972). Mott proposed that the greatest contribution to conductivity arises from hopping for which the transition rate, ν^{-1}, as defined by eqn. 2.1, is a maximum. This assumes that there is at least one state within a given spatial and energy separation. Hence

$$W = \frac{3}{4\pi R^3}(N(E_F))^{-1} \qquad (2.2)$$

where $N(E_F)$ is the density of states at the fermi level, E_F.

The distance in space that an electron is most likely to hop is defined as R_{opt}, and is evaluated by using the above value of W and minimizing the exponential factor in (2.1), giving :

$$2\alpha = \frac{9}{4\pi R_{opt}^4 N(E_F)kT} \qquad (2.3) \qquad R_{opt} = \left(\frac{9}{8\pi N(E_F)kT\alpha}\right)^{1/4} \qquad (2.4)$$

The most probable hopping energy is :

$$W_{opt} = \frac{3}{4\pi R_{opt}^3 N(E_F)} \qquad (2.5)$$

The conductivity is given by :

$$\sigma = N(E_F)kTe\mu \qquad \text{where the mobility, } \mu = \frac{e\nu_{AB}R^2}{6kT} \tag{2.6}$$

$$\sigma = \sigma_0' \exp(-2\alpha R_0 - W/kT) \tag{2.7}$$

Substituting R_{opt} and W_{opt} into the above equations gives

$$\sigma = \sigma_0 \exp\left(\frac{T}{T_0}\right)^{-1/4} \quad \text{where} \quad T_0 = \frac{18\alpha^3}{N(E_F)k} \tag{2.8}$$

Eqn. 2.8 is the Mott $T^{1/4}$ law which describes variable range hopping conductivity. In the samples of the type used in the present work $T^{1/4}$ behaviour is seen up to room temperature (N. Balkan, Ph.D. thesis 1979). This is not expected from the above model as W_{opt}, the optimum hopping energy given by (2.5), is much greater than the maximum phonon energy at such temperatures. Emin (1974) calculated a phonon assisted transition rate for a multiphonon process and obtained a $T^{1/4}$ type temperature dependence, from the transition rate alone, upto the Debye temperature; this suggests that the multiphonon process must be taken fully into account when calculating the hopping rates. However it is not clear that the Emin process leads to the dispersion required to explain the a.c. data.

The pre-exponential factor, σ_0 is theoretically expected to be of the following form by most workers :

$$\sigma_0 \sim [N(E_F)T]^p \qquad \text{where } |p| <= 1 \tag{2.9}$$

Experimentally it has little temperature dependence but it can be changed by orders of magnitude by annealing, even though T_0 remains almost constant. This failure of the theory has been ascribed to the assumption that hopping takes place in a homogeneous material. An inhomogeneous microstructure may explain the behaviour of the

pre-exponential factor while the variable range hopping model may still be valid (Aspley et al., 1977).

Aspley & Hughes (1974,1975) calculated the hopping conductivity between localized states as a function of applied electric field as well as temperature. Using (2.1) they calculated the probability of hopping to be :

$$\text{Probability} \sim \exp\left(-2\alpha R - \frac{(W+eFR\cos\theta)}{kT}\right) \qquad (2.10)$$

This is for a hop upwards in energy where θ is the angle between the direction of hop and the field,F. Taking into account the possibility of downward a hop down in energy, they defined a "range" in four dimensional space, $\langle R_{nn} \rangle$. This range (three spatial coordinates and one energy coordinate) is the average nearest neighbour range. The conductivity is then expressed as follows :

$$\sigma \sim \exp\left(\langle R_{nn} \rangle\right)$$

They then estimate the most probable nearest neighbour range $|R_{nn}|$ from $\langle R_{nn} \rangle$ and so calculate the field dependent hopping conductivity in the form :

$$\text{For } \beta \ll 1 \qquad \sigma(\beta,T) = \sigma_0 \exp\left[-\left(\frac{T_0}{T}\right)^{1/4}\left(1-\frac{\beta^2}{4}\right)\right] \qquad (2.11)$$

$$\text{For } \beta \geq 10 \qquad \sigma(\beta,T) = \sigma_0 \exp\left(\frac{-64\alpha^4}{\pi N(E_F)e}\right)^{1/4} \frac{1}{F^{1/4}} \qquad (2.12)$$

$$\beta = \frac{Fe}{2\alpha kT} \qquad T_0 = \frac{24\alpha^3}{N(E_F)\pi k}$$

They assume : i) the field does not change the occupation probability of a particular localized state, ii) the average distance hopped by carriers depends on the direction of the field and iii) the density of states is flat, $N(E)=N(E_F)$

The above theory can be used to evaluate α^{-1} and $N(E_F)$ values. The predicted high field behaviour has been seen

experimentally (Apsley et al., 1977). Pollak and Reiss (1976) used percolation theory to obtain similar results at high fields. At low fields the two approaches were not consistent.

2.2 : A.C. Loss - The Pair Approximation

The usual approach to the theory of a.c. loss is to consider the polarizability of an isolated pair of states and then to sum the losses of such pairs over the whole sample. This is known as the pair approximation. It was first introduced by Pollak & Geballe (1961), and was modified by Pollak (1964, 1971, 1975) and by Austin and Mott (1969). Figure 2.1 shows a pair of single electron states separated by an energy Δ_{12} and the distance R_{12}. If the states are occupied by only one electron and f_1 and f_2 are the occupation probabilities of the states then the transfer rate equations are :

$$\dot{f}_1 = \omega_{21} f_2 - \omega_{12} f_1 = -\dot{f}_2 \qquad (2.13)$$

The transition rates ω_{ij} involve inelastic processes

$$\omega_{ij} = \frac{1}{\tau_0} \exp\left(\frac{|\Delta_{ij}| + \Delta_{ij}}{2kT}\right) \qquad (2.14)$$

for i=1,2 and j=2,1. In thermal equilibrium f_1 & f_2 take the following form

$$f_1^o = \frac{1}{1 + \exp\left(\frac{-\Delta_{12}}{kT}\right)} \qquad f_2^o = \frac{1}{1 + \exp\left(\frac{\Delta_{12}}{kT}\right)} \qquad (2.15)$$

When a sinusoidal field $\mathcal{E}$, of frequency ω is applied the energy between the two states decreases by $e\mathcal{E}R$ perturbing the occupation values. If the response in linearized for a small field, $\mathcal{E}$, the polarizability is :

$$\alpha = \frac{e^2 R_{12}^2}{4kT} \frac{1}{\cosh^2(\Delta_{12}/2kT)} \frac{1}{1+i\omega\tau} \qquad (2.16)$$

where the effective relaxation time is given by

$$\tau = \frac{\tau_0}{2}\left[\cosh\left(\frac{\Delta}{2kT}\right)\right]^{-1} \quad \text{for } e\mathcal{E}R \ll kT \qquad (2.17)$$

It can be seen that the polarizability has a Debye form $1/1+i\omega\tau$ with an imaginary (lossy) part that peaks at $\omega \sim \tau^{-1}$. Loss will occur principally for states separated by < kT because of the $[\cosh(\Delta_{12}/2kT)]^{-2}$ factor.

Miller & Abrahams (1960) suggested that for low energy single phonon transfer processes a more correct form of the transition rate is

$$\omega_{ij} = \frac{\beta\Delta_{ij}}{\exp(\Delta_{ij}/kT) - 1} \qquad (2.18)$$

where β contains details of the interaction. The polarizability is unaffected by the new transition rate but the relaxation time becomes

$$\tau = \frac{1}{\beta|\Delta_{12}|}\tanh\left(\frac{\Delta_{12}}{2kT}\right) \qquad (2.19)$$

As $\Delta_{12} \rightarrow 0$ at very low temperatures, this result also becomes inaccurate due to quantum mechanical splitting of the states.

The pair approximation is the basis of most of the theoretical models of a.c. loss in amorphous semiconductors. The above calculations apply to an isolated, singly-occupied pair of states. The pair approximation will work best at high frequencies. For a random distribution of states those pairs which are closer together will have a shorter relaxation time and will respond to a higher frequency. Coupling between the pairs of states decreases with their separation. Hence closely spaced pairs are less likely to overlap and interact

with other pairs. At lower frequencies the separation between the active a.c. loss states will increase and interactions between them and the surrounding states will no longer be negligible.

The next stage of the analysis is to consider electron states distributed uniformly over an energy range Δ_0 and with N states per unit volume. We take a pair of states at energies E_1 & E_2 and calculate the statistical factors by considering the pair of states as a whole. We assume that the intrasite correlation energy is much greater than Δ_0 and that all energies are measured from $\mu+kT\ln(2)$ where μ is the chemical potential. The partition function then simplifies to

$$Z = 1 + e^{-\beta E_1} + e^{-\beta E_2} + e^{-\beta(E_1+E_2+E_{12})} \qquad \text{where} \quad \beta = 1/kT \tag{2.20}$$

(For full partition function see Long (1982)).

If the intersite correlation energy, $E_{12}=0$ then the occupation probability of site 1 is

$$h_1^0 = Z^{-1} e^{-\beta E_1} \tag{2.21}$$
$$= \frac{\exp\left((\beta/2)(E_1-E_2)\right)}{2\left[\cosh\left((\beta/2)(E_1-E_2)\right) + \cosh\left((\beta/2)(E_1-E_2)\right)\right]}$$

By using similar rate equations to those used in the previous section and by solving them for a small sinusoidal field the polarizability can be deduced

$$\alpha(E_1,E_2,R_{12}) = \frac{e^2R_{12}^2}{2kT} \frac{\omega_{21}^0 h_2^0 + \omega_{12}^0 h_1^0}{\omega_{21}^0 + \omega_{12}^0} \frac{1}{1 + i\omega\tau} \tag{2.22}$$
$$= \frac{e^2R_{12}^2}{4kT} \frac{1}{\cosh\left((\beta/2)(E_1 - E_2)\right)\left[\cosh\left((\beta/2)(E_1 + E_2)\right) + \cosh\left((\beta/2)(E_1 - E_2)\right)\right]}$$
$$\times \frac{1}{1 + i\omega\tau}$$

The relaxation times are given by (2.17) for a multiphonon process and by (2.19) for single phonon hopping.

The total a.c. loss can be calculated from the polarizability. Firstly it is necessary to integrate over all possibile site 2's for a given site 1 to obtain the average polarization.

$$\bar{\alpha}(E_1) = \iiint \alpha(E_1, E_2, R_{12}) 2\pi \frac{N}{\Delta_0} R_{12} \sin\theta \, dE_{12} dR_{12} d\theta \qquad (2.23)$$

The complex conductivity is calculated by integration over all initial states.

$$\sigma = \frac{i\omega}{2} \int \bar{\alpha}(E_1) \frac{N}{\Delta_0} dE_1 \qquad (2.24)$$

$$= \frac{\pi}{6} e^2 \beta g_0^2 \iiint R^4 \frac{1}{1 + i\omega\tau}$$

$$\times \frac{dR dE_1 dE_2}{\cosh((\beta/2)(E_1 - E_2))\left[\cosh((\beta/2)(E_1 + E_2)) + \cosh((\beta/2)(E_1 - E_2)\right)}$$

where g_o is the density of states. This expression is used later to calculate the loss for different cases of single electron transfer.

2.3 : A.C. Loss - Charge Transfer Models

2.3.1 : Electron Transfer by Tunnelling

Deep within the energy gap of an amorphous semiconductor the states are isolated, single particle states which have a broad range of energies about the Fermi level. The adherence of these materials to the Mott $T^{1/4}$ law over many decades of conductivity variation supports the theory that transport

is by electron tunnelling close to E_F (see § 2.1). The relaxation time is similar to eqn. 2.17 except τ_0 is replaced by

$$\tau_0 \rightarrow 2\tau_{0t}\exp(2\alpha R) \qquad (2.25)$$

where α is the decay parameter for the s-like wavefunction on the sites and τ_{0t}^{-1} is approximately an optic phonon frequency (Mott 1969). By using this expression in eqn. 2.24 the a.c. loss predicted by the tunnelling model can be calculated. The integration over R is replaced by integration over τ, giving the real part of the conductivity to be

$$\sigma_1 = \frac{\pi}{6}\frac{e^2\beta g_0^2\omega}{2\alpha}\int \frac{R^4\omega d\tau}{1+\omega^2\tau^2}\iint \qquad (2.26)$$

$$X \frac{dE_1 dE_2}{\cosh((\beta/2)(E_1-E_2))[\cosh((\beta/2)(E_1+E_2)) + \cosh((\beta/2)(E_1-E_2))]}$$

The exponential factor in eqn. 2.17 means that τ is a rapidly changing function of R but the Debye form implies the conductivity will peak strongly where $\omega\tau \sim 1$, for a very restricted range of R. The slowly varying R can be approximated by a constant R_ω with $\tau \sim \frac{1}{\omega}$ given that $\tau_{max} \gg \omega^{-1} \gg \tau_{0t}$ where τ_{max} is the largest relaxation time.

Eqn. 2.17 implies that R_ω will be effected by the factor E_1-E_2. However the denominator of the integral in eqn. 2.26 suggests that the contributions to the conductivity are negligible except when E_1-E_2 is small. If follows that the energy factors in eqn. 2.26 can be discounted and that

$$R_\omega = -\frac{1}{2\alpha}\ln(\omega\tau_{0t}) \qquad (2.27)$$

From the above it can be seen that the tunnelling distance at a fixed frequency is independent of temperature, this is

characteristic of loss by tunnelling.

Using these approximations and evaluating the integral for the wide band case gives

$$\sigma_1 = \frac{\pi^4}{12}\frac{e^2 g_o^2 kT}{2\alpha}\omega R_\omega^4 \qquad (\text{for } \beta\Delta_o >> 1) \tag{2.28}$$

or more simply

$$\sigma_1 \sim \omega^s T^n \quad \text{where} \quad s = 1 + \frac{4}{\ln(\omega\tau_{0t})} \tag{2.29}$$

For this model, s is independent of T and about 0.8 for a frequency of 10kHz. For single electron tunnelling, n=1.

Eqn 2.28 was derived by Bottger & Bryksin (1976) and Efros (1981); Other workers (Pollak, 1971, Butcher & Hayden, 1977, Long et al., 1982) obtained a similar functional form but with different numerical factors. Eqn. 2.28 has the form of the formula first derived by Austin & Mott (1969) on the basis of the same physical argument but with less mathematical analysis.

2.3.2 : Correlated Barrier Hopping

In this model of charge transfer we first consider a single electron hopping over a potential barrier between positive defect centres. The barrier height will be reduced by coulomb interaction; the barrier height W is correlated with the separation R

$$W = W_m - \frac{e^2}{\pi\varepsilon\varepsilon_o R_{12}} \tag{2.30}$$

Here W_m is the energy needed to remove an electron to the conduction band. The barrier profile for the correlated barrier hopping (CBH) model in shown in fig 2.2. It was first

introduced by Pike (1972). Using eqn. 2.17 the transition rate is

$$\omega_{12} = \frac{1}{2\tau_{0h}} \exp\left(-\frac{W}{kT}\right)\exp\left(-\frac{\Delta_{12}}{2kT}\right) \qquad (2.31)$$

In general W>>kT (except for very low temperatures) so the activation energy is much greater than the Debye energy and τ_{0h} is approximately the inverse Debye frequency. It is assumed that any dependence of τ_0 on R due to overlap of the excited state wavefunctions is weak.

The relaxation time for the CBH model has the form

$$\tau = \tau_{0h}\exp\left(\frac{W}{kT}\right)\frac{1}{\cosh(\Delta/2kT)} \qquad (2.32)$$

the site energies E_1 & E_2 are measured from $\mu + kT\ln(2)$

Starting from the linearized expression for the conductivity (2.24) the way forward is similar to that used in the previous section. τ varies rapidly with respect to R, as before, and the integral is transformed to an integral over τ by substitution.

$$dR = \frac{kT}{\tau}\frac{1}{dW/dR}d\tau \qquad (2.33)$$

Hence $$\sigma_1 = \frac{\pi}{6}e^2 g_0^2 \omega \int \frac{[R^4(dR/dW)]\omega d\tau}{1+\omega^2\tau^2} \iint \qquad (2.34)$$

$$\times \frac{dE_1 dE_2}{\cosh\left(\frac{1}{2}\beta(\Delta_1 - \Delta_2)\right)\left[\cosh\left(\frac{1}{2}\beta(\Delta_1 - \Delta_2)\right) + \cosh\left(\frac{1}{2}\beta(\Delta_1 + \Delta_2)\right)\right]}$$

The integral over τ is approximated by $(\pi/2)[R^4(dR/dW)]_{opt}$, if dR/dW is evaluated at R_ω, the value of R at $\omega\tau = 1$.

As for the tunnelling process, R_ω is in principle dependent on E_1 and E_2. However, for $\Delta <= kT$, that is, for hopping close to the chemical potential, (2.34) can be simplified; R_ω is given by a solution of the following eqn.

$$W(R_\omega) = -kT \ln(\omega\tau_{0h}) \tag{2.35}$$

From (2.35) R_ω is deduced.

$$R_\omega = \frac{e^2}{\pi\varepsilon\varepsilon_o[W_m + kT\ln(\omega\tau_{0h})]} \tag{2.36}$$

Also

$$\left[R^4\frac{dR}{dW}\right]_{opt} = R_\omega^6\frac{\pi\varepsilon\varepsilon_o}{e^2} \tag{2.37}$$

The conductivity is calculated by integrating over the energy terms.

$$\sigma_1 = \frac{\pi^2}{24}N^2e^2\omega\left[R^4\frac{dR}{dW}\right]_{opt} \qquad \text{for } (\Delta_o << kT) \tag{2.38}$$

$$\sigma_1 = \frac{\pi^2}{12}g_o^2(kT)^2e^2\omega\left[R^4\frac{dR}{dW}\right]_{opt} \qquad \text{for } (\Delta_o >> kT) \tag{2.39}$$

Following the notation of the previous section, the frequency exponent, s and the temperature exponent, n are calculated to be

$$s = 1 - \frac{6kT}{W_m + kT\ln(\omega\tau_{0h})} \tag{2.40}$$

$$n = -(1-s)\ln(\omega\tau_{0h}) \tag{2.41}$$

These equations give a very different picture from that given with the tunnelling model. For correlated barrier hopping n, the temperature exponent is frequency dependent. The frequency exponent, s, decreases from unity with increasing temperature.

2.3.3 : Polaron Tunnelling

Polaron assisted tunnelling occurs when the transfer of an electron from one state to another causes lattice relaxation and a lowering in energy of the states. Mott and Davis (1979, Ch3) showed that the process of electron

transfer between degenerate states has an activation energy $W_H = W_p/2$ where W_p is the energy decrease caused by the lattice deformation at the occupied site.

There are two different types of polaron tunnelling. Firstly we consider the small or molecular polaron. In this case, the energy decrease comes from local bonding changes and the deformation around the two sides does not overlap; W_p is independent of R, the site separation. Emin & Holstein (1969) calculated the probability of transfer at high temperatures to be

$$\tau = \tau_{0p}\exp\left(\frac{W_H}{kT}\right)\exp(2\alpha R) \qquad (2.42)$$

Here we assume that hopping occurs between states of similar energy i.e. $\Delta \simeq 0$. W_H is independent of T at lower temperatures because the distorted lattice is in its ground state at each site.

As the temperature term in (2.42) does not contain the site separation we can treat small polaron tunnelling in the same way as simple tunnelling but with the transition time τ_0 replaced by $\tau_{0p}\exp(W_H/kT)$

The a.c. loss is given by (2.28) but with

$$R_\omega = -\frac{1}{2\alpha}\left[\ln(\omega\tau_{0p}) + \frac{W_H}{kT}\right] \qquad (2.43)$$

The frequency exponent increases with temperature

$$s = 1 + \frac{1}{[\ln(\omega\tau_{0p}) + W_H/kT]} \qquad (2.44)$$

The large or dielectric polaron is the second case to be considered. Here, the polaron energy comes from polarization changes in the deformed lattice. Such a polaron, because of the long range coulomb force, will extend over a number of

interatomic distances. The potential wells of the two states are now likely to overlap and the activation energy of the particle transfer will drop (Austin & Mott, 1969, Mott & Davis, 1979) according to

$$W_H = W_{H0}\left(1-\frac{r_0}{R}\right) \tag{2.45}$$

The polaron radius is r_0. W_H is now a function of site separation. The empirical expression for the relaxation time becomes

$$\tau = \tau_{0p}\exp\left\{\frac{W_{H0}}{kT}\left(1-\frac{r_0}{R}\right)\right\}\exp(2\alpha R) \tag{2.46}$$

Following the same procedure as before, the integral over R is replaced by one over τ . The term evaluated at $\tau = \omega^{-1}$ is

$$\left[\frac{R^4}{2\alpha kT + dW_H/dR}\right]_{opt} = \left[\frac{R^4}{2\alpha kT + W_{H0}r_0/R^2}\right]_{opt} \tag{2.47}$$

The frequency exponent, s follows the CBH model at low temperatures but is similar to pure tunnelling at high temperatures

$$s = 1 - \frac{1}{2\alpha R_\omega}\,\frac{4+6(W_{H0}r_0/2\alpha kTR_\omega^2)}{[1+(W_{H0}r_0/2\alpha kTR_\omega^2)]^2} \tag{2.48}$$

2.3.4 : Intersite Correlation Effects

So far in this discussion of the pair approximation, the intersite correlation energy E_{12} has been neglected. E_{12} is best approximated by the positive electrostatic repulsion of two electrons which are a distance of R_{12} apart.

$$E_{12} = \frac{e^2}{4\pi\varepsilon\varepsilon_0 R_{12}} \tag{2.49}$$

If one site is occupied, the second site is raised by E_{12} making the second site less likely to be occupied. The unoccupied second site allows the pair to respond to an applied a.c. field and contribute to the loss. Hence the correlation energy causes the loss due to carrier transfer to be increased.

If $E_{12} \ll kT$ the occupation of a state is largely unaffected by the correlation energy. However if $E_{12} > kT$ the occupation factors will be altered. Superficially, therefore, this appears to be a low temperature effect. However the substitution of some numerical values into (2.49) reveals that the onset of correlation effects may occur at about room temperature for tetrahedral semiconductors. These ideas apply to nearest neighbour sites, the coulomb interaction will be screened for a high density of states at larger separation distances

The effect of the intrasite correlation energy was first considered by Pollak (1971) who derived the low temperature results in the tunnelling case. We will now return to the simple tunnelling model and take into account the correlation energy. Using the partition function (2.20) with a non-zero E_{12} the state occupation function of site 1 is

(2.50)

$$h_1^0 = \frac{\exp\left((1/2kT)(E_1-E_2)\right)}{2\left[\cosh\left((1/2kT)(E_1+E_2+E_{12})\right)\exp(-E_{12}/2kT) + \cosh\left((1/2kT)(E_1-E_2)\right)\right]}$$

The expression for the conductivity is equivalent to eqn. 2.24 with a revised energy integral. Evaluating the integral for $E_{12} \gg kT$ gives $4E_{12}/kT$. The dependence of the loss on E_{12} is because all the states between $\mu+kT\ln(2)$ and $\mu+kT\ln(2)-E_{12}$ contribute, so the number of pairs involved

in the loss is proportional to E_{12}. The real part of the conductivity becomes

$$\sigma_1 = \frac{\pi^2}{3} \frac{e^4 g_o^2}{4\pi\varepsilon\varepsilon_o} \frac{1}{2\alpha} \omega R_\omega^3 \qquad (2.51)$$

Further results taking correlation into account can be derived for the tunnelling model and for the CBH and polaron models. These are summarized in table 4 of Long (1982). From that table it will be seen that the temperature exponent, n is in general less by one than for the uncorrelated results. This is connected to the dependence of the number of the contributing pairs on E_{12}kT rather than $(kT)^2$ as in the uncorrelated case (Pollak, 1971). The pairs of states with mean energies between $\mu+kT\ln(2)$ and $\mu+kT\ln(2)-E_{12}$ are essentially occupied by one electron.

2.4 : The Imaginary Component of the Loss

For a constant frequency exponent independent of frequency, the imaginary part of the loss is connected to the real part by the Kramers-Kronig transform (see, for example, Pike, 1972)

$$\frac{\sigma_2}{\sigma_1} = \tan\left(\frac{s\pi}{2}\right) \qquad (2.52)$$

However, the value of s is usually weakly frequency dependent and a more sophisticated approach is required. From (2.24), the imaginary component is

$$\frac{\sigma_2}{\omega} \alpha \int_{\tau_0} F(R) \frac{d\tau}{\tau(1+\omega^2\tau^2)} \qquad (2.53)$$

For simple tunnelling, this expression becomes :

$$\frac{\sigma_2}{\omega} \alpha \frac{1}{5(2\alpha)^4}\int_{\tau_0}[\ln(\tau/\tau_{0t})]^5 \frac{2\omega^2\tau d\tau}{(1+\omega^2\tau^2)} \qquad (2.54)$$

Integration by parts gives

$$\frac{\sigma_2}{\omega} \alpha \int_{\tau_0}\frac{[\ln(\tau/\tau_{0t})]^4}{\tau}\frac{d\tau}{(1+\omega^2\tau^2)} \qquad (2.55)$$

The function $\tau/(1+\omega^2\tau^2)^2$ peaks at $\tau=\omega^{-1}$. The logarithmic term is now removed and evaluated at $\tau=\omega^{-1}$ The integral becomes

$$[-\ln(\omega\tau_{0t})]/5(2\alpha)^4$$

Using the value of σ_1 for tunnelling gives

$$\frac{\sigma_2}{\sigma_1} = -\frac{2}{5\pi}\ln(\omega\tau_{0t}) \qquad (2.56)$$

The method outlined above can be employed for other models of charge transfer (see Long, 1982).

2.5 : Atomic Relaxation

In amorphous semiconductors with a wide band gap and a low density of electronic states within the gap, atomic relaxation, as opposed to electronic relaxation, may play an important part in the loss (Hunklinger & von Shickfus, 1981). It should be possible to differentiate between the two mechanisms from experimental results. One distinguishing property of atomic relaxation is that although the atom (or group of atoms) is allowed to transfer between two potential wells, it is unable to leave the pair and go to another site. Hence, unlike electronic relaxation, we can be certain of the accuracy of the pair approximation and the results of §2.2 can be used with $f_1 + f_2 = 1$. We have no particular

reason to assume that the dipole moment associated with transfer is correlated with R so in the following calculations, the dipole moment, p is taken to be constant and the atomic transition is assumed to change the dipole from parallel to anti-parallel i.e. a change of $2p\mathcal{E}$ in energy. The polarizability of the pair is

$$\alpha = \frac{\eta p^2 \cos^2\theta}{kT} \frac{1}{\cosh^2(\Delta/2kT)} \frac{1}{1+i\omega\tau} \tag{2.57}$$

where θ is the angle between dipole and field and η is a mean field correction.

The potential barrier between the sites may be crossed in two ways by the atom, thermal excitation over the barrier or tunnelling through it. The former case has been analysed by Pollak & Pike (1972) and Le Cleac'h (1979). Following these authors we assume the relaxation time is a modified form of (2.17).

$$\tau = \tau_{0a} \exp\left(\frac{W}{kT}\right) \frac{1}{\cosh(\Delta/2kT)} \tag{2.58}$$

W is allowed to vary over a range W_m to take into account changes in the atomic environment. The mean polarizability is

$$\bar{\alpha} = \frac{\eta p^2}{kT} \iiint \cos^2\theta \frac{1}{2} \sin\theta d\theta \frac{d\Delta}{\Delta_0 \cosh^2(\Delta/2kT)} \frac{1}{1+i\omega\tau} \frac{dW}{W_m} \tag{2.59}$$

The real and imaginary parts of the conductivity are deduced using the methods previously applied.

$$\sigma_1 = i\omega N\bar{\alpha} \tag{2.60}$$

$$\sigma_1 = \frac{\pi}{3} \frac{\eta\omega N p^2}{W_m} \frac{kT}{\Delta_0} \tanh\left(\frac{\Delta_0}{2kT}\right) \tag{2.61}$$

$$\frac{\sigma_2}{\sigma_1} = -\frac{2}{\pi} \ln(\omega\tau_{0a}) \quad \text{for } 1/\tau_{0a} >> \omega >> 1/\tau_{0a}\exp(-W_m/kT) \tag{2.62}$$

For the tunnelling case, at low temperatures, we follow

the development of Frossati et al. Following eqn. 2.17, the relaxation time in the form appropriate for single-phonon transitions is:

$$\tau = \frac{B}{\Delta} \exp(2\lambda) \tanh\left(\frac{\Delta}{2kT}\right) \tag{2.63}$$

Here, λ is a tunnelling parameter, a measure of the barrier height and width, which is randomly distributed over a range λ_0. The mean polarizability is

$$\bar{\alpha} = \frac{\eta p^2}{3kT} \int_0^{\Delta_0} \int_0^{\lambda_0} \frac{d\lambda d\Delta}{\lambda_0 \Delta_0 \cosh^2(\Delta/2kT)} \frac{1}{1+i\omega\tau} \tag{2.64}$$

giving

$$\sigma_1 = \frac{\pi}{6} \frac{\eta N p^2 \omega}{\lambda_0 \Delta_0} \tanh\left(\frac{\Delta_0}{2kT}\right) \tag{2.65}$$

and

$$\frac{\sigma_2}{\sigma_1} = -\frac{2}{\pi} \ln\left(\frac{\omega B}{kT}\right) \quad \text{for } 1 >> \omega B/kT >> \exp(-2\lambda_0) \tag{2.66}$$

The frequency exponent of both the tunnelling and the activated transfer is equal to one. Physically, this represents the independence of the dipole moment of the contributing states from any of the parameters associated with the state distribution. For the wide band case ($\Delta_0 >> kT$), the temperature exponent is less by one than for uncorrelated electron transfer processes and this is derived from the unity occupation of the atomic pair state. The unity occupation of a pair of sites is also a feature of correlated electron processes (§2.3.4) and this leads to a similarity between the results of correlated transfer models and the atomic relaxation model. As a consequence it is sometimes difficult to determine the exact nature of the loss mechanism from experimental data.

2.6 : The Extended Pair Approximation (EPA)

All the models considered so far for a.c. loss make no provision for the continuous passage of electrons through the material. In the d.c. limit, where the pair approximation fails, the d.c. component of the conductivity is analysed using the Mott $T^{1/4}$ law. In order to interpret both components of the conductivity with a single theory, Summerfield and Butcher (1982) extended the pair approximation to take into account the effects of neighbouring states on the response of the pair. Miller and Abrahams (1960) introduced an equivalent circuit representing the linearized rate equations for a pair of sites. Summerfield and Butcher added elements to account for the rest of the network in an average way and solved Kirchhoff's equations for this extended equivalent circuit. Similar results have been obtained using a random-walk model to represent the network of interacting localized states (Movaghar & Schirmacher, 1981, Movaghar, Pohlmann & Sauer, 1980)

Measurements on sputtered a-Ge (Long et al., 1982, 1983) and a-Si (Long et al., to be published) revealed a loss peak in the a.c. conductivity and the differential form of the permittivity. The frequency at which the loss peak occurs, ω_c, was found to be strongly temperature dependent. The loss peak was associated with the transition to non-dispersive behaviour. Such behaviour cannot be explained by any model based on the pair approximation.

Summerfield (1985) noted that the shape of the curve in the region of the onset of dispersive behaviour is

approximately independent of temperature. A critical assessment of results calculated from many different models showed that ω_c is proportional to the d.c. conductivity, $\sigma_1(0)$ Summerfield found the following scaling hypothesis fitted the conductivity in the low frequency region.

$$\frac{\sigma_1(\omega)}{\sigma_1(0)} = 1 + \left(\frac{\omega}{\omega_c}\right)^{0.725} \qquad (2.67)$$

For dimensional reasons ω_c is given by

$$\omega_c = \frac{A\sigma_1(0)kT}{e^2\alpha} \qquad (2.68)$$

where A is a dimensionless constant. Summerfield found that the scaling relations, eqns. 2.67 and 2.68, fitted a number of different models when the value of A was adjusted. When the frequency dependent conductivity is normalized to its d.c. value at a particular temperature, it follows a quasi-universal function of the reduced frequency, $\tilde{\omega}$.

$$\frac{\omega}{\omega_c} = \frac{\omega e^2\alpha}{A\sigma_1(0)kT} = \frac{\tilde{\omega}}{A} \quad \text{where} \quad \tilde{\omega} = \frac{\omega e^2\alpha}{\sigma_1(0)kT} \qquad (2.69)$$

If the value of A is calculated using the EPA, the one unknown parameter in eqn. 2.69, α^{-1}, may be evaluated by fitting the experimental data. In fig. 2.3, we give a schematic representation of $\sigma_1(\omega,T)$ as predicted by the EPA and how it is related to $\sigma_1(0)$ and to the prediction using the pair approximation.

2.7 : Experimental Review

The a.c. conductivity of a-Ge and a-Si films has been studied by many workers. The results of different groups are not always consistent and are difficult to compare because of different sample preparation conditions and because the

measurements have been taken in different temperature and frequency ranges. This section is a summary of the more recent work in this field.

Butcher & Hayden (1977) compared the loss in evaporated a-Ge films measured by several workers (Chopra & Bahl, 1970, Hauser & Staudinger, 1973, and Gilbert & Adkins, 1976). They established that the Austin-Mott tunnelling model of loss was not acceptable. The measured loss is orders of magnitude too large. Long (1982) also rejects the Austin-Mott model because the temperature dependence at constant frequency is much stronger than the n=1 relationship of (2.28) and because the s value of the data at high frequencies is lower than the 0.8 predicted and is a decreasing function of temperature.

Long & Balkan (1980) applied the CBH model of Elliott (1977). They associated the loss peak with a spatial cut-off in the separation of contributing states ($=R_\omega$). The loss peak frequency should then follow an simple activated form. Although better than the Austin-Mott theory, the CBH model was still inadequate. Eqn. (2.40) predicts a linear relationship between s and temperature; in reality, s is approximately temperature independent above the cut-off frequency. Also the relaxation time parameter derived from the application of CBH is five orders of magnitude greater than the expected value of 10^{-13} (the inverse phonon frequency).

Long, Balkan, Hogg & Ferrier (1982) showed that the effect of hydrogen in sputtered a-Ge films was to scale the a.c. loss to higher temperatures. The scaling was explained using the polaron tunnelling model (§2.3.3) in which carriers hop between states around which polaron wells are formed. The hydrogen increases the dielectric constant in the vicinity of

the wells and so increases the polaron activation energy.

Long & Hogg (1983) proposed two distinct temperature regimes in the loss observed in sputtered a-Ge films. In pure a-Ge at low temperatures (T< 15K) n is about 0.4 and s=0.9. This region is also characterised by a strong a.c. field effect. Above 15K the conductivity increases rapidly with temperature (n=3 or 4) and s drops to about 0.6. A loss peak is seen in the a.c. conductivity and in the differential form of the permittivity data . Similar results are seen in a-Si (J. McMillan, Ph.D. Thesis, 1987, unpublished).

Small angle scattering measurements (Patterson et al., 1983) show that defects or voids of about 1nm in extent are common in sputtered material. These voids are identified as the active centres for low temperature loss (Long, Hogg, Holland, Balkan & Ferrier, 1985) (see next section). The authors suggest that at low temperatures, charge is trapped within defect clusters and that loss is due to polarisation of such clusters. The high temperature loss represents carrier hopping between clusters.

The EPA of Butcher & Summerfield (1982,1983) was applied to a.c. loss in sputtered a-Ge and a-Si by Balkan, Butcher, Hogg, Long & Summerfield (1985). Balkan et al. plotted the a.c. loss data using the reduced frequency, $\tilde{\omega}$, and found that the data does lie close to the universal curves describing the theoretical fit. The EPA successfully explains i) the loss peak in both the real and imaginary parts of the loss, ii) the gradient in the high frequency power-law region, above the loss peak, iii) the scaling of the loss peak to higher temperatures as the d.c. conductivity falls. The values of the inverse decay length, α, chosen to fit the EPA

were physically reasonable.

2.8 : The Low Temperature Regime

At low temperature there is little thermal energy for an activated process. Only tunnelling is likely to be possible. Initially Long et al. (1985) took the ideas of atomic relaxation (§2.5) and extended the model to take account of correlation between the dipole moment of the tunnelling state and the tunnelling parameter

$$p^2 = p_o^2 f(\lambda) = \frac{p_o^m (m+1)\lambda^m}{\lambda_o^m} \qquad (2.70)$$

The conductivity becomes

$$\sigma_1 = \frac{\pi}{6} \frac{\eta N p_o^2 \omega}{\Delta_o \lambda_o} f\left(\frac{1}{2}\ln\left(\frac{2kT}{\omega B}\right)\right) \quad \text{for } \Delta >> k_0 T >> \omega B \omega B \qquad (2.71)$$

The above predicts the temperature and frequency exponents

$$1-s = n = m/\ln(2kT/\omega B) \qquad (2.72)$$

The equality between s and n-1 comes directly from the assumption of inelastic tunnelling involving single phonons.

The atomic model is successful in explaining the low temperature properties of bulk glasses (Phillips, 1981). However the loss in a-Ge is a thousand times larger than that in vitreous silica. This can only be explained using the atomic tunnelling model by assuming a density of states three orders of magnitude greater in a-Ge or a dipole moment of 30 times the value in a bulk glass. The latter in the light of field effect results (see below) is more believable. The dipole in a-Ge must be of the order of an electronic charge multiplied by a distance of 4Å. This is a much higher value

than even for highly polar atomic groups and forces the conclusion that low temperature loss in a-Ge is by electronic tunnelling.

At these low temperatures we should consider correlated processes. It was shown in §2.5 that there is a similarity between the atomic and correlated electronic mechanisms, so the above results can be used with N, the number of tunnelling states per unit volume, replaced by $E_{12}g$, the correlation energy multiplied by the density of states. However there is one problem with the formulation. With s=0.9, the value of the temperature exponent (n=0.4) is too high to be satisfied by the simple tunnelling model (eqn. 2.71).

To investigate the nature of the low temperature loss further we turn to the dependence of the a.c. conductivity on the exciting electric field. Pairs of states whose asymmetry energy is less than or of the order of kT will relax at low fields. A field effect will be observed when the field-induced asymmetry becomes larger than kT. The critical condition for the onset of an effect is

$$e\mathcal{E}R \sim kT \qquad (2.73)$$

All pairs having asymmetry energies below $2e\mathcal{E}R$ will now contribute to the loss. The relaxation times (2.63) of the contributing states will drop allowing more states to contribute. By applying the above condition to experimental data, Long et al. (1985) calculated the electronic hopping distance to be 1nm; this is in agreement with the figure estimated above from consideration of the loss magnitude.

We have already dismissed simple tunnelling between defects because of the value of the temperature exponent

compared with the frequency exponent. This strong temperature dependence together with the strong field effect suggests a coupling mechanism which is energy-dependent. It is also unlikely that the losses are caused by the electronic tunnelling between the defects dominant in the high temperature regime. Balkan et al. (1985) derived a tunnelling distance of 20nm at 3kHz using parameters derived from the high temperature loss; this figure is not compatible with the 1nm tunnelling decay length observed. It appears that the electronic polarization is accompanied by some activated lattice relaxation and atomic relaxation.

Polaronic models have been discussed in §2.3.3. Small polarons would not be mobile at helium temperatures (Phillips, 1976). A large dielectric polaron is possible, extended defects in which the electronic wells are on closely spaced overlapping sites, so reducing activation energy. The 1nm voids detected by small angle scattering would provide a suitable environment for relaxation involving overlapping large polaron wells.

Other experimental results support this assertion. The helium temperature conductivity increases with 1/d where d= the film thickness. However, unlike the high temperature loss, the increase is not exactly proportional. This is readily explained because the voids in sputtered material are more prevalent towards the surfaces of the films. The hydrogenation of films reduces the conductivity in the high temperature regime whilst the data at low temperatures is hardly effected. Single dangling bonds, which are removed by hydrogen, could be the active defects above 15K. Below this temperature the dominant process probably occurs at extended

defects of 1nm in extent and involves significant activated atomic reorganization.

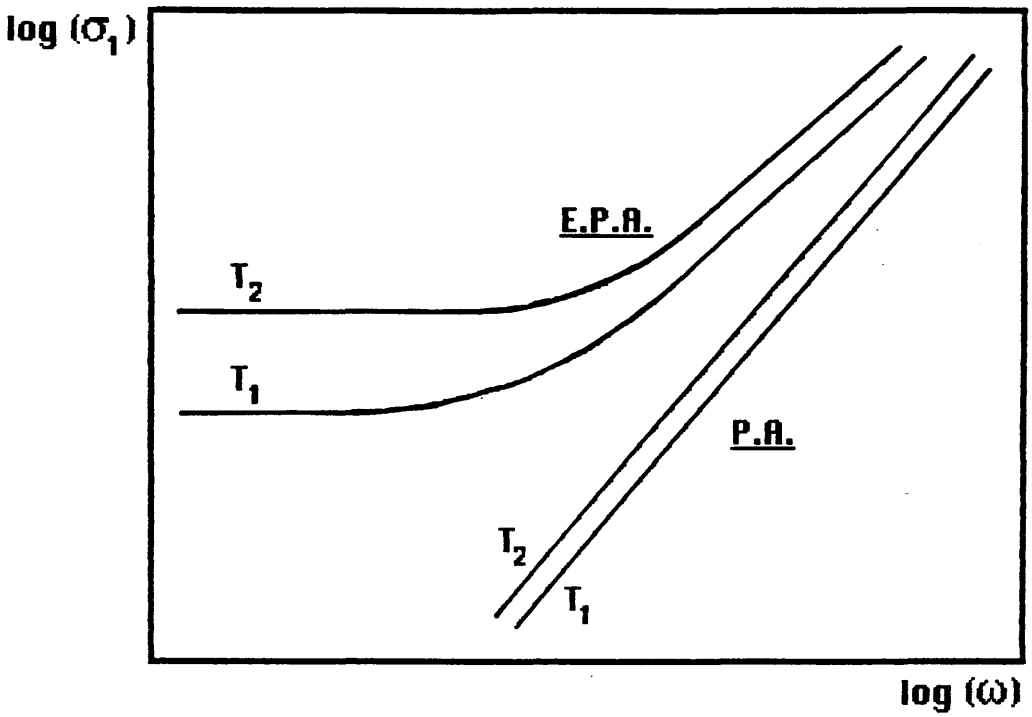

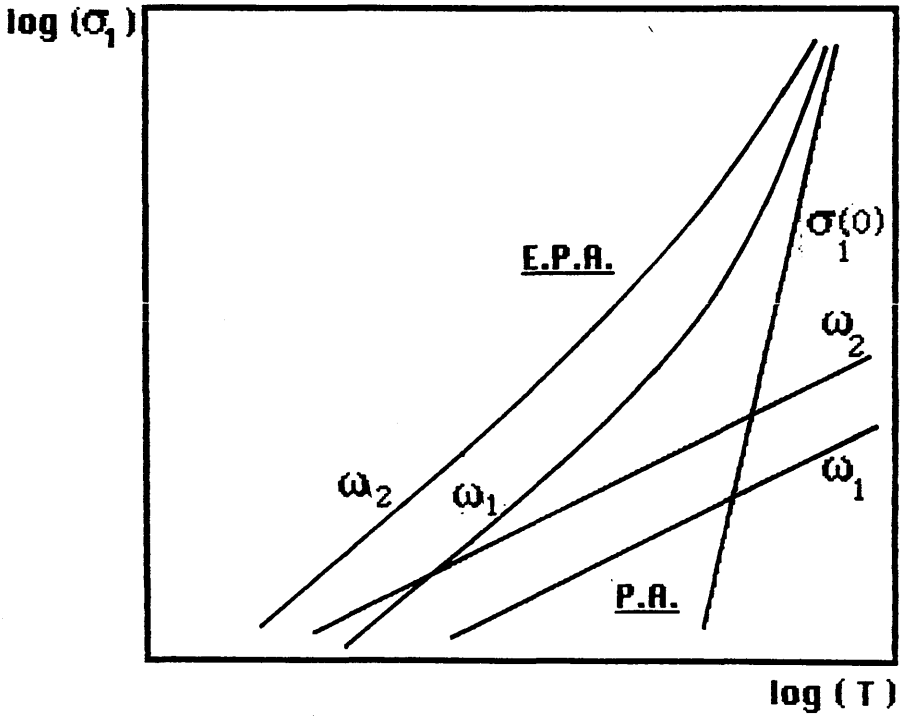

Figure 2.3 : Diagram showing schematically the predictions of the pair approximation (PA) and the extended pair approximation (EPA) for the (a) frequency and (b) temperature dependent conductivity of a hopping system. ($T_2 > T_1$ and $\omega_1 > \omega_2$).

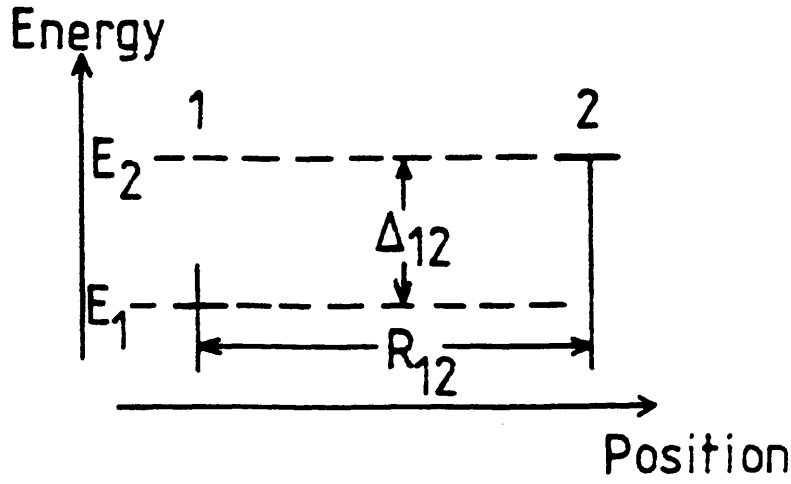

Figure 2.1 : Parameters for a pair of states 1 and 2.

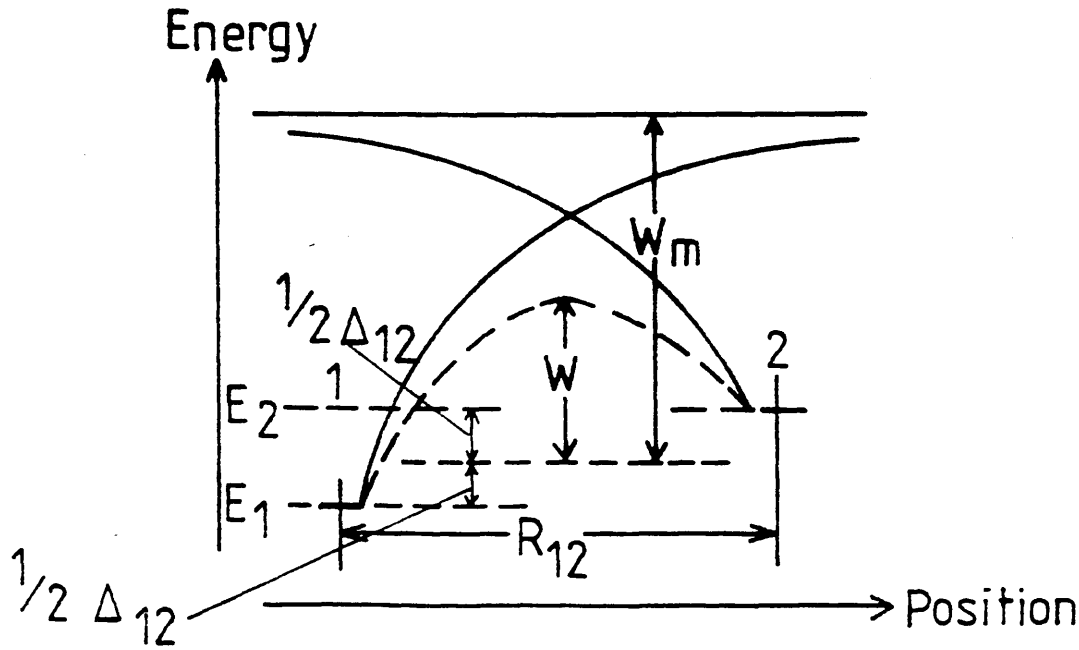

Figure 2.2 : Parameters for a CBH hop between states 1 and 2.

CHAPTER 3 : Optically and Electrically Induced Long-Lived States in Amorphous Semiconductors

The following chapter covers some techniques used for inducing and studying states with long lifetimes and metastable states in amorphous materials. Much of the work in this area has been done on the Staebler-Wronski effect.

3.1 : The Staebler-Wronski Effect

In 1977, D. L. Staebler and C. R. Wronski found that the dark conductivity and the photoconductivity of both doped and undoped a-Si:H films decreased when the films were exposed to light for long periods. Such changes were perfectly reversible and perfectly stable at room temperature and were a bulk effect between what may be considered a thermally stable state A and a new metastable state B. State A is obtained by annealing the films in the dark at a temperature above 150°C; the annealing time being dependent upon temperature. State B results after the exposure of the sample to light. The conductivity of state B is dependent upon the light exposure used in contrast to state A which has a clearly defined conductivity.

3.1.1 : Dark Conductivity Changes

A light intensity of between 100 and 200mWcm^{-2} of red light applied for 4 hours can result in a "light-soaked"

state for most a-Si:H films. When the film has reached this state, further illumination will not produce additional change. If the illumination is periodically interrupted, it is seen that the dark conductivity decreases rapidly at first and then saturates after about four hours (Fig. 3.1). The rate of decay depends on the illumination intensity.

By using different film thicknesses and electrode configurations, Staebler and Wronski (1980) showed that the conductivity changes occur in the bulk of the film. The continuous decrease in dark conductivity that occurs under illumination is primarily due to a decrease in the density of free carriers. Such a decrease requires a movement of the fermi level and this is reflected by a corresponding increase in the activation energy, E_A (fig. 3.2). The conductivity follows the form

$$\sigma(T) = \sigma_0 \exp(-E_A/kT) \qquad (3.1)$$

The picture is complicated by the dependence of the pre-exponential factor, σ_0 on E_A which can be written

$$\sigma_0 = C \exp(D E_A) \qquad (3.2)$$

where C and D are constants. This exponential dependence of σ_0 and E_A is known as the Meyer-Neldel rule (Meyer & Neldel, 1937). The simultaneous decrease in free carrier concentration (reflected in the increases of E_A) and the increase in σ_0 lead to the observed asymptotic approach of the conductivities to the light soaked state. This pattern of behaviour is similar to that caused by doping the material, except that it is the opposite sense.

The photo-induced changes in the activation energy reflect the displacement of the Fermi level brought about by the introduction of metastable defects in the gap of a-Si:H.

Heavy doping greatly decreases the conductivity changes under illumination. In such cases, the densities of photo-induced defects are too small to overcome the pinning of the Fermi level by significantly larger densities of donors and acceptors. Tanielian et al. (1981) reported a small increase, rather than a decrease in dark conductivity in slightly n-type films. This behaviour suggests both donors and acceptors are created in the photo-induced effects.

3.1.2 : Reversal of Light Induced Changes

The early work on the S-W effect showed that the change in dark and photoconductivity could be reproducibly reversed by annealing the a-Si:H films at 150°C for an hour or less (Staebler & Wronski 1977). It was found that, just as the rate of transition from state A to state B depends upon the light exposure, the rate at which the conductivities revert back to state A depends upon the annealing temperature.

Fig. 3.3 shows the temperature dependence of the annealing process for an undoped film. The transition from state B to state A is activated with an energy equal to 1.5eV. The same value of activation energy was obtained for the diffusion constant of hydrogen in a-Si:H by Carlson & Magee (1979).

Other photo induced properties of a-Si:H appear to be susceptible to the annealing process reported above. Pankove & Berkeyheiser (1980) found a photo-induced photoluminescence peak at 0.8eV which could be annealed away. The deep centres responsible for this peak could also contribute to the decrease in carrier lifetimes observed in light induced

photoconductivity changes. Dersch et al. (1981) found that the electron spin densities in their a-Si:H films increase under prolonged illumination and these extra spins could be removed at a temperature of 220°C. The number of dangling bonds and deep-lying defects with spin which act as recombination centres was estimated to be $2 \times 10^{+16} cm^{-3}$. The similarity of the kinetics of the conductivity, photoluminescence and e.s.r. changes imply that dangling bonds and deep-lying defects are involved in the S-W effects.

3.1.3 : Photoconductivity Changes

The photoconductivity σ_p, is determined by the generation rate of free carriers, F and their lifetimes, τ_n.

$$\sigma_p = e\eta\mu_n n = e\eta\mu_n\tau_n F \qquad (3.3)$$

where η is the photogeneration efficiency, n is the number of free electrons and μ_n their mobility (assuming that electrons dominate holes). The free carrier lifetimes are determined by the recombination kinetics which are reflected by the relationship between the photoconductivity and the light intensity, I.

$$\sigma_p \alpha I^{\gamma} \qquad (3.4)$$

Fig. 3.4 illustrates the change in photoconductivity between the annealed state A and states at successive exposures to light of $200 mWcm^{-2}$ until the light-soaked state B is attained. The values of γ = 0.8 and 0.5 in state A convert to a single γ = 0.89 after prolonged exposure to light. These changes indicate that not only is there a decrease in the recombination lifetime upon illumination, but also there are significant changes in the recombination

kinetics. The changes in photoconductivity cannot be explained by the change in the mobility of carriers. If the mobility had been decreased by illumination a parallel shift downwards would be seen by the curves in fig. 3.4; however, the Y = 0.5 portion is unchanged by the light exposure. The model suggested by Rose (1963) implies the Y = 0.8 section is associated with deep gap states whereas the Y = 0.5 region is connected with shallow traps. Hence the decrease in photoconductivity under illumination must be due to a decrease in carrier lifetimes resulting from metastable states being produced in the gap.

Photo-induced changes in carrier lifetimes, τ_n, and in the photoconductive response time have been observed (Fuhs et al.,1979, Wronski & Daniel, 1980). The light exposure caused much reduced carrier lifetimes and a change from bimolecular ($\tau_n \alpha I^{-0.5}$) to monomolecular recombination (τ_n independent of I) confirming the photoconductivity results. Wronski & Daniel (1980) showed that the deep-lying centres of state B have electron capture cross-sections significantly larger than those that control the carrier recombination in state A. They estimated the number of defects to be 10^{16} to $10^{17} cm^{-3}$. This small number is consistent with the light induced e.s.r results and the small S-W effect in heavily doped films. The larger capture cross sections of these states causes a decrease in the recombination lifetime of carriers so affecting the density of photogenerated carriers.

3.1.4 : Models for the S-W Effect

We have seen that the dark conductivity results are

consistent with a metastable change in gap states and a subsequent lowering of the Fermi level towards the middle of the gap. The mechanism by which these states are introduced does not appear to be a direct absorption process as the S-W effect is correlated with the photoconductivity. Staebler & Wronski (1977) used light of wavelengths between 600nm and 900nm; they found that light that produced a given photoconductivity also produced nearly the same S-W change irrespective of the photoconductivity per absorbed photon. Between these wavelengths the quantum efficiency varies by an order of magnitude (Loveland, Spear & Sharbaty, 1974).

The correlation between the S-W effect and the photoconductivity suggests that the new gap states are created after recombination or trapping occurs at a localised defect. This could release the energy to cause a local band reorientation or displacement into a new metastable position. The hydrogen which passivates the dangling bonds in a-Si:H is likely to be the active centre. The annealing of a film back to state A would represent the relaxation of the centre back to its original orientation. We have already noted the equality of the activation energy for annealing with the diffusion energy of hydrogen in a-Si:H.

Besides the bond reorientation model, Staebler & Wronski proposed a second model. This involves centres which are in poor communication with the extended state. During illumination, free electrons are trapped by these weakly-coupled centres and can no longer participate in the detailed balance that establishes thermodynamic equilibrium. The film has fewer free carriers, the Fermi level drops and the dark conductivity decreases. The decrease in

photoconductivity would have to come from larger recombination cross-sections. Defects could be ionized by the charge-transfer process or by the drop in the Fermi level causing an increase in the cross-sections of the defects.

The thermal relaxation process would be the electrons being excited out of the weakly-coupled centres. The ground state of the centres must be within about 0.2eV of the mobility edge otherwise the centres would be below the Fermi level and would not be emptied by annealing. The 1.5 eV activation energy for annealing suggests these centres are surrounded by a strong repulsive barrier and are therefore isolated from the bulk.

During illumination, charges are transfered to the centres via the extended state. Free carriers are lost and the dark conductivity decreases. The photoconductivity can see the weakly coupled centres and is affected by them. The centres could be simple localized defects or larger regions such as a microvoid surrounded by a repulsive barrier.

In the last few years a variety of more specific models for the metastable defects have been proposed. Elliott (1979) suggested that the photogenerated excitons can become self-trapped and produced intimate, oppositely charged dangling bonds that are stabilized by their Coulomb interaction and a "soft" lattice that occurs near weak bonds. Wautelet et al. (1981) suggested the light induced metastable centres result from two neutral configurations of a single dangling bond. Dersch et al. (1981) proposed that the defects are created by the breaking of weak Si-Si bonds and the subsequent transfer of hydrogen atoms to these broken bonds from extended clusters of Si-H bonds which occur at the

internal surfaces of voids.

3.2 : Electrical Injection and Long-Lived Traps in a-Si:H

We will see that that trap relaxation can be studied by looking at the variation of e.s.r signal produced by trapping excited carriers and following the emptying of these traps after the excitation is terminated (§3.3). Light can be used for excitation. Another method is to use a "heat step" i.e. fast cooling which freezes a high temperature distribution of carriers in the sample. These processes usually involve both electrons and holes. A third method of excitation into traps is electrical injection of carriers; this has the advantage of only involving one type of carrier.

Hallerdt, Solomon & Tran-Quoc (1985) used an n^+-i-n^+ structure which allowed the injection of electrons into the slightly n-type intrinsic layer. After the removal of the injecting voltage, the conductance decay of the sample was monitored using a low voltage (less than 50mV) (see fig. 3.5). The data was taken at room temperature. After a very rapid decrease, the conductance shows a long, slowly decreasing tail, reaching the equilibrium conductance value after a number of hours. The decay is clearly not exponential.

The analysis of this transient conductance is based on the assumption that the Fermi level, E_F, is shifted by an amount ΔE_F, in proportion to the charge density of the trapped carriers.

$$\Delta E_F = -\beta N \qquad (3.5)$$

where β describes the emptying of the states to take account of the negative charge of trapped electrons. $\beta = 1/g_{\infty}$ where g_{∞} is the density of states at the unperturbed Fermi level; g_{∞} was measured using space-charge limited current techniques. If n_{∞} is the equilibrium density of conduction electrons then n, the density of electrons after excitation is given by

$$n = n_0 \exp(\Delta E_F / kT) \tag{3.6}$$

Using the above two relationships the conductivity can be deduced.

$$\ln[\sigma(t)/\sigma_0] = -N(t)/g_0 kT \tag{3.7}$$

where σ_0 is the equilibrium conductivity. The conductivity is a direct measure of the trapped electron density.

If recombination is constant for a given trap then

$$dN(t)/dt = -\nu N(t) \quad \Rightarrow \quad N(t) = N(0)\exp(-\nu t) \tag{3.8}$$

As this is not seen experimentally Hallerdt et al. suggested a distribution of relaxation times as follows:

$$N(t) = \int_0^{\infty} \Pi(\nu)\exp(-\nu t)d\nu \tag{3.9}$$

where $\Pi(\nu)$ is the relaxation rate distribution of the initial trap population i.e. $\Pi(\nu) = dN(0)/d\nu$ so that N(t) is the laplace transform of $\Pi(\nu)$ and the conductance is intimately related to the rate distribution.

It was found that $\log(1/\{\sigma(t)/\sigma_0\})$ had a linear relationship with time in the range t=1s to t=2500s. Hence

$$N(t) \propto t^{-1} \tag{3.10}$$

and from eqn. 3.9

$$N(t) = \Pi_0 t^{-1} \tag{3.11}$$

This implies a uniform distribution of relaxation rates for

the initial trap population.

If the traps are emptied by thermal means, the relaxation rates depend on energy, E, with respect to the Fermi level.

$$\nu = \nu_o \exp(E/kT) \qquad (3.12)$$

The range of relaxation rates extends over three orders of magnitude which corresponds to an energy spread of 0.2eV for the traps involved.

3.3 : Light Induced ESR Studies

At low temperatures, a non-equilibrium distribution of trapped carriers, which persist with long lifetimes after excitation with optical light, has been detected using light induced spin resonance (LESR) in a-Si-H (Street & Biegelsen 1982, Carius & Fuhs 1984, Boulitrop 1984). LESR decay measurements are recorded with the magnetic field set at the peak of the electron band tail absorption derivative; the general form of the signal consists of a rapid decay followed by an extremely slow long time decay (see fig. 3.11). The data presented in fig. 3.6 is that of Street et. al. at 30K.

The long lifetimes measured indicate that diffusion of carriers is negligible at this temperature. The LESR lifetimes decrease with excitation intensity (fig. 3.6A) and the number of light induced spins varies with intensity in a sublinear relationship (fig. 3.6B). These results are characteristic of bimolecular recombination. The decays are linear with log(t) over most of the decay; such a broad distribution is characteristic of a tunnelling process. It is clear that LESR is bimolecular suggesting distant pair rather

than geminate recombination which contradicts luminescence data taken under the same conditions (Street 1981).

At low temperature rapid thermalization by band tail states limits the separation of an optically induced electron-hole pair to about 50 to 100Å. Hence for weak excitation radiative recombination is expected to be geminate. This monomolecular process is characterized by a decay independent of pair densities and luminescence measurements probe such a process. However for large pair densities where the average inter-pair separation is comparable to the average intra-pair separation, the recombination kinetics have been shown to convert to bimolecular behaviour, that is, higher pair densities lead to shorter lifetimes.

Street distinguished between the two types of decay outlined above by their response to pulsed excitation. A sequences of pulses of 20ms duration with a 10s period is used to excite the system. For distant pair recombination the first pulse generates a small number of electrons and holes which leave a random distribution and a large average separation. Luminescence is therefore negligible for times shorter than 10s and the LESR creation is 100%. Subsequent pulses increase the electron-hole population, the e-h separations drop and the recombination rate and luminescence increases. For the geminate case, assuming a distribution of intra-pair separations such that the largest lifetime is shorter than 10 seconds, each pulse generates the same distribution of pairs, which recombine before the next pulse. Thus a very low LESR density and a high luminescence efficiency are expected, independent of the number of pulses.

The experimental results of Street & Bielgelsen showed a high luminescence efficiency in the first pulse and a very low LESR creation efficiency indicating a geminate process and cannot be explained by distant pair recombination.

Street points out that the basic geminate photogeneration model can be used to explain both the LESR and luminescence results. After band gap excitation, electrons and holes thermalize rapidly by sequence of short tunnelling transitions. The random walk between carriers before recombination occurs leads to an intra-pair radial distribution function.

$$G(r) = (\sqrt{\pi/2\bar{r}^3})r^2 \exp(-r^2/\bar{r}^2) \qquad (3.13)$$

where r is the average intra-pair separation (Lindgren & McElrath, 1964). In fig. 3.7A the distribution is plotted for r=50Å. The radiative tunnelling the lifetime is

$$\tau = \tau_0 \exp\left(\frac{2R}{R_0}\right) \qquad (3.14)$$

where $\tau_0 = 10^{-8}$s and R_∞ = 10Å, the radius of the band tail electron.

Using the above expression the abscissa in fig. 3.7B is converted to log(τ). After the first pulse pairs whose separation is less than a certain radius, R_x will recombine; the distribution just before the second pulse is shown in fig. 3.7B. With a 10 second time period and T=30K the great majority of e-h pairs recombine causing luminescence before the next pulse. However a small fraction remains and forms the basis of a steadily increasing density of essentially metastable states. The number of these long-lived states is limited by a different mechanism. As

the density of these states increases, recombination between non-geminate pairs becomes important and a bimolecular regime begins to replace monomolecular recombination. Further excitation creates a distribution which shifts to lower lifetimes at higher excitation intensities. The recombination process is therefore a mixture of geminate recombination of short-lived pairs and non-geminate bimolecular recombination of metastable pairs.

The luminescence signal measures the rate of recombination and is controlled by the faster geminate process; LESR measures the number of excited states and is dominated by slow bimolecular recombination. The logarithmic decay of the metastable population implies that the number of carriers which recombine per unit time decays as t^{-1} . The photoluminescence decay at long times has been observed to be of the t^{-1} form. This confirms that it is the metastable carriers that are in radiative states even though they are in long lifetime configurations (Boulitrop 1984).

The work reported above concentrated on measuring LESR decay fixed on the electron band tail signal. The ESR spectra did not change shape during the decay. Carius & Fuhs (1985) reported the same behaviour in their undoped a-Si:H films. However, in p-type samples, they observed a change in the shape of the ESR signal during decay. They analysed the relative contribution of the broad line produced by holes trapped in the valence band, $N_s(h)$, and the narrow line which arises from the superposition of resonances of D^- states and band tail electrons, $N_s(e\text{-}db)$, and found that the e-db line decreased more rapidly than the h line. This behaviour is consistent with the assumption that the band

tail electrons rapidly transfer to dangling bond states to create D^0 and D^- states after the cessation of illumination. The time limiting step for recombination is the tunnelling transition of band tail holes to D^0 and D^- states.

When the films are annealed above 70K or exposed to IR radiation the h-line decreases more strongly, cancelling the effect of the initially more pronounced decay of the e-db line. Above 70K holes diffuse in the valence band and then recombine.

The residual spin density N_s(e-db) is an order of magnitude less than N_s(h) so a considerable amount of negative charge must reside in D^- states undetected by ESR techniques. The strong annealing of the h-line then results because there are two recombination channels available for holes (3a and 3b in fig. 3.8) which generate (3a) and destroy (3b) D^0 states.

We will return to LESR measurements in the next section to examine the effect of IR quenching on the residual metastable states.

3.4 : Recombination Probed by Subbandgap Excitation

At low temperatures in a-Si:H photoexcited carriers are trapped in bandtail states from where they recombine radiatively with a carrier in the other bandtail, producing luminescence or non-radiatively by tunnelling to defects. The recombination process has been studied using photoluminescence (PL), photoconductivity (PC) and ESR.

In dual beam experiments IR excitation of non-equilibrium carriers leads to quenching and enhancement of luminescence and photoconductivity. Fig. 3.9 displays the transient PC and PL responses of undoped a-Si:H when the film is excited with band gap light (1.92eV) and subbandgap light (<0.7eV) is turned on and off (Carius & Fuhs 1984).

3.4.1 : Photocurrent

The PC transients exhibit a short enhancement which in the steady state is followed by quenching at 130K and by enhancement at 30K. Similar results have been seen by other workers (Vanier & Griffith, 1982; Varmazis, Hirsch & Vanier, 1984) and have been interpreted as the enhancement of recombination by optical excitation of trapped minority carriers.

The PC quenching phenomena can be explained in terms of the recombination scheme proposed by Dersch, Schweitzer & Stuke (1983) (fig. 3.8). After generation (E) and thermalization (t_h, t_e) carriers are trapped in tail states from where they are either re-emitted (1a,1b) or recombine via dangling bond defect states (2,3). The first recombination step is tunnelling of band tail electrons to neutral dangling bonds, D^0, creating D^- states (2a). The second step is the transition from D^- to a trapped hole in the valence band tail (3a). If the mobility of trapped holes is raised by the IR radiation the holes will be more able to move towards D^- states enhancing recombination (in n-type films).

Fuhs (1985) points out that PC quenching can be achieved

in another way within the above model. The spectral dependence of the PC quenching shows an onset at about 0.6eV in all samples; this implies that the transitions excited by IR light are from D^- states. Such transitions would lead to quenching. In n-type samples IR excitation of electrons from D^- states would initially lead to enhanced PC. However because of the strong dependence of the tunnelling rate (2) on the concentration of D^o states, a small increase in the number of D^o will decrease the lifetime in the steady state. Just this sort of behaviour is seen in the PC transient in fig. 3.9.

3.4.2 : Photoluminescence

IR quenching of photoluminescence (PL) has been observed at temperatures below 100K in a-Si:H (Varmazis, Hirsch & Vanier, 1984, Carius, Fuhs & Hoheisel, 1984). The effect is usually larger in p-type films. In duel beam experiments the spectral distribution of the PL becomes unsymmetric and shifts to a lower energy; the magnitude of the quenching decreases with decreasing excitation energy (fig.3.10). Raising the temperature has a similar effect on the spectral distribution. The thermal effect has been explained by the activation of electrons from the band tail, shifting the demarcation level to a lower energy as electrons tunnel to D^o states (2a) (Street, 1981). The spectral dependence of IR quenching could be explained in this way. The high energy side of the PL peak corresponds to radiative recombination of electron-hole pairs in shallow traps. The carriers in these

shallow traps are more delocalized than the deeply trapped carriers which radiate at the lower energy side of the peak. The carriers in shallow traps are therefore the ones most likely to recombine non-radiatively and are therefore more susceptible to quenching.

The PL quenching exhibits a cut-off near 0.5eV as the energy of the IR light is reduced; this is the same cut-off energy as that reported in the previous section for PC quenching suggesting that the absorption processes are similar. The excitation of trapped holes and subsequent transfer to defects could enhance the non-radiative recombination rate leading to PL quenching.

Varmazis et al. (1984) suggest that photoexcited holes are trapped at about 0.5eV above the valence band edge where they are strongly localized and have low recombination rates. Trapped electrons and D^- states maintain charge neutrality. IR excitation causes holes to move to shallow traps; there they are less localized and more able to recombine directly with trapped electrons producing enhanced luminescence. However within a few milliseconds, tunnelling transitions produce more neutral dangling bonds. A new steady state is established with an increased rate of non-radiative recombination for the electron-hole pairs delocalized enough to interact with dangling bonds. The data of Fuhs (fig 3.9) shows just such a transient increase in PL followed by steady state quenching.

3.4.3 : IR-Induced Transients

Carius & Fuhs noted that exposure to IR light quenches

the residual LESR signal and is accompanied by transients in the photocurrent and photoluminescence (fig. 3.11) indicating that the IR effects reported here originate from the same non-equilibrium carrier distribution. They studied the metastable trap population by varying the time delay between the beginning of the LESR decay and the application of IR light, t_d. For t_d = 10s all carriers with a recombination time of less than 10s have recombined. The average separation of the remaining pairs is estimated to be 125Å using eqn 3.14. This limits the concentration of trapped carriers to $10^{17} cm^{-3}$ in agreement with the figure calculated from residual LESR spin densities (Street & Biegelsen, 1982). In order to compare the decay of the residual LESR and the peak heights of the PC and PL transients of different doped samples it is convenient to plot the logarithmic derivative of the peak heights. Fig 3.12 demonstrates that the LESR, PC and PL decays are similar in form.

The LESR decay signal shows a faster decay in n-type and undoped material than for p-type films, in agreement with the results presented in §3.3. The PC decays of all samples coincide with the lower values of the LESR in p-type films whereas the PL decays of all samples match the n-type LESR results. The peak height of the PL transient is proportional to the product of the concentration of the trapped electrons and holes, $p_t.n_t$. As electrons have more extended wavefunctions than holes, recombination is controlled mostly by the trapped electrons. The PL signal height is related to the relaxation of band tail electrons. The PC transients are more difficult to understand. The photocurrent would be

expected to be proportional to n_t+p_t and so be determined by the majority carrier. This is not observed.

Carius & Fuhs pointed out that the form of these decays is typical of a broad spectrum of time constants which originates from the distribution of intra-pair separations according to eqn 3.14. They showed that the difference between n-type and p-type decays can be accounted for by stronger localization in the valence band. Using a model based on a simple rectangular distribution of tunnelling distances (the full lines in fig. 3.12) they calculated the radius of the band tail electrons and holes to be 10Å and 8Å respectively; both figures agree with other estimates in the literature.

The long-time decay of the metastable trap population was found to be independent of temperature below 80K. Above this temperature thermal detrapping of band tail carriers appears to enhance recombination.

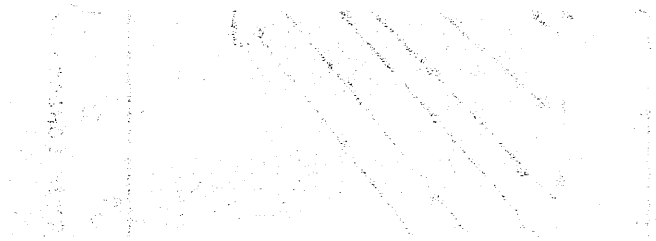

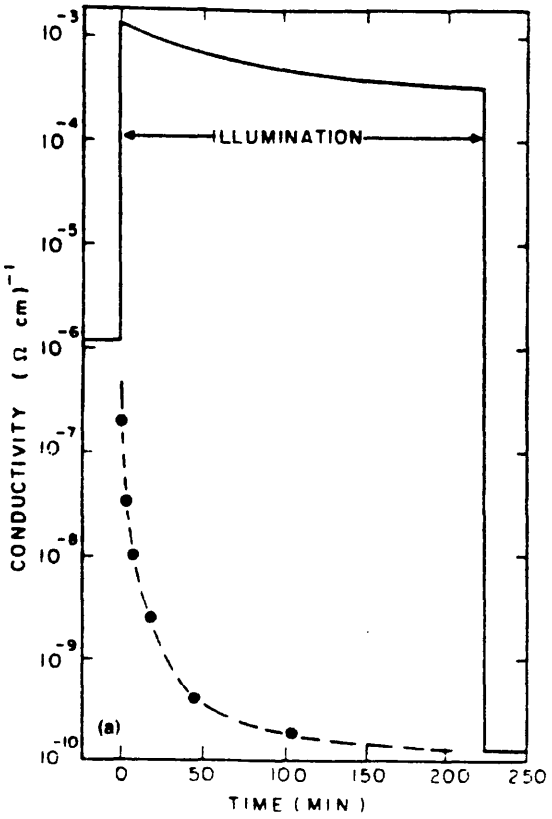

Figure 3.1 : Decrease in the photoconductivity (solid line) and dark conductivity (dashed line) of an undoped a-Si:H film during illumination with 200mWcm^{-2} filtered tungsten light. (Staebler & Wronski, 1980)

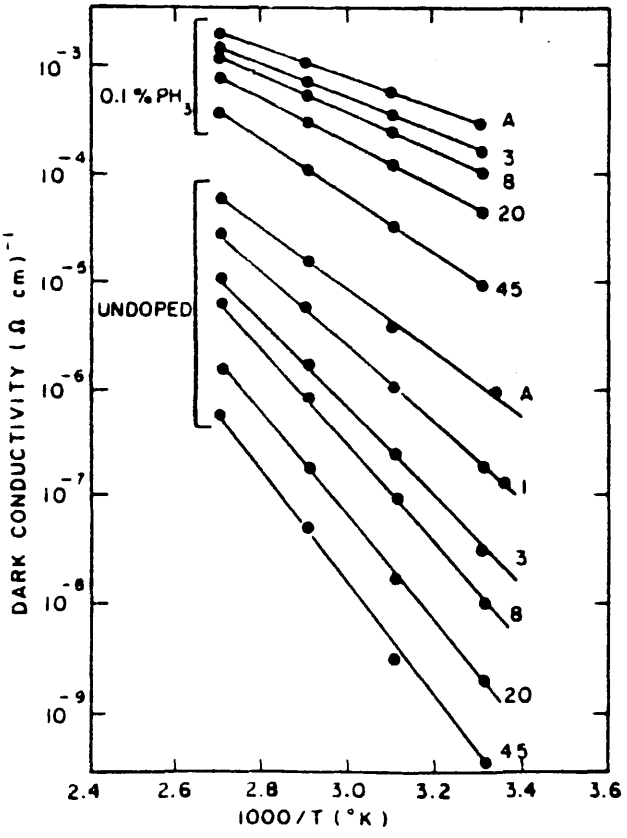

Figure 3.2 : Temperature dependence of the dark conductivity for the a-Si:H film of fig. 3.1 and a doped a-Si:H film. The A lines are for annealing and the others for after optical exposure. The numbers indictate the exposure time in minutes. (Staebler & Wronski, 1980).

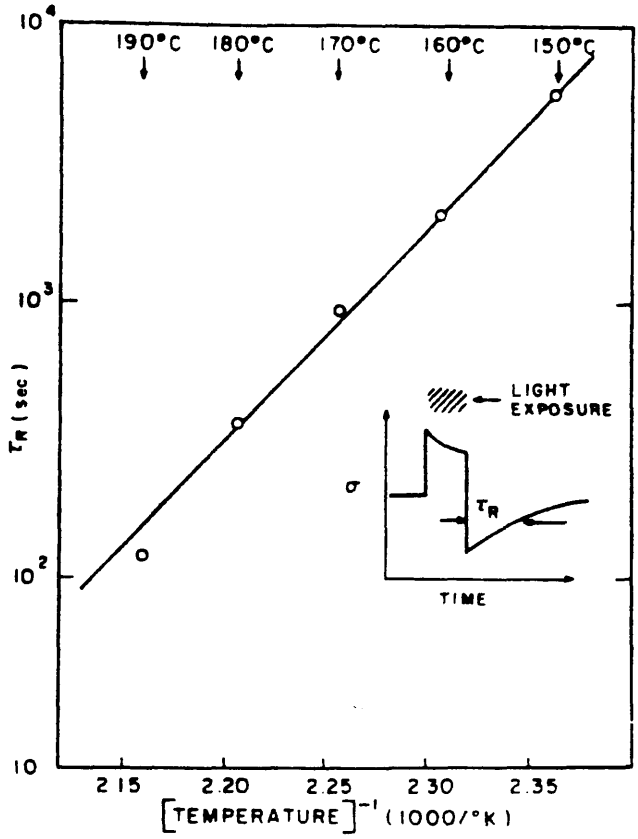

Figure 3.3 : Thermal relaxation time as a function of temperature. The measurements were made at the indicated temperatures shown in the inset. (Staebler & Wronski, 1980).

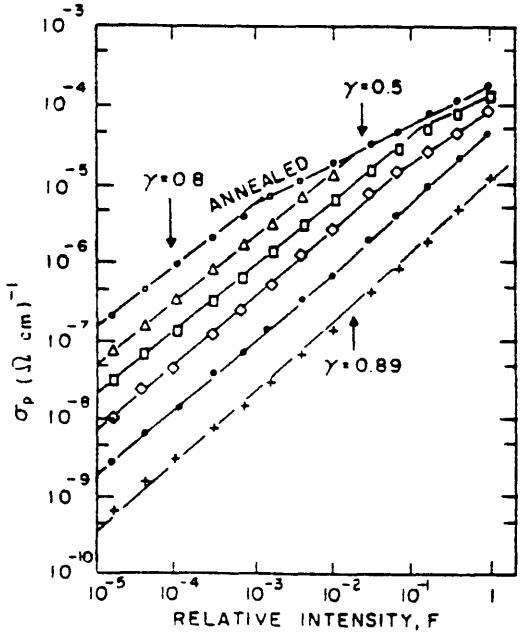

Figure 3.4 : Photoconductivity generated by penetrating light as a function of relative light intensity for the film of fig. 3.1 after annealing and subsequent prolonged exposure to light to a maximum of 4 hours. (Staebler & Wronski, 1980).

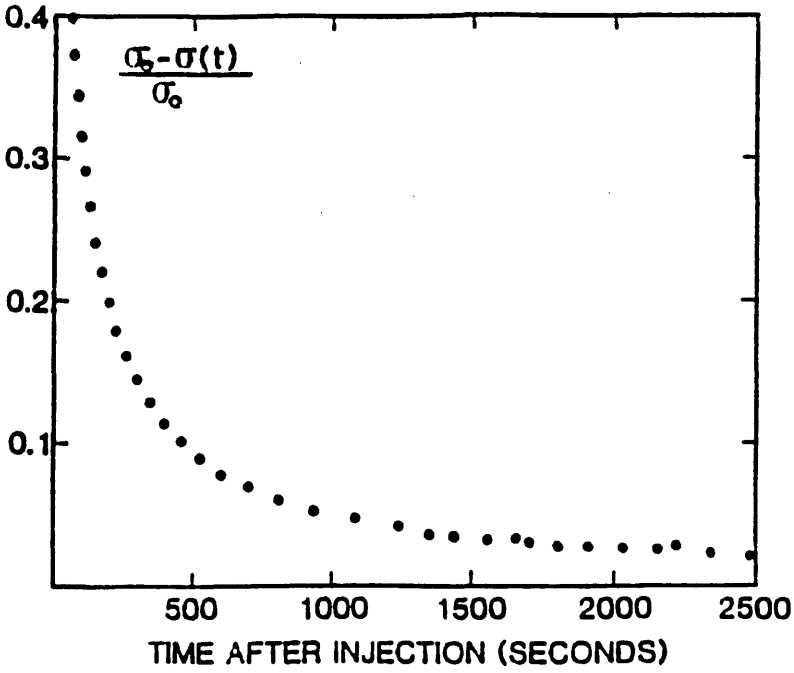

Figure 3.5 : Typical transient conductance curve for an a-Si:H thin film sandwich structure after an electrical injection. The curve shown is for a sample with an i-layer thickness of 2.05um and a room temperature conductivity of $3x10^{-10}Sm^{-1}$
An injecting voltage of 4.0V was applied for 5 minutes. The transient conductance was then measured at 20mV. (Hallerdt et al., 1985).

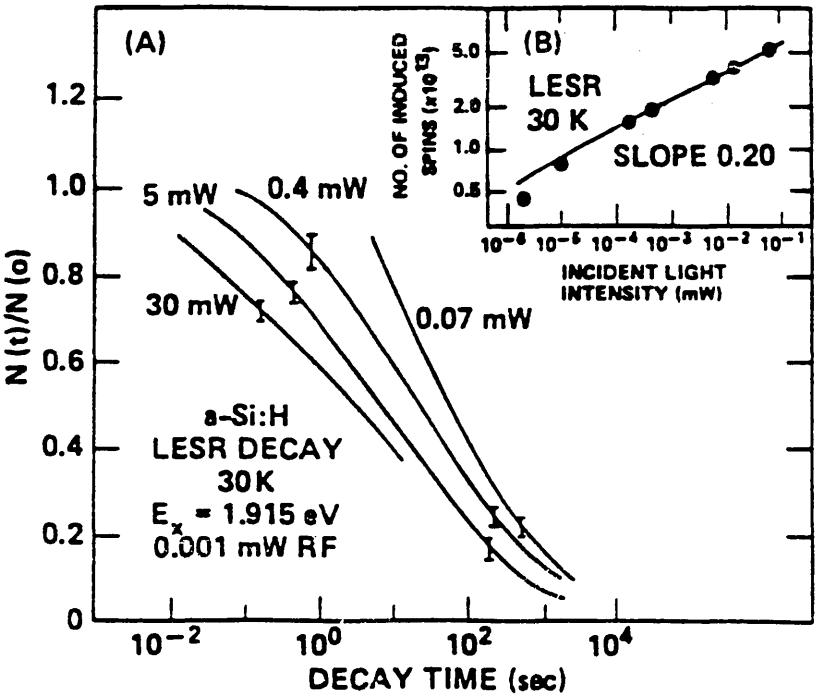

Figure 3.6 : (A) The decay of the LESR in a-Si:H at different excitation intensities. The excitation pulse was chosen to be long enough for a steady state to be reached.
(B) Dependence of steady state LESR on the incident light intensity.
(Street & Biegelsen, 1982)

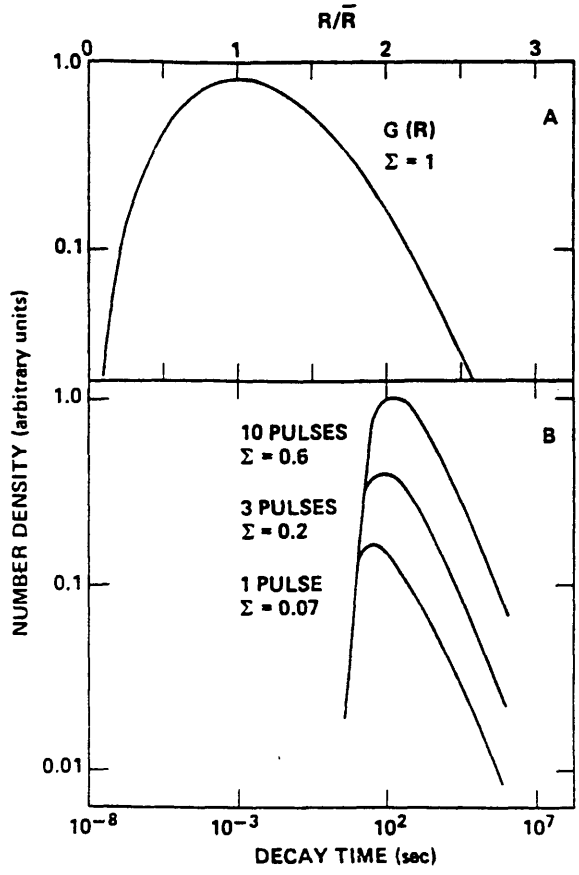

Figure 3.7 : (A) Model distribution of the pair separation of the germinate electron-hole pairs.
(B) The remaining distribution just before the 2nd, 4th, and 11th pulse.
(Street & Biegelsen, 1982)

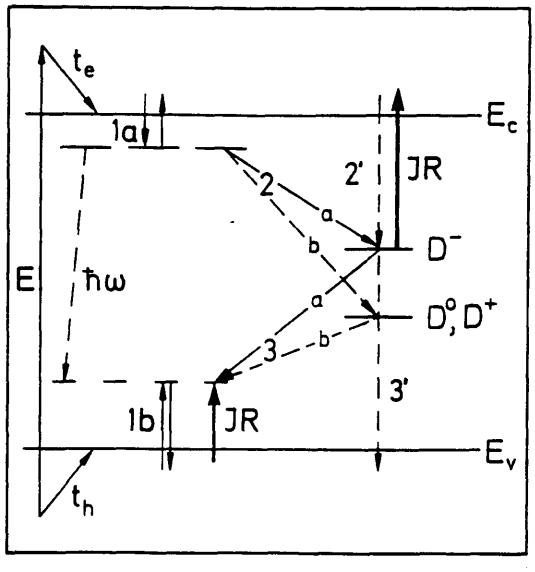

Figure 3.8 : Recombination model, for details see text. (Dersch et al., 1983).

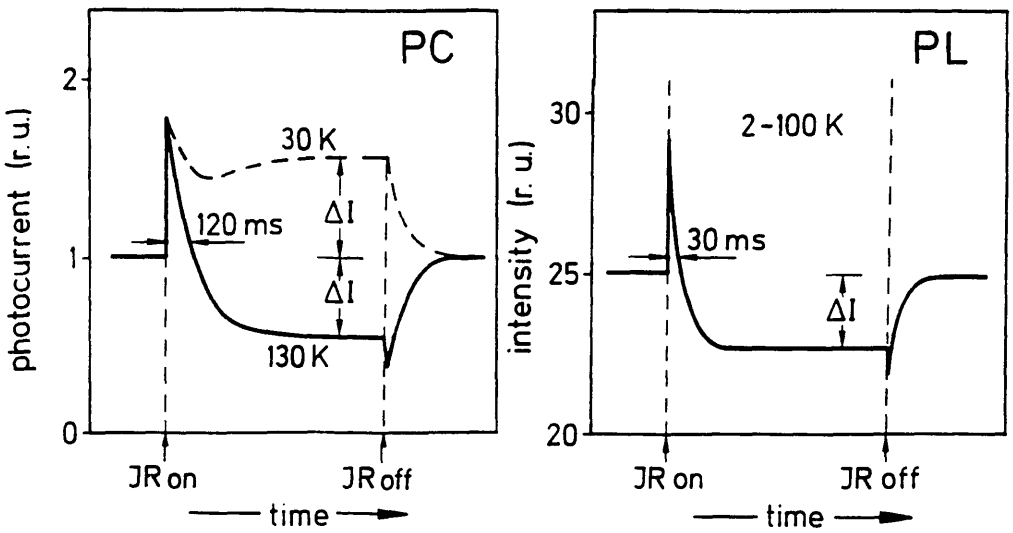

Figure 3.9 : Transient behaviour of the photoconductivity and the photoluminescence in a duel beam experiment. (Carius et al., 1984).

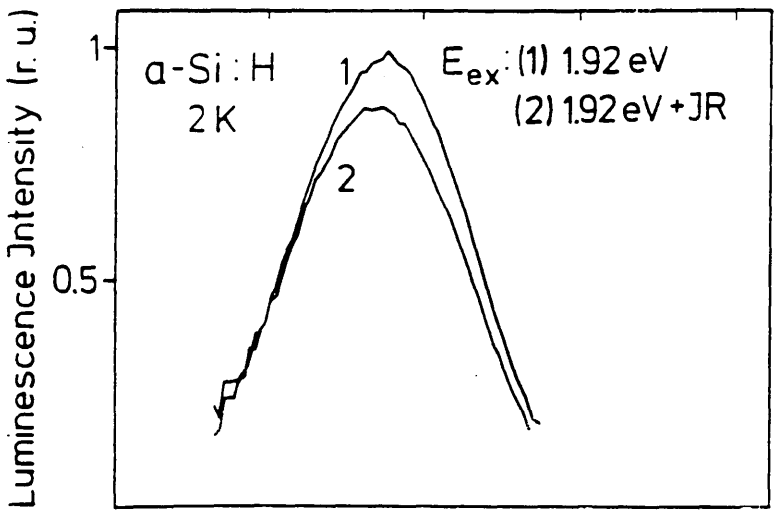

Figure 3.10 : Photoluminescence spectra with a single beam and duel beam excitation. (Fuhs, 1985).

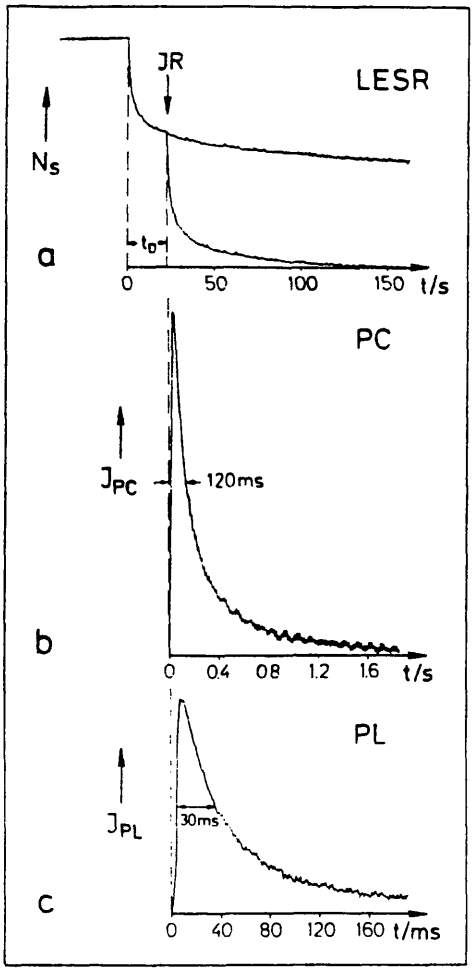

Figure 3.11 : Transients of LESR (a), PC (b) and PL (c), when after a dark period, t_D, the films are exposed to IR-light (energy < 0.7eV). The same light intensity is used for (b) and (c) whereas that for (a) was much lower. T = 15K. Note different time scales. (Carius et al., 1984).

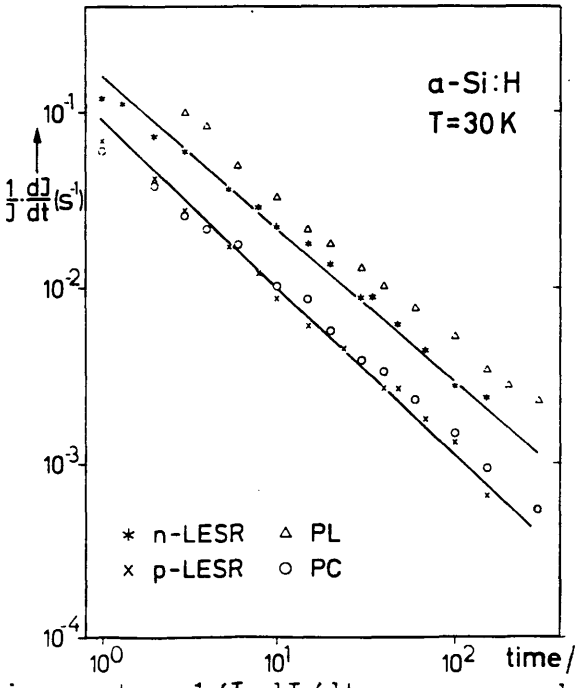

Figure 3.12 : Relaxation rate 1/I.dI/dt versus delay time. LESR, PC- and PL-peak height of n-type and p-type samples at 30K (full curves calculated). (Carius et al., 1984).

CHAPTER 4 : Experimental Techniques

The first part of this chapter discusses the methods used for sample preparation. This is followed by a detailed description of the experimental techniques used to characterise the samples.

4.1 : Sample Preparation

The physical properties of amorphous substances vary considerably depending on the method of preparation. The amorphous silicon & germanium films examined in this work were prepared by R.F. sputtering in argon or argon-hydrogen atmospheres onto room-temperature substrates. Sputtered a-Ge shows properties, such as d.c. conductivity, to be reproducible to within $\pm$50% of one another when produced under the same conditions (Long et al. 1982). The a-Si samples appear to be even more reproducible (Long, McMillan, Balkan to be published).

4.1.1 : Sample Geometry

Low frequency loss measurements involving electrical contact to the samples can be made with either sandwich or coplanar geometry. All the samples reported here are of the former geometry, with an amorphous semiconductor film sandwiched between metal electrodes defining a junction area of about 4×10^{-6} m^2.

The sandwich sample is more appropriate for use with an a.c. bridge. Its conductance ($\sigma_1 A/d$) is higher than the coplanar geometry making characterization more straightforward. The sample capacitance is dominated by the bulk, edge effects are less significant, so σ_2 can easily be studied. The Kramers-Kronig relations (see §2.4) can be applied to sandwich data with confidence, providing a good check on experimental results as follows :

$$\frac{\sigma_2}{\sigma_1} = \omega \frac{C_{ac}}{G_{ac}} = \tan\left(\frac{s\pi}{2}\right) \qquad (4.1)$$

where $G_{ac} \alpha \omega^s$ and s is constant with respect to frequency. Hence given a value of a.c. conductance at a particular frequency, a capacitance value can be predicted. In practice G_{ac} and C_{ac} agree to within 2%.

A disadvantage of sandwich geometry is the possibility of effects caused by the metal-semiconductor interface. Fritzsche (1973) showed that in pure a-Ge and a-Si films there is a high density of states within the energy gap which means the electronic properties of these films are not likely to be determined by charge carriers at the metal-amorphous semiconductor interface. Further evidence of this from the present work is that the magnitude of the d.c. and a.c. conductivities are independent of film thickness. Also, the high bias, non-linear regions of the current voltage characteristics of the optical samples are symmetric despite having a bottom electrode of aluminium and a top electrode of gold. It can be concluded that any formation of a barrier at the surface of these films is negligibly small and that the electronic properties are determined by the bulk.

Figure 4.1 shows the masks used for the optical samples.

Mask I provided the bottom sputtered aluminium electrode which was typically 6000Å thick; 30 minutes sputtering time at a rate of 3.3Å/s. Masks II & III were used during the sputtering of the semiconductor to produce two different junction thicknesses. The two junctions were completed with the evaporation of the top gold electrode (Mask IV) and by the sputtering of the aluminium tabs on top of the ends of the gold electrode (Mask V). These tabs were to allow indium pressure contacts to be made; thin gold is simply scraped away if physical contact is attempted.

It was important to have a reliable method of measuring the gold thickness - too thick an electrode would be opaque to light whereas too thin an electrode would lead to an unacceptably high junction series resistance (see § 4.5). To this end, the thickness was continually monitored during deposition using a quartz crystal oscillator mounted close to the substrate. The resonant frequency of the crystal changes linearly with the mass deposited on it

$$\text{i.e.} \quad \Delta\text{frequency} = K_1 \times \Delta(\text{mass}) \qquad (4.2)$$

$$\text{hence} \quad = K_1 \times \Delta(\text{vol.}) \times \text{density}$$

$$= K_2 \times \Delta(\text{thickness}) \text{ for fixed area}$$

where K_1 & K_2 are constants

The resonant frequency was read with a Racal universal counter 9835. The electronic oscillator circuit used was made in the department (see N. Balkan, Ph.D. thesis, 1979). The system was calibrated for gold (the thickness measured by a Varian Å-scope interferometer) giving $K_2 = (9 \pm 2)$ cycles/Å. The optimum gold thickness was about 110Å. This caused a

junction series resistance of 40 ohms and had an optical transmittance of approximately 0.5.

The gold evaporation took place within the sputterer immediately after the semiconductor deposition in a vacuum of < 10-7 T. This procedure avoided any problems which might have been caused by oxide barrier formation between the semiconductor and the top electrode.

99.999% pure gold wire on a "V" shaped Tungsten wire was the source material for the evaporation. Gold was used for the thin top electrode because of its inert properties. A thin film of gold is not susceptible to oxidization on contact with the atmosphere unlike other more reactive metals. A thin film of aluminium, for instance, would become aluminium oxide when the sample was removed from the sputterer. This transformation of the whole of the top electrode or of the surface of the electrode would lead to an increase in the series resistance of the sample and to changes in the transmittance of the electrode.

The sample thickness was measured at the end of each experiment using the Varian Å-scope which has a specified resolution of ±30Å. However, this accuracy was not attainable because the film edge of sputtered films, as deposited, is not sharp. Values of thickness obtained at the film edge tended to present the lower limit of the actual thickness at the centre of the film, due to spatial variations crossing from film edge to film edge. To improve the accuracy of thickness measurements the semiconductor film was scraped adjacent to the junction to provide a sharp edge, spatially close to the junction. The error of the thickness measurement obtained using this technique was ±10%. A travelling

microscope was used to measure the area to within ±1%.

4.1.2 : Radio Frequency (r.f.) Sputtering

The Nordiko sputtering unit used to produce amorphous silicon and germanium films is shown in figure 4.2. The sputterer is basically a chamber filled with low pressure gas (about 5 mT) which consists of two electrodes, a target of the source material and a work table which holds the substrate. When a r.f. voltage is applied between the electrodes, a plasma can be sustained. The potential of the target surface can be described as an r.f. potential with a super-imposed negative d.c. bias. This bias accelerates the ions of the plasma to the target where they remove material which is then deposited on the substrate. With magnetron sputtering a permanent magnet is mounted behind the target which creates a faster deposition rate, a smaller d.c. bias and a less energetic deposition to the substrate (see Nordiko sputtering handbook).

The sputterer was powered by a 1250W R.F. power supply made by R. D. Mathis inc. A vacuum of better than 10^{-7}Torr was obtained by an Edwards 160/700M type diffusion pump with the aid of a liquid nitrogen trap for removal of water vapour. The semiconductor and aluminium targets were 10 cms in diameter and were earth-shielded to avoid contamination of the sputtered film by the surrounding material. The target substrate distance was 8 cm and with an R.F. power input of 100W a deposition rate of 0.1Å/s was attained for pure silicon. Magnetron sputtering more than tripled these deposition rates. Each target would be "presputtered" before

deposition onto the substrate began to remove any contaminated surface layer. The aluminium target was susceptible to surface oxidization and had to be polished to remove the damaged layer and give a uniform surface from which the oxide layer could be removed by sputtering.

The pressure of sputtering gas in the chamber was measured by a Furness Micromanometer. Mixtures of 99.99% pure argon and hydrogen were prepared in an 80 litre tank. The films were deposited onto Corning 7059 glass substrates held at room temperature.

4.2 : Cryostat and Themometry

4.2.1 : Cryostat Design

Two different cryostats were used during the course of this project. The first optical samples were characterized using an insert, or sample holder, made by N. Balkan (see N. Balkan, Ph.D. Thesis, 1979). The insert was placed into the glass He^4 dewar of a double cryostat. For measurements in the temperature range 1.3K to 40K, the outer stainless steel dewar was filled with liquid N_2 and the inner with liquid He^4. The lowest temperature of 1.3K was obtained by pumping the helium. For measurements in the range 50K to 120K both dewars were filled with liquid N_2.

The later samples were mounted on a long-term low-temperature insert details of which can be seen in figure 4.3 and in the photograph (figure 4.4). Figure 4.3 shows the copper tailpiece onto which the substrates are mounted

together with the fibre optic and aluminium coated mirror used to guide the exciting light to the sample. It was designed for use with a L'Air Liquide, 38 litre, wide neck helium dewar. The insert is lowered directly into the helium bath and will then remain at a temperature of 4.2K for about 15 days. This stability provides an opportunity for the sample to "relax" thermally and for the study of photocapacitance decay over long periods (see §6.7). Temperatures of up to 30K were produced by a constantan wire heater. A liquid nitrogen bath was used for measurements at T > 77K.

The following is a summary of the design of the newer insert; these design principles apply equally to the older insert.

The ideal insert has minimum heat leakage between the environment and the insert in order to reduce the boil off of the refrigerant. Also the sample should be thermally decoupled from the refrigerant bath to allow heating above the bath temperature. Thin stainless steel tubing was used between the sample can and the top section of the insert as this causes low heat leakage and has low thermal capacity and still has high mechanical strength. Five such tubes were used, three of which carried the themometry and signal wires; the 3mm diameter tube carried a fibre optic whilst the fifth central tube served to pump the vacuum can round the sample.

To reduce heat leakage by room temperature radiation, a radiation shield was attached around the steel tubes. The signal wires were cooled to liquid helium temperature by the helium and then fed into the can which was sealed with stycast. The wire used was vinyl acetate coated copper; wires

with this coating can be vacuum sealed. The vacuum in the can was about 10^{-3} Torr at room temperature and was sealed by an indium ring. Once the insert was cooled cryopumping would reduce the pressure in the can considerably further. No helium leaks were observed.

The copper tailpiece was $15cm^2$ in area and was attached to the rest of the insert by a thin stainless steel tube. The sample leads were connected to the electrodes via a stycast insulated tag board ; pressed indium contacts were used between the electrodes and the sample leads. The glass substrates were glued to the copper tailpiece by a 50/50 mixture of Bostick (No. 1 Adhesive) and acetone for good thermal contact. A heater, and copper and germanium thermometers were glued and tightly screwed to the back of the copper piece.

In figure 4.3 it can be seen that the upper section of the long-term, low-temperature insert consists of a 38mm diameter stainless steel tube encasing the smaller tubes. The purpose of this tube (and of the assembly shown in figure 4.4 where the insert meets the top of the wide neck dewar) is to seal the helium bath from the atmosphere during the process of lowering the insert into the bath. The helium boil-off resulting from the cooling process was directed to the helium recovery system via the top of the insert. This outlet, at the top of the 38mm steel tube, was also necessary to deal with the oscillations caused by a tube closed at the top end being immersed in liquid helium.

4.2.2 : Temperature Measurement

The temperature measurement and control unit (TCU) shown schematically in figure 4.5 is based on a design by A. Rosiewicz. The circuit consists of three sections :

i) A constant current supply to the thermometers

ii) Amplification and measurement of the voltage signal from the thermometers

iii) Generation of a reference signal for the required temperature to be compared with the thermometer signal.

iv) A controlled power supply to the heater.

The first two sections concern the measurement of the thermometer resistances. These measurements were made four terminally with the use of a constant current supply of between 1μA and 10mA. After amplification the voltage signal was displayed on a Keithley 177 D.V.M.

For temperatures of > 50K copper wire thermometers were used whereas the sensitive range of the germanium sensors was between 1.3K and 40K. The former was calibrated at the melting point of ice and the boiling point of liquid nitrogen; the tables of Dauphinee and Preston-Thomas (1954) were then used to interpolate for temperatures of 50K to 300K. The Ge thermometer was obtained from Lake Shore Cryotronics (Type : GR-200A-1500) and was calibrated against a similar commercially calibrated thermometer.

The constant current supply was produced by a fixed voltage (±10V) across an accurately adjustable resistance which was a combination of fixed and 10-turn variable components. The supply was periodically checked and found to be correct to ± 0.2%. The main sources of error for the temperature measurement were the thermometer calibrations and the possibility of bad thermal contact between the samples

and the temperature sensors. The magnitude of error is estimated to be less than 0.5K

The third stage of the T.C.U. is for stabilization. A reference signal, which is a measure of the desired temperature, is produced and after amplification it is compared with the thermometer signal. The difference signal is passed to an integrator and proportional circuit to control the output time response and then to a high gain power transistor which drives the constantan wire heater.

For optical experiments, using the long-term low-temperature insert, it was desirable to achieve constant temperatures above 4K over periods of time of about 72 hours. The stability of the T.C.U. centres on the ability of the ±10V fixed voltage supply of the constant current section. It was found that prolonged use of the stabilizer lead to overloading of this voltage supply and lack of temperature control. The solution to this problem was to upgrade the power rating of the supply by use of a larger I.C. as well as better heat-sinking of the I.C. and use of voltage regulators on the I.C. outputs. After these modifications a temperature of 10K could be maintained for up to 3 days to within ±0.1 K.

4.3 : Light Production & Measurement

4.3.1 : Experimental Arrangements

Two light sources were used during this project, a 2mW Coherent He-Ne laser and a water-cooled, tungsten lamp, giving a wide-band source in conjunction with a PRT Optics

MC1-04 mini monochromator (wavelength range 500nm to 1.2μm). The arrangement of the optical bench used to mount these components is shown in figure 4.6.

Before each optical run,the intensity of light emitted at the end of the 3m connecting optical fibre was measured by putting the fibre end at a known distance from a Radio Supplies photodiode device (RS308-067). This device was a Si photodiode integrated with an amplifier; the operational circuit of the photodiode is shown in figure 4.7. The intensity of the emitted light was adjusted by changing the laser/fibre input distance and by moving the fibre inlet slightly out of the laser beam (the beam was defocused by a lens for safety reasons and to prevent small movements of the fibre input causing large changes in the amount of light entering the fibre).

All the items on the optical bench were mounted on X-Y movement stands for ease of manipulation. On completion of an optical experiment the intensity would usually be remeasured to see if any variation in output had occurred during the run. The laser was stable to within ±3%; the wideband source stability was better (±1%).

The 3m fibre was connected to the fibre fitted in the cyrogenic insert in order to shine light on the sample. The light travelled from its source through the fibre system to the insert can . It emerged from the insert fibre to be reflected through 45° by an aluminium coated mirror onto the sample. After the initial calibration of the input intensity, the intensity of light arriving at the sample was varied by introducing neutral density filters into the source beam.

When attempting low intensity measurements (less than 0.1nWcm^{-2}) certain precautions were essential. The section of the optical bench between the light source output and the connecting fibre input was protected from ambient light by black boards and cloth. The ND filters were placed as close as possible to the fibre input to further exclude the ambient light.

The "intensity' measured by the photodiode was, in reality, a voltage on a DVM. To convert this to a reading in terms of nWcm^{-2} arriving at the sample, a calibration was carried out with a Photodyne light meter (model 88XLA, sensitive range .001nWcm^{-2} to 2000nWcm^{-2}). The source and the 3m connecting fibre were arranged to produce the same intensity of light as registered during experiments. The Photodyne meter was then placed at the end of the copper tailpiece of the insert at a known distance (about 2cm) from the insert fibre output. The mirror was removed for calibrations and black tape was used to cover the tailpiece to prevent possible reflections. ND filters were then put in the light path and the intensity arriving at 2cm from the insert fibre output was measured for each set of ND filters used in the experimental runs. How these readings were converted to an intensity measurement for the semiconductor junction is described in the next section.

4.3.2 : The Intensity Calibration

The reading taken at 2cm from the insert fibre outlet must be multiplied by a number of factors to produce an estimate of the light intensity incident on the semiconductor

film. Absorption within the amorphous semiconductor and its effect on the loss measurements is treated using the distributed trapping model (see §7.8).

The corrections are as follows :

1) The junction was usually closer to the fibre outlet than 2cm. Assuming the intensity varies as the inverse square of the distance from the source the appropriate correction is

$$\frac{(\text{insert fibre - Photodyne detector distance})^2}{(\text{insert fibre - plane of junction distance})^2} \qquad (4.3)$$

2) The junction being measured was rarely in the exact centre of the cone of light produced by the fibre. The variation of intensity as the distance from the centre of the cone increases is shown in figure 4.8. for λ=500nm and λ=800nm. It can be seen that the distribution of the light in the cone has no wavelength dependence within the visible range. The position of the centre of the circle of light on the sample was estimated, taking into account the angle of the deflecting mirror. The junction - cone centre distance was calculated and, using the relative intensity graph, a positional factor was calculated. Values of this factor ranged from 0.2 to 1.0.

3) Light will be absorbed by the top gold electrode and reflected by the semiconductor surface, leading to a factor = $T_{Au}(1-R_{Si})$ where T_{Au} is the transmittance of the top gold electrode and R_{Si} is the reflectance of the semiconductor thin film. However with a sample of high transmittance, the light which travels straight through and is reflected back into the sample by the bottom aluminium electrode will not be negligible. In this case there will be an additional term :

$$T_{Au}.R_{Al}(1-R_{Si})$$

where R_{Al} is the reflectance of the bottom aluminium electrode, giving the total correction :

$$T_{Au}(1-R_{Si})(1+R_{Al}) \qquad (4.4)$$

4) The aluminium mirror is not 100% reflective. For a wavelength of 633nm this factor=0.9.

5) The Photodyne meter has an active area of 0.42cm². At a distance of 2cm from the fibre outlet the active area does not measure the intensity at the centre of the cone of light but gives an average reading corresponding to the centre and to the less intense outer regions of the cone. The positional factor (2) assumes the Photodyne reading represents the intensity at the centre. The reading must be increased by 1/0.84 to alter the averaged result to the expected central reading.

4.3.3 : Transmittance and Reflectance Measurements

The reflectance and transmittance values of the following were measured for the optical samples: the top gold electrode; the semiconductor film; the gold and semiconductor together; the junction (i.e. the gold plus the semiconductor plus the bottom aluminium electrode). This was done at different wavelengths using a conventional spectrophotometer (see I.Gibb, Ph.D. thesis, 1982).

4.4 : D.C. Measurements

Figure 4.9 shows the circuit used in d.c. measurements.

The circuit is based on a differential operational amplifier (LM725C) with high input impedance, operating in constant voltage mode. The input of the operational amplifier is taken from a digital sweep generator, which generates a ramp voltage varying between ±10V, in 1024 steps. An internal clock allowed the total sweep time to be varied from 1.024s to 1024s. The sample was connected to the output of the swept supply by a switch box. All I-V characteristics were taken four terminally to avoid series resistance problems.

Current and voltage were measured in analogue form by plotting I vs. V with an HP 7000 AMR X-Y recorder. This instrument has an input impedance of 1 megaohm for both inputs so, in order to avoid errors when studying to low conductance samples, two high impedance Keithley 604 differential electrometers were used at the X,Y inputs. Errors were < 1% for conductances greater than 10^{-10}S.

4.5 : A.C. Loss Measurements

The interpretation of a.c. loss data involves a number of potential sources of difficulty. The first concerns the d.c. limit. The d.c. conductivity in amorphous semiconductors is usually a stronger function of temperature than any a.c. current so the a.c. loss will be dominated at high temperature by the d.c. conductivity and must be decomposed from it. This is done by subtracting the d.c. conductance G_0 from the total conductance as follows :

$$G_{total} = G_0(T) + G_{ac}(\omega,T) \qquad (4.5)$$

This equation assumes that the mechanisms responsible

for a.c. conduction are independent of the d.c. current and that G_0 is non-dispersive. In hydrogenated material and chalcogenides G_0 is usually due to band conduction and G_{ac} is derived from fermi level processes, so these assumptions are reasonable. In pure material, all conduction processes occur at E_F, therefore the above equation may not have any physical meaning. Experimental evidence, however, validates the use of the d.c. subtraction method to determine important parameters of the a.c. loss (Long et al., to be published).

The capacitance may also be split into dispersive and non-dispersive components :

$$C = C_\infty + C_{ac}(\omega,T) \qquad (4.6)$$

The non-dispersive component, C_∞, arises from high frequency atomic and dipolar vibrational transitions. C_{ac} is the contribution from relaxation processes. To isolate C_{ac} from the total capacitance requires an evaluation of C_∞ for each sample. This can be done in one of the following ways.

If the frequency is increased sufficiently C_{ac} becomes negligibly small and hence C_∞ may be directly measured. Such high frequency techniques however introduce new problems which mean C_∞ cannot be accurately judged from such data. A second method is to assume C_{ac} follows the empirical ω^s relationship. C_∞ can then be chosen to give a linear relationship between C_{ac} and ω on a logarithmic plot. Probably the best technique and the one used for the optical samples is to differentiate the capacitance data numerically with respect to frequency, eliminating the constant C_∞. C_{ac} can then be calculated by integrating the differential capacitance at a particular frequency. Subtracting this value from the total capacitance gives C_∞.

The next interpretive problem discussed here is one that is particularly relevant to optical samples, that of series resistance in electrodes and leads. The thin top gold electrode of our samples will inevitably have a higher resistance than the conventional aluminium electrode (typically 60 ohms for Au, 15 ohms for Al at T=4.2K). This series resistance distorts the a.c. loss data at the higher frequencies. The problem can be considered by analysis of the equivalent circuit (fig. 4.10). The effective capacitance and conductance are given by

$$G_{eff} = \frac{(R_0 + R) + (\omega CR)^2 R_0}{(R_0 + R)^2 + (\omega CR)^2 R_0^2} \qquad (4.6)$$

$$C_{eff} = \frac{R^2 C}{(R_0 + R)^2 + (\omega CR)^2 R_0^2} \qquad (4.7)$$

At low frequencies $G_{eff} = R^{-1}$ and $C_{eff} = C$ assuming $R_o << R$. As the frequency, ω, rises, the series resistance, R_o, begins to cause the measured conductance to rise above G.

$$G_{eff} = G + \omega^2 C^2 R_0 \qquad (4.8)$$

Such a spurious dependence in the conductance is seen in the experimental results plotted in figure 4.11.

The value of R_o can be calculated and its effect removed. This is done by taking advantage of the ω^s relation that the conductance follows in amorphous semiconductors over many decades at helium temperatures. The ideal logarithmic plot of conductance vs. frequency is linear; the value of R_o can be adjusted until such a linear plot is produced. This is done by the computer programme 'accalc' and the relevant routine is summarised in fig. 4.12 . The R_o values derived from this technique are self-consistent, when calculated from different frequency sweeps at different

temperatures for the same junction, and agree with rough estimates from direct measurements of electrode series resistances. Care must be taken when applying the linear fit technique to frequency sweeps taken at temperatures other than 4K; the ω^s relation should hold for the frequency range used for the fit, and this is only approximately correct in some temperature ranges.

An estimate of the series resistance at helium temperatures was also made by measuring the resistance of the cross strip (top electrode) and vertical strip (bottom electrode) using an multimeter from the top of the insert. However, it is difficult to estimate the proportion of the cross strip or vertical strip resistance that constitutes $R_\square$. The series resistance cannot be measured directly, of course, as the semiconductor thin film lies in series with the electrode resistances that make up $R_\square$.

4.5.1 : The Manual A.C. Bridges

Two different manually-operated bridges were used during the course of this work; the first, a home-made version was used for all the germanium samples and is shown schematically in figure 4.13. The a.c. signal is derived from a Levell TG2000M oscillator. The variable arm consists of parallel resistance and capacitance boxes from J. J. Lloyd Instruments Ltd. (accurate to about 0.1%). Metal oxide resistors with an accuracy of 0.1% were used in the ratio arms of the bridge. A Brookdeal 9503-SC lock-in amplifier, fitted with a differential pre-amp, was used as a detector. This phase sensitive amplifier has two advantages over the more usual

filtered amp. with rectified output; the balance point is a true zero, not just a minimum and the signal to noise ratio is improved because noise is detected only over a limited bandwidth.

Stray capacitances and direct interaction of the signal source and the detector were minimized by symmetrically positioning each component with respect to the other and by enclosing the circuit components with earthed metal boxes. The variable arm resistance box stray switch capacitances were measured for a number of dummy samples. Using these calibrations an appropriate value of stray capacitance was chosen depending on frequency and sample resistance (typically about 200pF) and this value was added to the measured capacitance. The insert leads had a capacitance of about 10pF, this was subtracted from the data.

The frequency range of 10Hz to 100KHz was determined by the detector. The capacitance measurement became less accurate below 350pF due to the resistance box stray values. Conductance was limited to between 10^{-2}S and 10^{-7}S by the resistance box. Data was accurate to about 1%

The second bridge used was a General Radio Capacitance Bridge (Type 1615-A). This instrument was employed mainly to take the helium temperature frequency sweeps on the silicon samples. The transformer ratio arms used in the bridge eliminate the stray capacitances to ground and give highly accurate data when measuring the sample three-terminally. In the range 10F to 10^{-5}pF the capacitance error would be typically 0.01% at mid-audio frequencies. Conductance could be measured down to 10^{-10}S.

4.5.2 : The Computer Controlled Measurement of A.C. Loss

The Hewlett Packard 4274A LCR meter is an automatic test instrument able to measure various impedances at 12 spot frequencies between 100Hz and 100KHz. The test signal was variable between 1mV and 5V; a signal of 10mV was usually used. A zero offset compensator facility is available which takes account of the stray capacitance and residual conductance of the test leads. The meter was always used in high resolution mode which averages ten data readings before displaying the result.

A Sinclair QL microcomputer was the centre of the computer system which allowed automatic a.c. loss measurement (see figure 4.14). A CST (Cambridge Systems Technology) IEEE 488 interface connected the QL to the LCR meter and to a Solartron 7150 DVM which reads the sample temperature (voltages developed across the Ge & Cu resistance thermometers). During an experimental run the temperature was recorded every ten minutes to check for drift. The capacitance and conductance of the semiconductor junction could be recorded every second but in practice data was taken less often but with more averaging and so greater accuracy (see next section).

The first results taken with the system had a surprisingly large scatter (see figure 4.15). This was isolated to interference generated by the QL. The problem was eliminated by connecting the sample lead earth to the LCR meter earth. When frequency sweeps were taken each point was averaged over 20 high resolution readings. Sweeps taken on Opt 4, a 20:1 hydrogenated Si sample, can be seen in figure

4.16 together with measurements taken using the General Radio Bridge. At 77K there is excellent agreement between the the two instruments; the error of the HP bridge is about 1% for conductance and 0.3% for capacitance. However as the temperature falls towards 4K the loss angle decreases, making measurement more difficult; the conductance error becomes approximately 10% and varies with frequency although the capacitance is still fairly accurate ($\pm$0.2%).

It can be seen that the General Radio Bridge provides more accurate results than the computer controlled system but the latter has a number of advantages when taking optically induced loss data. The speed of data acquisition is vital for monitoring rapid decays in capacitance or conductance which occur when the light source is extinguished. The computer controlled system is able to take one point/second compared to at least two minutes which is required to balance the bridge manually. It often takes 2 to 3 days for the sample parameters to return to their original values after illumination, so overnight recording of data is desirable and can only be provided by automatic recording of data. Finally the errors above are quoted with respect to absolute values of capacitance and conductance. As these errors are additive in nature, the change that occurs in sample parameters, when the junction is illuminated, can be measured to a much greater accuracy (typically $\pm$0.005%).

The computer controlled system was used for frequency sweeps at liquid nitrogen temperatures and all optical runs whereas sweeps at helium temperatures were taken using the General Radio Bridge.

4.5.3 : Programmes for Data Acquisition and Analysis

The LCR programme used to record capacitance and conductance values is shown in appendix A. Data can be recorded at various rates between one point/second (no averaging) and one point every 600 seconds (an average of 30 readings). The QL internal clock times the optical runs. When the light intensity is changed a flag can be placed in the data to record the time of change. Data can be written to disc or a frequency sweep can be taken at any point during the experiment.

Appendix B contains the Lcrgraph programme. This takes the optical data from disc and plots out capacitance, conductance or temperature against time on the Epson printer in the form of a continuous line of screen dumps.

The Lcredit software is a data editor. The data files (usually about 1000 points in length) can be rapidly paged through. If strange values are found (caused by the accidental disconnection of the sample, perhaps) they can be edited out. Multiple files which represent one experiment can be merged into a single file. The recorded temperatures can be used to correct the capacitance and conductance according to the routine shown in figure 4.17. In this way any temperature drift during the experimental run can be compensated for. Further averaging of data can be carried out. Finally, particular decay curves can be isolated and plotted using logarithmic scales or against 1/time.

The accalc programme is used to analyse and plot frequency sweeps taken by the LCR meter. It performs the series resistance correction and can cope with multiple

frequency sweeps taken at different intensities of light. A similar programme (acgenrad) exists for use with manually recorded frequency sweeps.

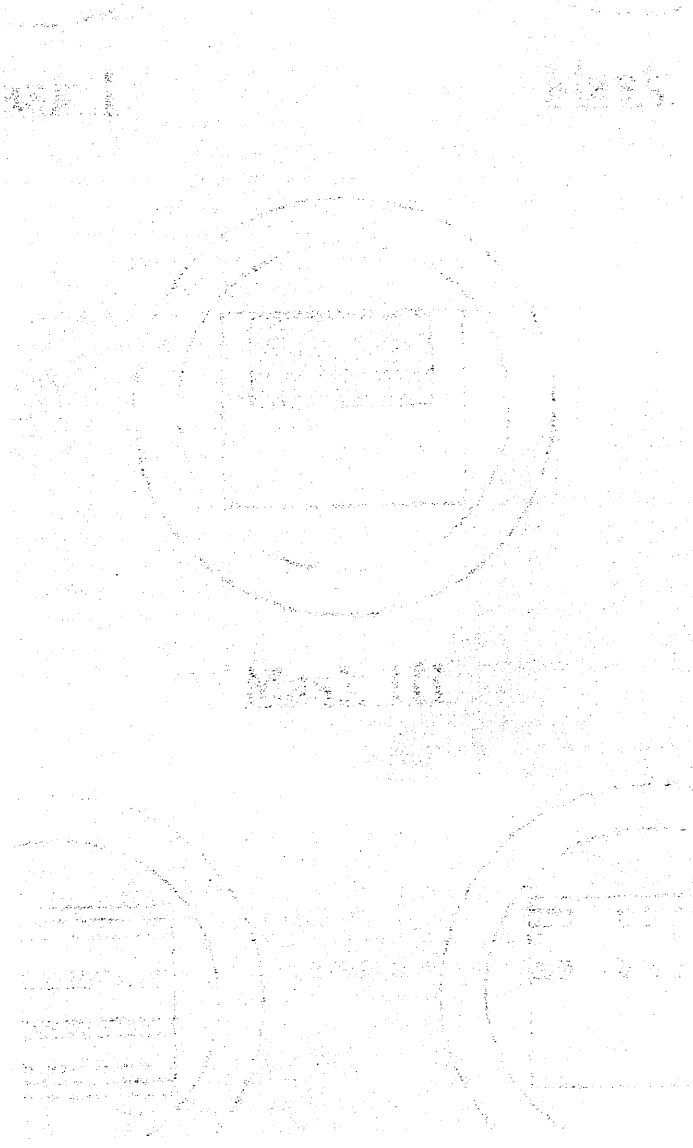

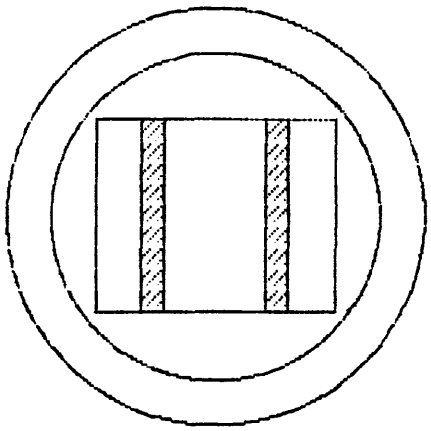

Mask I

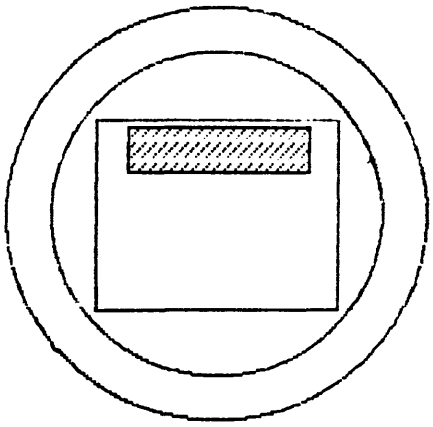

Mask II

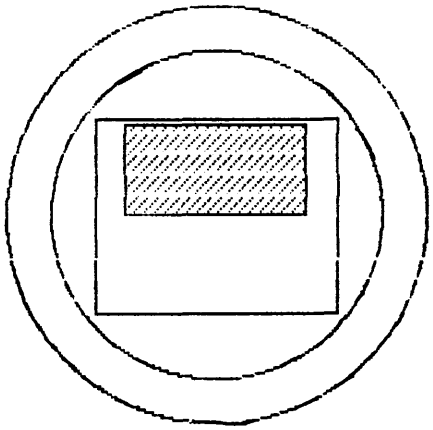

Mask III

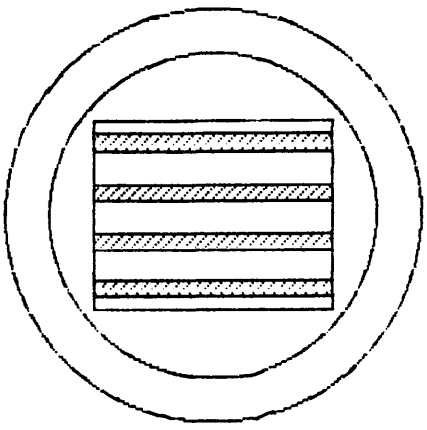

Mask IV

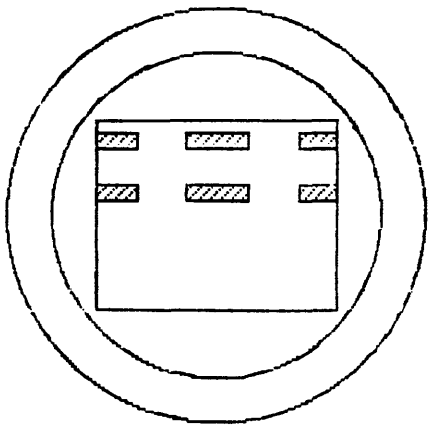

Mask V

Figure 4.1 : Masks used in the preparation of the optical samples.

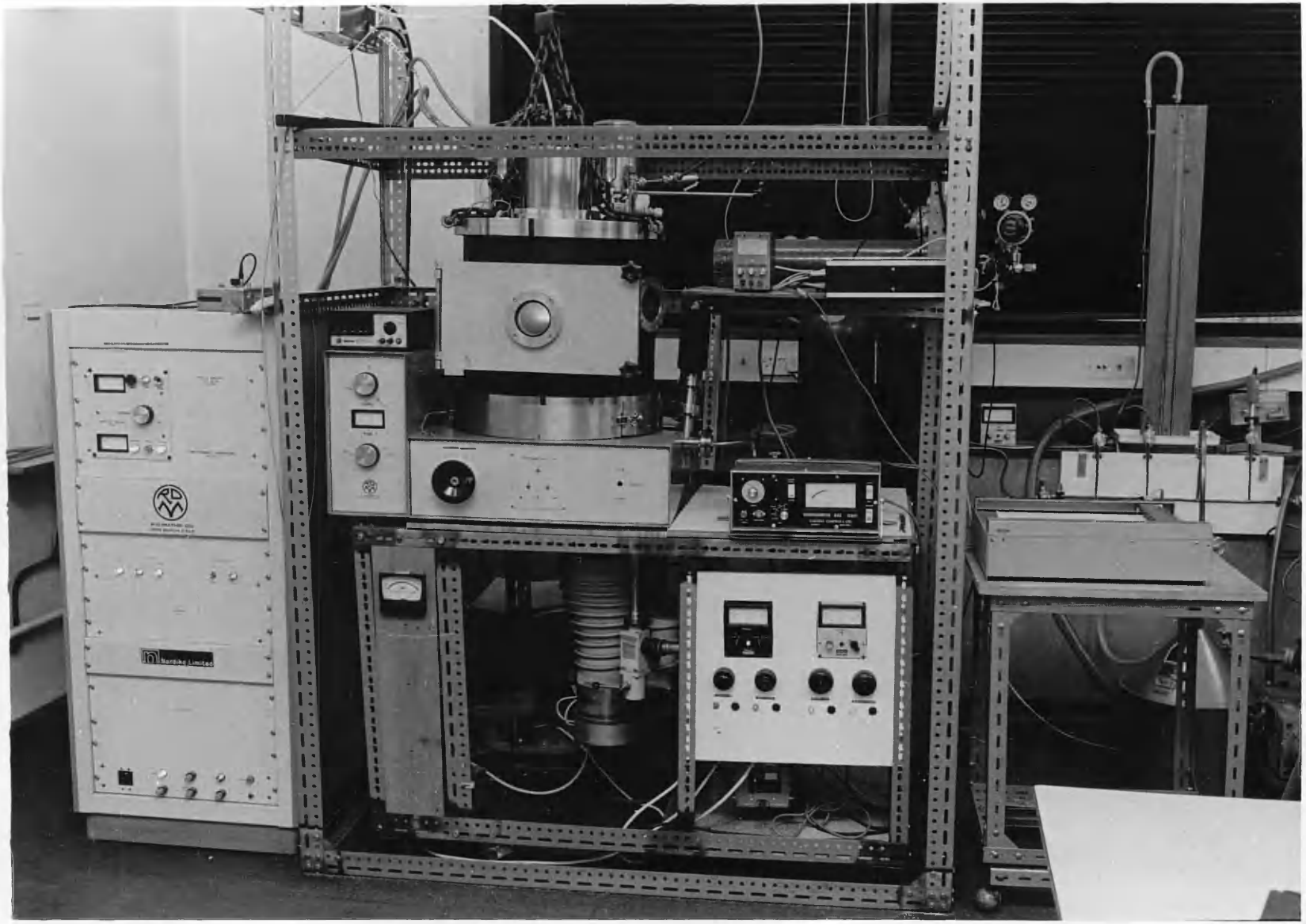
Nanjike Limited

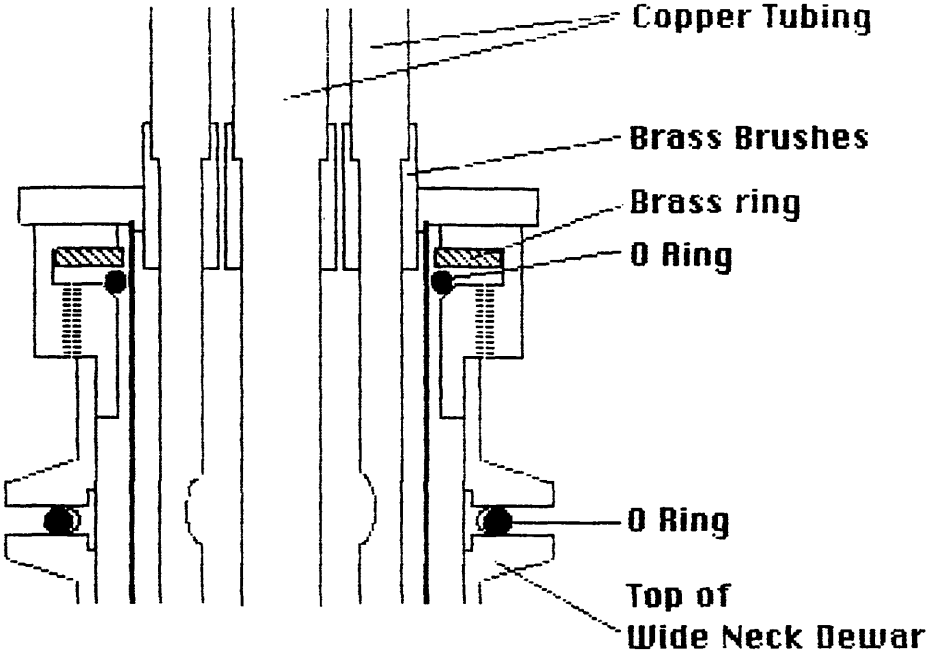

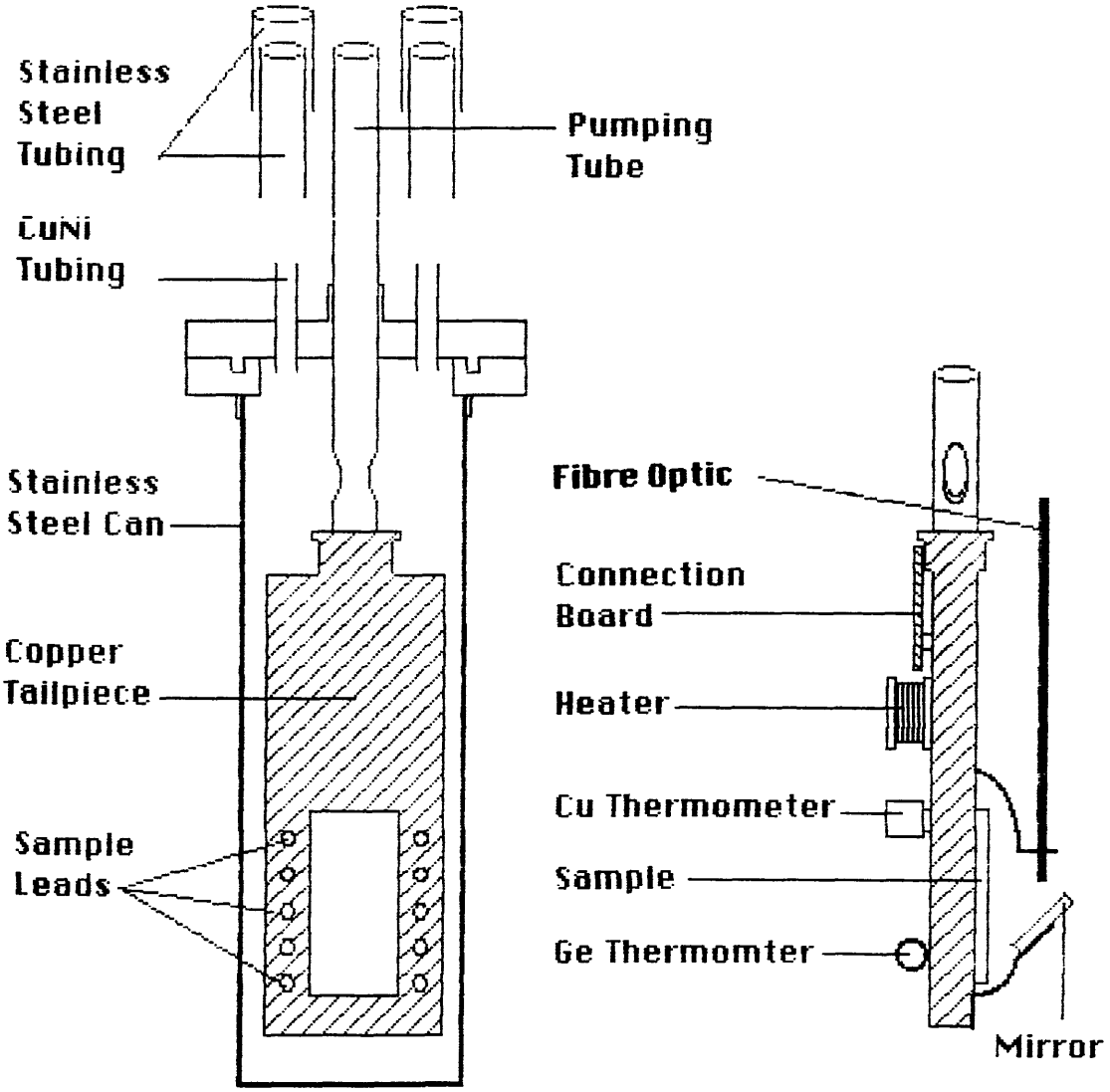

Figure 4.3 : The long-term, low-temperature insert (the top fig. shows how the insert is connected to the wide neck helium dewar).

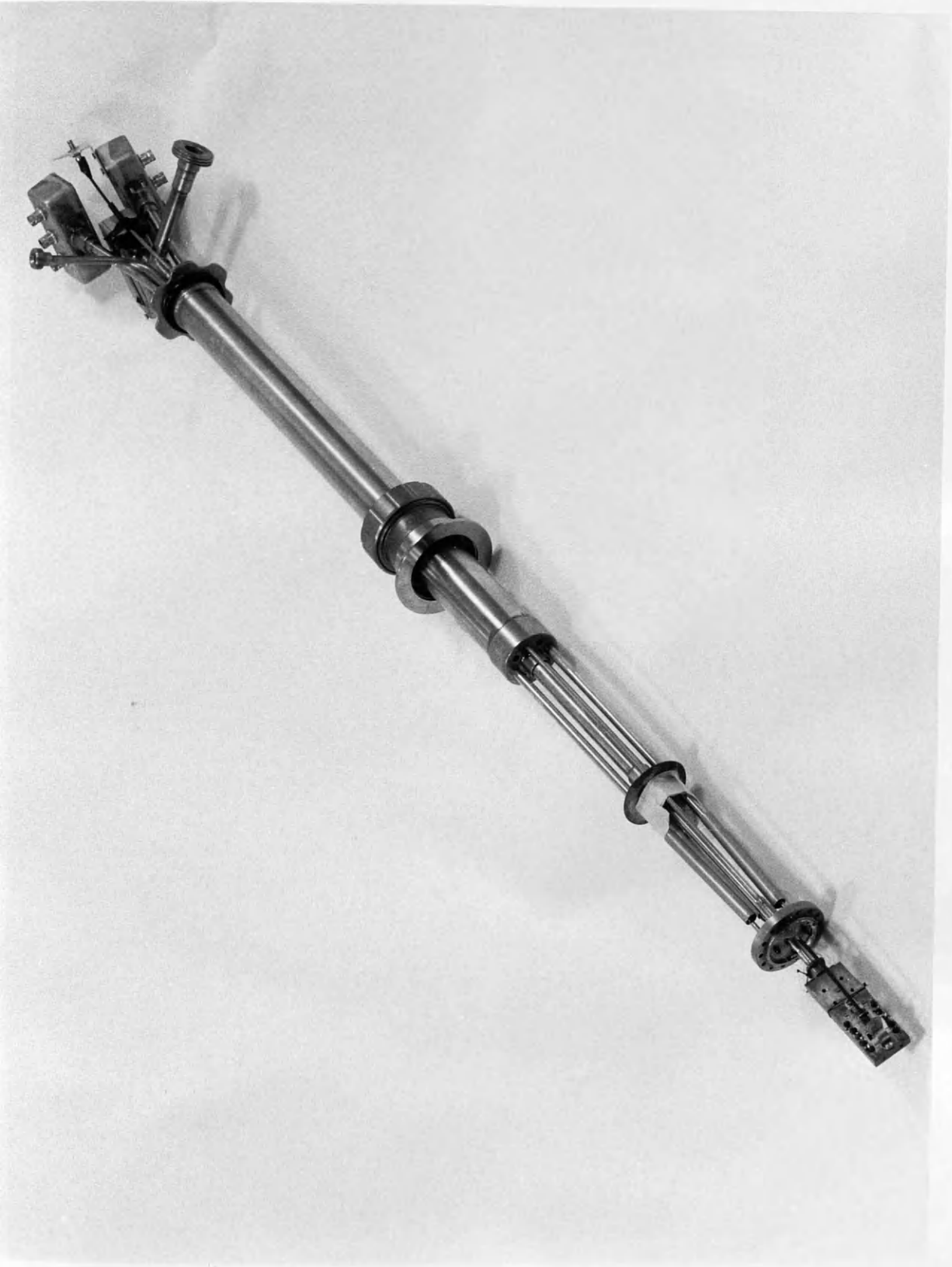

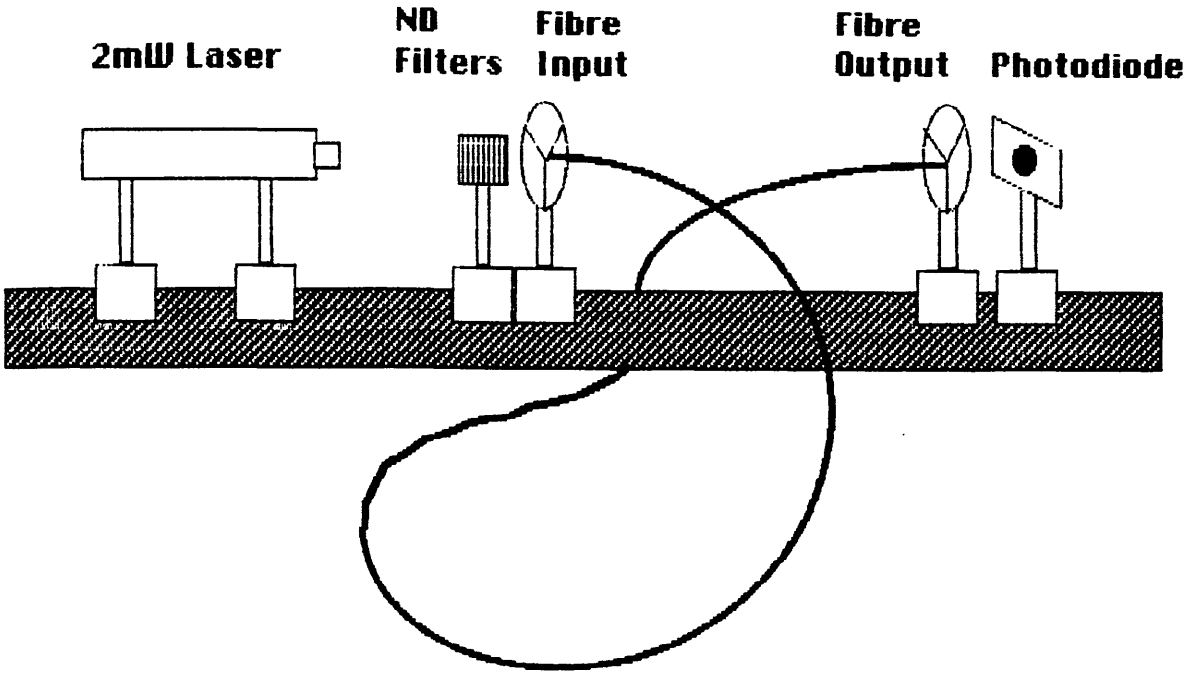

Figure 4.6 : Optical bench arrangement used for intensity calibrations.

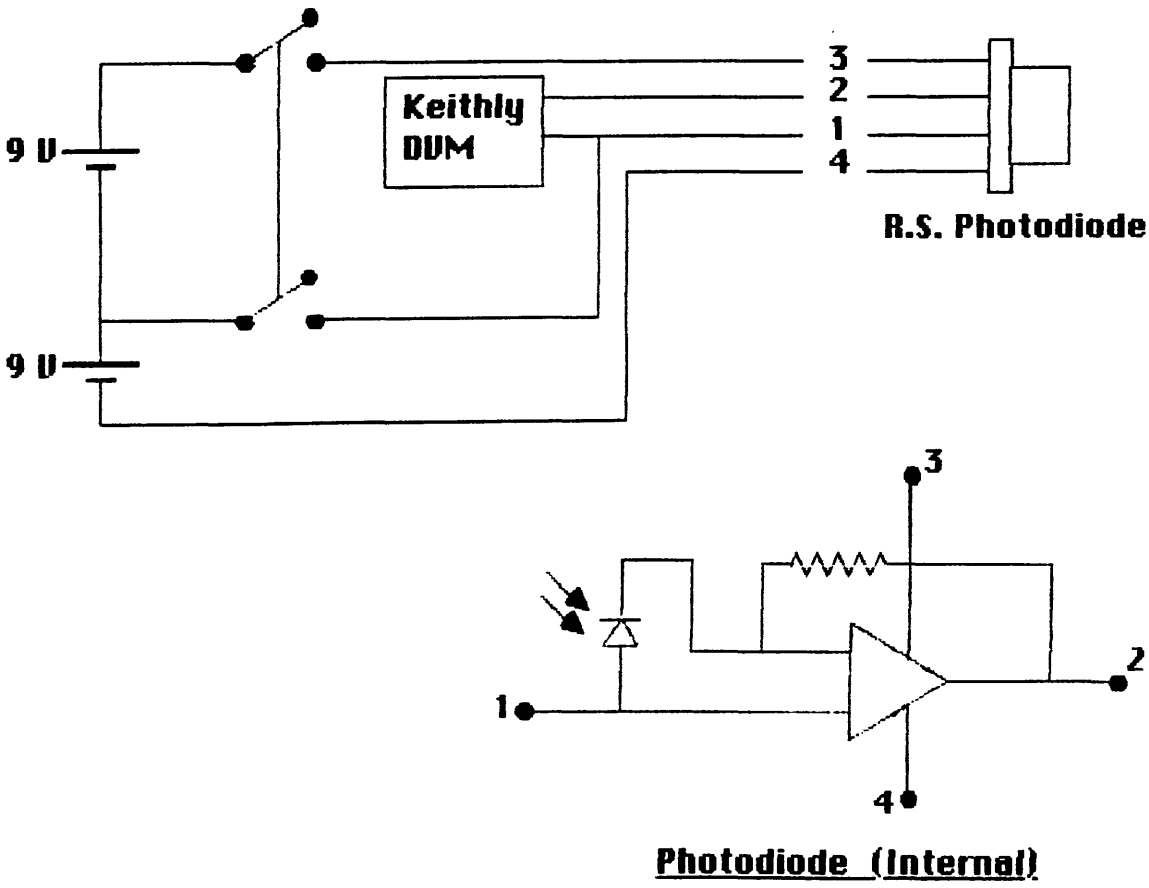

Figure 4.7 : Photodiode supply circuit.

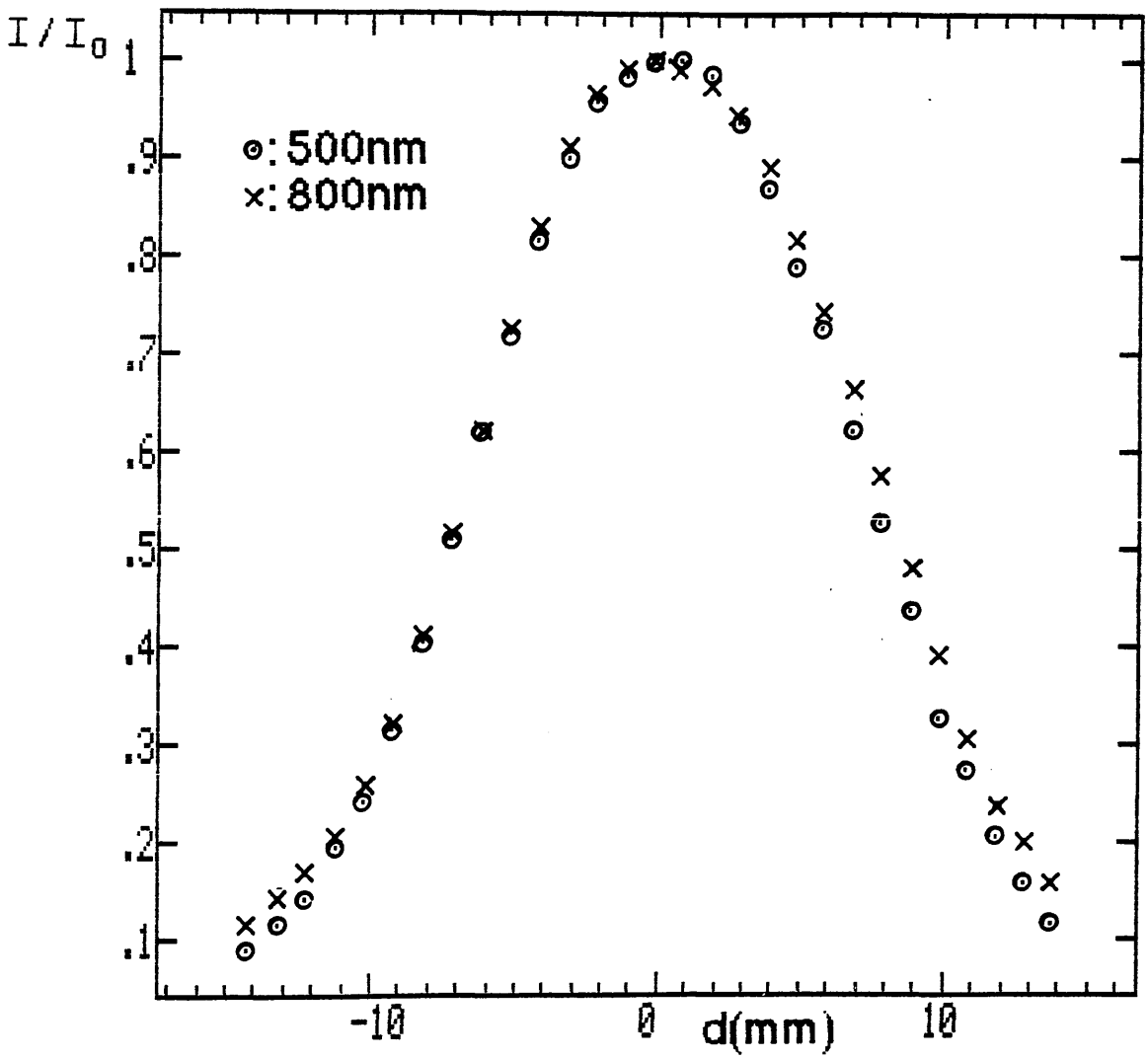

Figure 4.8 : Variation of intensity with d, the distance from centre of light cone produced by a fibre optic.

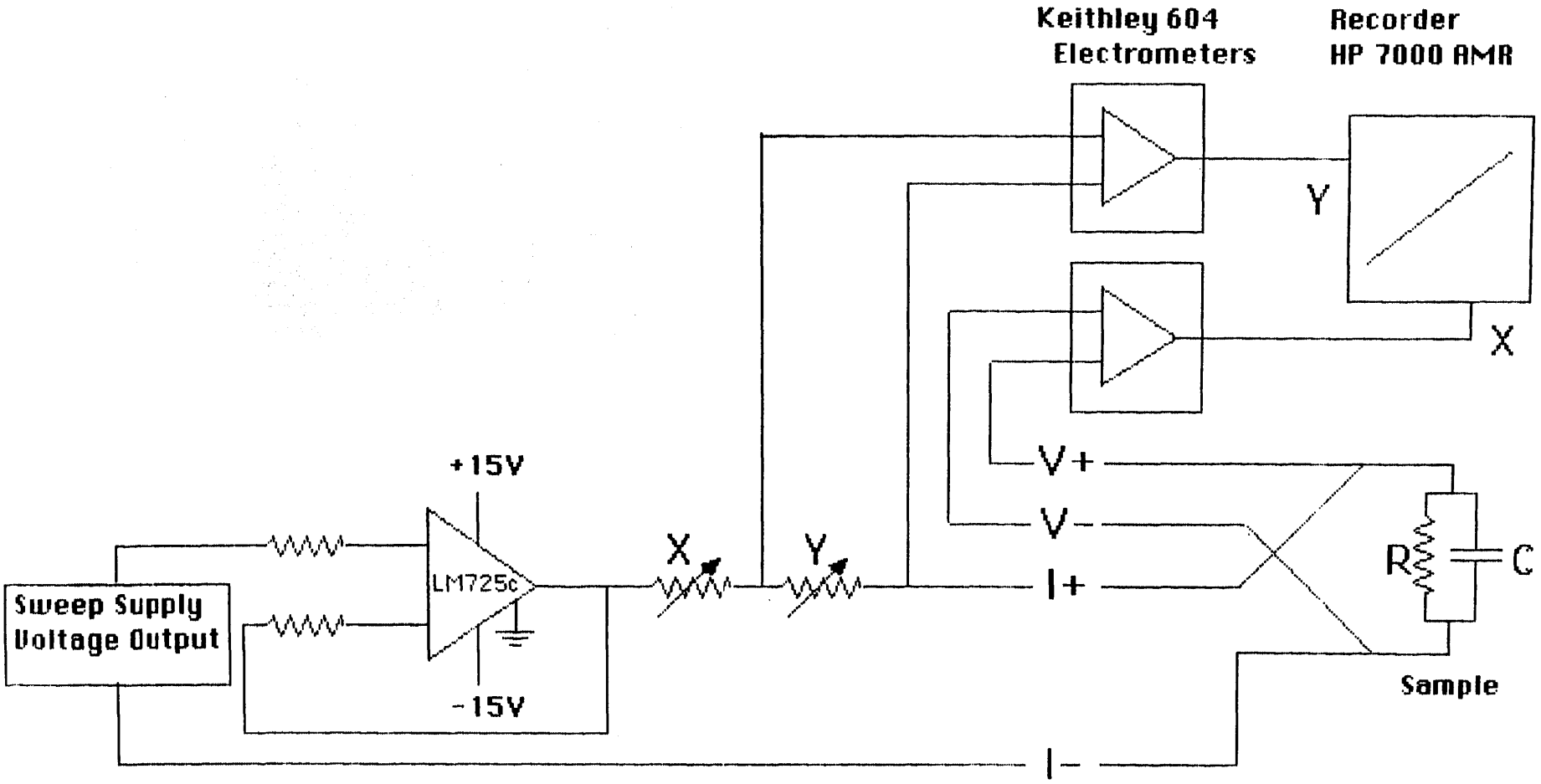

Figure 4.9 : Schematic diagram of the d.c. measurement circuit.

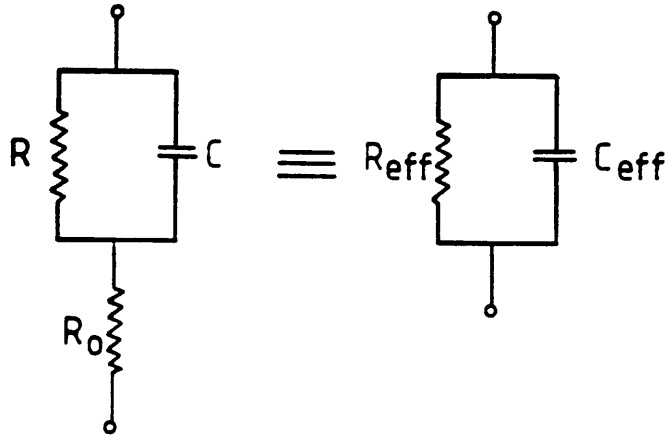

SAMPLE

MEASURED EQIVALENCE OF THE SAMPLE

R: Bulk resistance
C: Bulk capacitance
R_0: Electrode and lead resistance.

R_{eff} : Measured resistance
C_{eff} : Measured capacitance

Figure 4.10 : Representation of the electrode and lead resistance effect in the a.c. measurements.

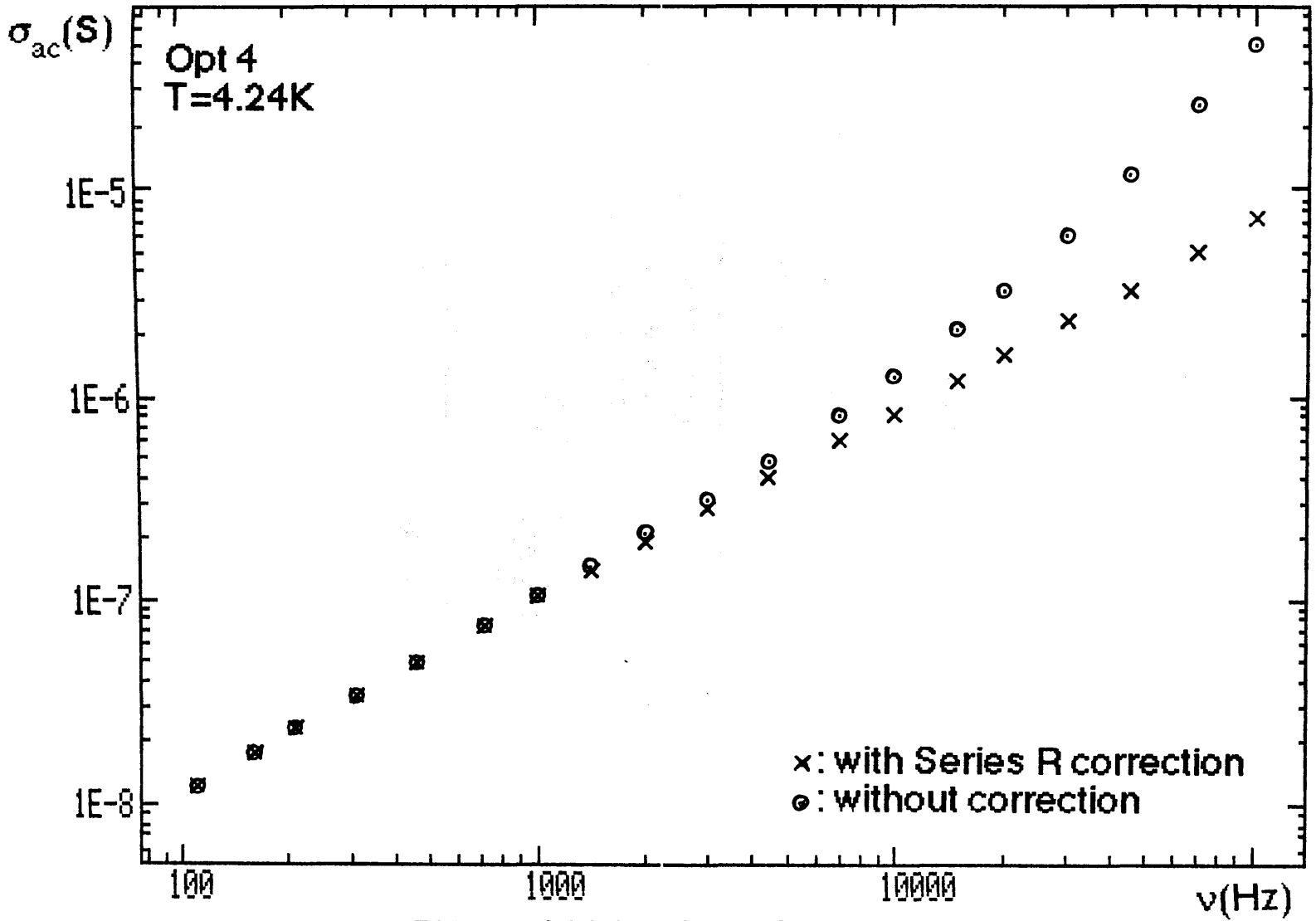

Figure 4.11 : Effect of high electrode series resistance on the accuracy of the a.c. conductivity measurements (Opt 4).

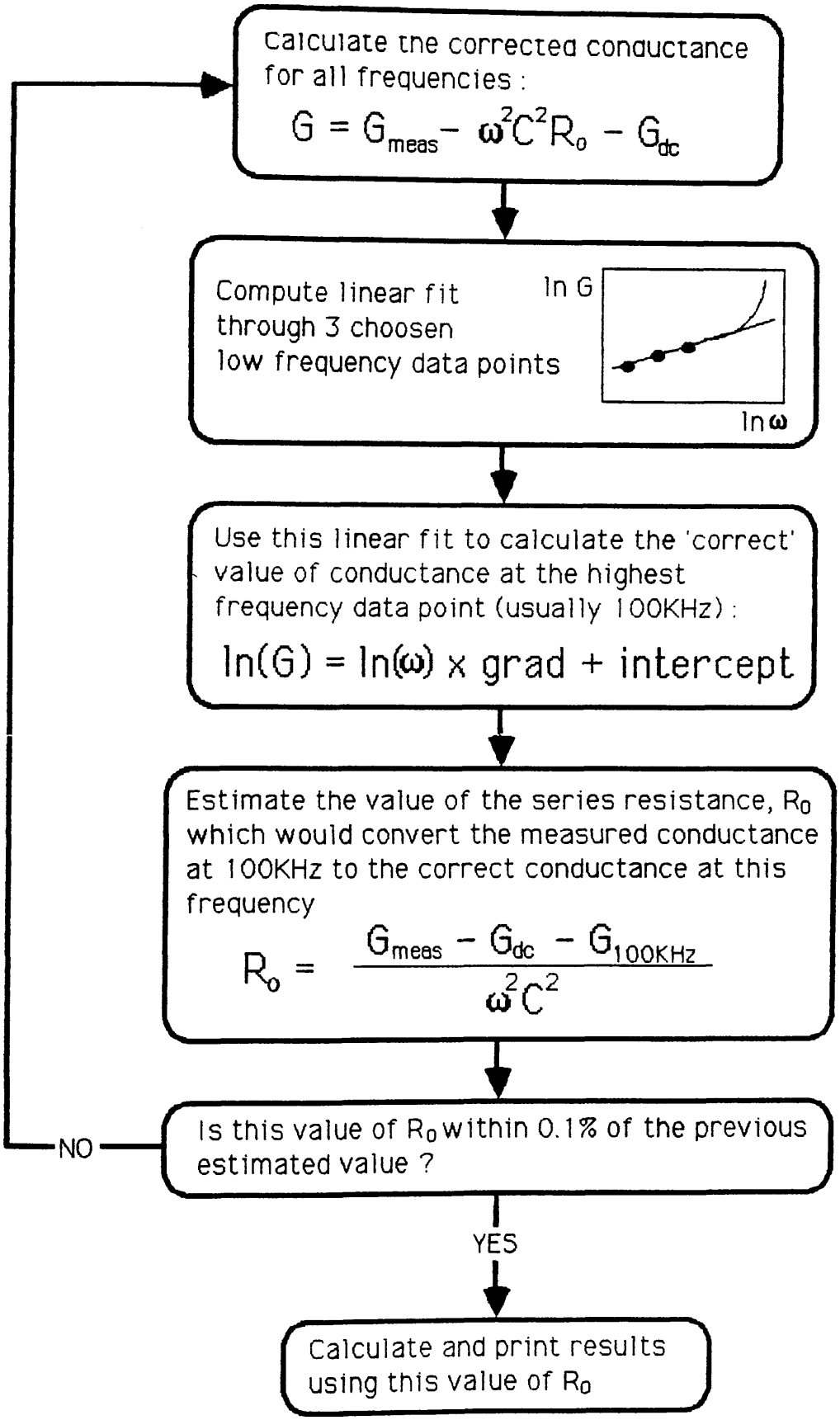

Figure 4.12 : Series resistance correction from 'accalc' program.

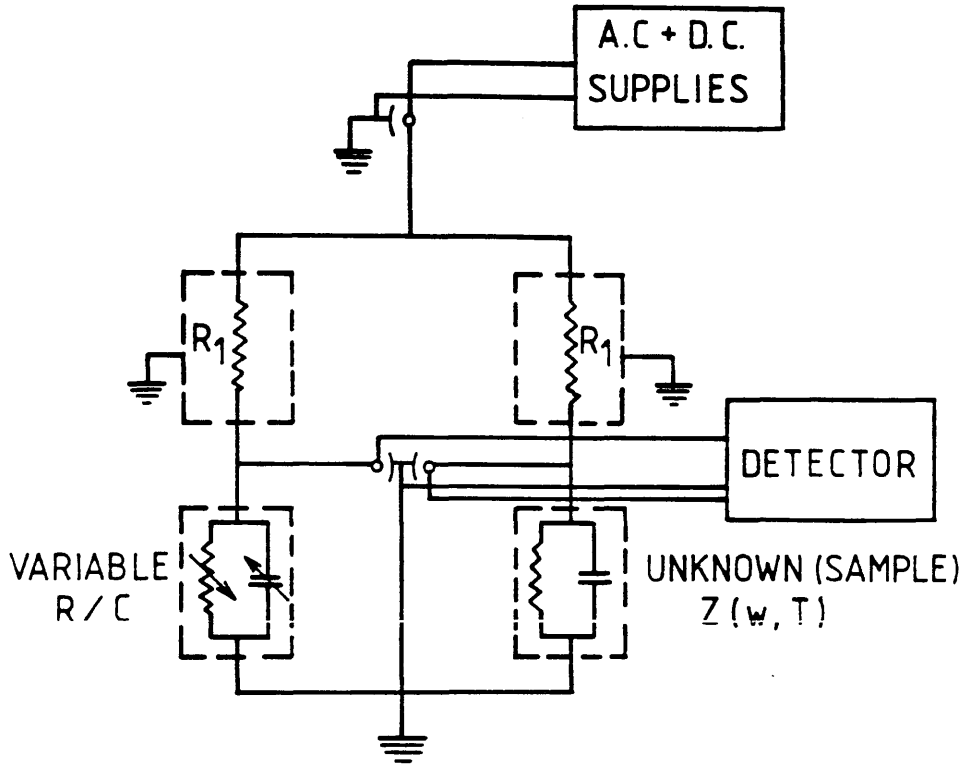

Figure 4.13 : Schematic diagram of manual a.c. bridge used in the experiments.

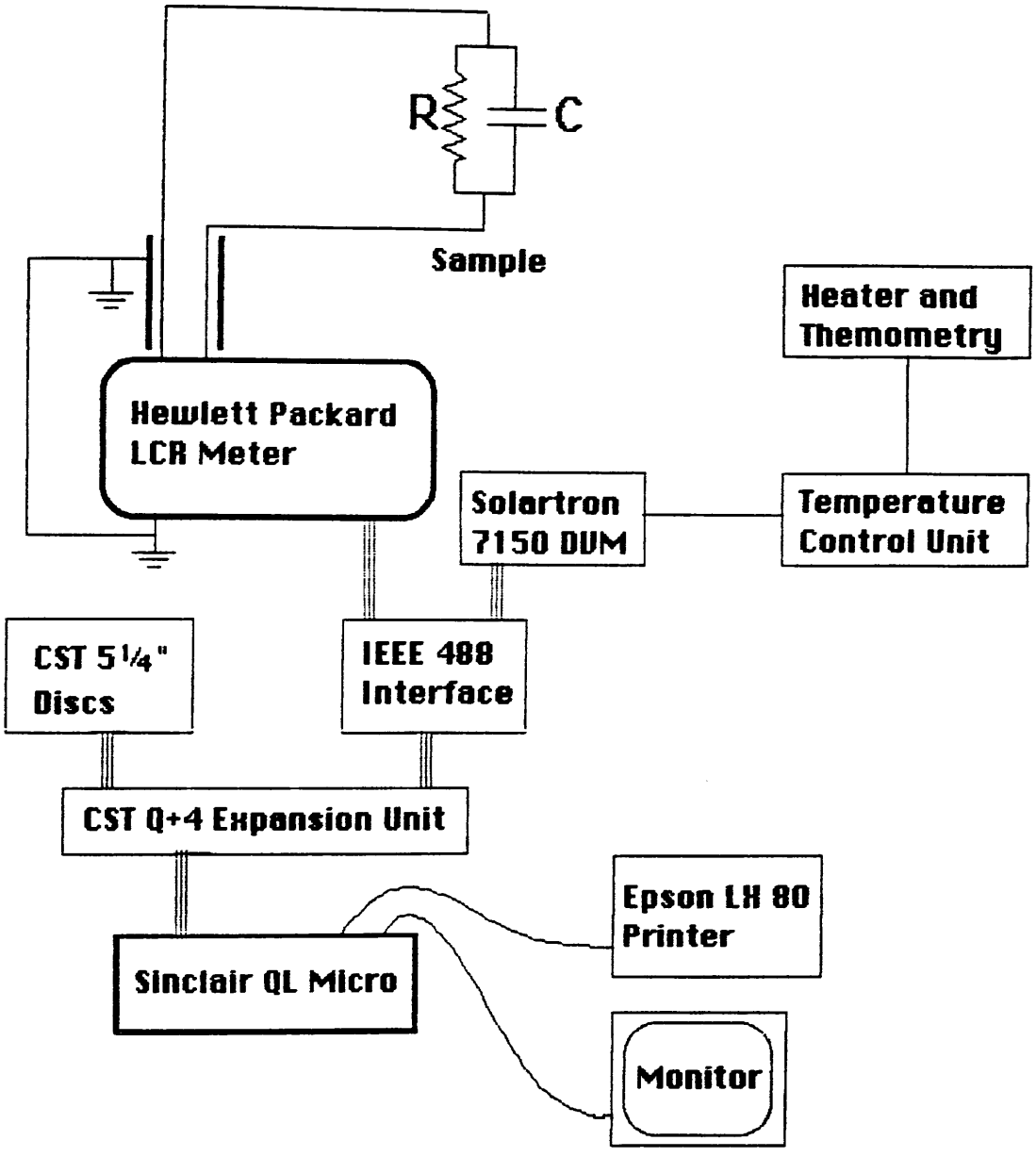

Figure 4.14 : System for the computer controlled recording of a.c. loss.

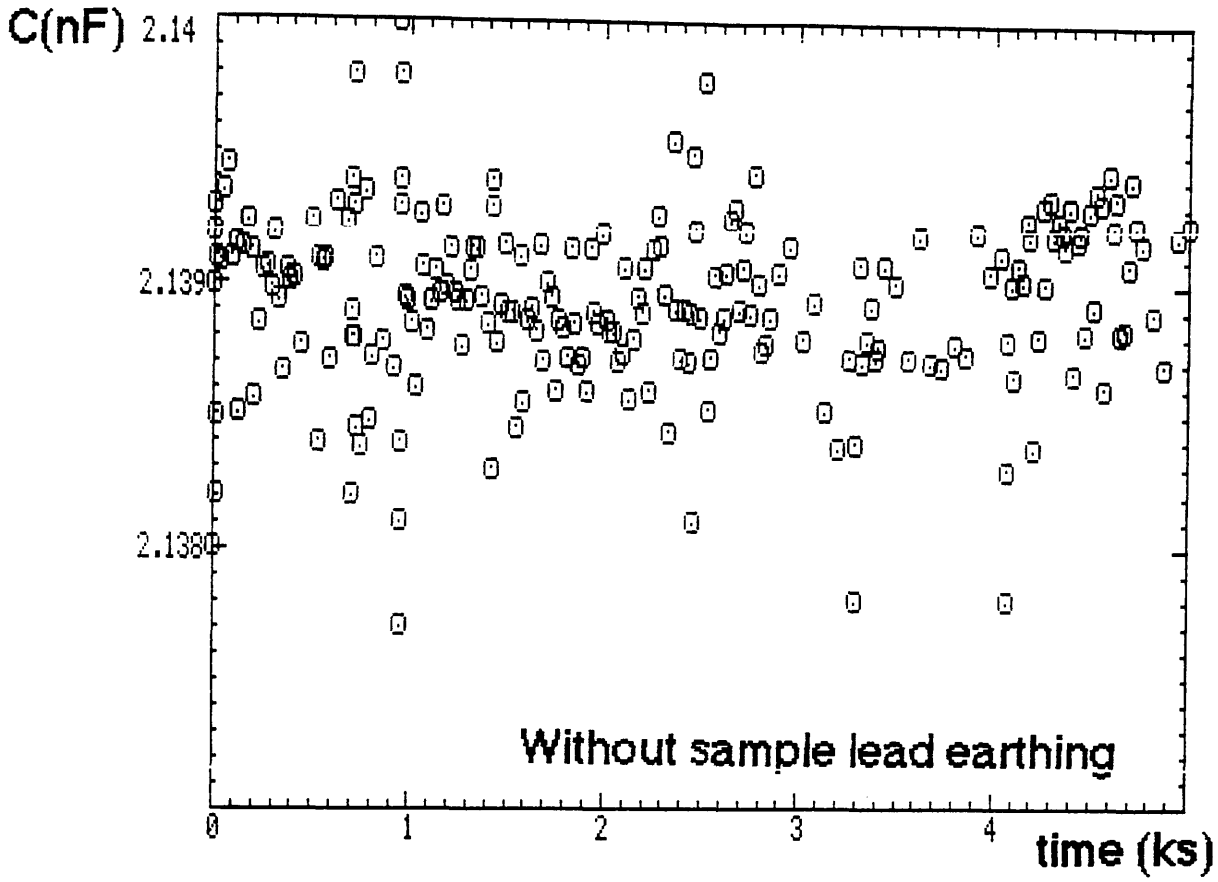

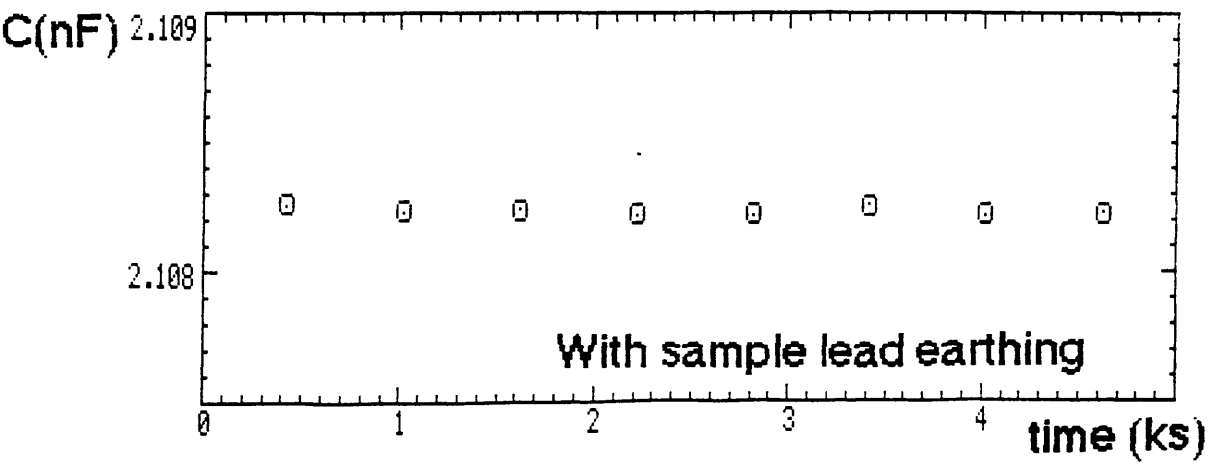

Figure 4.15 : The large scatter in capacitance data caused by inadequate earthing of the QL computer (top). The problem was solved by improved earthing and by data averaging procedures (above).

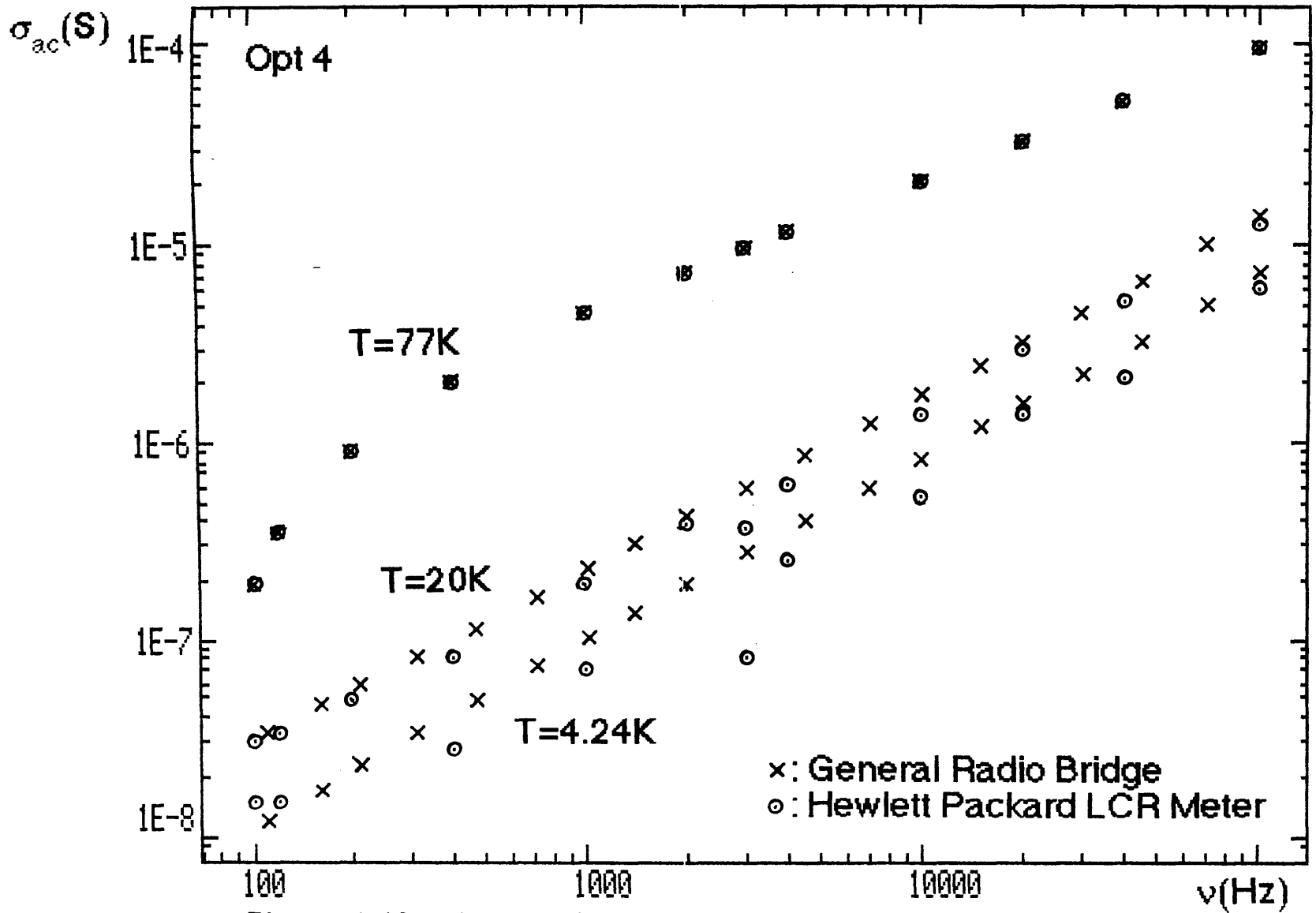

Figure 4.16 : A comparison of frequency sweeps taken with the computer controlled system and the manual General Radio bridge (Opt 4)

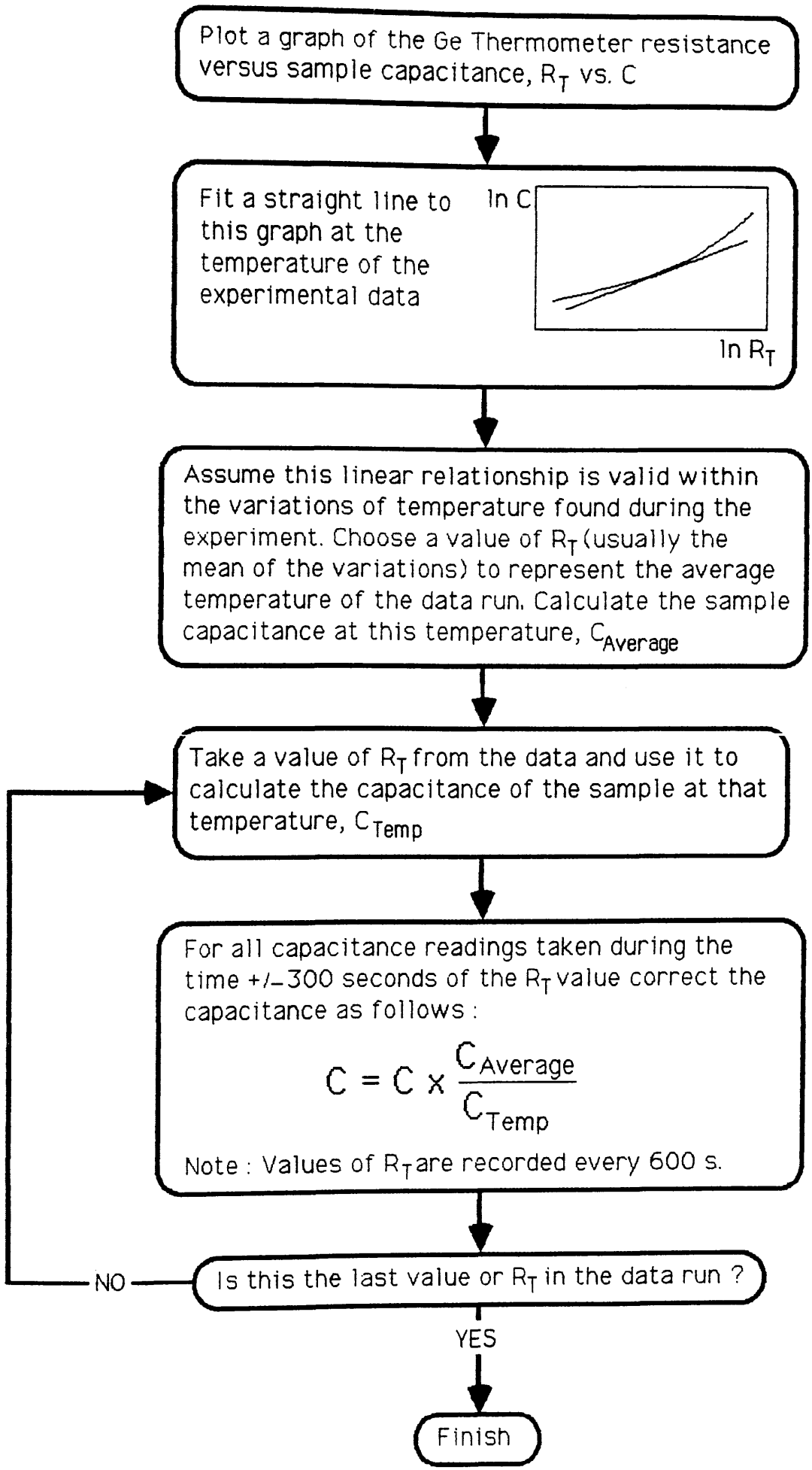

Figure 4.17 : Temperature correction routine from 'lcredit' program.

CHAPTER 5 : Sample Characterization

Table 5.1 summarizes the characteristics of the a-Si and a-Ge samples used during the course of this work. This chapter presents some of the data taken on these samples and shows their behaviour follows that measured on sputtered material by other workers (Long et al., 1982, 1985, Long, McMillan & Balkan, to be published).

The work cited above reports on samples which have aluminium top and bottom electrodes. The use of a gold top electrode with the optical samples (the "Opt" samples) creates the possibility of gold diffusion into the sputtered thin film and a subsequent change in electrical characteristics. Such effects have been seen with device quality glow discharge material (Shimakawa, Long, Anderson & Imagawa, 1987) where the use of gold led to an increase in the loss at helium temperatures of an order of magnitude. Sputtered material has a greater density of states than glow discharge material and therefore a greater value of a.c. conductivity at low temperatures. It is likely that any increase in the density of states caused by gold diffusion, in sputtered films, will be masked by the intrinsically high density of states. No evidence could be found in the optical samples of an abnormally high loss. However, this does not rule the possibility of gold diffusion and some of the optical results presented in chapter 6 could be explained by electrode diffusion.

5.1 : A.C. Conductivity

The frequency dependent conductance, G versus ν is shown for Opt 4 (a-Si:H 20:1) in fig. 5.1. Each curve was measured at a different temperatures in the range 1.3K to 126K and is corrected for series resistance (see §4.5). Fig 5.2 shows the dispersive component of the conductance, with the d.c. value subtracted. From this figure it can be seen that G_{ac} follows a power law relationship of the form $G_{ac} \alpha \nu^{s}_{down}$ to a certain frequency at a given temperature and then "rolls off" more rapidly as the frequency is further decreased. These loss peaks are associated with the transition to non-dispersive behaviour. At liquid helium temperatures the roll-off does not occur within the measurement range.

The results of fig. 5.2 are plotted as G_{ac}/ν in fig 5.3. Now the loss peaks and the cut-off frequencies (ν_c) are clearly visible. The differential capacitance results (fig 5.4) also highlight the loss peaks. A graph of $\log(\nu_c)$ versus $T^{-1/4}$ for Opt 4 (fig. 5.5) shows a linear dependence. The d.c. conductivity of Opt 4 follows the Mott $T^{-1/4}$ law over the temperature range of these measurements (see fig. 5.11). Hence it is clear that the loss peak frequencies are proportional to the d.c. conductivity in this sample, as predicted by Summerfield's scaling hypothesis (§2.6).

5.2 : Temperature Dependence

A feature of the frequency dependence of the a.c. conductivity for Opt 4 is the temperature dependence of the

frequency exponent s in the high frequency range. In fig. 5.6 we plot s values, measured above ν_c where appropriate, against T for three a-Si samples (Opt 3, Opt 4 and Opt 5) and a pure a-Ge sample (B11). They show similar features, a minimum of s=0.6 at high temperatures and s=0.9 at low temperatures. The transition region between these regimes varies in a systematic way with the amount of hydrogen in the sample.

The temperature dependence of σ_{ac} measured at 3kHz is shown in fig. 5.7 for B11. In the low temperature regime there is a weak T dependence (n=0.32) and s is close to 1. The transition to the high temperature region occurs at around 15K; beyond this temperature the loss is strongly temperature dependent (n=3.5) and s falls towards 0.6. The a.c. conductivity for the two different film thicknesses of B11 is shown in fig. 5.7. The values of σ_{ac} observed in the high temperature regime are in agreement to within the estimated error of the thickness measurement and must therefore be bulk properties of the film. Below 10K however the thinner film has a higher conductance suggesting that the defects responsible for low temperature loss are more numerous in the surface region of the film (Long et al., 1985).

Fig. 5.8A shows σ_{ac} of three a-Si samples measured at 20kHz. The temperature at which the loss peak occurs scales with the hydrogen content of the samples. The relative permittivity data behaves in a similar way (fig 5.8B).

5.3 : A.C. Field Effect

The a.c. loss measured at low temperatures shows a strong dependence on exciting electric field. This effect was first reported by Long et al. (1985). The data in fig. 5.9 obtained at 1.25K, 4.2K and 10K for B11 is normalized to zero field conductivity and is plotted against the log of the electric field. This shows the effect is a genuine field effect because the data for junctions of different thicknesses plot about the same curve. The onset of the effect occurs at a higher field at higher temperature. The critical condition for the onset (eqn. 2.74) can be used to calculate the electronic hopping distance. The field effect is defined to have begun when the a.c. conductivity is 50% above its minimum value. The arbitrary nature of this definition has the consequence that absolute values of the hopping distances are only order of magnitude figures. For B11 the hopping distance is 6Å, values for other samples are given in table 5.1.

5.4 : D.C. Conductivity

The temperature dependence of the d.c. conductivity in the range 1.25K to 60K is shown in fig. 5.10 for B11. It is apparent that the observed conductivity follows the $T^{-1/4}$ dependence as expected from the variable range hopping model. The d.c. conductivity data taken on the silicon samples in the liquid nitrogen temperature range is plotted in fig. 5.11. It can be seen that the d.c. properties of these

samples scale with hydrogen content. The T_o and σ_o values of the d.c. plots for all the samples are given in table 5.1.

Non-linear I-V characteristics were measured at high fields and the Aspley and Hughes theory (§2.1) was applied to this data to estimate values for the electronic overlap parameter, α^{-1} . A value of (15±1)Å was calculated for Opt 3 at liquid nitrogen temperatures which compares to (17±1)Å for Opt 4 in the same temperature range.

5.5 : Characterization of Arsenic Selenide

A sputtered Arsenic Selenide sample, prepared at the Dundee College of Technology with a semi-transparent gold top electrode, was characterized prior to study of optically induced loss within it and the results are summarised in the following paragraphs.

The a.c. conductivity followed a power law relationship with a frequency exponent of unity (±3%) between 1.3K and 300K. The d.c. conductivity was at least an order of magnitude less than σ_{ac} even at the lowest frequency (100Hz) and highest temperature (300K) at which measurements were taken. No loss peaks were observed.

Fig 5.12 shows the temperature dependence of the a.c. conductivity of the sample measured at 2kHz. There is a rapid increase in σ_{ac} between 2K and 8K; the value of the temperature exponent, n, is unity (±3%). Between 10K and 50K, n=0.5 (±5%) and as the temperature rises further the value of n falls.

One possible mechanism for the a.c. loss in this

material was proposed by Elliott (1977, 1983). He adapted the single-electron CBH model (§2.3.2) to electron-pair hopping in chalcogenides. However the CBH model predicts that the frequency exponent, s, should decrease from unity with increasing temperature (eqn. 2.40). The temperature independent value of s for this sample implies that the CBH model is not applicable to these results. The absence of loss peaks suggests that there is no common hopping mechanism to explain the a.c. and the d.c. conductivity. The large magnitude of the a.c. loss compared to other data in the literature implies an additional mechanism, possibly due to contact diffusion as observed in glow discharge a-Si:H (Shimakawa et al., 1987).

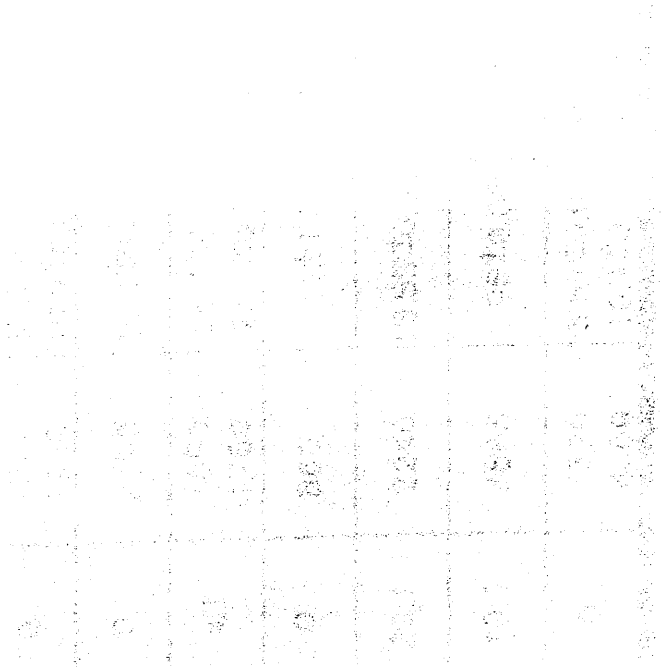

Sample	Argon Hydrogen Ratio	Thickness (Å ±5%)	Area / Thickness (m)	Deposition Rate (Å/s)	ε_∞	T_0 /K^{-1}	σ_0 ($\Omega^{-1}m^{-1}$ ±1%)	Hopping Distance (Å ±3%)
B11 (a-Ge)	0	1050 1950	33.7±0.8 19.9±0.6	0.58±1% 0.54	18.6±0.5 17.4±0.5	$(9.0\pm0.1)\times10^{7}$	1.80×10^{11}	6.2
Opt 1 (a-Ge)	0	2390	15.3±0.04	0.66	19.2±0.3	$(9.3\pm0.1)\times10^{7}$	4.06×10^{11}	8.2
Opt 2 (a-Ge:H)	4:1	1690 1760	26.1±0.9 23.9±0.9	0.23 0.24	16.2±0.6	$(2.6\pm0.2)\times10^{8}$	7.20×10^{10}	4.0
Opt 3 (a-Si)	0	860	51±1.5	0.08	12.3±0.2	$(1.33\pm0.06)\times10^{8}$	7.21×10^{10}	7.9
Opt 4 (a-Si:H)	20:1	2240	18.55±0.08	0.10	12.1±0.1	$(2.05\pm0.03)\times10^{8}$	6.28×10^{10}	4.2
Opt 5 (a-Si:H)	10:1	3865	9.98±0.08	0.13	13.9±0.1	$(3.57\pm0.09)\times10^{8}$	2.52×10^{10}	—
Opt 6 (a-Si)	0	7320 4000	5.67±0.03 10.1±0.1	0.68 0.74	15.5±0.2	$(1.15\pm0.03)\times10^{8}$	6.77×10^{9}	7.6

Table 5.1

Sample	σ_{dc} (77K) $\Omega^{-1}m^{-1}$ ±10%	σ_{ac} (77K) (ν = 3KHz) $\Omega^{-1}m^{-1}$ ±10%	σ_{ac} (4.2K) (ν = 3KHz) $\Omega^{-1}m^{-1}$ ±10%	s (77K) ±1%	s (4.2K) ±1%	n (4.2K) (ν = 3KHz) ±2%	α^{-1} E.P.A. Fit (Å ±8%)
B11 (a-Ge)	8.46×10^{-4}	—	4.18×10^{-8}	—	0.88	0.31	15
Opt 1 (a-Ge)	1.08×10^{-3}	—	3.99×10^{-8}	—	0.87	0.41	19
Opt 2 (a-Ge:H)	1.88×10^{-8}	4.25×10^{-7}	1.88×10^{-8}	0.64	0.94	0.49	8.5
Opt3 (a-Si)	5.53×10^{-5}	1.26×10^{-6}	4.86×10^{-8}	0.70	0.91	0.51	12.5
Opt 4 (a-Si:H)	1.97×10^{-7}	5.22×10^{-7}	1.49×10^{-8}	0.62	0.92	0.39	10
Opt 5 (a-Si:H)	2.43×10^{-10}	1.11×10^{-7}	8.91×10^{-9}	0.73	0.93	0.47	—
Opt6 (a-Si)	3.31×10^{-6}	2.19×10^{-6}	2.16×10^{-8}	0.57	0.90	0.52	8

Table 5.2

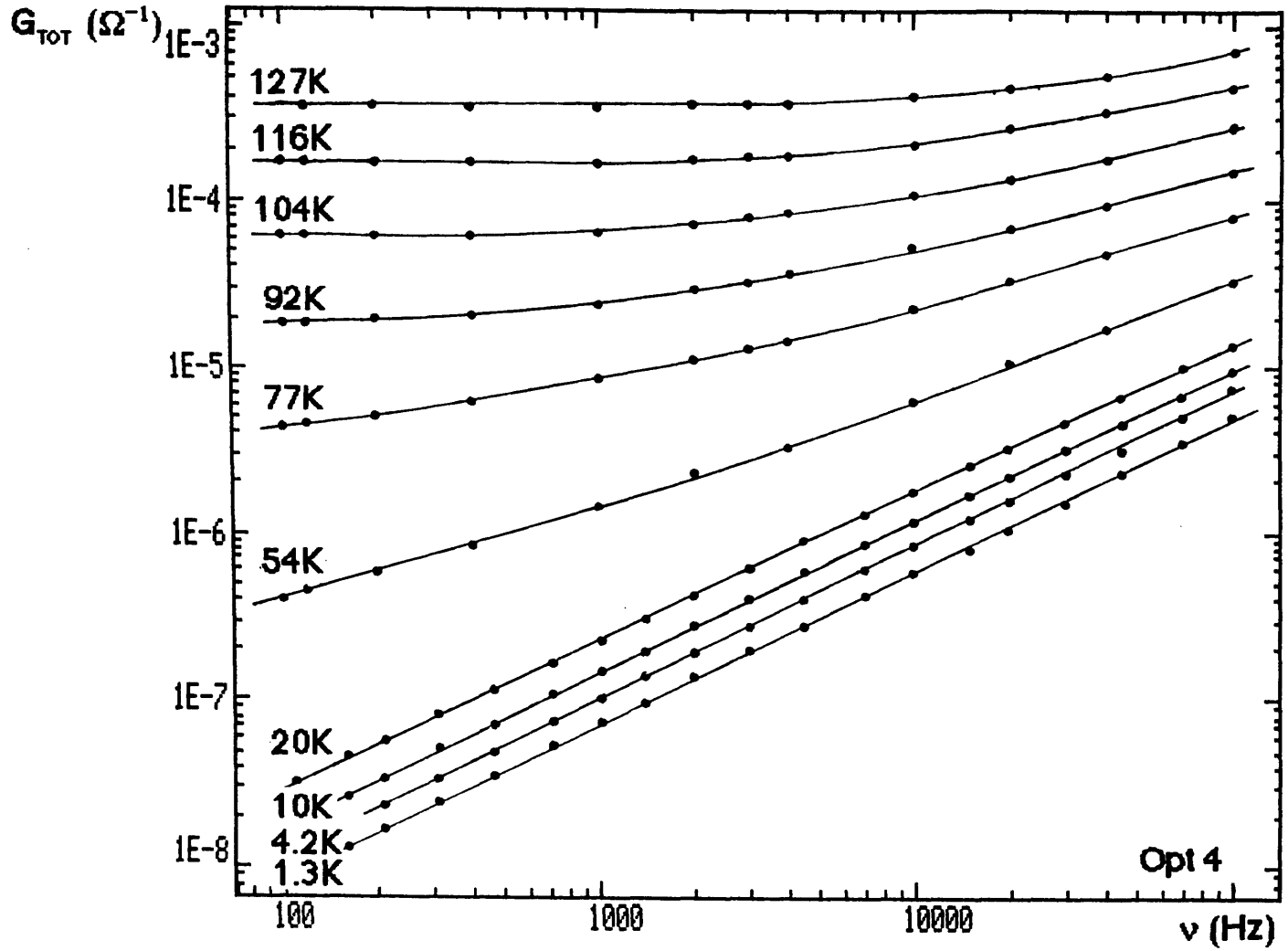

Figure 5.1 : Frequency dependence of the measured conductance for Opt 4.

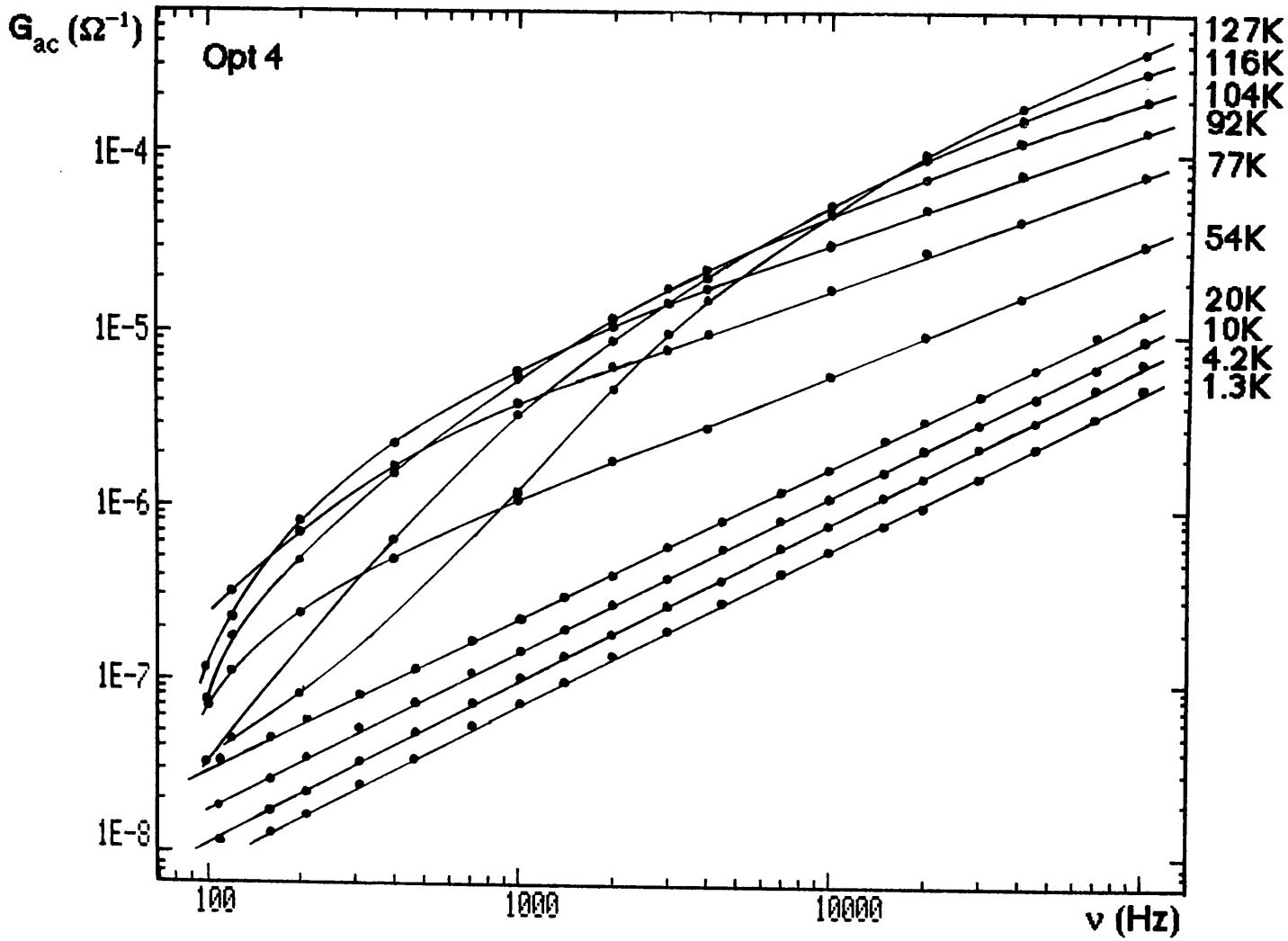

Figure 5.2 : Frequency dependence of the a.c. conductance for Opt 4.

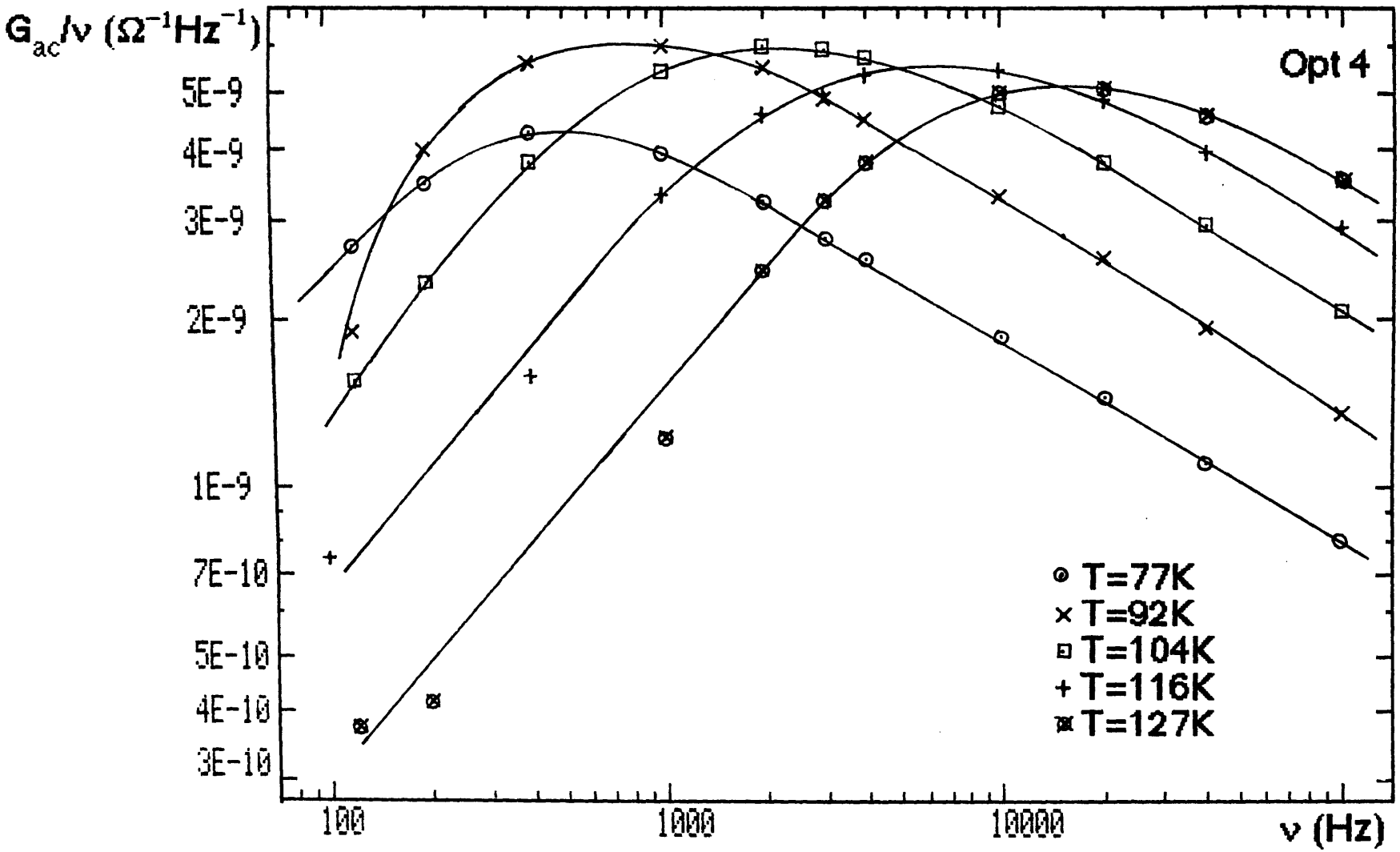

Figure 5.3 : The a.c. conductance divided by frequency for the data of fig. 5.2.

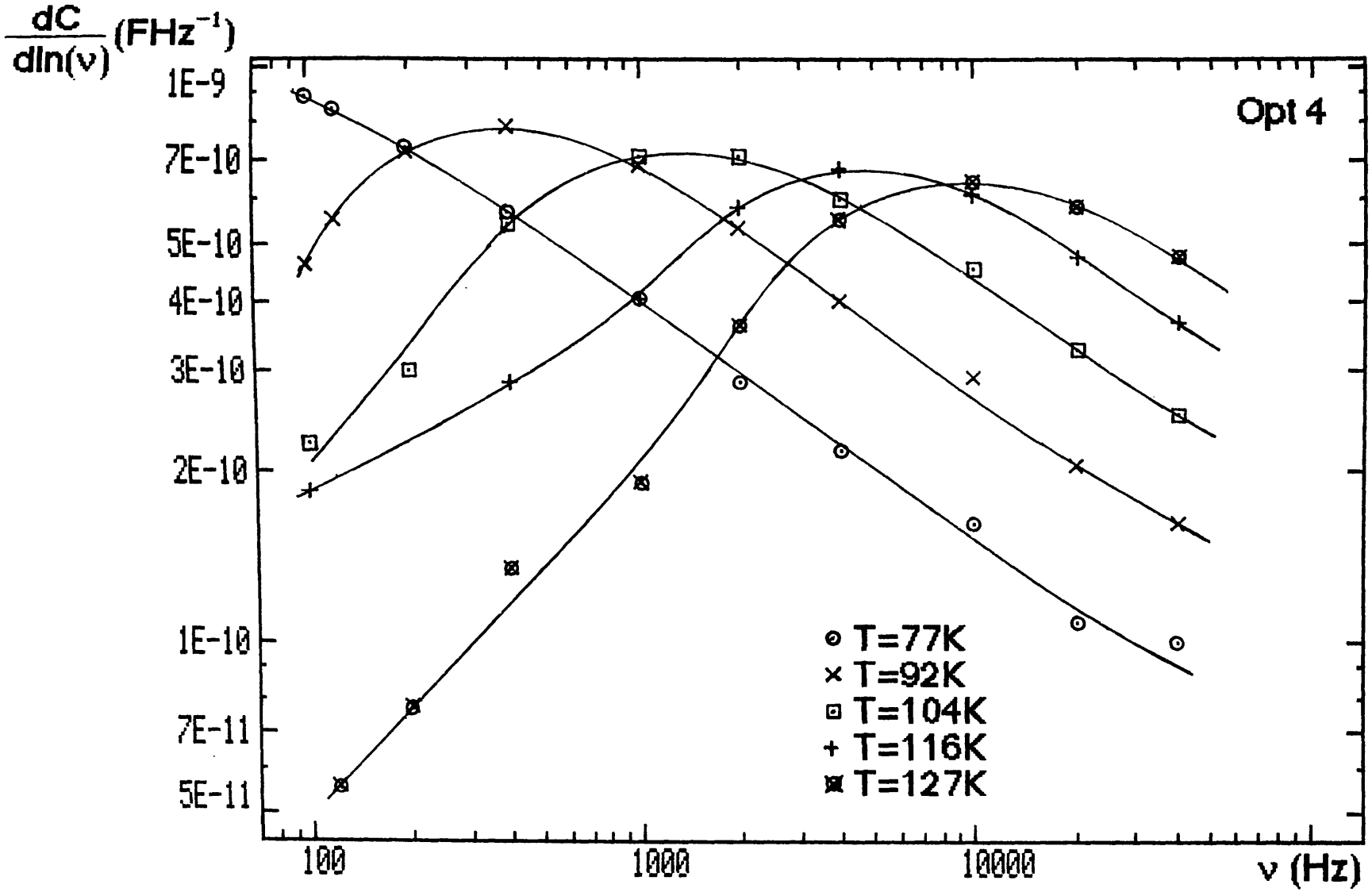

Figure 5.4 : The differential form of the capacitance versus frequency for Opt 4.

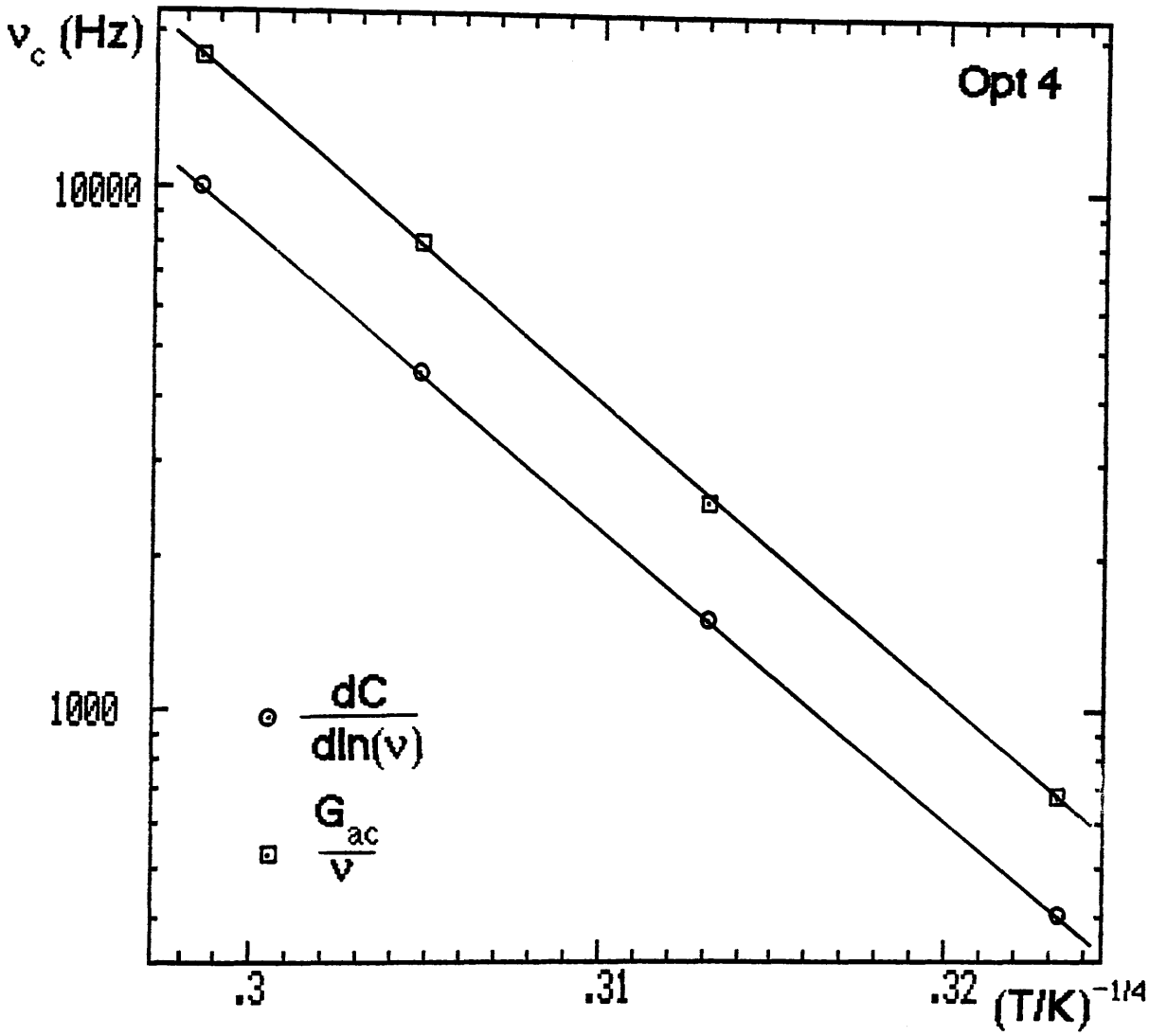

Figure 5.5 : The cut-off frequency (as derived from figs 5.4 and 5.5.) as a function of $T^{-1/4}$.

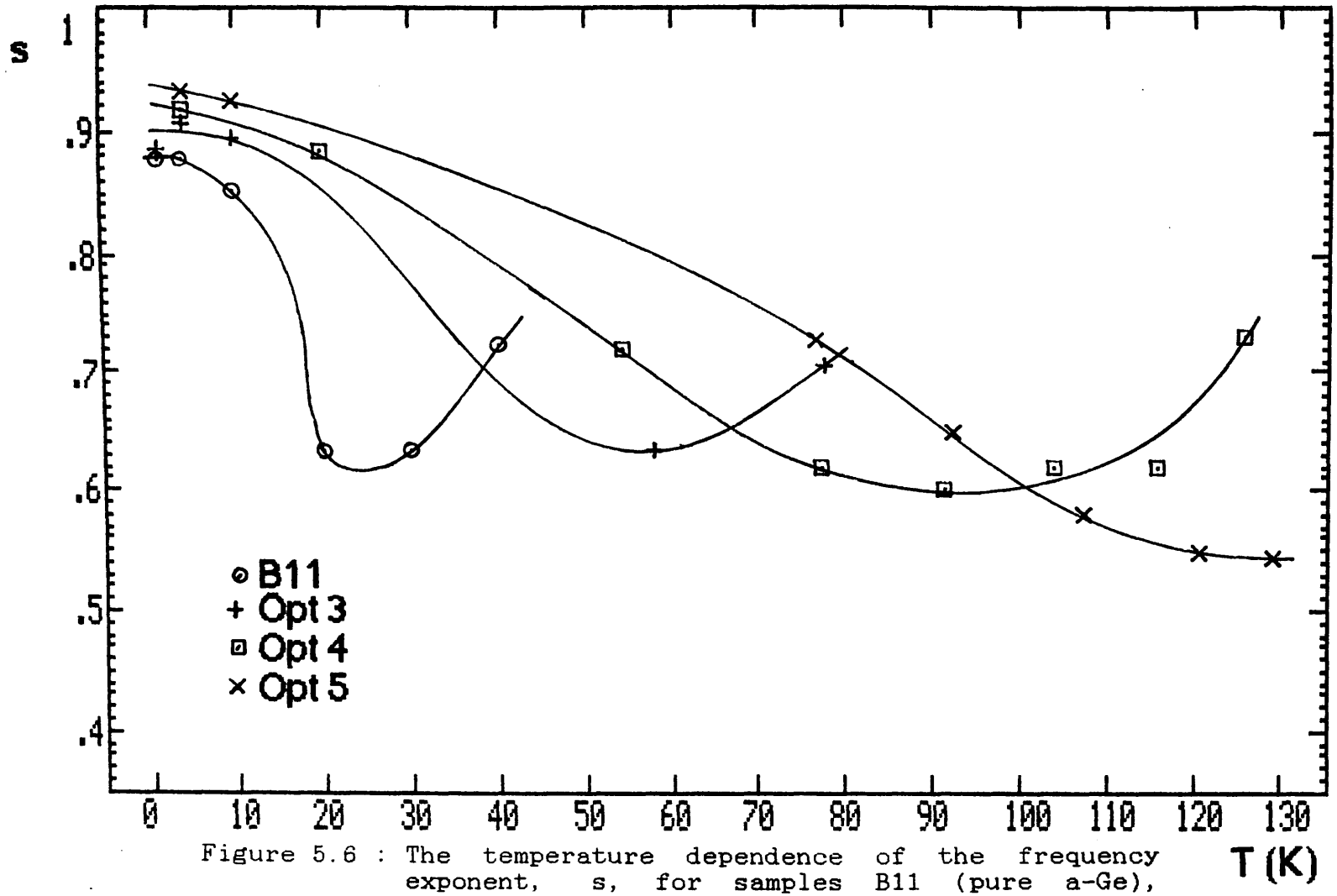

Figure 5.6 : The temperature dependence of the frequency exponent, s, for samples B11 (pure a-Ge), Opt 3 (pure a-Si), Opt 4 (a-Si:H 20:1) and Opt 5 (a-Si:H 10:1).

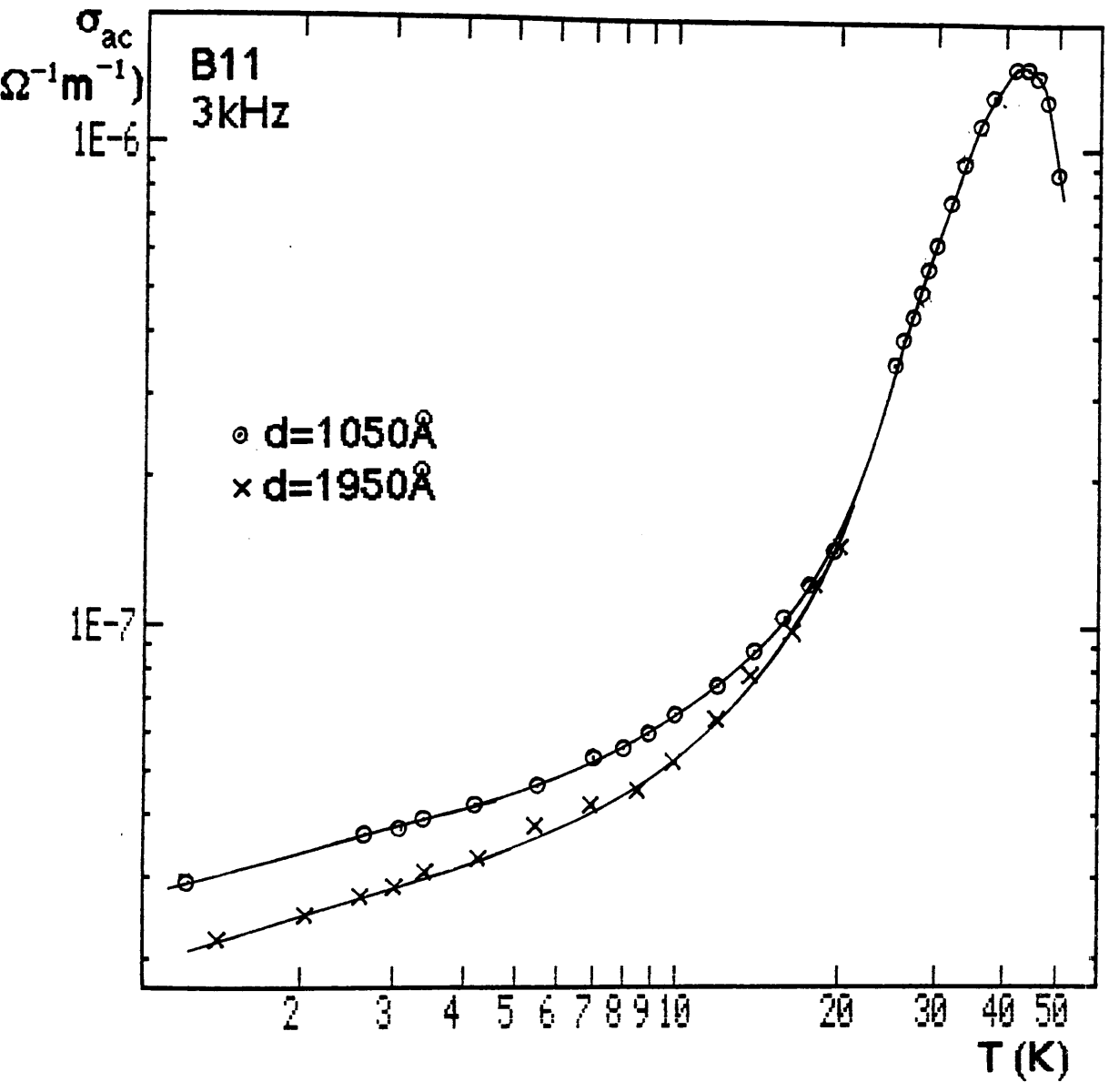

Figure 5.7 : The temperature dependence of the a.c. conductivity measured at 3kHz for B11.

Figure 5.8A

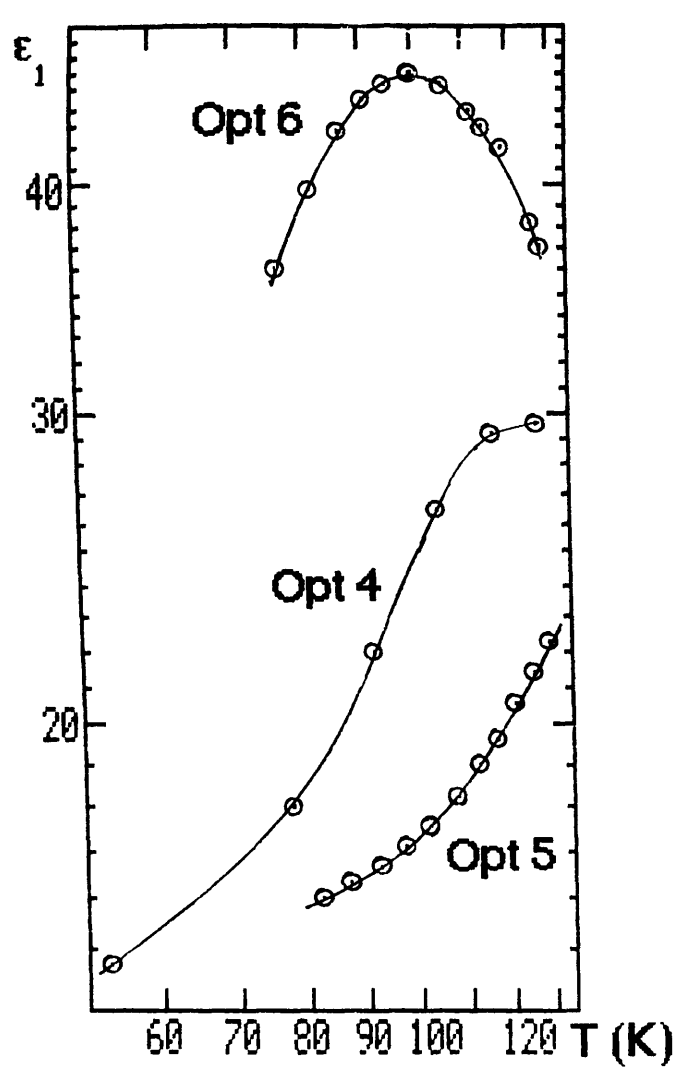

Figure 5.8B

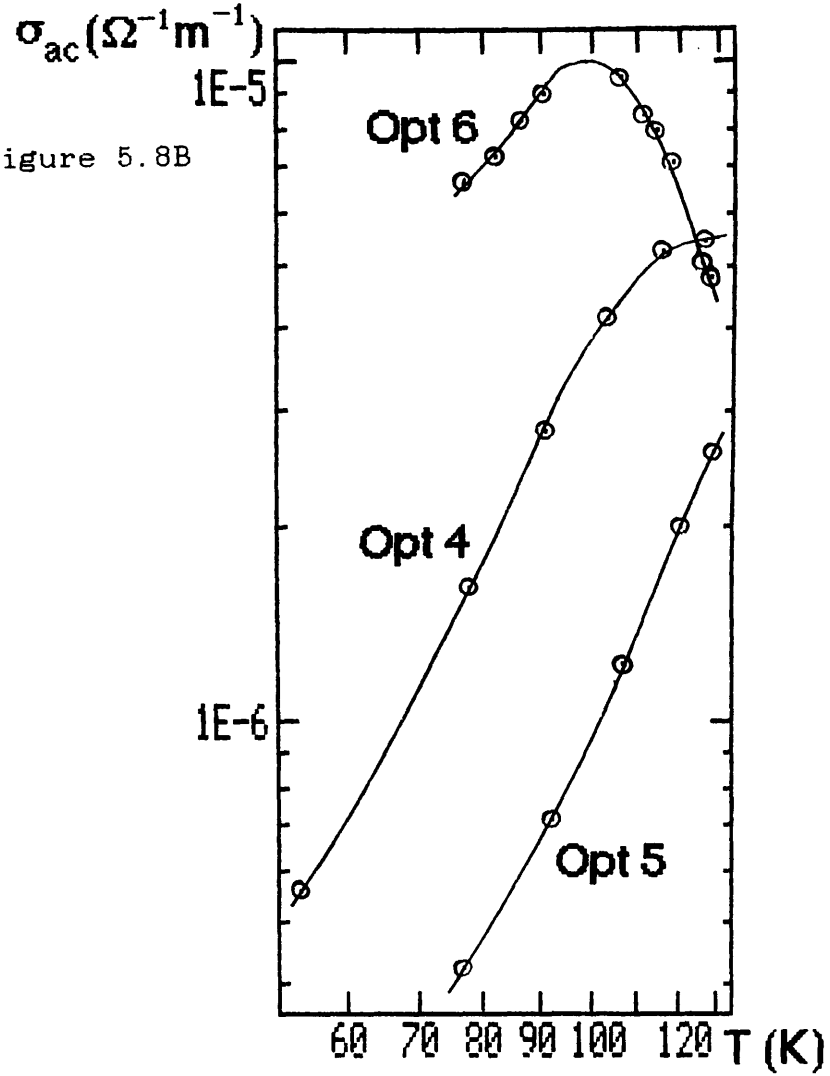

Figure 5.8 : The temperature dependence of the relative permittivity and the a.c. conductivity measured at 2kHz for Opt 4 (a-Si:H 20:1), Opt 5 (a-Si:H 10:1) and Opt 6 (a-Si).

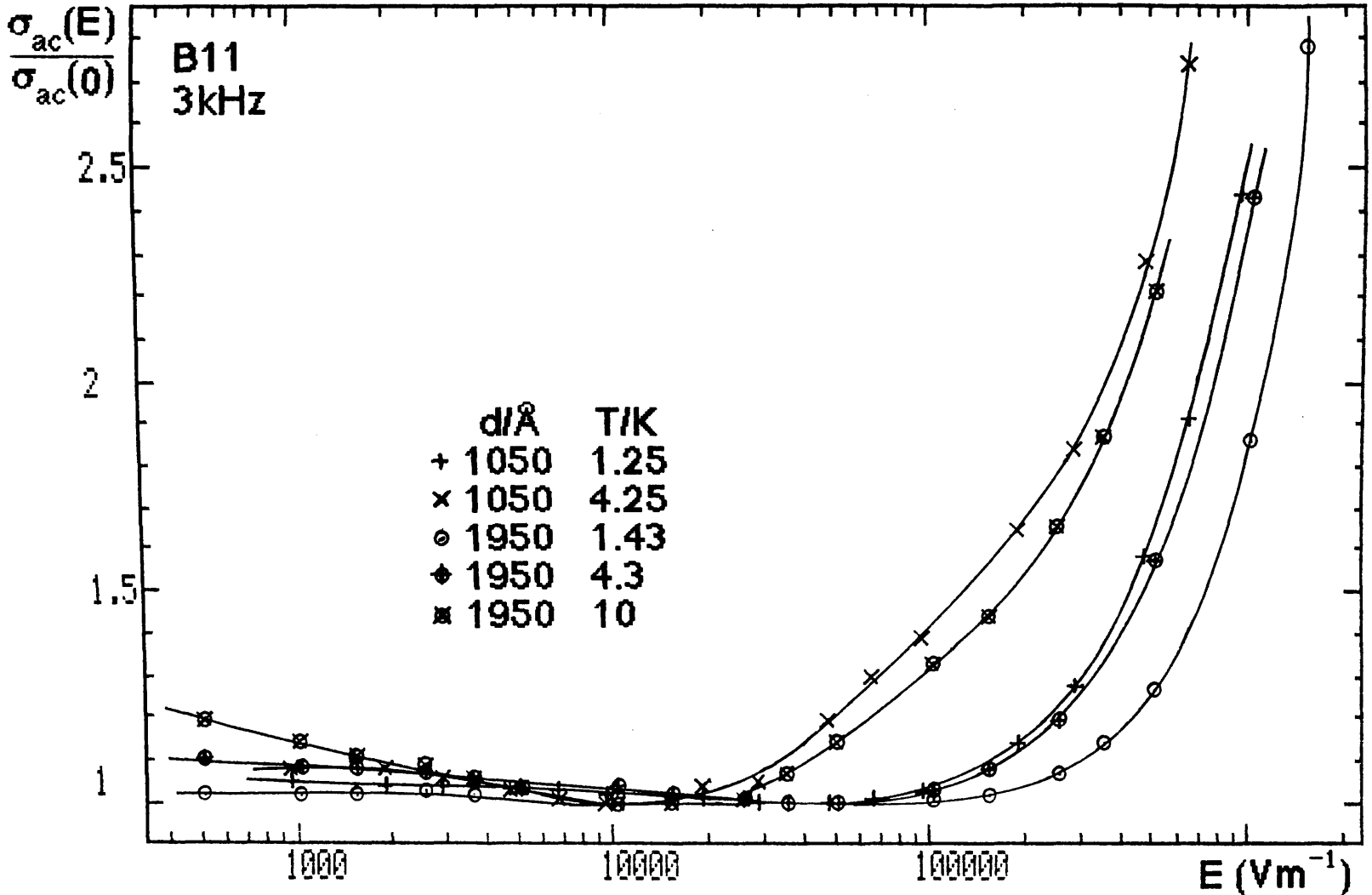

Figure 5.9 : The a.c. conductivity (measured at 3kHz) at different exciting fields normalized to that at low field for B11.

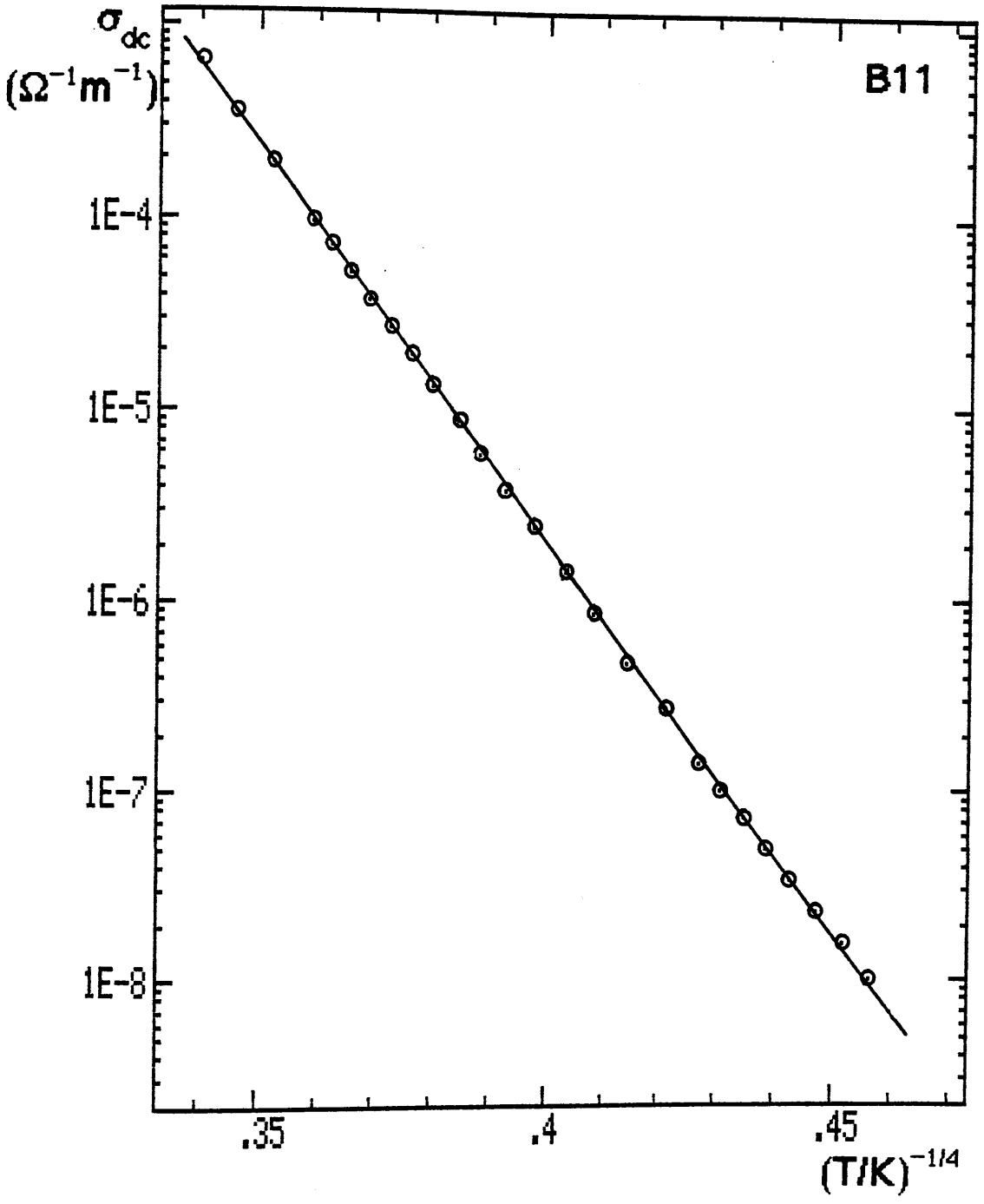

Figure 5.10 : The d.c. conductivity of B11 plotted against $T^{-1/4}$.

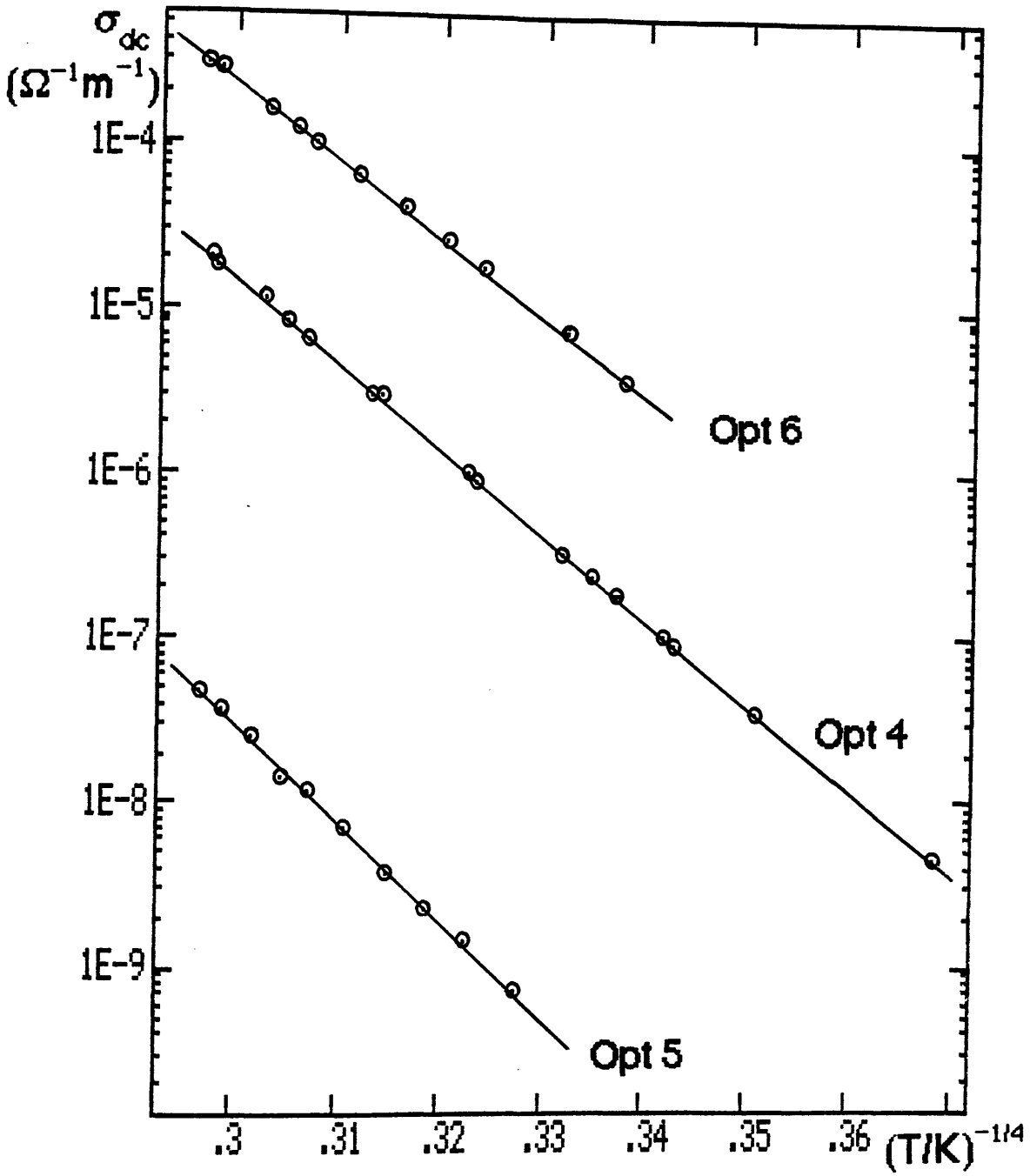

Figure 5.11 : The d.c. conductivity plotted against $T^{-1/4}$ for three silicon samples, Opt 4 (a-Si:H 20:1) Opt 5 (a-Si:H 10:1) and Opt 6 (pure a-Si).

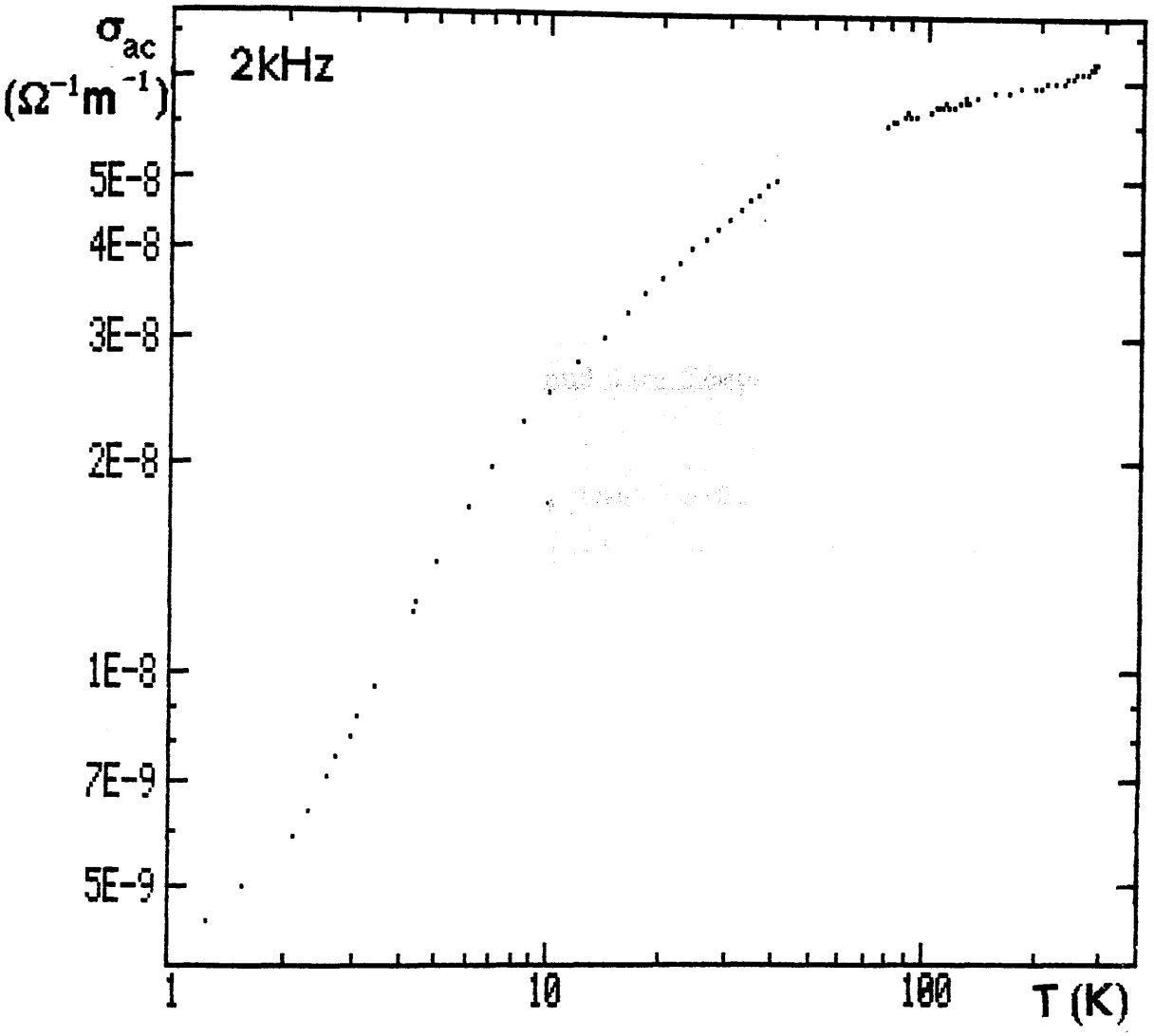

Figure 5.12 : Temperature dependence of the a.c. conductivity of the sputtered arsenic selenide sample.

CHAPTER 6 : Optically Induced Loss

In the following sections the results of optically excited changes in the low temperature capacitance and a.c. conductivity in amorphous tetrahedral thin films will be presented. The initial work on optically induced loss was done on a-Ge samples. The data, however, is more limited than that taken on a-Si. Some data on a-Ge samples will be presented to show the similarities between the two materials.

6.1 : The High Temperature and Low Temperature Effect

For most experiments, the a-Si thin films were illuminated with light derived from a He-Ne laser at 633nm through a semi-transparent top electrode. Illumination intensities of 1000nWcm^{-2} or less were used. Fig. 6.1 shows a change in the capacitance measured at 3kHz, for Opt 3, a pure a-Si sample, at different intensities and part of the recovery to the equilibrium state, at a temperature of 4K. Each increase in intensity causes an increase in permittivity which stabilizes at a new equilibrium value within about 1ks (1000s) at the lower intensities and more rapidly at higher intensities. Once the light is extinguished, at first, the permittivity rapidly falls towards the dark state value. At longer times the excess loss is inversely proportional to time ($\Delta C \propto 1/t$ for t>4ks). The recovery to equilibrium is non-exponential and usually many hours elapse before no further decrease can be detected.

The behaviour of the optically induced loss is similar

at 1.2K and 10K (see figs. 6.2 & 6.3). At 20K (fig. 6.4) and high intensity, the sample does not reach equilibrium under illumination in the time of measurement (1.6ks). Moreover the recovery to the dark state is not as rapid as at lower temperatures. At 60.2K (fig. 6.5) these effects are more pronounced. Little sign of capacitance saturation is seen at any intensity of illumination. After removal of the optical illumination return to equilibrium is much slower than at lower temperatures.

The data presented so far was taken using manual bridges. Figs. 6.6, 6.7 and 6.8 show measurements taken at 10K and 77K by the computer controlled system on Opt 5, a a-Si:H (10:1) sample. The return to the dark value of the capacitance can be followed over a much longer period of time. The initial rapid decay at 10K contrasts with the slow recovery of the capacitance at 77K. Fig 6.8 follows the decay at 77K over a period of 580ks or 6.7 days and 25% of the photo-induced capacitance change still remains.

Manual readings can only be taken once every two minutes, the time required to balance a bridge, whereas the HP LCR meter can take one reading a second. Figs. 6.9 and 6.10 take advantage of the rapid response of the computer controlled system. Fig 6.9 is an enlarged version of fig. 6.6 and shows the initial rise on the application of the highest intensity used. The rise is instantaneous (<1s) on the time scale of this experiment at 4K. Fig. 6.10 is a plot on the same time scale for the 77K data. The slow rise of the capacitance at this temperature can easily be followed.

All data taken by the automatic system has been corrected for temperature drift as described in §4.5.3. The

inset of fig 6.6 illustrates the distortion of the capacitance-time plot caused by temperature drift at the end of a long experiment, carried out at 10K.

Finally a capacitance-time plot taken at 4K on Opt 6 (pure a-Si) is shown in fig 6.11.

Two separate optical effects are apparent in all this data, one at helium temperatures which responds at intensities of less than $5x10^{-3}nWcm^{-2}$ and another at nitrogen temperatures which require higher intensities of light ($I_o>2nWcm^{-2}$). The former is characterized by instantaneous rises in permittivity to new equilibrium values and equally rapid falls on the removal of excitation. The latter is more gradual by nature, involving slow continual changes and no stable equilibrium values within the time scale of the experiment. The 20K data shows characteristics of both the high and low temperature effects.

The differences between the two effects can also be seen by measuring the response of the loss to pulses of light. Figs. 6.12 to 6.14 show the response of Opt 3 to 5s, 30s and 120s pulses of equal intensity, at 4K, 20K and 77K. These results were taken with the home-made manual bridge. A 5s pulse of intensity $950nWcm^{-2}$ has no effect at 77K. A limited response to a 5s pulse is seen at 20K. The response at 4K is almost equal to that for a 30s pulse, however, after the 5s pulse a more rapid return to equilibrium is observed. The high temperature effect has a response time of greater than 5s at this intensity.

6.2 : The Intensity Dependence at Low Temperatures

In fig. 6.15 the changes in the relative permittivity associated with the equilibrium behaviour at each intensity level are plotted against intensity, on a logarithmic scale, for Opt 3. The response is non-linear; at high intensities the permittivity increases at a low power of intensity, typically $I^{1/4}$, but at low intensities the response is closer to $I^{1/2}$. At high intensities the temperature dependence is weak; at low intensities there is a stronger temperature dependence. There is no measureable response at temperatures of 10K and above at lowest intensities used. Fig. 6.16 shows the a.c. conductivity changes at each intensity for the same experiment. The form of the data is very similar to that for the permittivity changes.

Fig. 6.17A is a plot of permittivity changes against temperature for two different intensity values. It can be seen that the value of $\Delta\varepsilon_1$ changes little between 1.28K and 20K. The same can be said for $\Delta\sigma_{ac}$ (see fig. 6.17B) even though the dark a.c. conductivity rises in this temperature range (the temperature exponent, n = 0.5).

The intensity dependence plot for Opt 6 (fig. 6.18) also shows a non-linear response. The transition between the low intensity region ($I^{1/2}$) and the high intensity region ($I^{1/4}$) is not as sharp as in Opt 3. The intensity used in these plots is the surface intensity, I_o. As the 633nm light penetrates the thin film, the intensity will begin to decrease below I_o. This effect is much more pronounced in Opt 6 (d=7320Å) than in Opt 3 (d=860Å). In Opt 6, at the intermediate intensities of light, the shallow sections of the

thin film may be in the high intensity, $I^{1/4}$, region while the deep layers are in the $I^{1/2}$ region. Hence the response of the Opt 6 thin films at this intensity is a mixture of the two regions and no definitive change change between the two regions can be seen.

The other tetrahedral thin films also showed a non-linear response. Figs. 6.19 and 6.20 are the intensity plots for the two a-Si:H samples, Opt 5 (10:1) and Opt 4 (20:1). The intensity dependence of Opt 1 (pure a-Ge) and Opt 2 (hydrogenated a-Ge, 4:1) are presented in figs. 6.21 and 6.22. The plots for Opt 1, Opt 2 and Opt 4 show a slightly reduced response at 1.3K compared to 4K in contrast to the trend of a decreased response with increasing temperature evident in the data at temperatures above 4K. A possible explanation of this anomaly is that the dark equilibrium value of capacitance at 1.3K may not be reached for many hours after the sample temperature reaches 1.3K. The limitations of the cyrogenic equipment do not allow the maintenance of a temperature of 1.3K over very long periods of time. The time taken for samples to "relax" into their dark equilibrium even at 4K can be considerable, especially in hydrogenated material (see §6.6).

Table 6.1 records the intensity exponent in the high and low intensity regions as deduced from the permittivity data for the silicon samples. Table 6.2 shows the same parameters deduced from the change in a.c. conductivity for Opt 1, Opt 2 and Opt 3.

6.3 : The Free Decay to Equilibrium

The recovery to the dark state at temperatures of 4K and 10K is presented in fig. 6.23 for Opt 6 The figure shows $\Delta\varepsilon_1$ as it decreases towards zero over a period of 90ks, after illumination with 633nm light of intensity = 2850nWcm^{-2}. The initial 1000s of the decay is shown in fig. 6.24. The two decay curves run parallel from a time of less than 10s after extinction of the light; the difference between the two remains constant at $\Delta\varepsilon_1 = 8\times10^{-3}$.

The recovery to the equilibrium state is shown for Opt 3 at 1.3K, 4K and 10K in fig 6.25. The time over which measurements were taken is rather shorter than for Opt 6. The 4K and 10K decays are parallel, separated by $\Delta\varepsilon_1 = 2\times10^{-2}$. The difference between the 1.3K and 4K curves starts at $\Delta\varepsilon_1 = 1\times10^{-2}$ and grows to 2×10^{-2} after 7ks.

The variation of $\Delta\varepsilon_1$ with 1/t has already been noted for Opt 3 at long times (t > 4ks). A plot of the excess permittivity against 1/t reveals a discontinuity in the decay (fig.6.26). The value of $\Delta\varepsilon_1$ at which the change in gradient occurs (4.2×10^{-2}) is approximately equal to the value of $\Delta\varepsilon_1$ at the change from $I^{1/2}$ to $I^{1/4}$ behaviour on the intensity plot (fig. 6.12). Similar discontinuities in the 1/t decays of Opt 5 and Opt 6 can be seen in figs. 6.27 to 6.30. Table 6.1 compares the transition values of $\Delta\varepsilon_1$ deduced from the intensity plot and those deduced from the free decays. The correlation between these results suggests that the two types of graph are different views of the same physical phenomenon.

The gradient changes in the 1/t plot for Opt 6 are less obvious than in the Opt 3 data in the same way that the

transition between between $I^{1/4}$ and $I^{1/2}$ behaviour for Opt 6 is not as distinct as the transition in the Opt 3 data. The thickness of Opt 6 is ten times that of Opt 3. The slow change in the gradient of the 1/t plot for the thicker sample can perhaps be explained by the lack of uniformity of excitation through the semiconductor film (as discussed in §6.2).

6.4 : Frequency Dependence of the Permittivity Change

The data presented so far in this chapter have been based on capacitance measurements at a frequency of 3kHz for the manual bridges and 2kHz for the HP LCR meter. The introduction of the HP instrument allowed a frequency sweep (the measurement of capacitance and conductance at frequencies between 100Hz and 100kHz) to be taken within a few minutes rather than the 90 minutes required for a manual bridge. Using the computer controlled system it was possible to take frequency sweeps at each equilibrium value of capacitance reached with each new intensity.

The results are shown in figs. 6.31 and 6.32 as the change in permittivity divided by the dispersive part of the dark permittivity $\Delta\varepsilon_1/(\varepsilon_1 - \varepsilon_\infty)$. At 4k and at high intensities, the response of Opt 6 decreases as the frequency increases with a frequency exponent of (-0.10 ± 0.01). The frequency exponent of the dispersive part of the dark permittivity, s'=s-1 (from eqn 4.1), hence s' at 4.24K = (-0.107 ± 0.005). At 10K the frequency exponent of the light induced response is (-0.12 ± 0.01) and for the dark

permittivity, s' = (-0.163 ± 0.005), at this temperature. From this evidence we can assert that the frequency dependence of the induced loss (at high intensities) is approximately equal to that of the dark loss.

The peaks recorded at 3kHz and 30kHz at the lower intensities seen at both temperatures could not be connected to inaccuracies in measurements by the LCR meter and may be a fundamental properties of the sample. The position of the peaks changed when different wavelengths of light (500nm and 800nm) were used to excite the loss.

6.5 : Response at Different Optical Wavelengths

A wide band source and a monochromator were used to produce light at wavelengths of 500nm and 800nm. The intensity dependence of the permittivity changes induced by these wavelengths of light is shown for Opt 6 in fig. 6.33.

The transition between the $I^{1/2}$ and the $I^{1/4}$ region is a little more distinct for 800nm light than for lower wavelengths. 800nm light penetrates a-Si more easily than 633nm or 500nm light (see Appendix C). Hence the radiation will be absorbed more uniformly at this wavelength. As the intensity is decreased the whole of the film will transfer from the $I^{1/4}$ to the $I^{1/2}$ region at a similar intensity. At lower, less penetrating wavelengths the deepest layer of the film will enter the $I^{1/2}$ region first. The transition is therefore more definite at 800nm.

The intensity scale on all the plots is based on surface intensity; no account is taken of the absorption coefficient

of a-Si at different wavelengths. The results presented here will be analysed further in §7.8.

6.6 : Thickness Dependence

The Opt 6 sample consisted of two semiconductor junctions. The first, on which most measurements were taken, was 7320Å thick; the second was 4000Å thick. By taking optically induced loss measurements on both junctions it was hoped that conclusive evidence would be produced that the changes in loss are bulk effects and not surface or electrode related phenomena. The intensity plots for the two junctions at 4K are shown in fig. 6.34.

The intensity scale is corrected for the different positions of the junctions with respect to the fibre optic output in the sample can,so the scale is representive of the surface intensity at each junction. However the surface intensity values are not adequate to compare the thick and thin junctions of Opt 6. Only 2% of the 633nm light entering the 4000Å a-Si layer is transmitted through to the other side (see Appendix 3). It is reasonable to assume that the deepest 3320Å of the thick junction will receive a very low intensity of light and will play little part in any photo-induced excess loss. A more sophisticated analysis of the data is therefore required (§7.8).

6.7 : The Relaxation of Samples at Helium Temperatures

The long-term low-temperature insert, which was used for Opt 5 and Opt 6, allowed the maintenance of helium temperatures over many days. The temperature stability of this system highlighted the length of time required for samples to achieve an electrical dark equilibrium value. The curves presented in figs. 6.35 and 6.36 show the fall in capacitance of Opt 5 and Opt 6 respectively after a stable temperature of 4.24K had been reached (as measured by the Ge thermometer attached to the copper tailpiece of the insert).

The heavily hydrogenated Opt 5 (10:1) took 30 hours to register a fall of 0.4%; the decrease continues in a slower, more erratic way for a further 60 hours. Even after this long period the capacitance is still 0.4% above its lowest recorded base value. Opt 6, the pure a-Si sample, decreases in capacitance by 0.1% in 15 hours and is still 0.05% above its base value.

6.8 : A Comparison of Capacitance and Conductance

The capacitance and a.c. conductance measurements show a similar response to optical light. If the intensity plots of the two sets of data for Opt 3 are compared (figs. 6.15 and 6.16) the same features are seen. The intensity exponents of in the high and low intensity regions are equal within error (see tables 6.1 and 6.2). The a.c. conductivity also mirrors the capacitance in such characteristics as the speed of the rise of the photo-induced loss at different intensities of

light and at different temperatures.

Capacitance is measured more accurately by the a.c. bridges and is not susceptible to photo-induced changes in the d.c. conductivity; hence the concentration on the capacitance data for most of this chapter.

6.9 : Photo-induced D.C. Conductivity

The d.c. conductivity of the samples would increase typically by an order of magnitude at helium temperatures on the application of the greatest intensities used. On the removal of light the d.c. conductivity appeared to fall rapidly towards its dark value. The measurement of a d.c. value at 4K takes a minimum of 600s. Within 2ks of the removal of excitation, the d.c. conductivity was usually sufficiently close to its dark equilibrium as to be equal to the equilibrium d.c. conductivity within the error of the measurement. For example, with Opt 1 (pure a-Ge), the application of 440nWcm^{-2} of 633nm light increased the d.c. conductivity from 4.2x10^{-10} Sm^{-1} to 1.3x10^{-9} Sm^{-1}. 1.5ks after the removal of the light, the d.c. conductivity had fallen to 5.6x10^{-10} Sm^{-1}, 15ks later this had fallen to 3.9x10^{-10} Sm^{-1}.

The primary purpose of measuring the d.c. photoconductivity was to check that its effect on the total conductivity, as measured by the a.c. bridges, was small. Where appropriate the enhanced d.c. conductivity was subtracted to calculated the a.c. photoconductivity. Fig. 6.37 compares $\Delta\sigma_{dc}$ and $\Delta\sigma_{ac}$ for Opt 2 between 1.2K and 77K

at a fixed intensity of 3670nWcm^{-2}. As no equilibrium value of $\Delta\sigma_{ac}$ can be recorded at 77K, the value used in this figure is the enhanced a.c. photoconductivity after 1ks. The ratio $\Delta\sigma_{dc}/\Delta\sigma_{ac}$ is 0.15 at 77K and .0075 at 4K. It is clear that the d.c. photoconductivity has little effect on the light induced a.c. loss.

Fig 6.38 shows the dependence of the d.c. photo conductivity on exciting intensity. Below 1000nWcm^{-2} $\Delta\sigma_{dc}$. increases as $I^{1/2}$, above this intensity $\Delta\sigma_{dc}$ varies linearly with intensity.

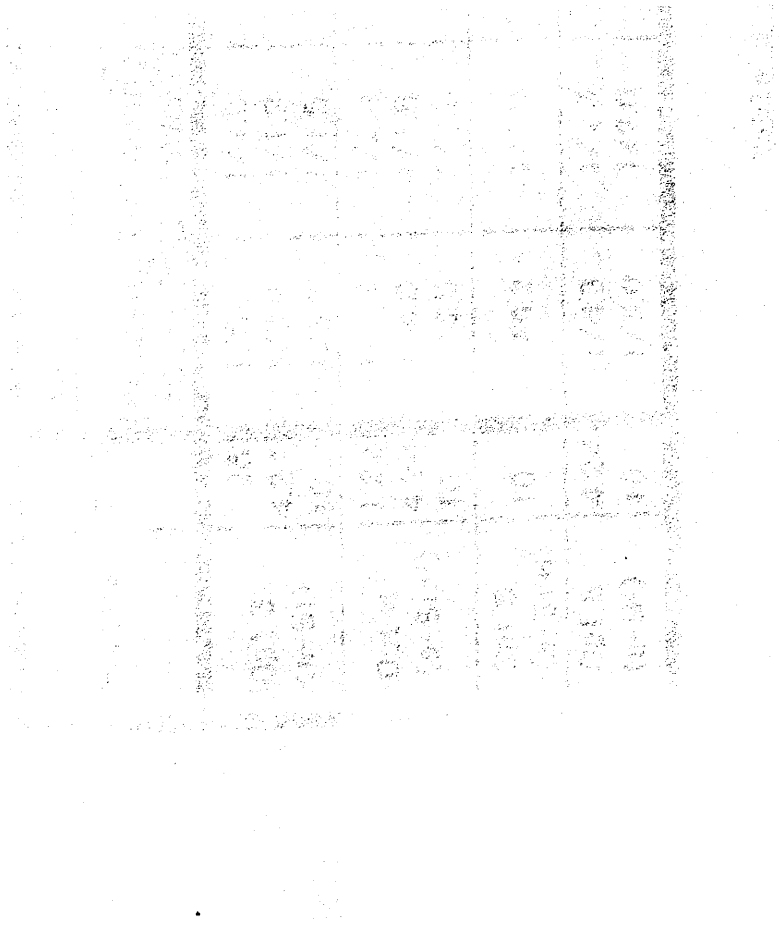

Sample	T(K)	$\Delta\varepsilon_1 \alpha I^A$ (Intensity >10nWcm^{-2})	$\Delta\varepsilon_1 \alpha I^B$ (.01nWcm^{-2}> I >1nWcm^{-2})	Transition Value of $\Delta\varepsilon_1$	
				$\Delta\varepsilon_1 \alpha I$	$\Delta\varepsilon_1 \alpha 1/t$
Opt 3 (a-Si)	1.28	1/5.3	1/1.6	$(5 \pm 1)\times10^{-2}$	$(5.0\pm0.2)\times10^{-2}$
	4.24	1/3.9	1/1.9	$(5.5 \pm 1)\times10^{-2}$	$(4.2\pm0.8)\times10^{-2}$
	10	1/3.8	1/1.5	$(5 \pm 1)\times10^{-2}$	$(2.9\pm0.1)\times10^{-2}$
Opt 4 (a-Si:H)	1.22	1/4.2	1/2.4	$(1.9\pm 0.4)\times10^{-2}$	——
	4.24	1/4.8	1/1.8	$(2\pm0.7)\times10^{-2}$	——
	10	1/3.5	1/1.9	$(2\pm0.6)\times10^{-2}$	——
Opt 5 (a-Si:H)	10	1/4.2	1/1.9	$(1.1\pm 0.5)\times10^{-2}$	$(1.5\pm0.1)\times10^{-2}$
Opt 6 (a-Si)	4.24	1/4.3	1/2.3	$(3.4\pm 1)\times10^{-2}$	$(4.0\pm0.2)\times10^{-2}$
	10	1/5.0	1/2.0	$(3.6 \pm 1)\times10^{-2}$	$(3.8\pm0.1)\times10^{-2}$

Table 6.1

Sample	T(K)	$\Delta\sigma_{ac} \alpha I^{A}$ (Intensity $>10nWcm^{-2}$)	$\Delta\sigma_{ac} \alpha I^{B}$ ($.01nWcm^{-2} > I > 1nWcm^{-2}$)
Opt 1 (a-Ge)	1.3	1/3.9	——
	4.24	1/3.5	——
Opt 2 (a-Ge:H)	1.3	1/3.7	——
	4.24	1/4.9	1/2.8
	10	1/4.1	——
Opt 3 (a-Si)	1.28	1/4.8	1/1.9
	4.24	1/4.8	1/2.4
	10	1/4.0	1/1.8

Table 6.2

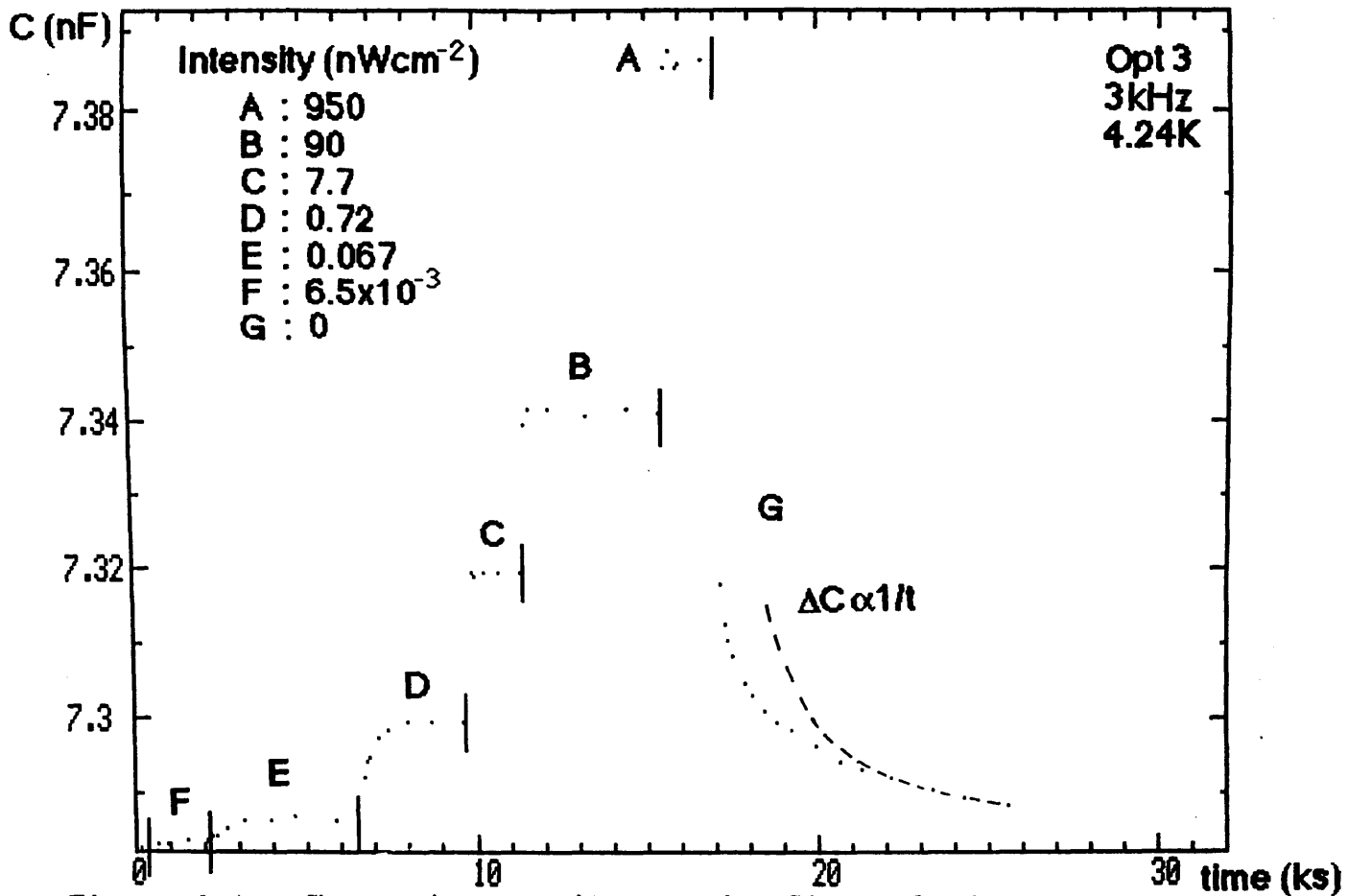

Figure 6.1 : Change in capacitance of a-Si sample Opt 3 under illumination at 4.2K versus time. Measurements made by the manual General Radio Bridge. Intensity values are corrected for Si reflectance and top electrode transmittance (error of I = ±25%). Light wavelength = 633nm. The free decay after 17ks is fitted to a 1/t relation.

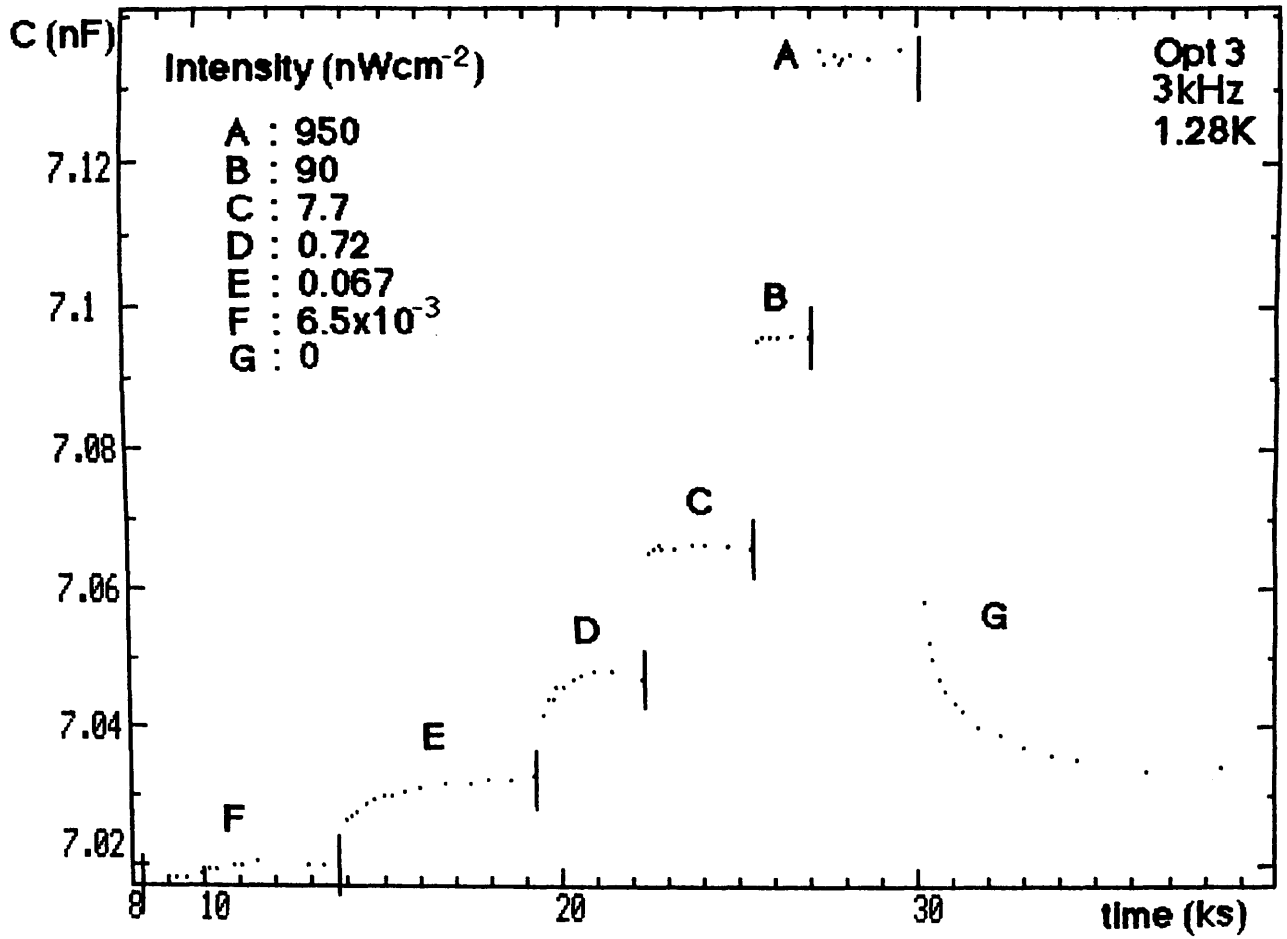

Figure 6.2 : Change in capacitance of Opt 3 versus time measured at 1.3K.

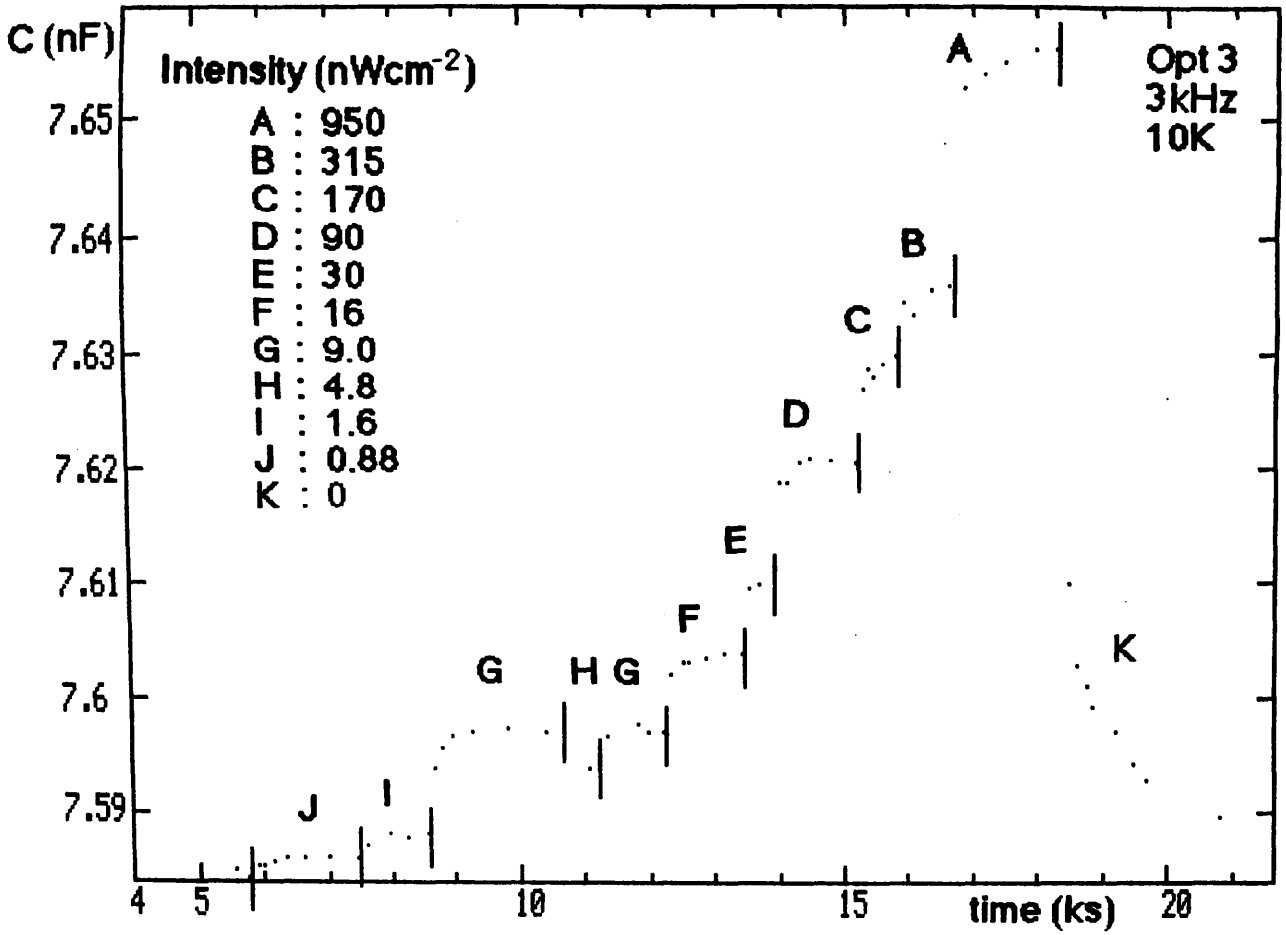

Figure 6.3 : Change in capacitance of Opt 3 versus time measured at 10K.

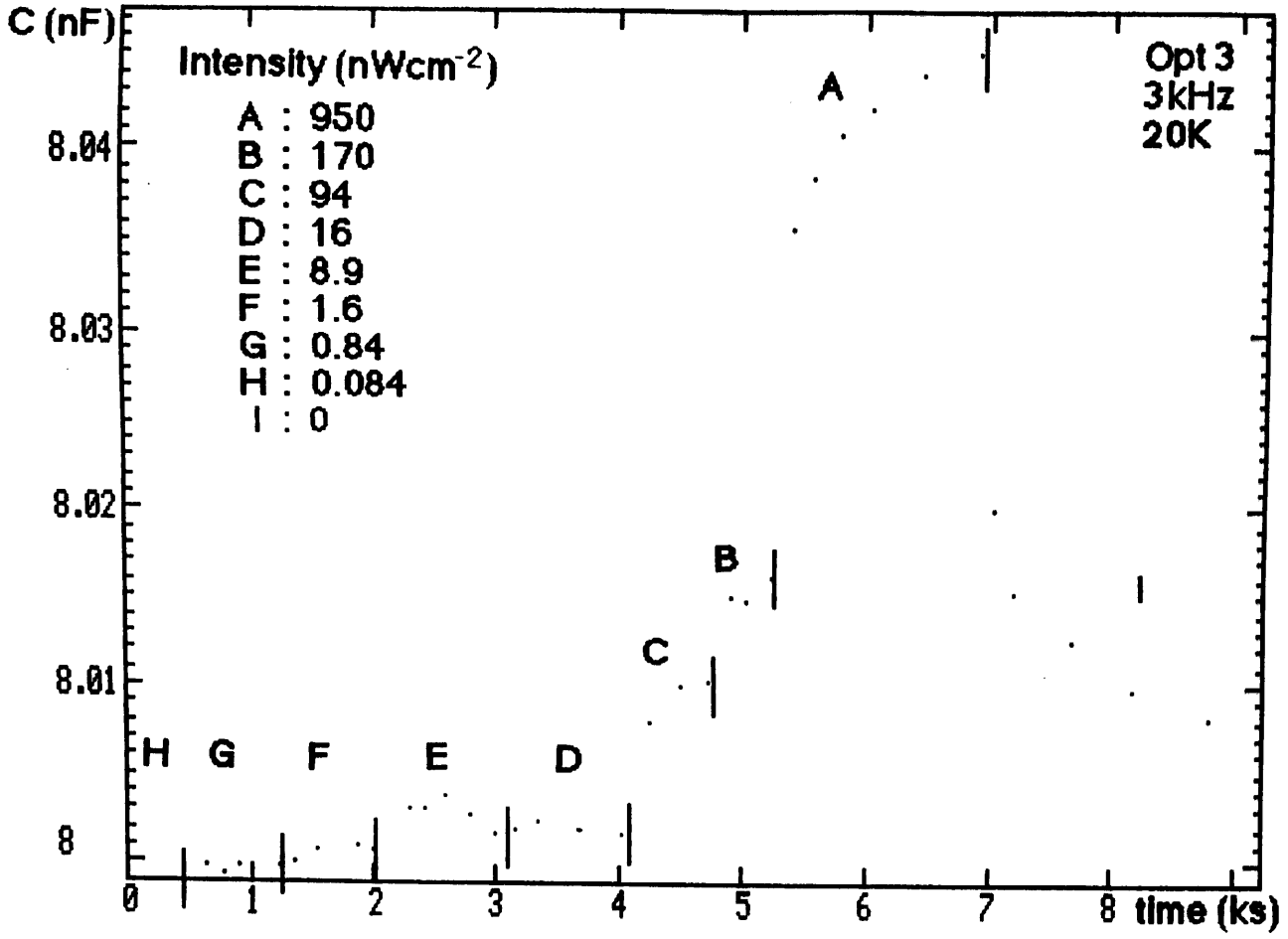

Figure 6.4 : Change in capacitance of Opt 3 versus time measured at 20K.

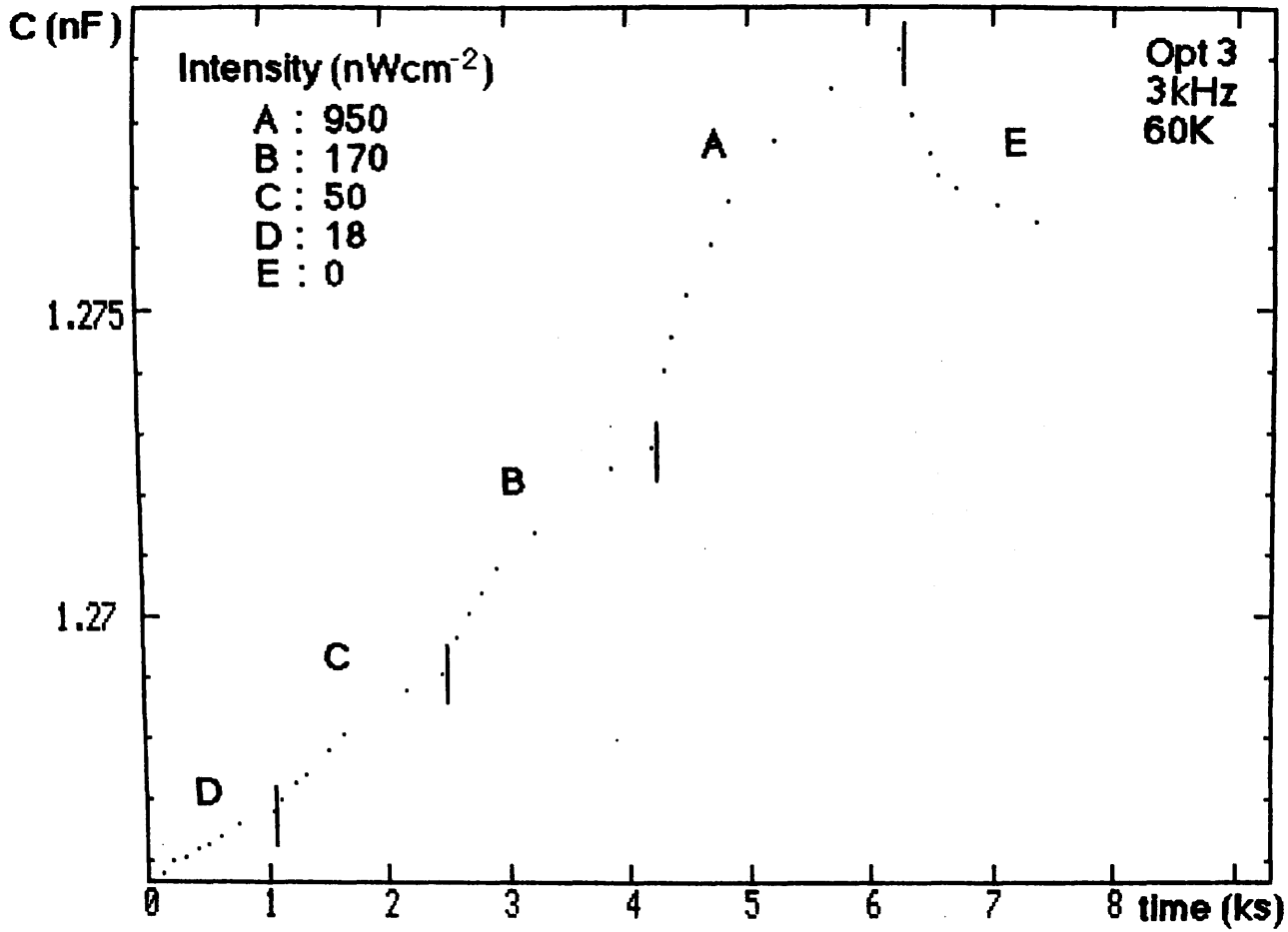

Figure 6.5 : Change in capacitance of Opt 3 versus time measured at 60K.

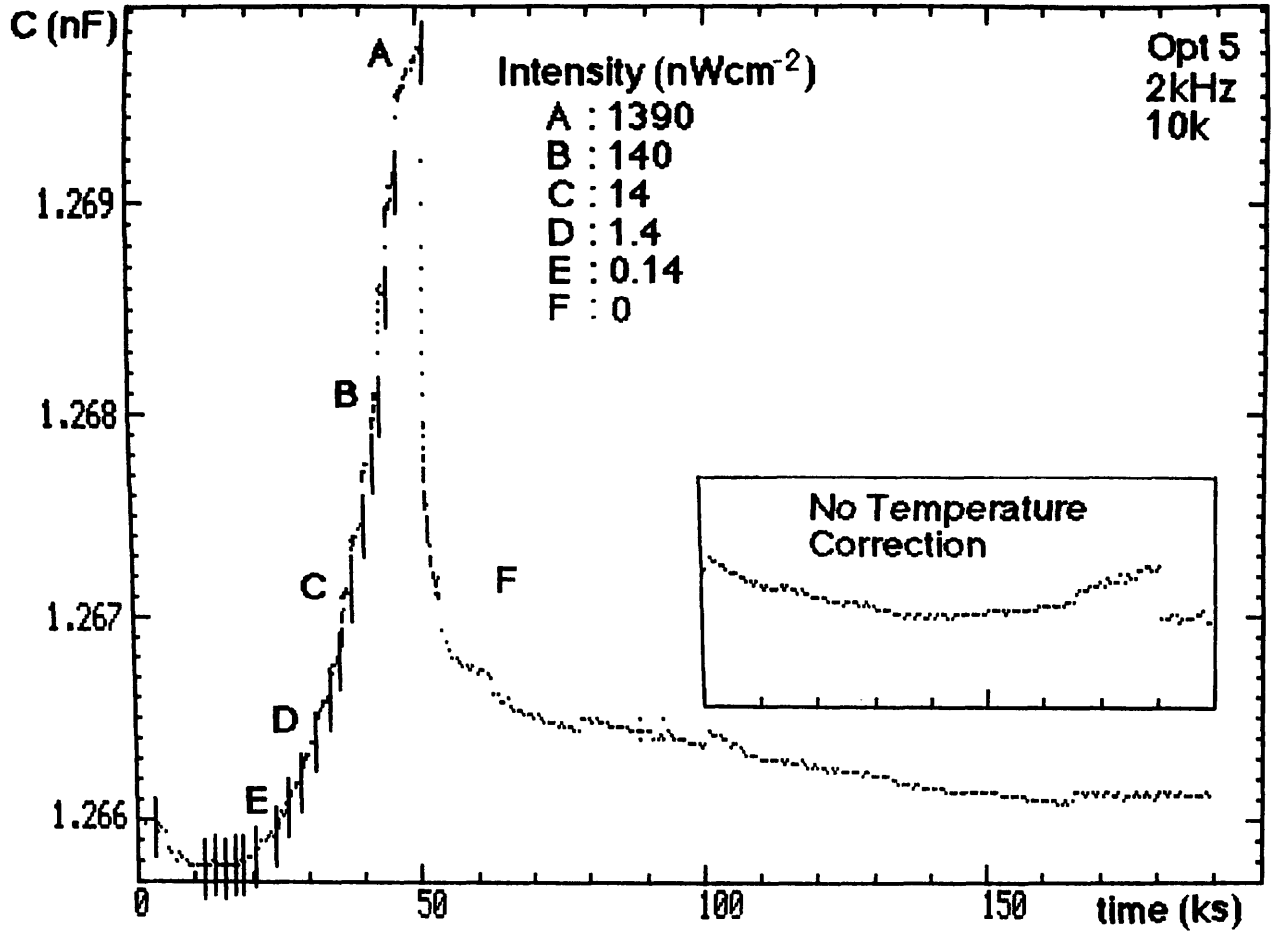

Figure 6.6 : Change in capacitance of Opt 5 (a-Si:H 10:1) versus time measured at 10K by the computer controlled system. The data has been corrected for temperature drift. Raw data is shown in the inset.

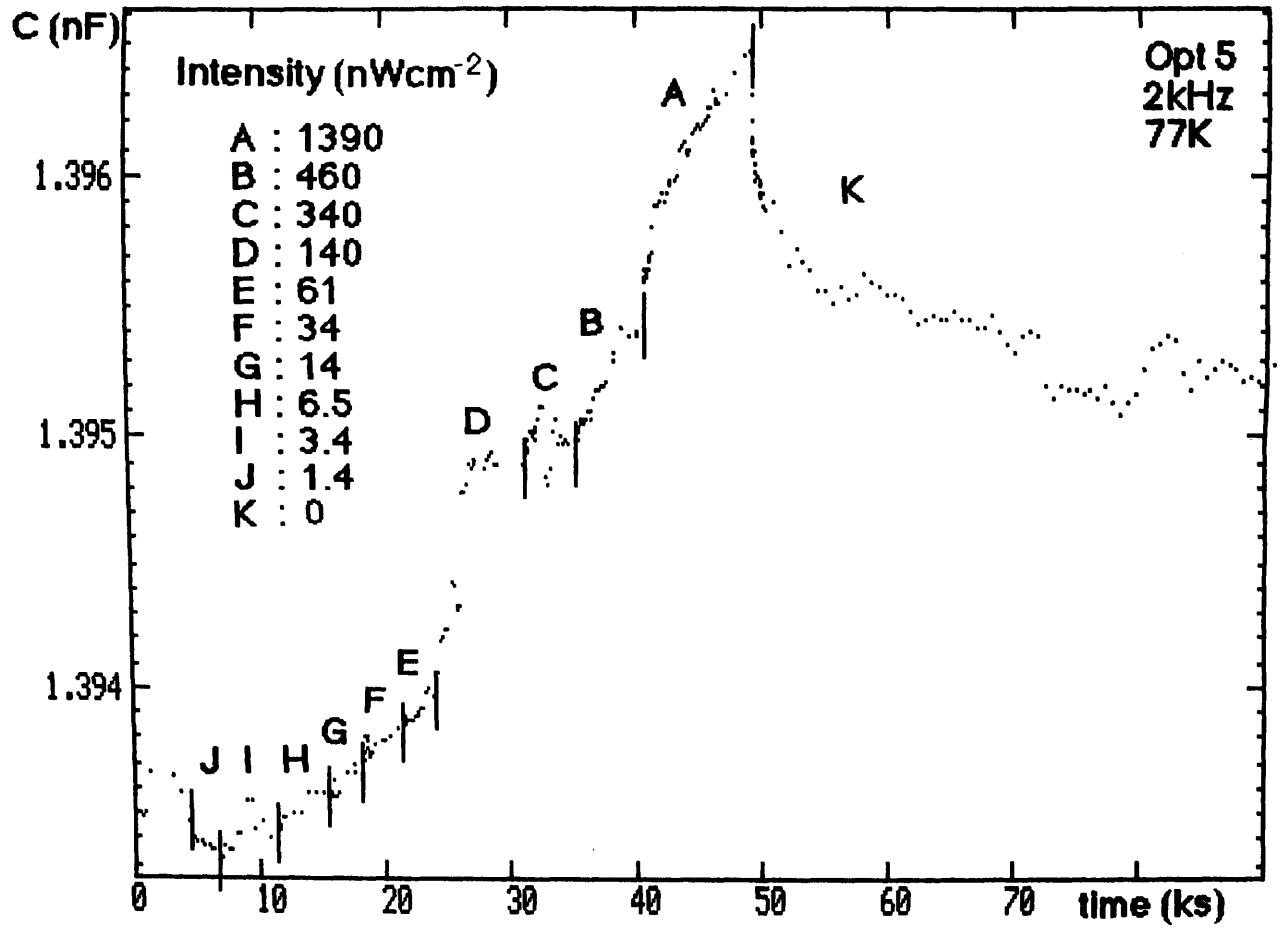

Figure 6.7 : Change in capacitance of Opt 5 versus time measured at 77K by the computer controlled system.

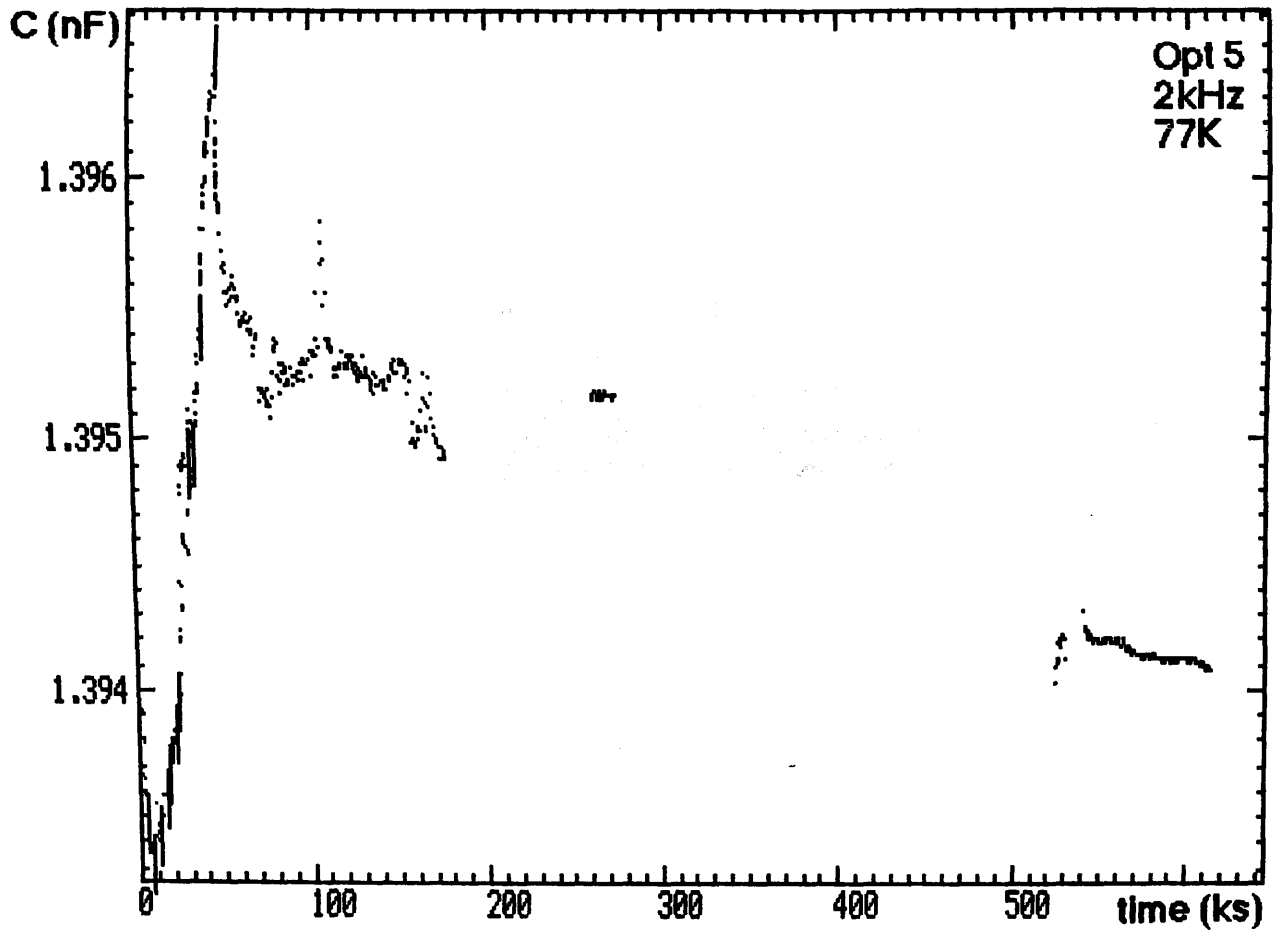

Figure 6.8 : Data of fig. 6.7 showing the decay to dark equilibrium after the exciting light has been extinguished.

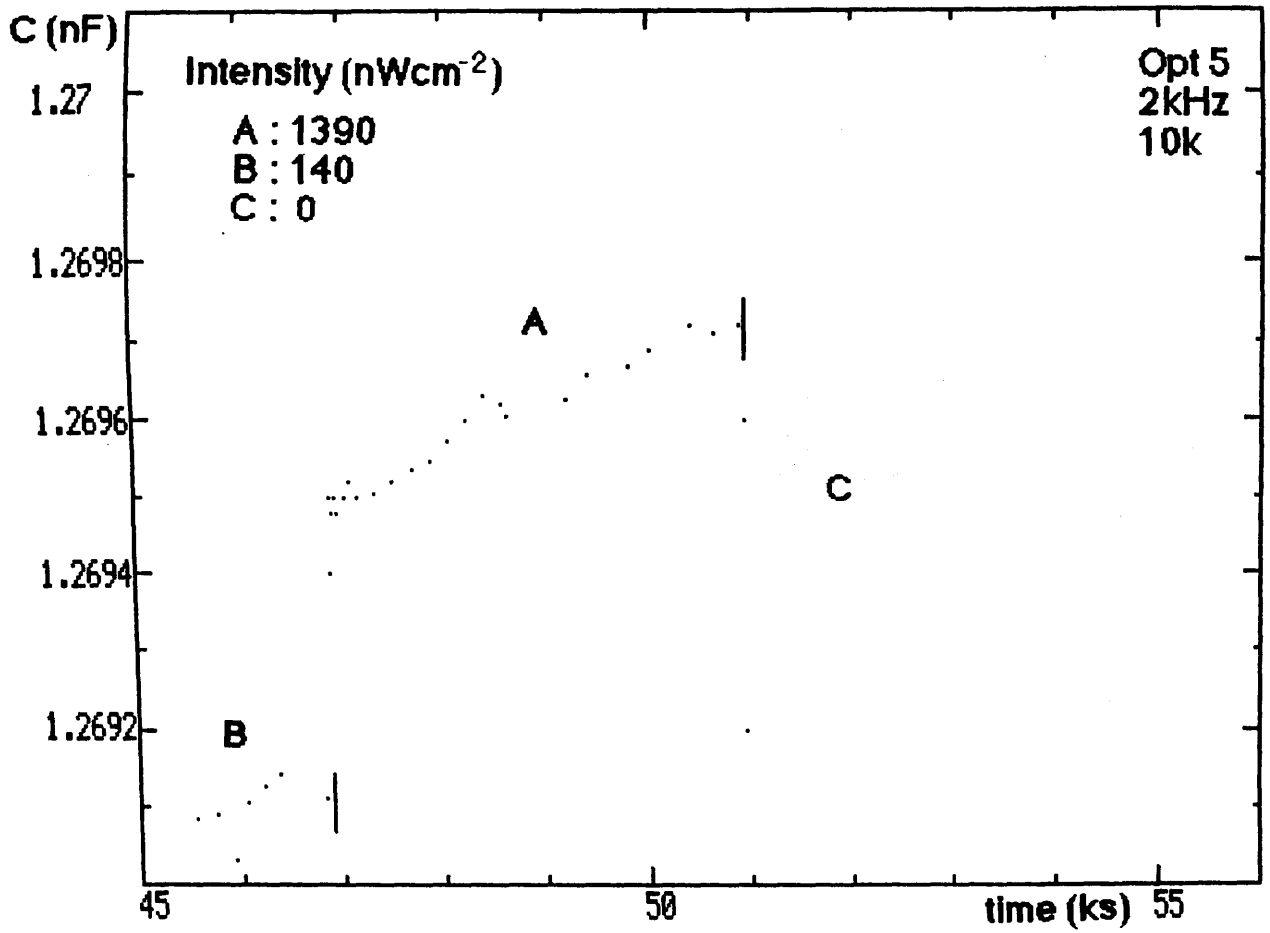

Figure 6.9 : Data of fig. 6.6 (Opt 5, T=10K) showing, in detail, the rise in capacitance on applying the highest intensity used and the beginning of the return to equilibrium.

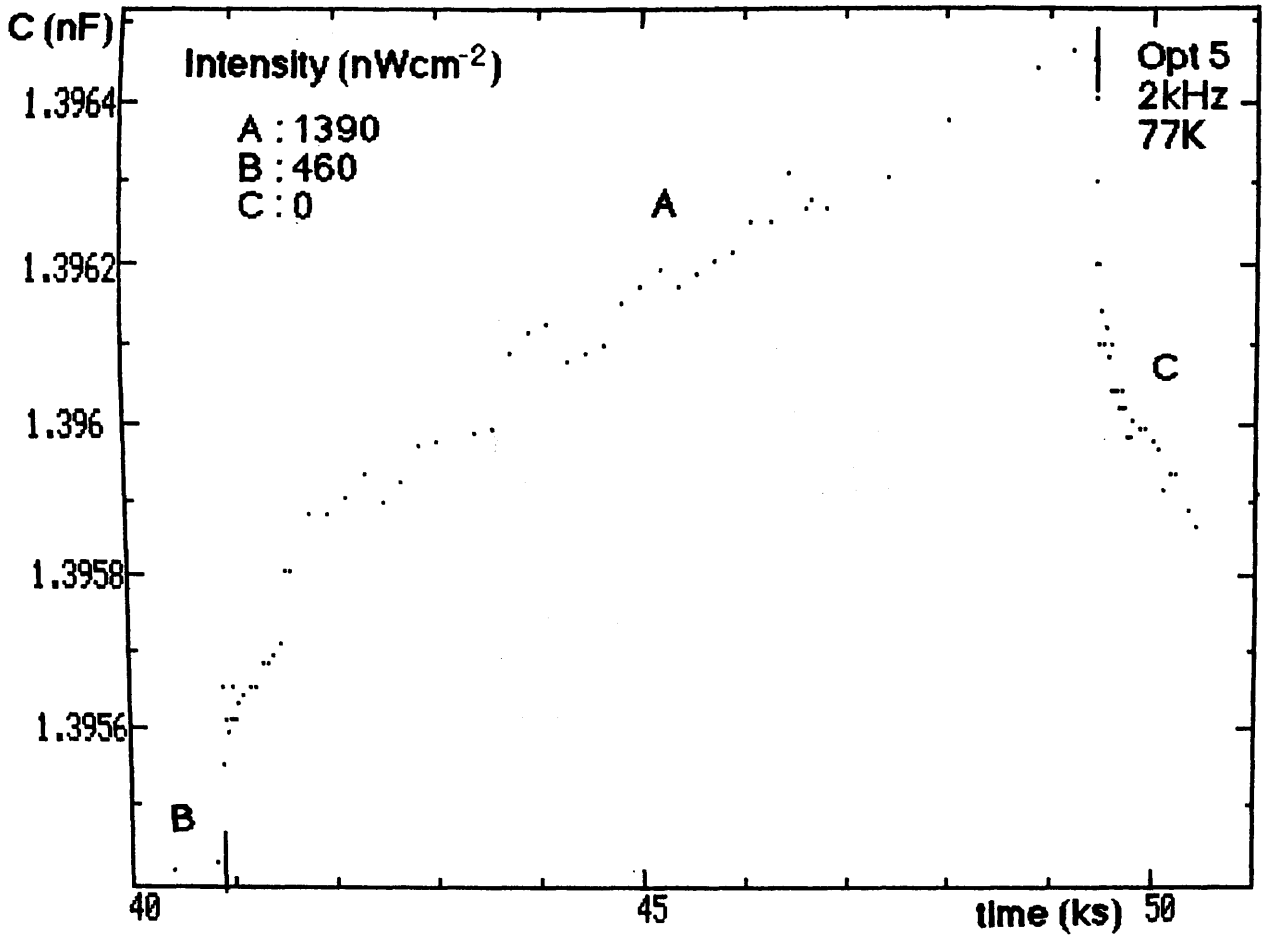

Figure 6.10 : Data of fig. 6.7 (Opt 5, T=77K) showing, in detail, the rise in capacitance on applying the highest intensity used and the beginning of the return to equilibrium.

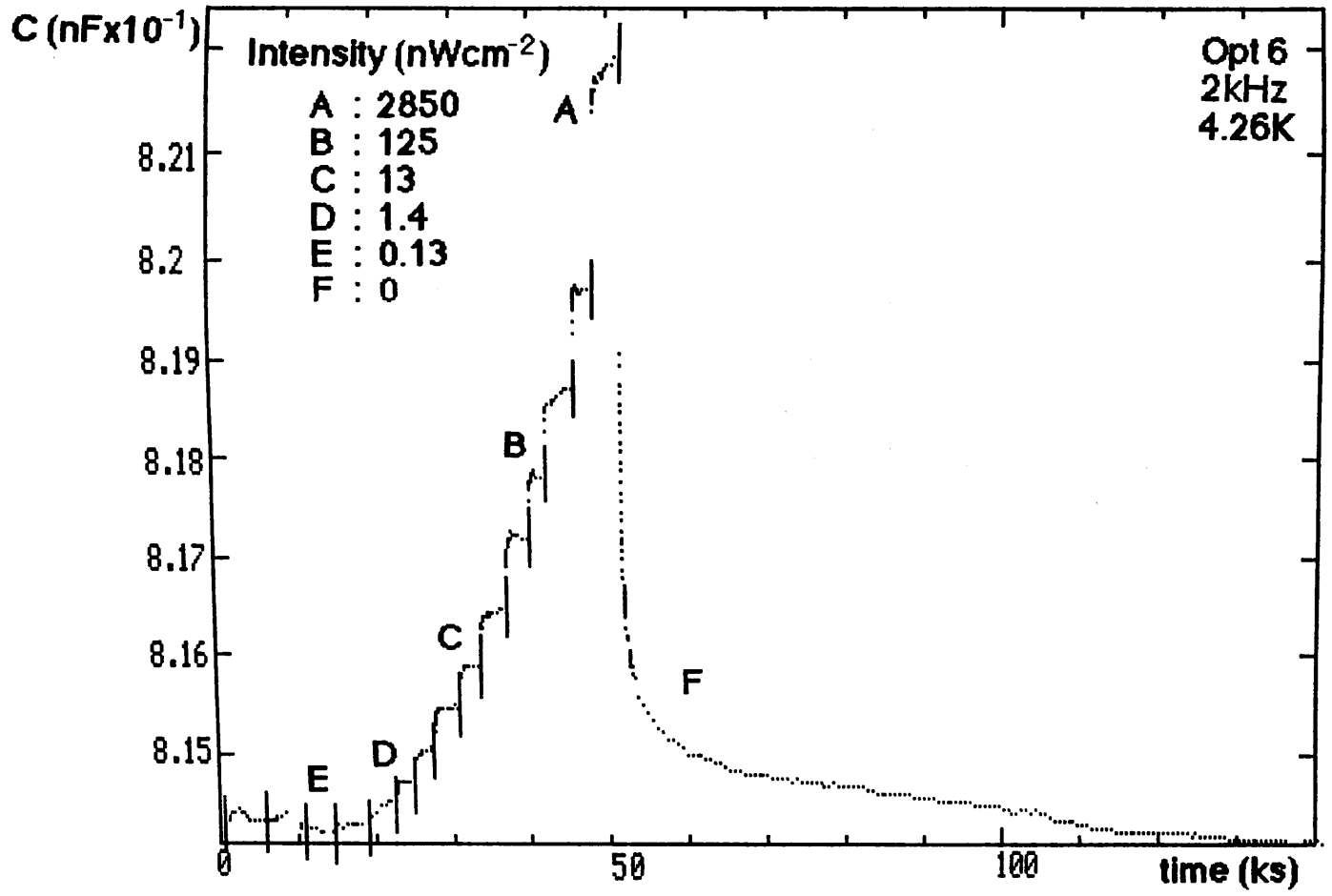

Figure 6.11 : Change in capacitance of Opt 6 (magnetron sputtered pure a-Si) versus time measured at 4.26K by the computer controlled system.

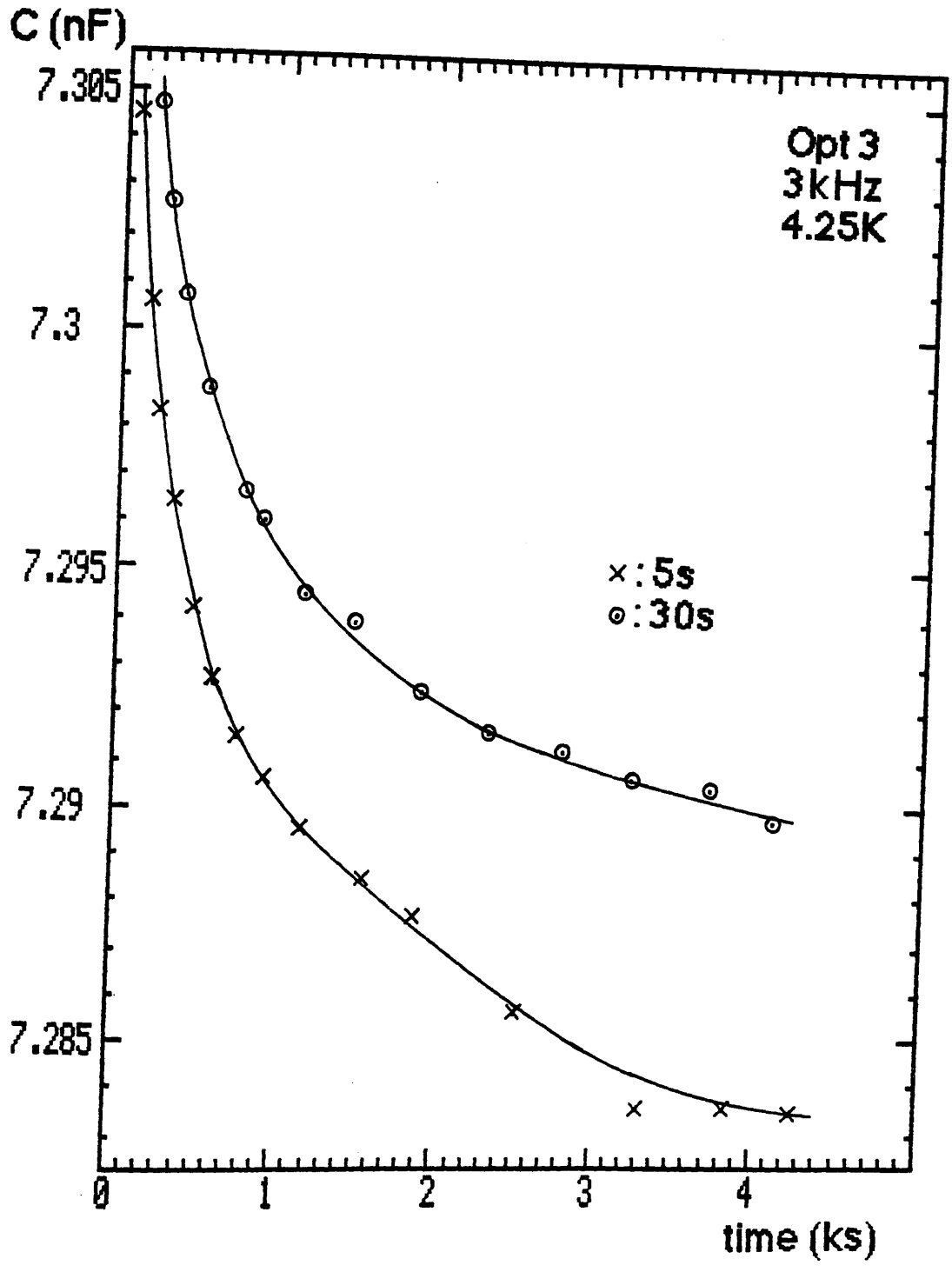

Figure 6.12 : The decay of the capacitance in the dark after short pulses (5s and 30s) of 633nm light were applied to Opt 3 (pure a-Si) at 4.25K. Pulse intensity, I_o = 950nWcm^{-2}. Measurements taken by the manual General Radio Bridge.

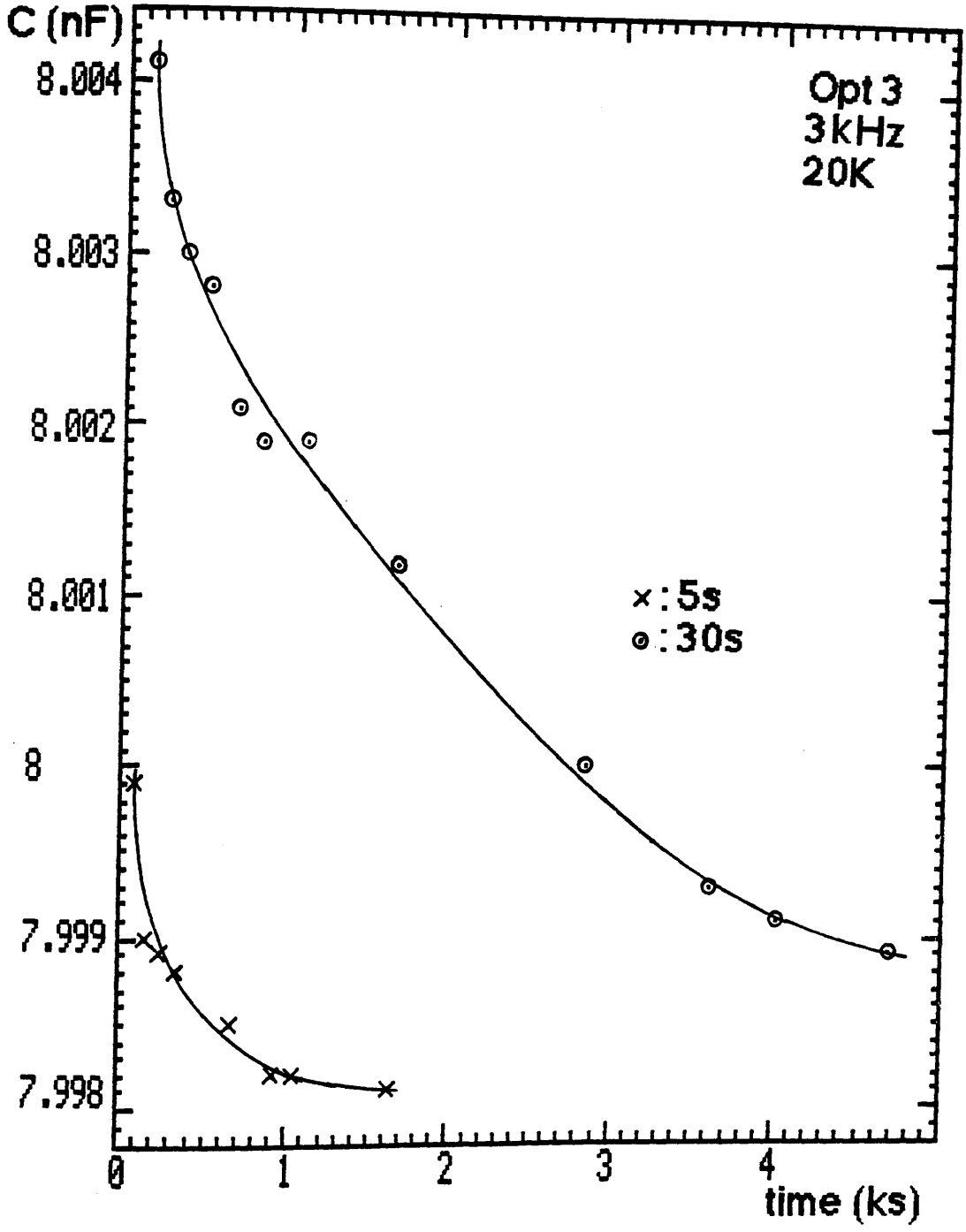

Figure 6.13 : The decay of the capacitance in the dark after short pulses of light were applied to Opt 3 at T = 20K.

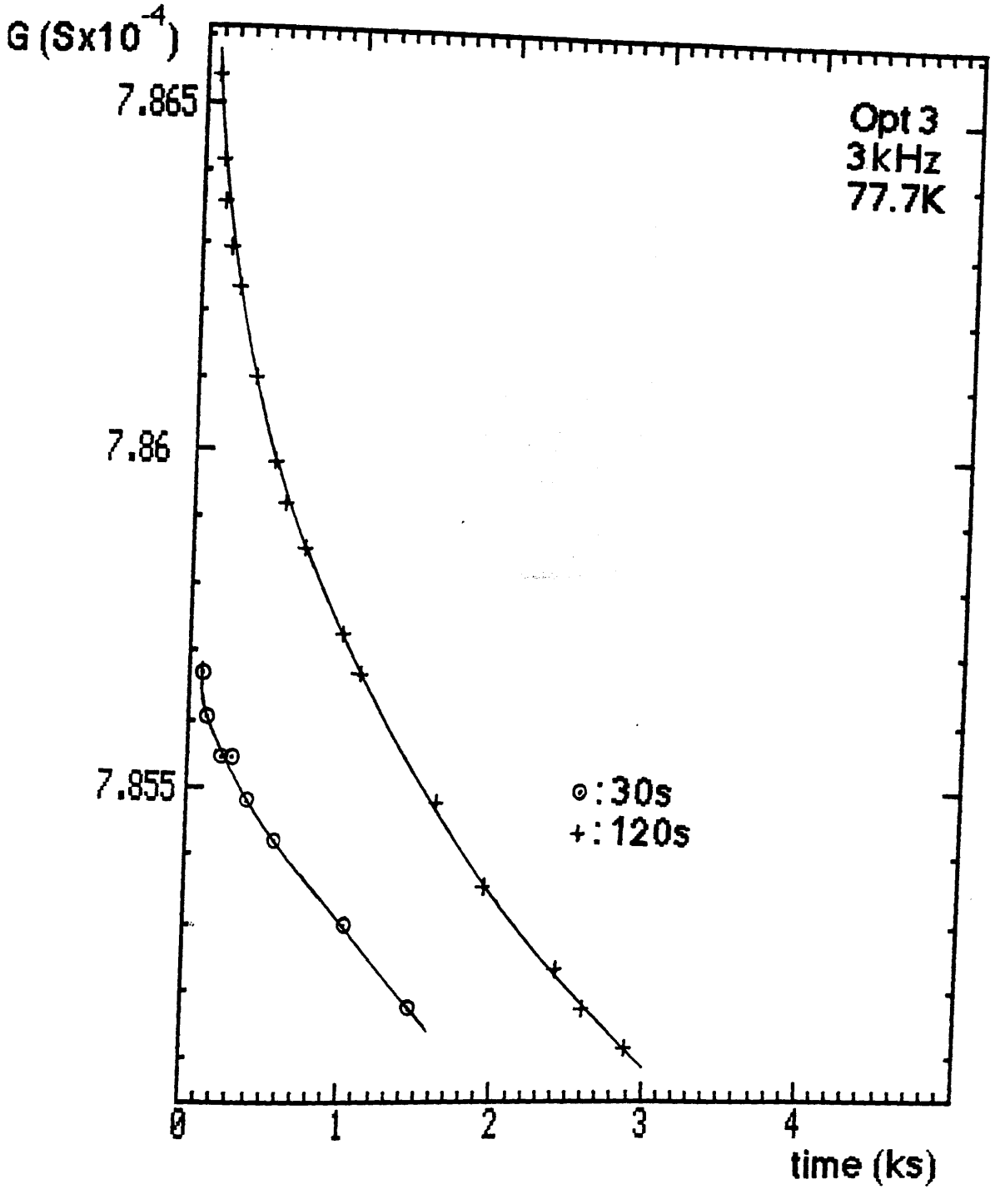

Figure 6.14 : The decay of the a.c. conductivity in the dark after short pulses of light were applied to Opt 3 at 77K. The sample did not respond to a 5s pulse. Value of G_{ac} = 7.86725×10^{-4}S during the 120s pulse. Pulse intensity same as figs 6.12 and 6.13.

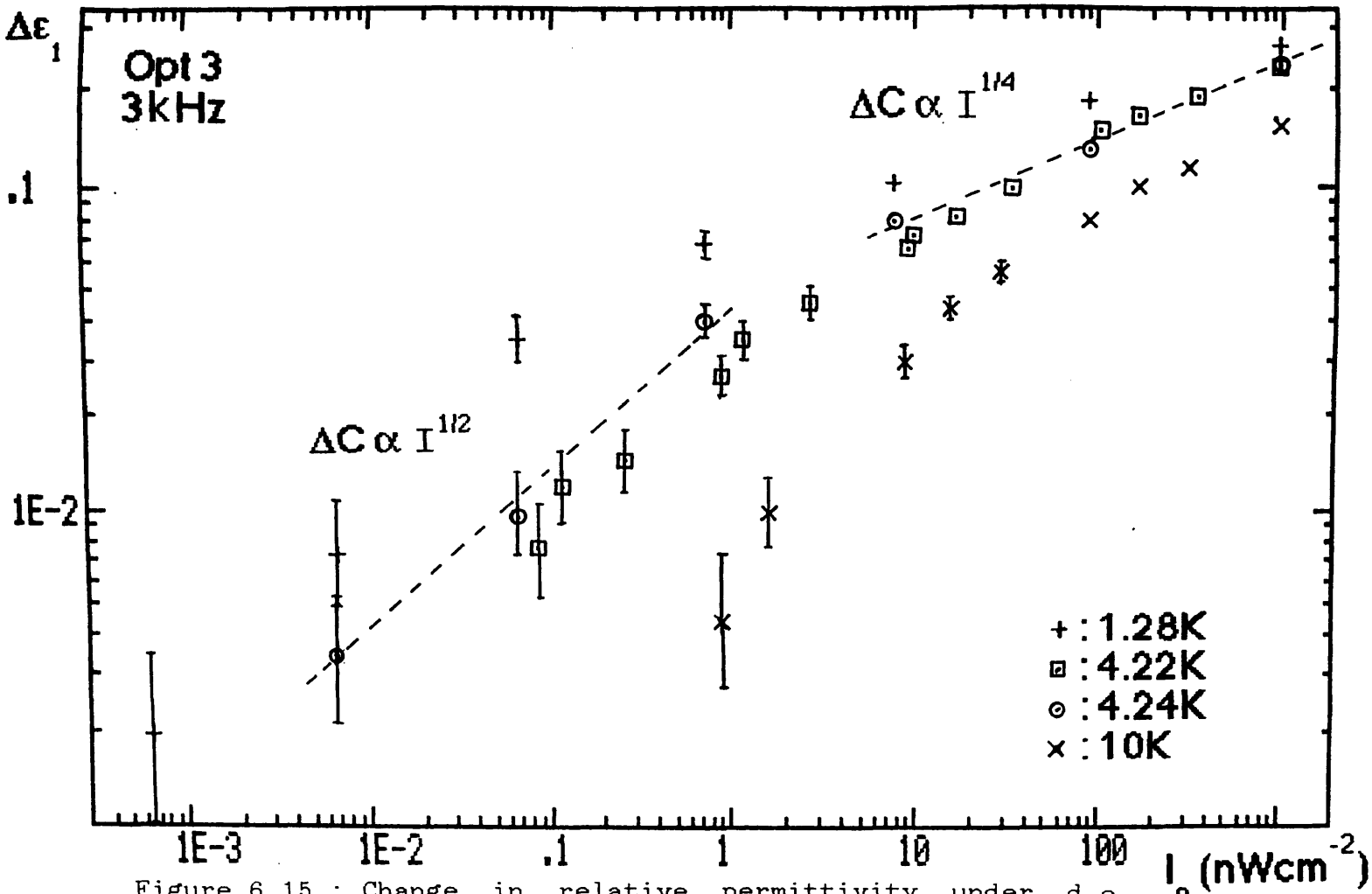

Figure 6.15 : Change in relative permittivity under d.c. illumination of intensity I_o for Opt 3. The 4.2K data was derived from fig. 6.1, the 1.3K data from fig. 6.2 and the 10K data from fig. 6.3.

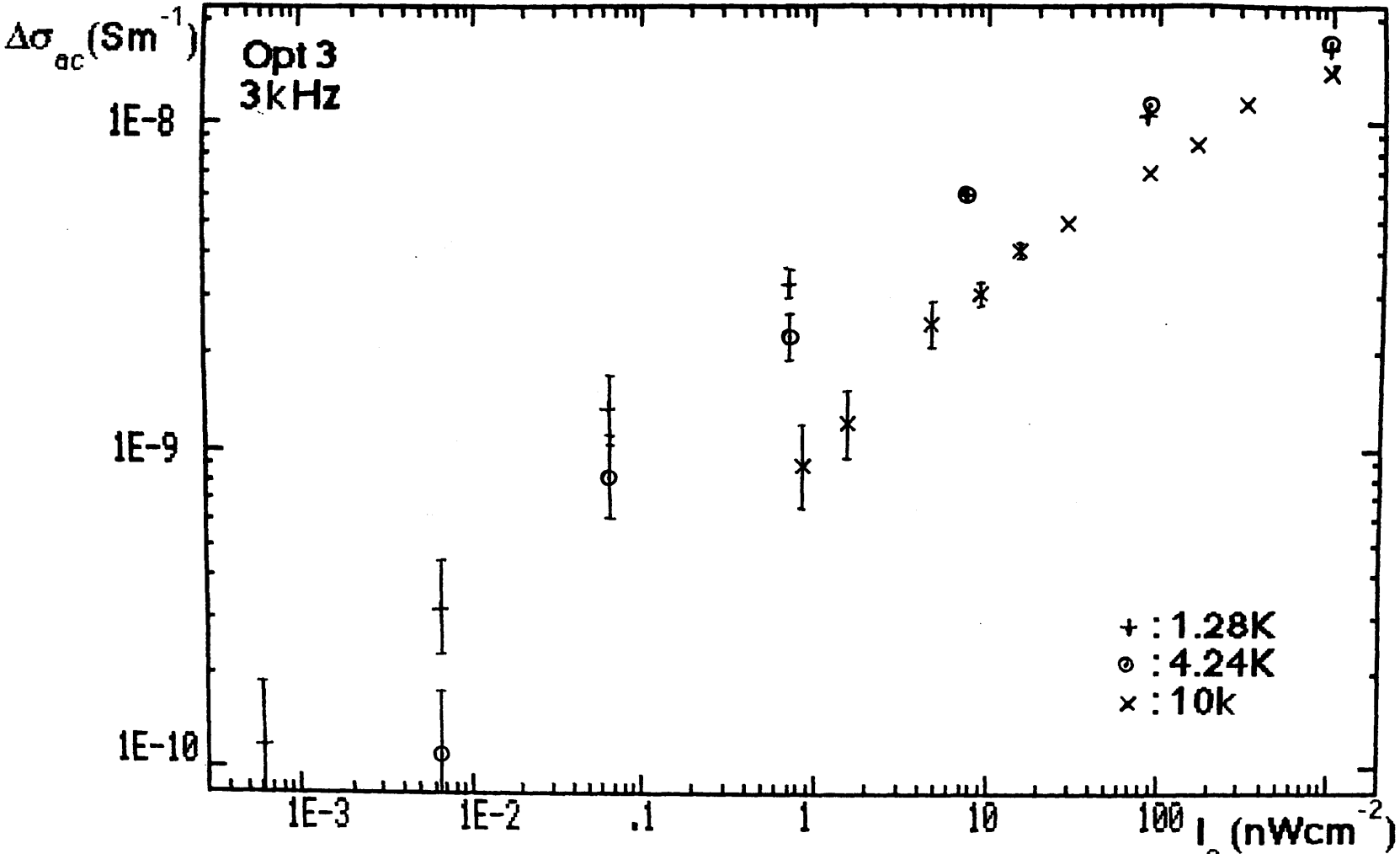

Figure 6.16 : Change in the a.c. conductivity under d.c. illumination for Opt 3. This data was taken during the same experimental runs as the previous figure.

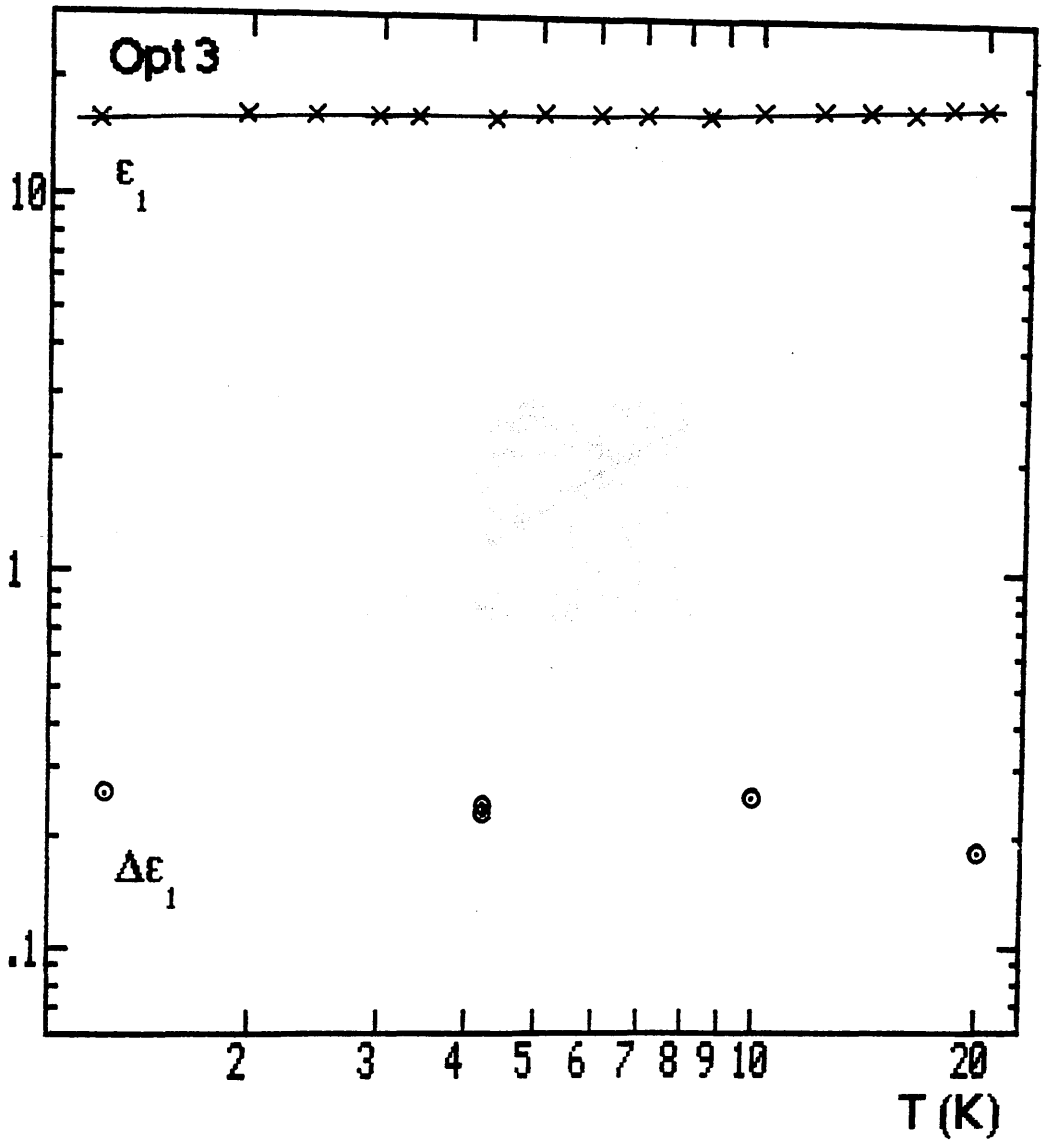

Figure 6.17A : Temperature dependence of the light-induced permittivity change and the dark values of permittivity for Opt 3 measured at a frequency of 3kHz. I_o =950 nWcm^{-2}.

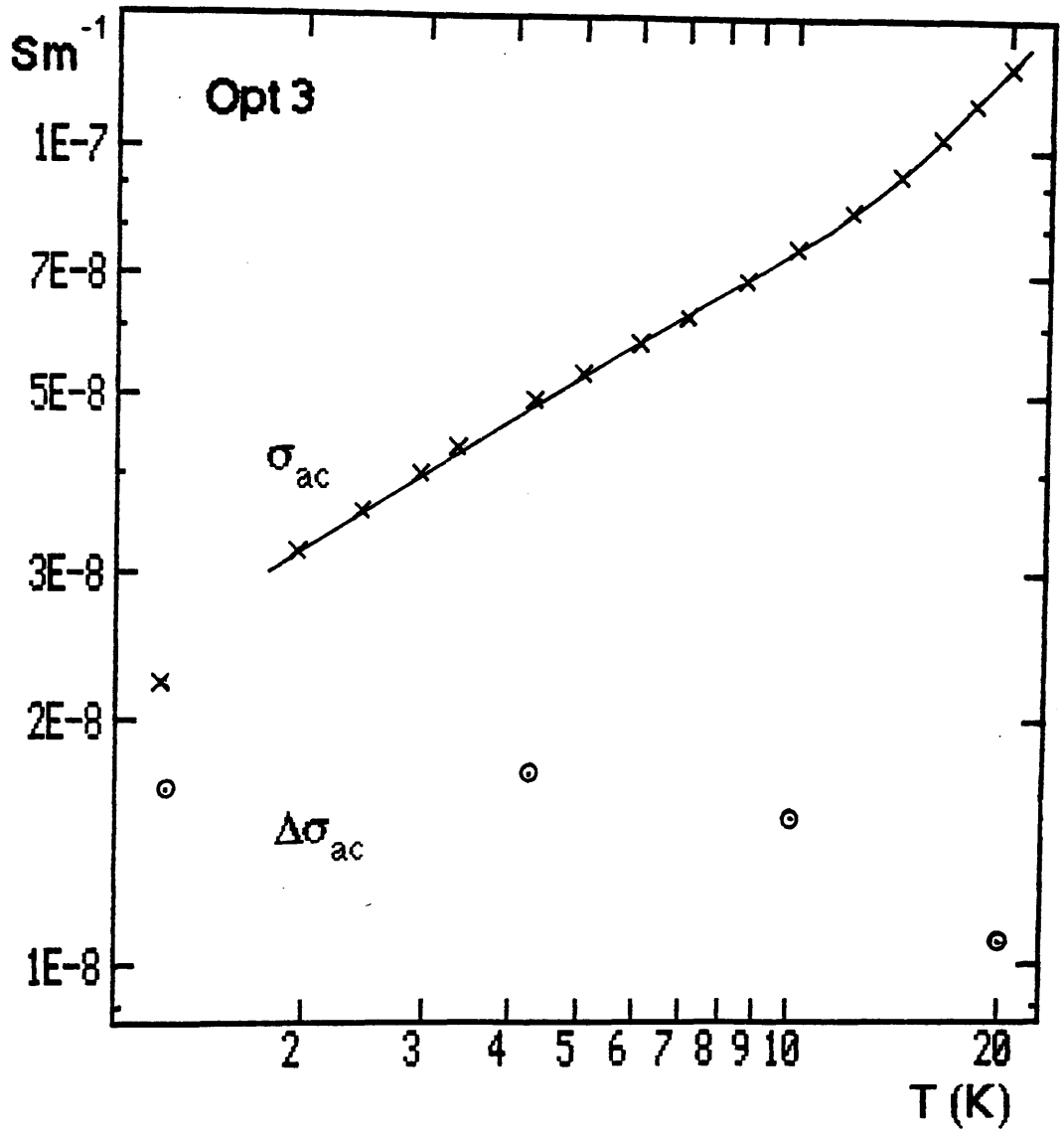

Figure 6.17B : Temperature dependence of the light-induced change in a.c. conductivity and the dark values of a.c. conductivity for Opt 3 at a frequency of 3kHz. I_o = 950nWcm^{-2}.

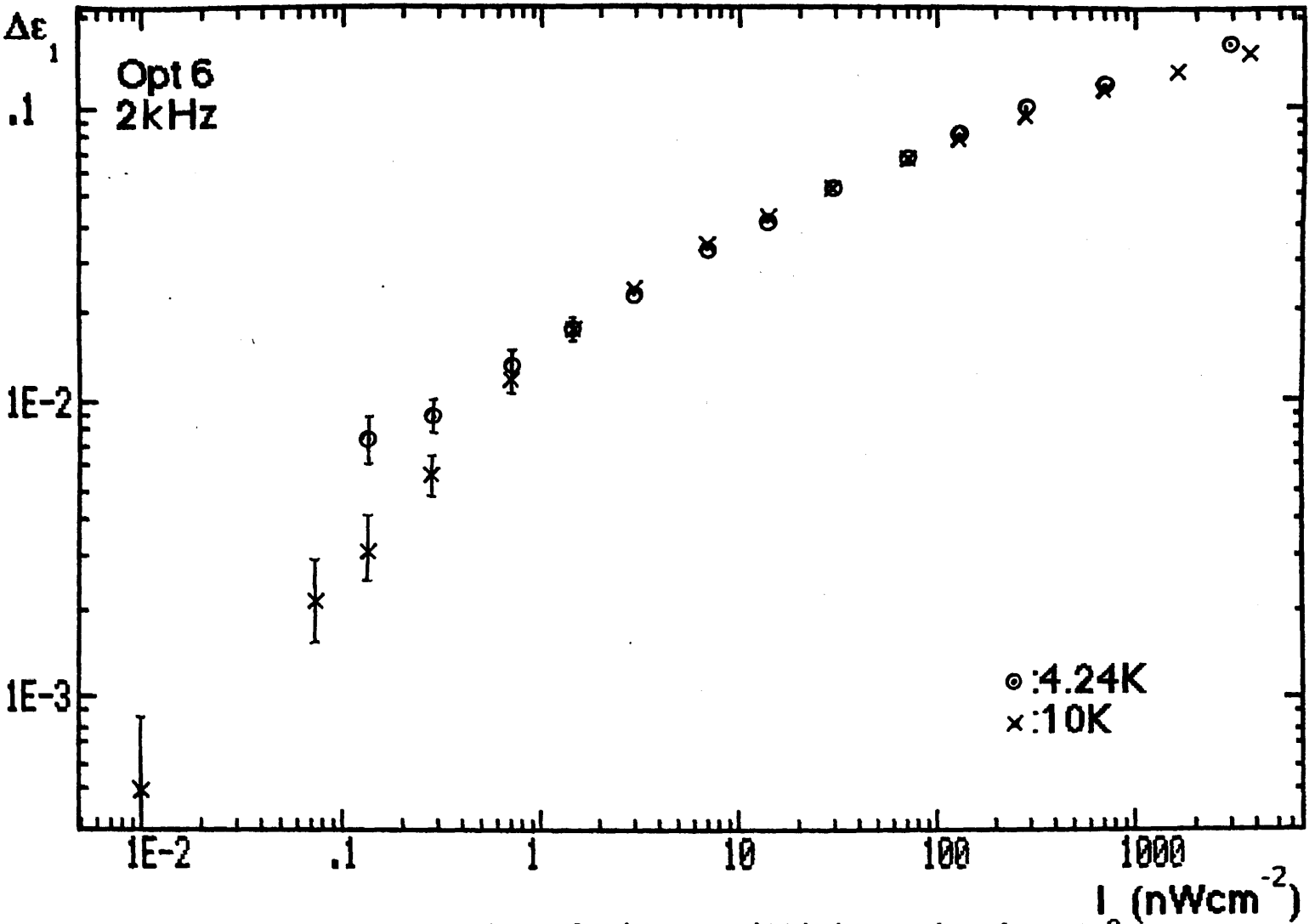

Figure 6.18 : Change in the relative permittivity under d.c. illumination for Opt 6 (magnetron sputtered pure a-Si) at 4.2K and 10K.

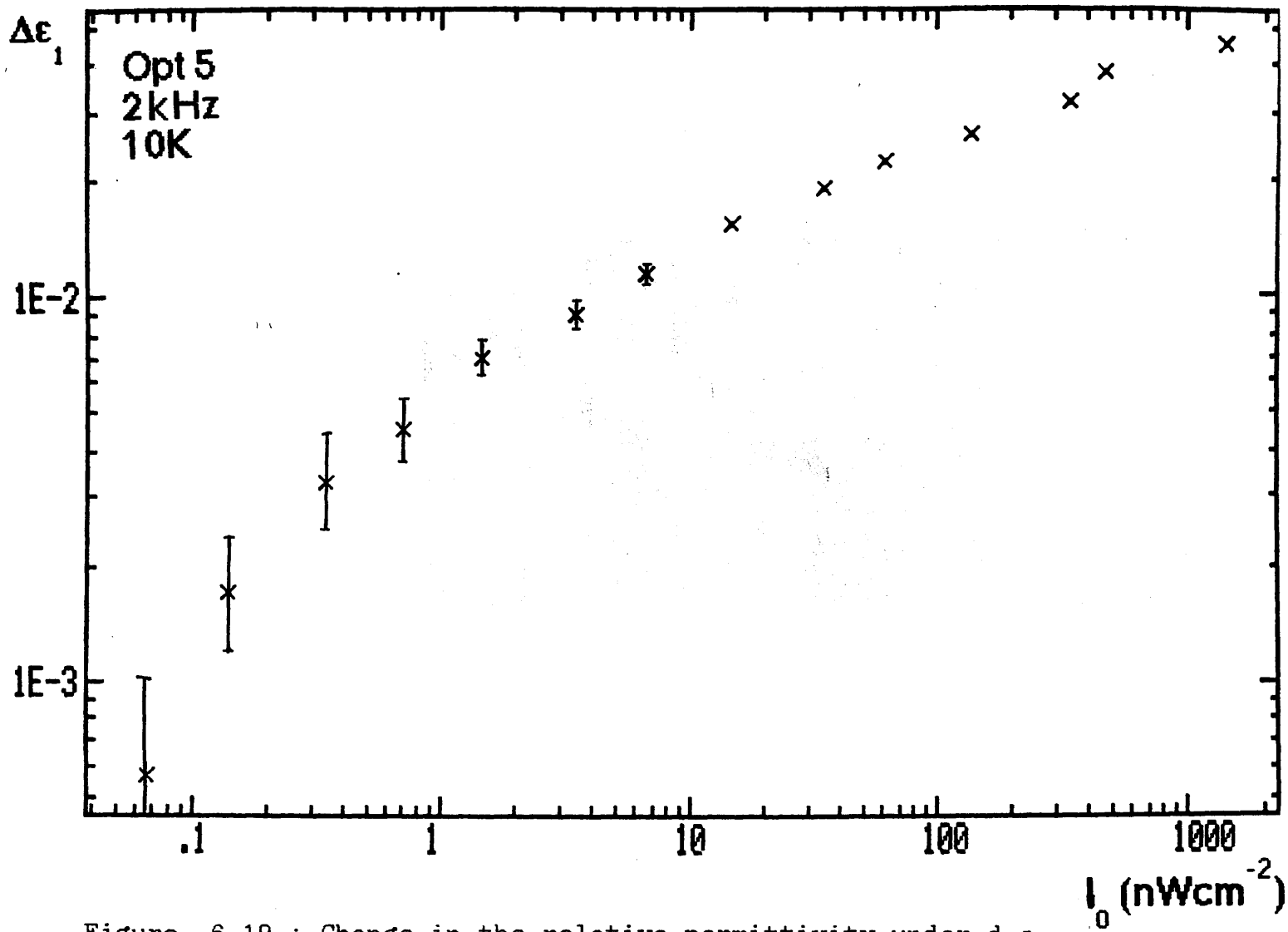

Figure 6.19 : Change in the relative permittivity under d.c. illumination for Opt 5 (a-Si:H 10:1) at 10K.

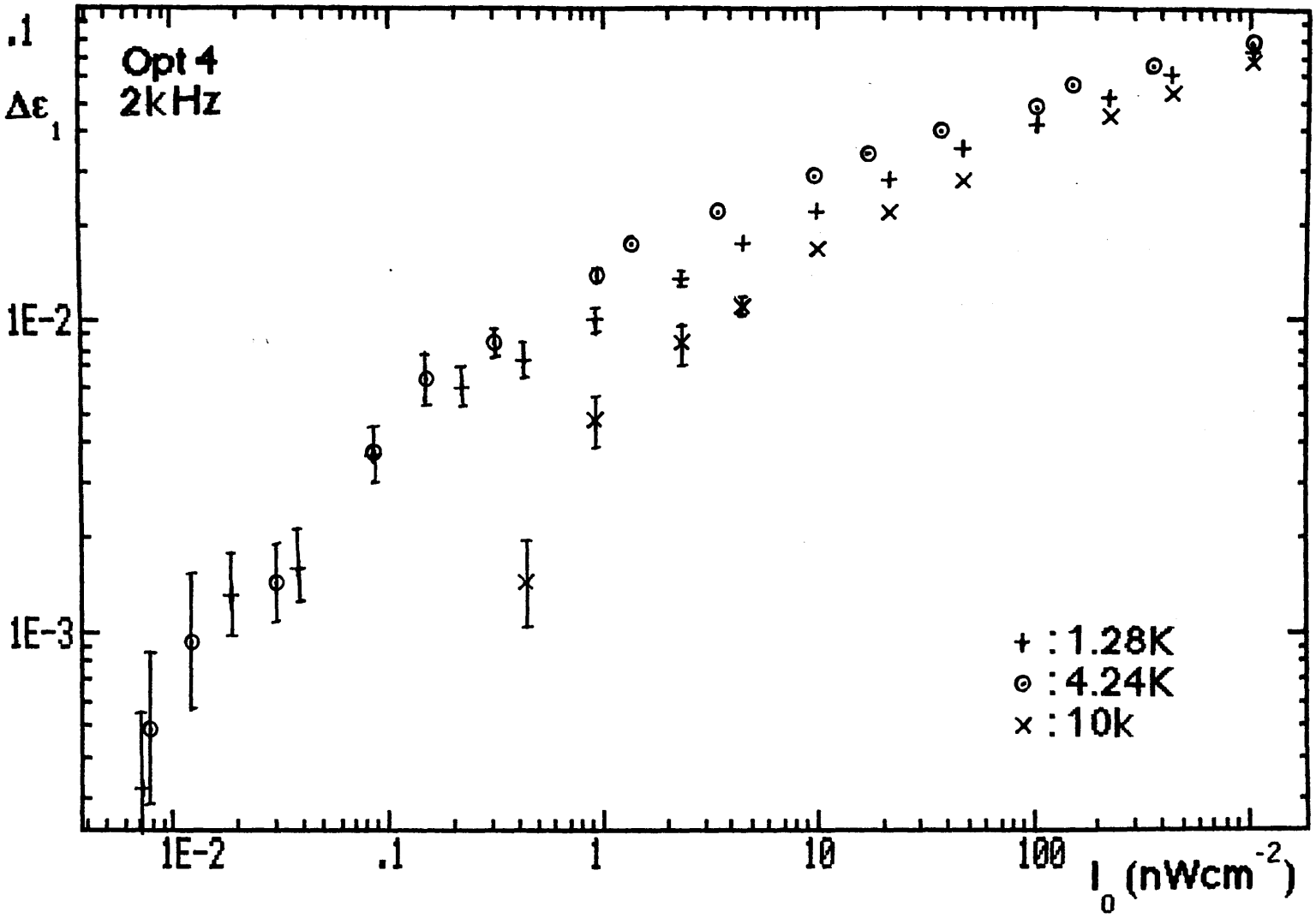

Figure 6.20 : Change in the relative permittivity under d.c. illumination for Opt 4 (a-Si:H 20:1) at 1.3K, 4.2K and 10K.

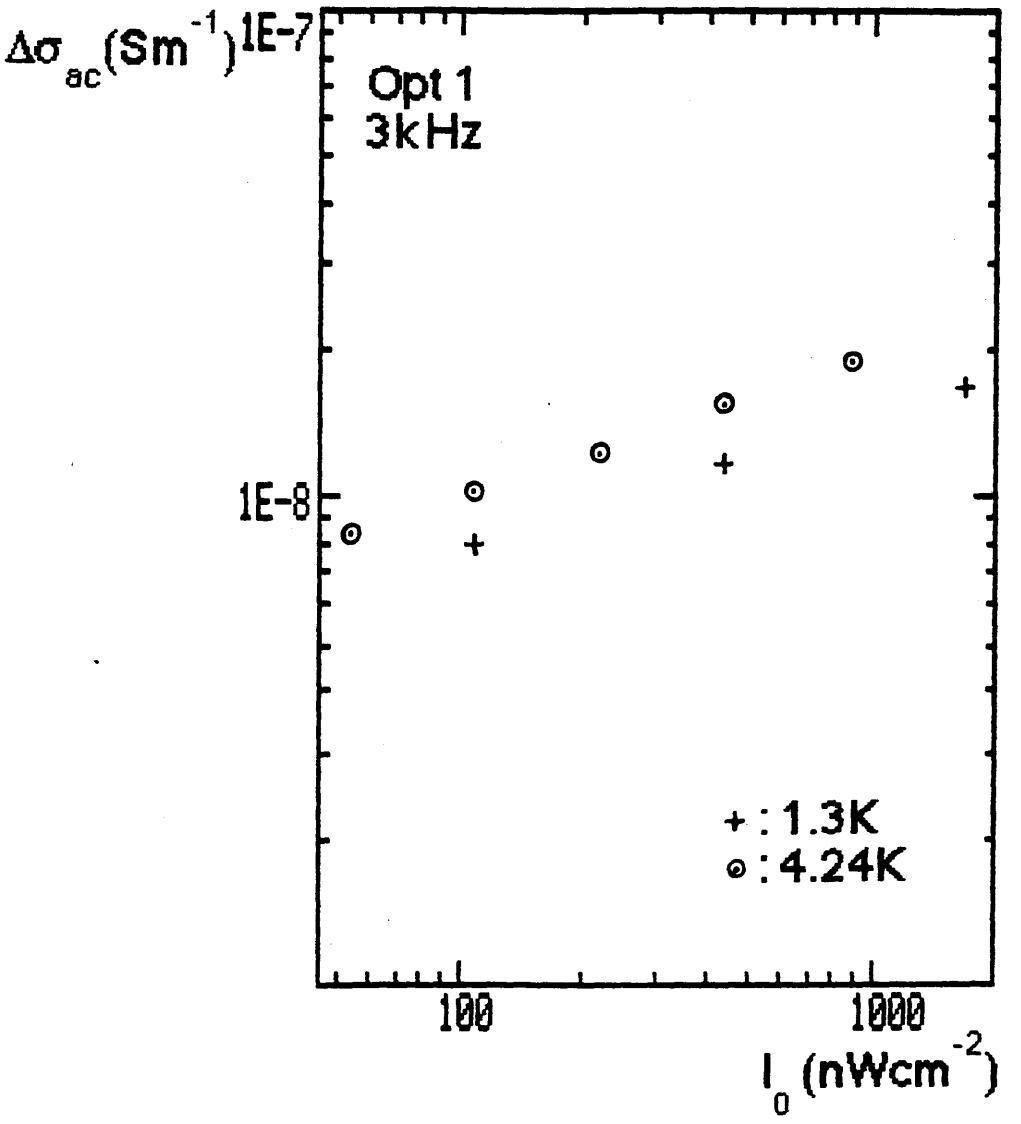

Figure 6.21 : Change in the a.c. conductivity under d.c. illumination for Opt 1 (pure a-Ge) at 1.3K and 4.2K.

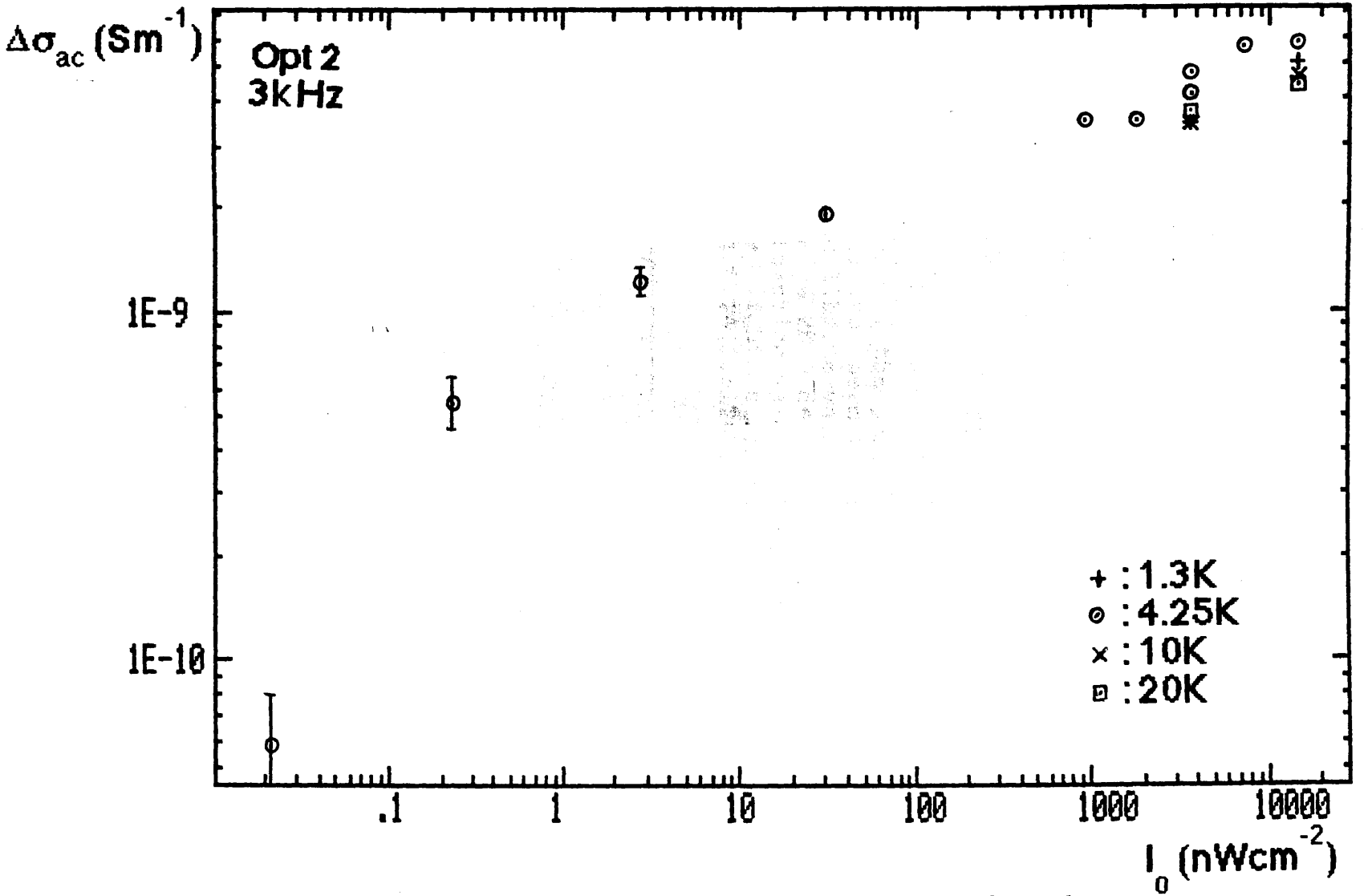

Figure 6.22 : Change in the a.c. conductivity under d.c. illumination for Opt 2 (a-Ge:H 4:1) at 1.3K, 4.2K, 10K and 20K.

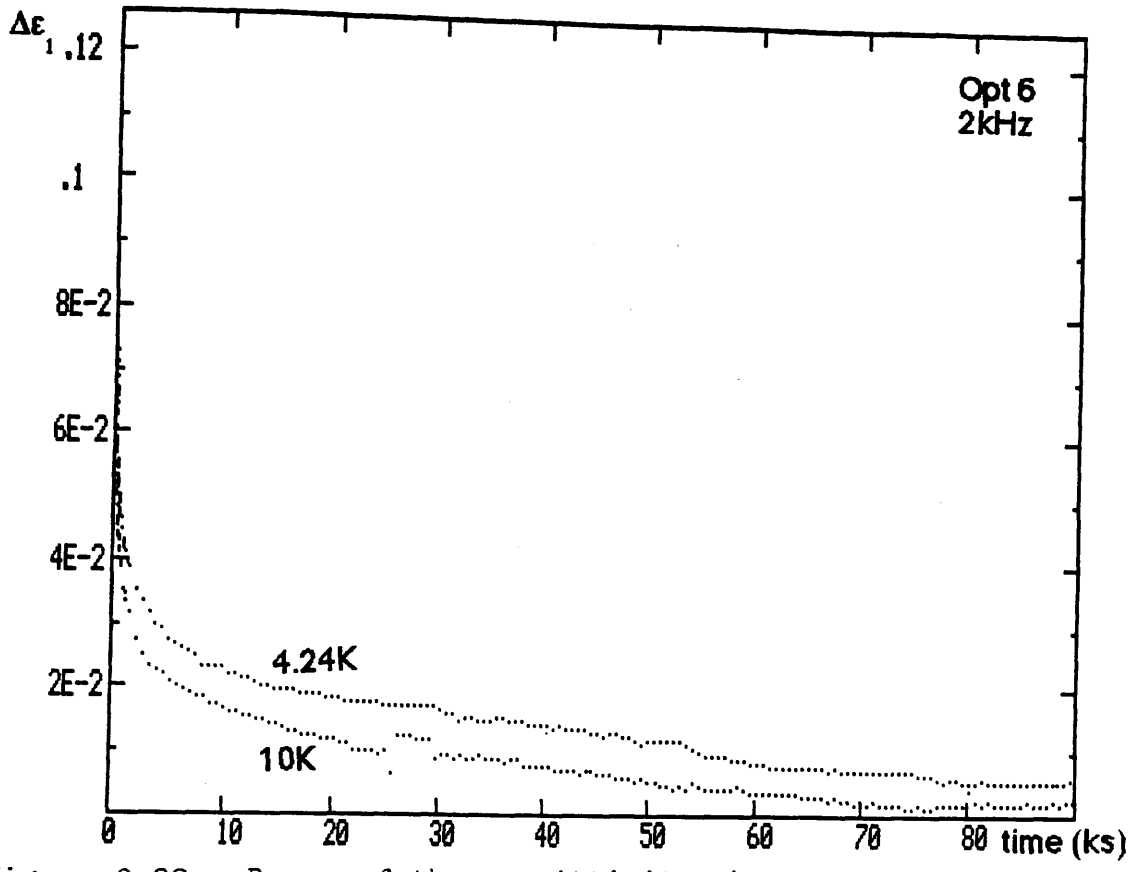

Figure 6.23 : Decay of the permittivity change to zero as the relative permittivity returns to it's dark equilibrium value for Opt 6 at 4.2K and 10K. The 4.2K data is taken from fig 6.11. Saturation values of permittivity change before the light is removed (t=0) are 0.15 for T=4.2K and 0.14 for T=10K.

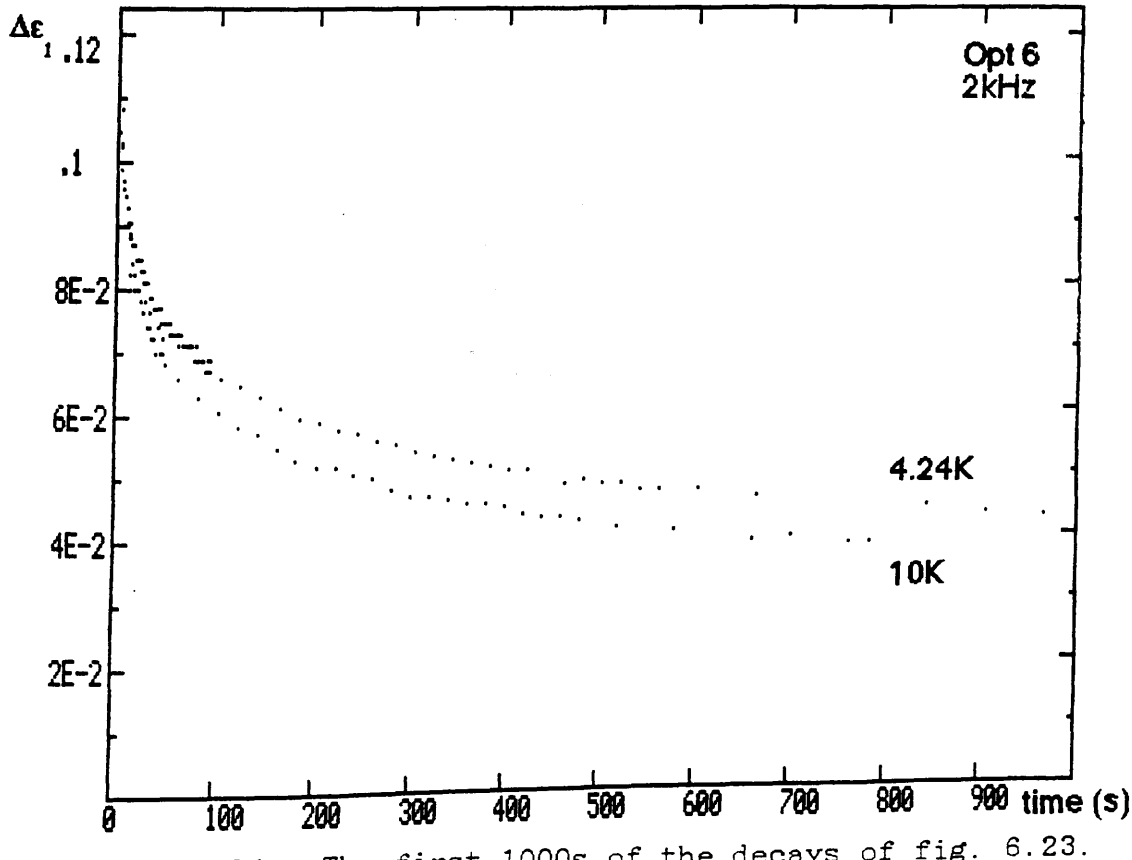

Figure 6.24 : The first 1000s of the decays of fig. 6.23.

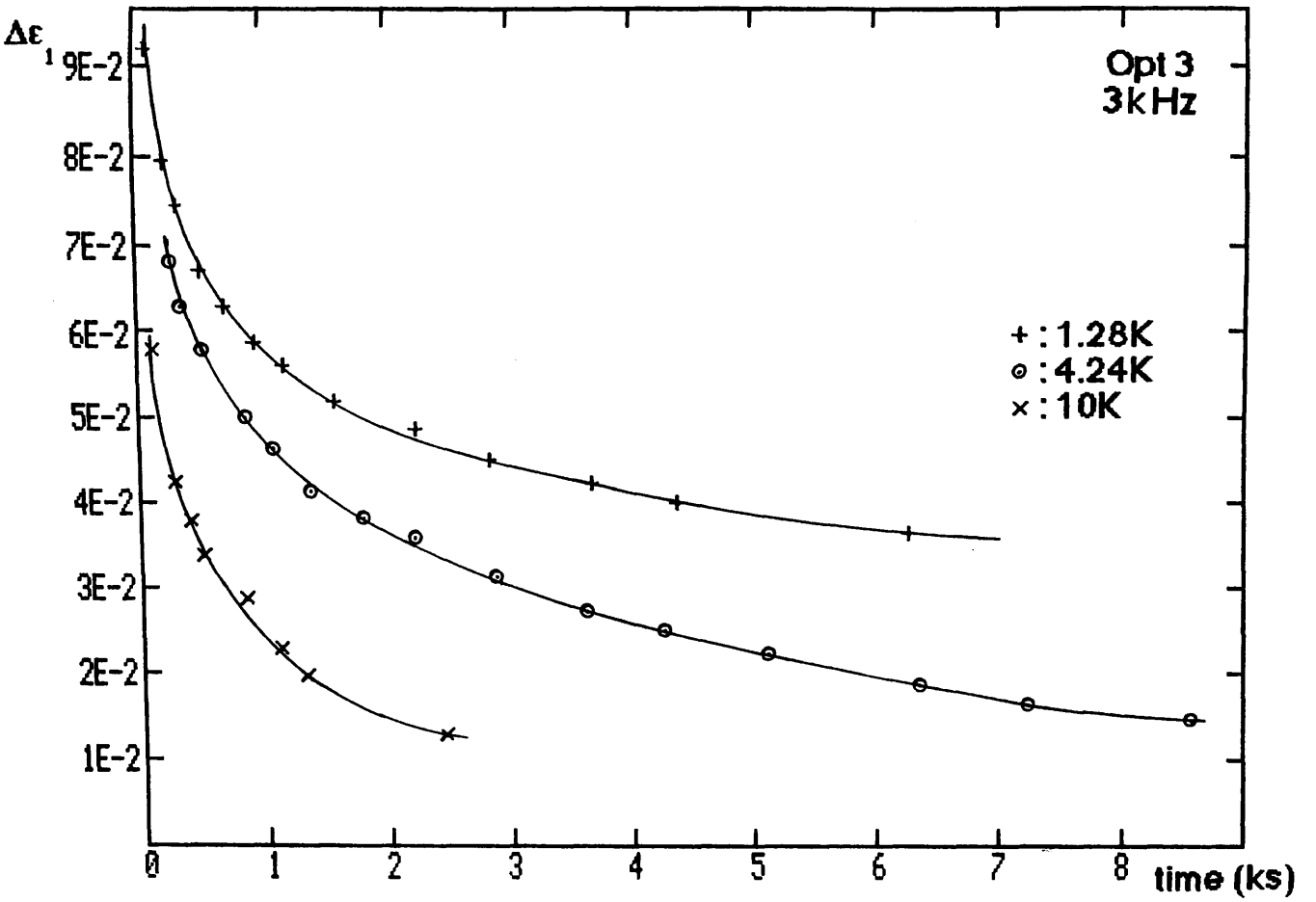

Figure 6.25 : Decay of the permittivity change in the dark for Opt 3 at 1.3K, 4.2K and 10K. The data is taken from figs. 6.2, 6.1 and 6.3 respectively. Saturation values of permittivity change before the light is removed (t=0) are 0.255 for T=1.3K, 0.225 for T=4.2K and 0.13 for T=10K.

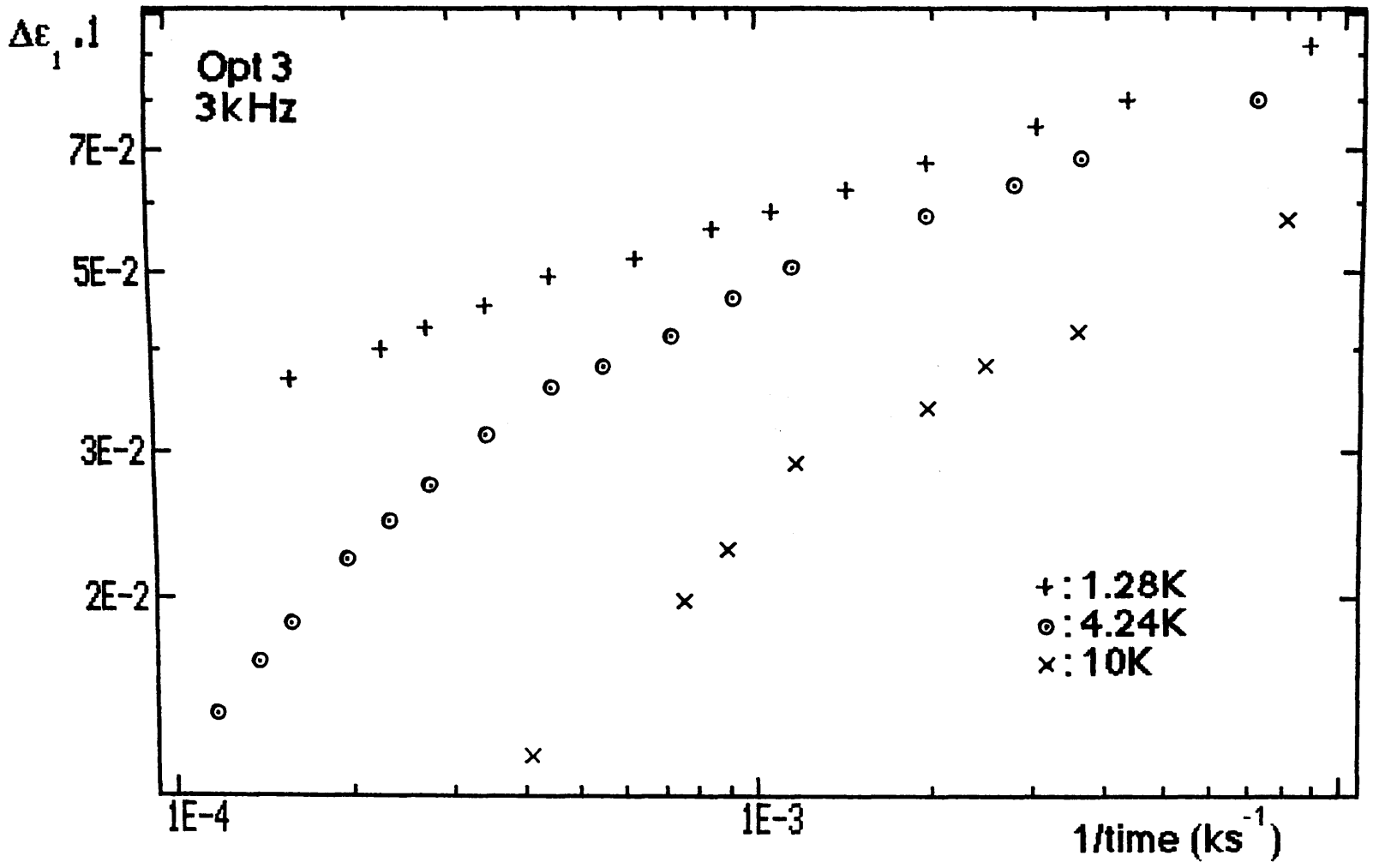

Figure 6.26 : The data of fig. 6.25 (for Opt 3) plotted against 1/t.

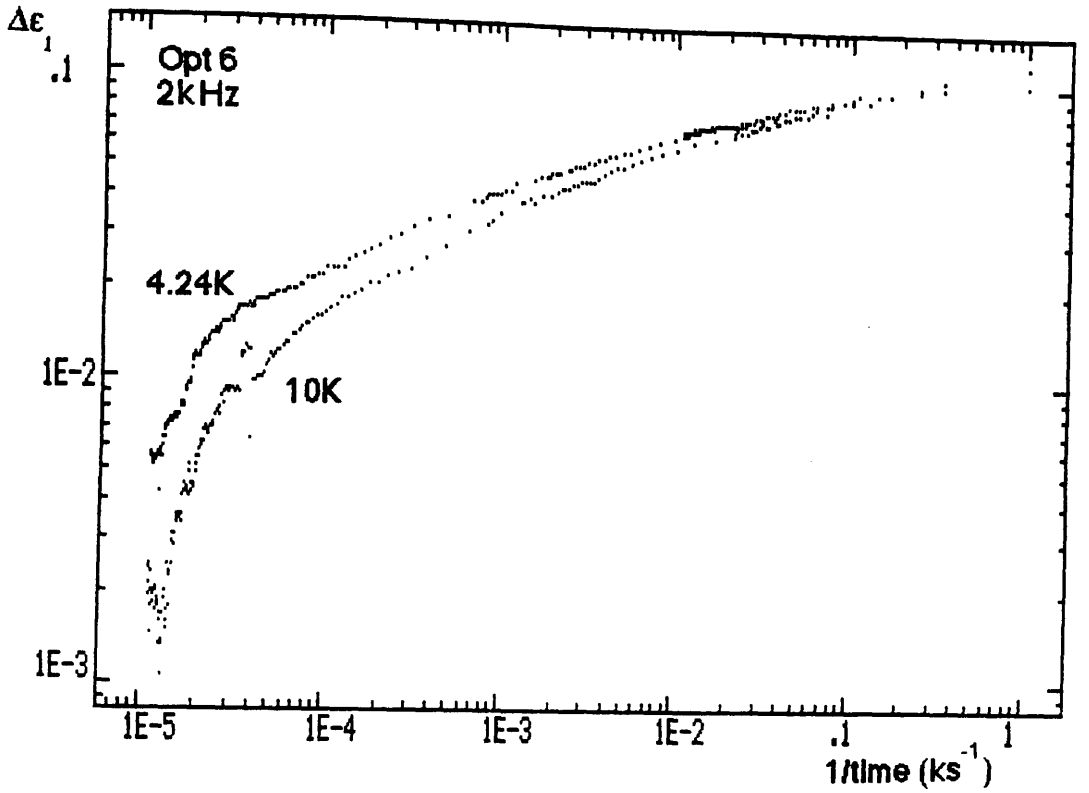

Figure 6.27 : The data of fig. 6.23 (for Opt 6) plotted against 1/t.

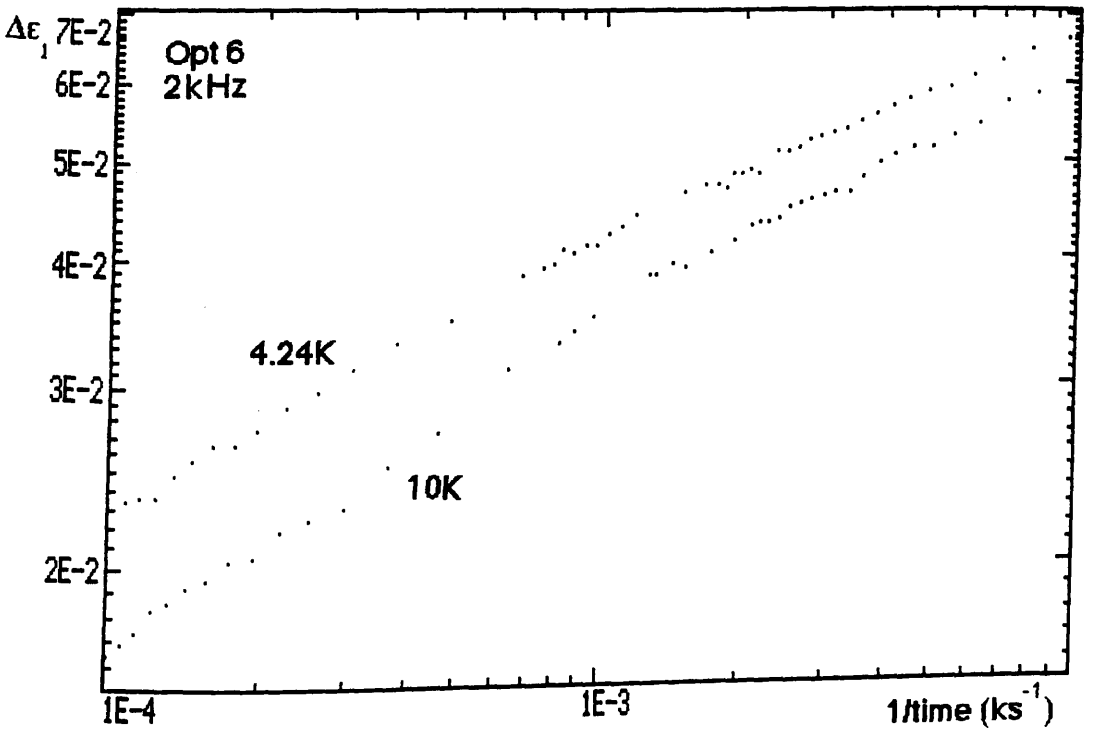

Figure 6.28 : Detail of the previous figure between t = 100s and t = 10ks.

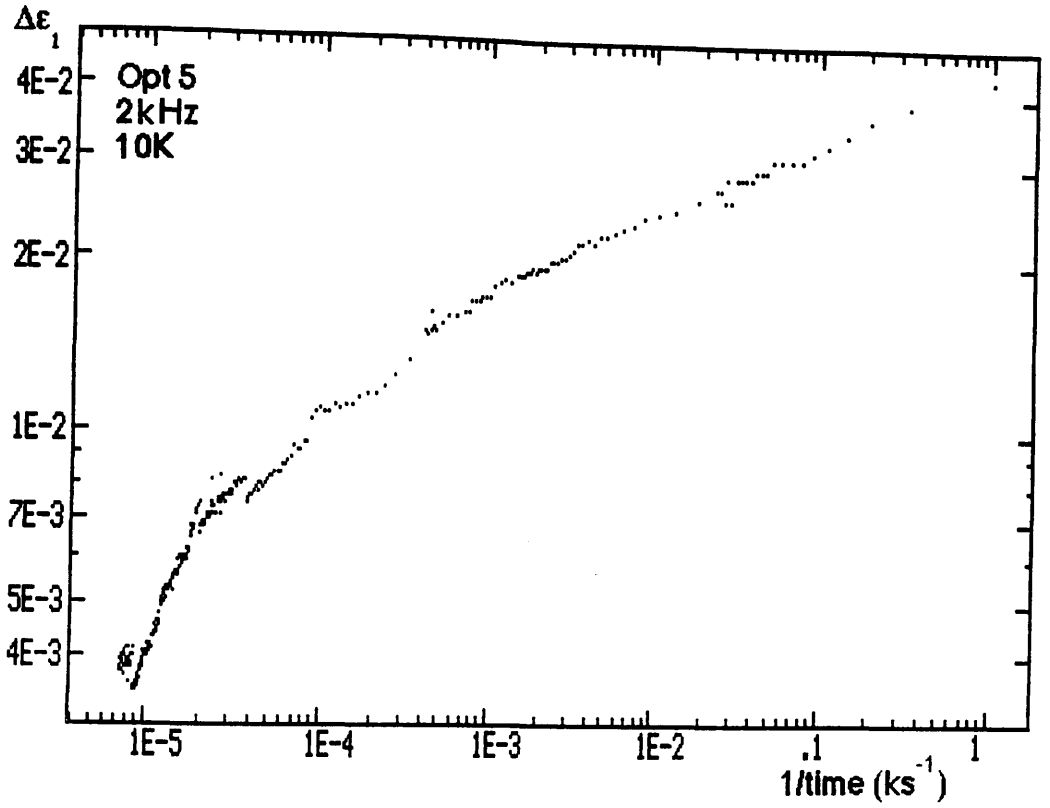

Figure 6.29 : Decay of the permittivity change in the dark plotted against 1/t for Opt 5 (a-Si:H 10:1) at 10K. The data is taken from fig. 6.6.

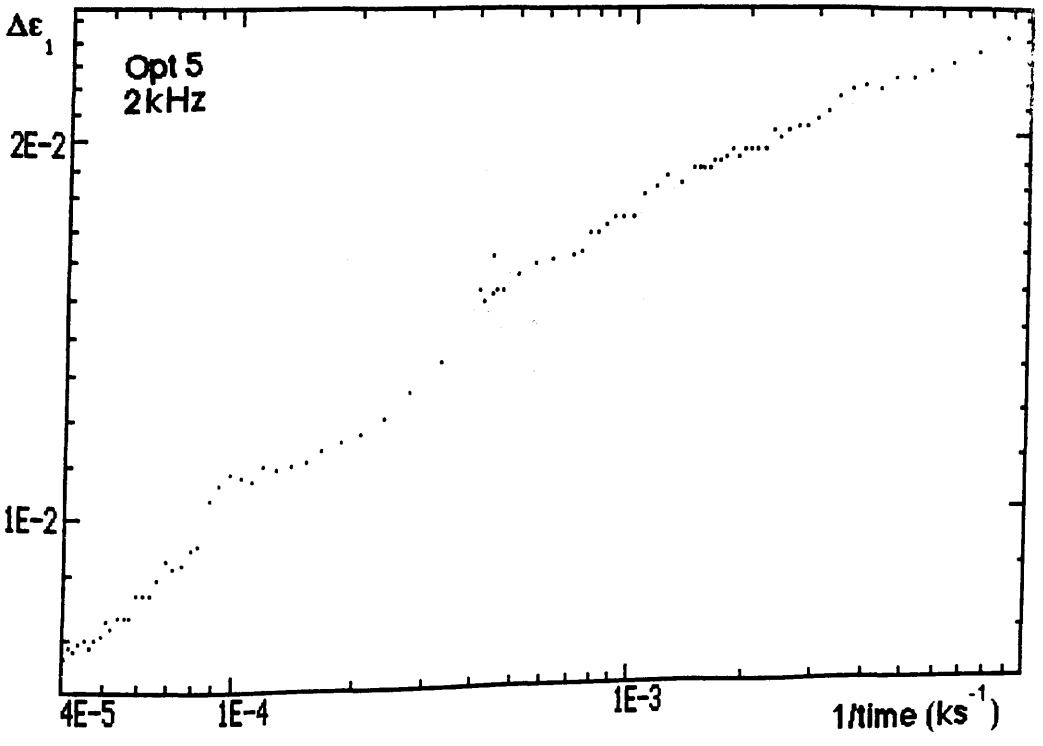

Figure 6.30 : Detail of the previous figure between t = 100s and t = 25ks.

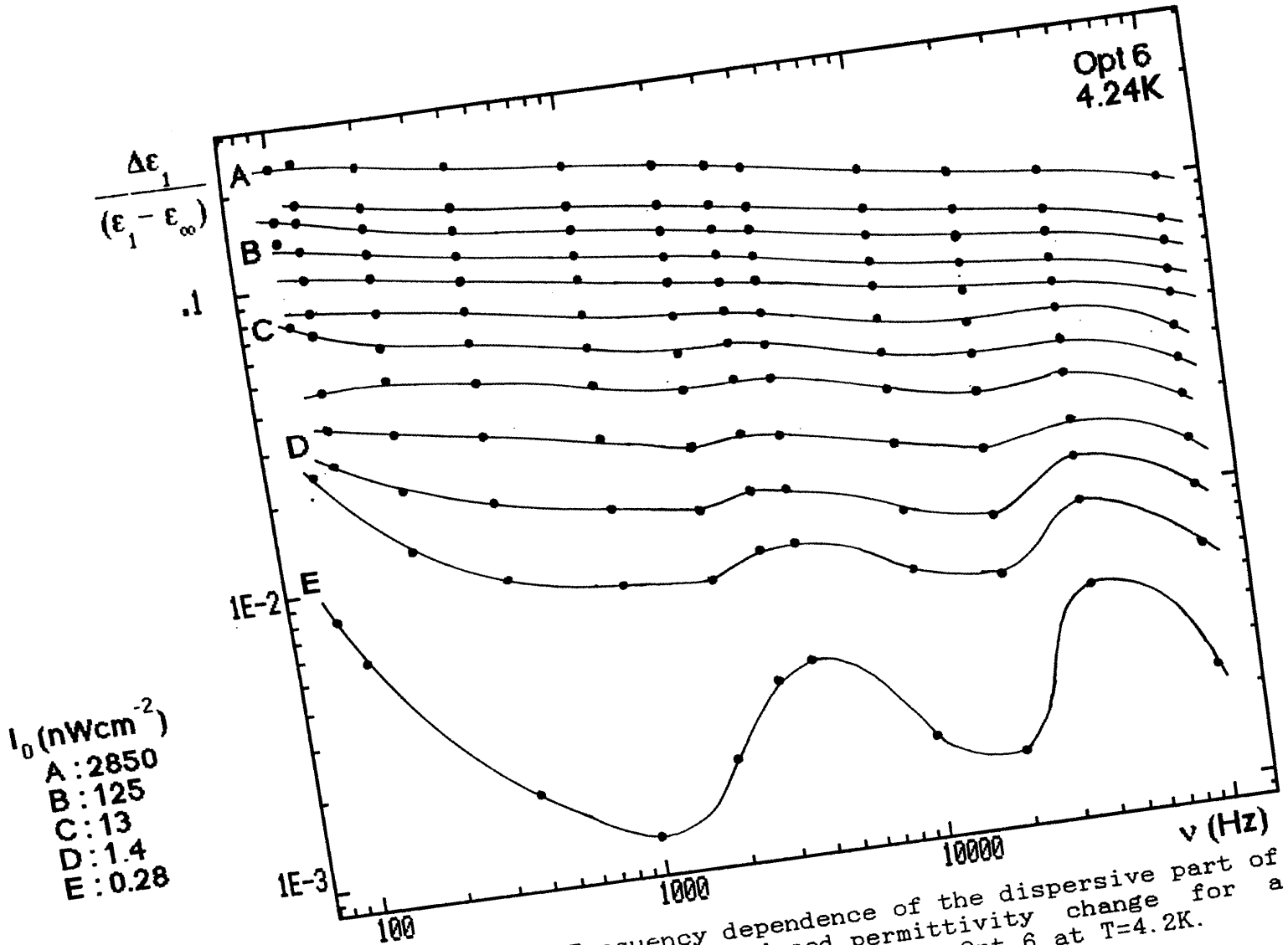

Figure 6.31 : Frequency dependence of the dispersive part of the light-induced permittivity change for a range of intensities for Opt 6 at T=4.2K.

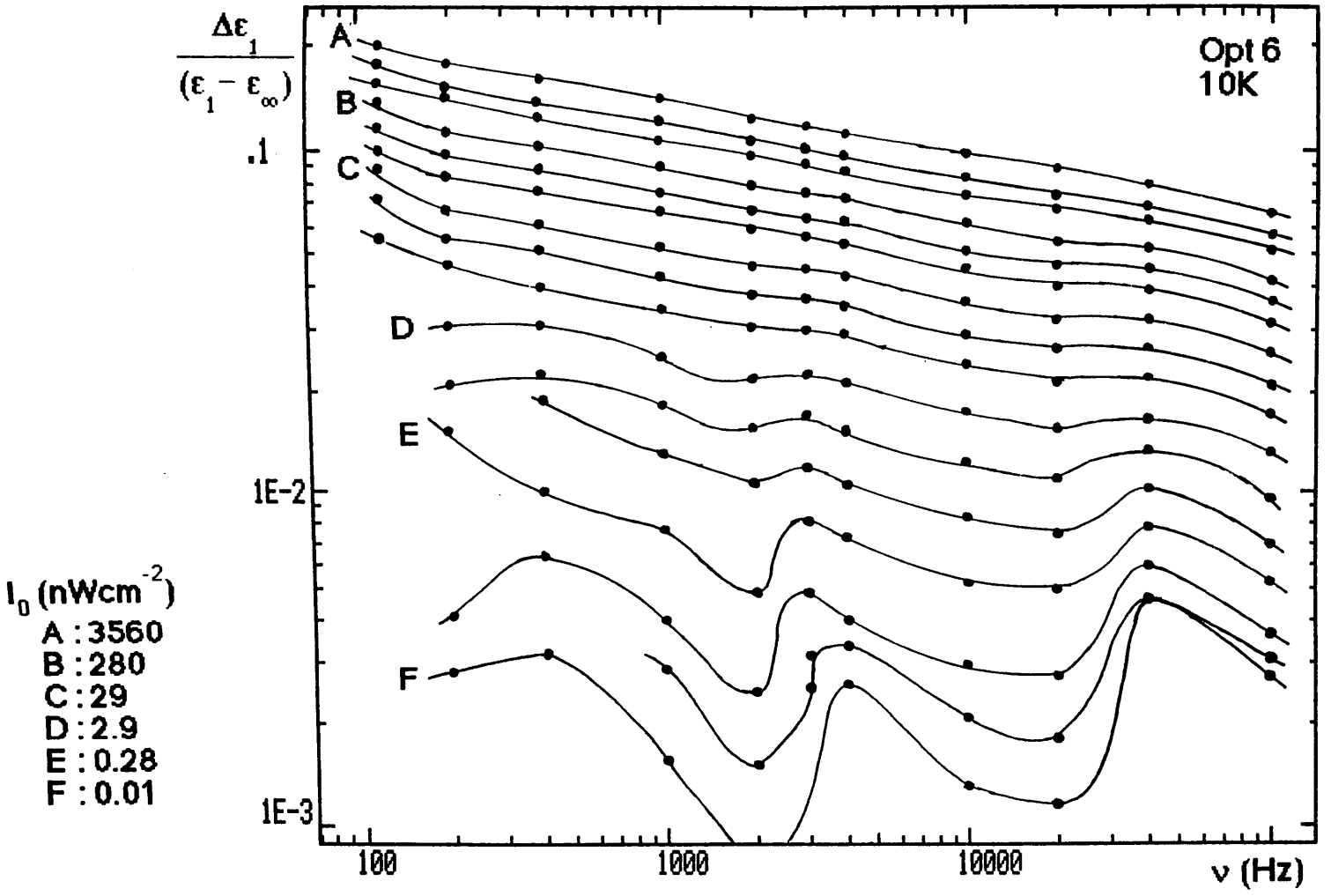

Figure 6.32 : Frequency dependence of the dispersive part of the light-induced permittivity change for a range of intensities for Opt 6 at T=10K.

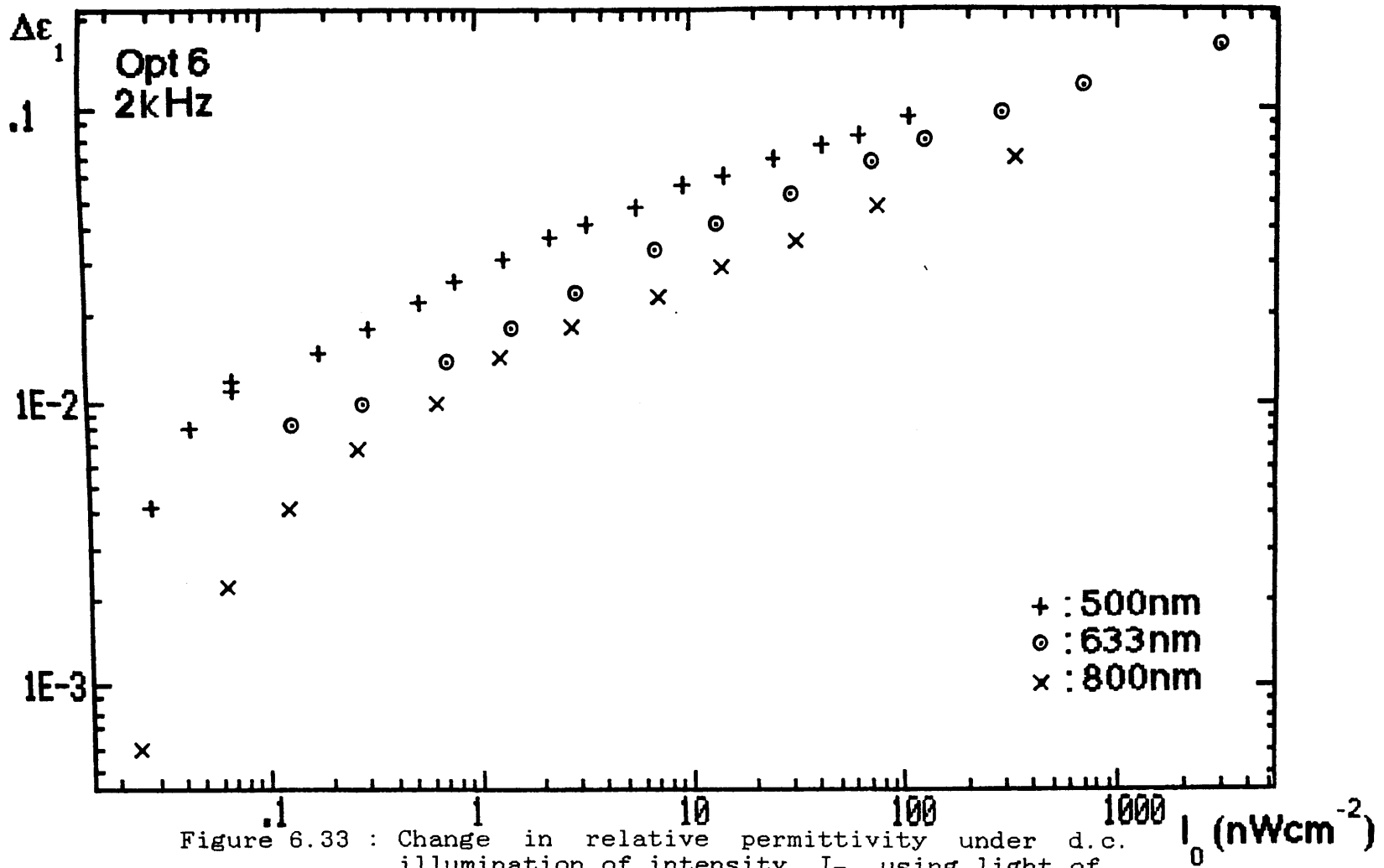

Figure 6.33 : Change in relative permittivity under d.c. illumination of intensity, I_o, using light of wavelengths 500nm, 633nm and 800nm for Opt 6 at 4.2K. The intensity is corrected for semiconductor surface reflectance and top electrode transmittance only (see text).

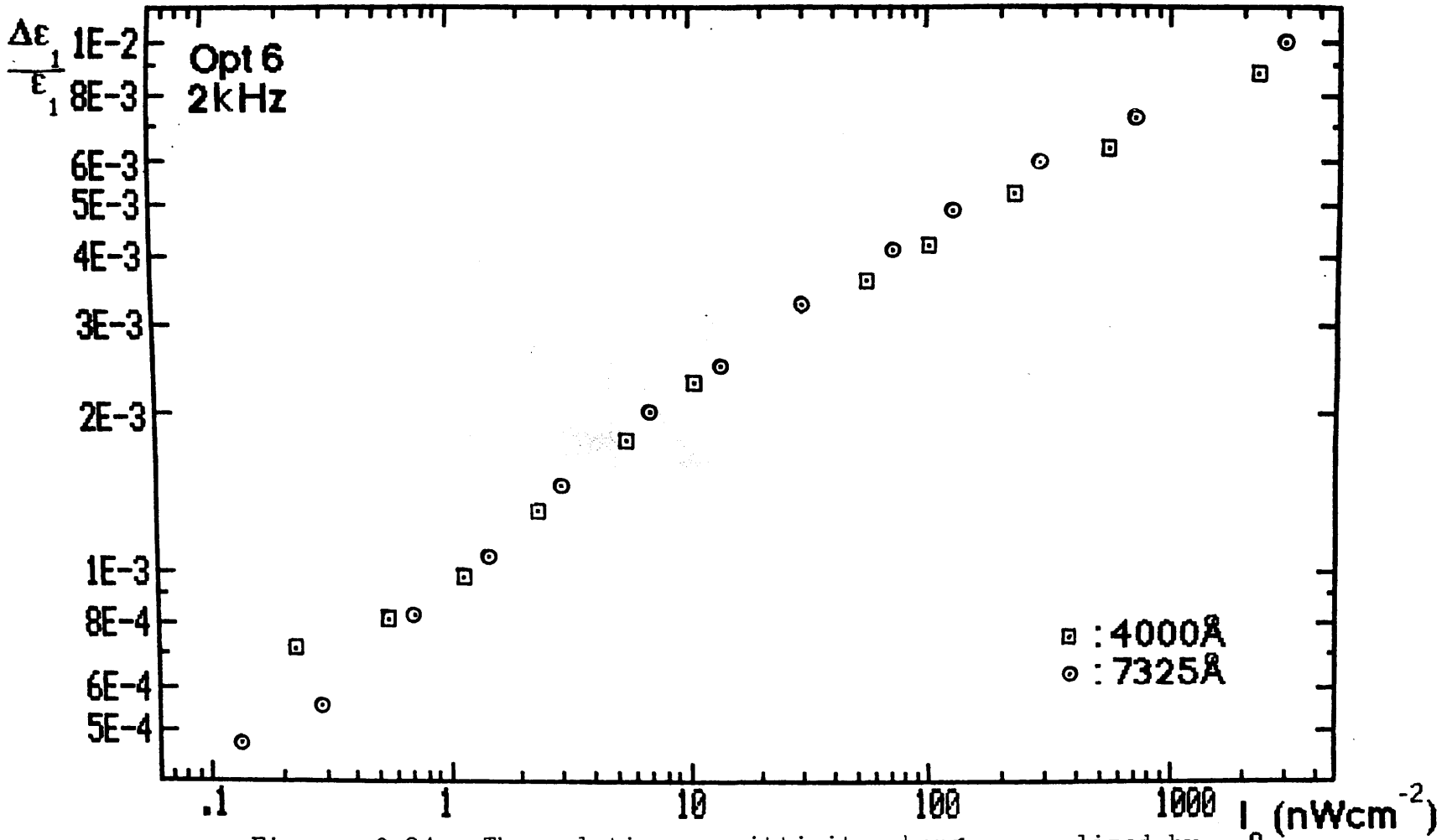

Figure 6.34 : The relative permittivity change normalized by the dark value of the permittivity for two film thicknesses for Opt 6 at 4.2K. Intensity corrected as for fig. 6.33.

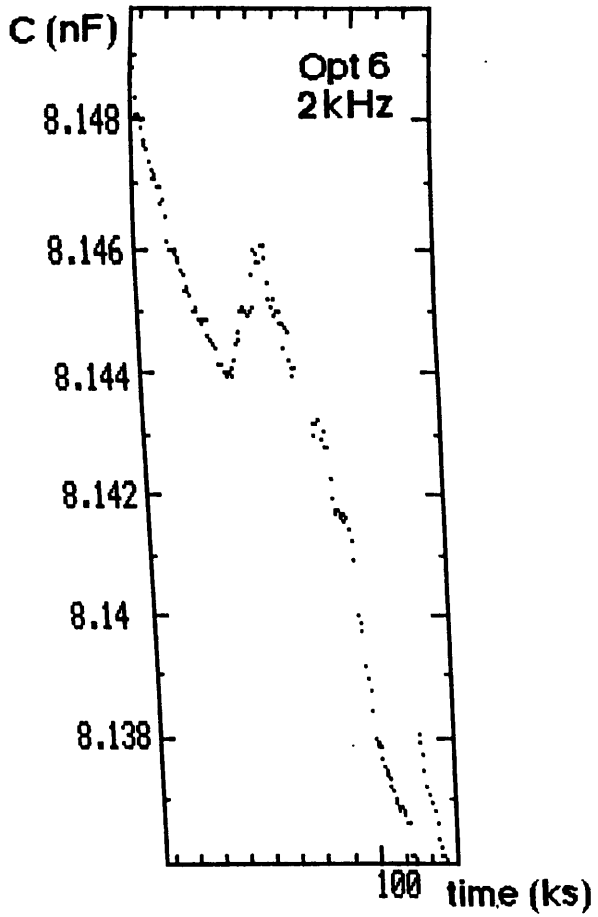

Figure 6.35 : Relaxation of Opt 6 (pure magnetron sputtered a-Si) after cooling to 4.24K, as shown by the decay of a thermally excited capacitance.

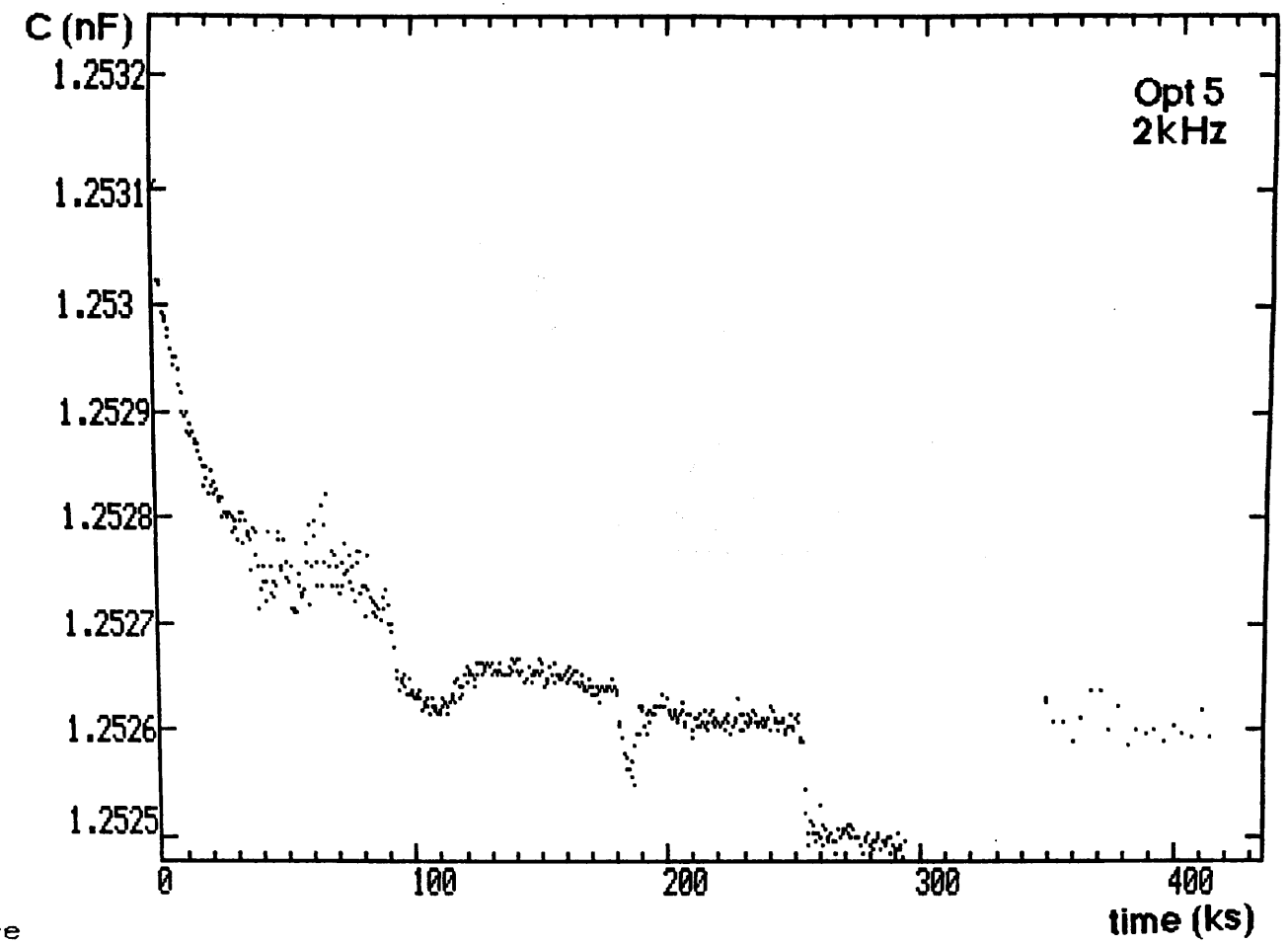

Figure 6.36 : Relaxation of Opt 5 (a-Si:H 10:1) after cooling to 4.24K.

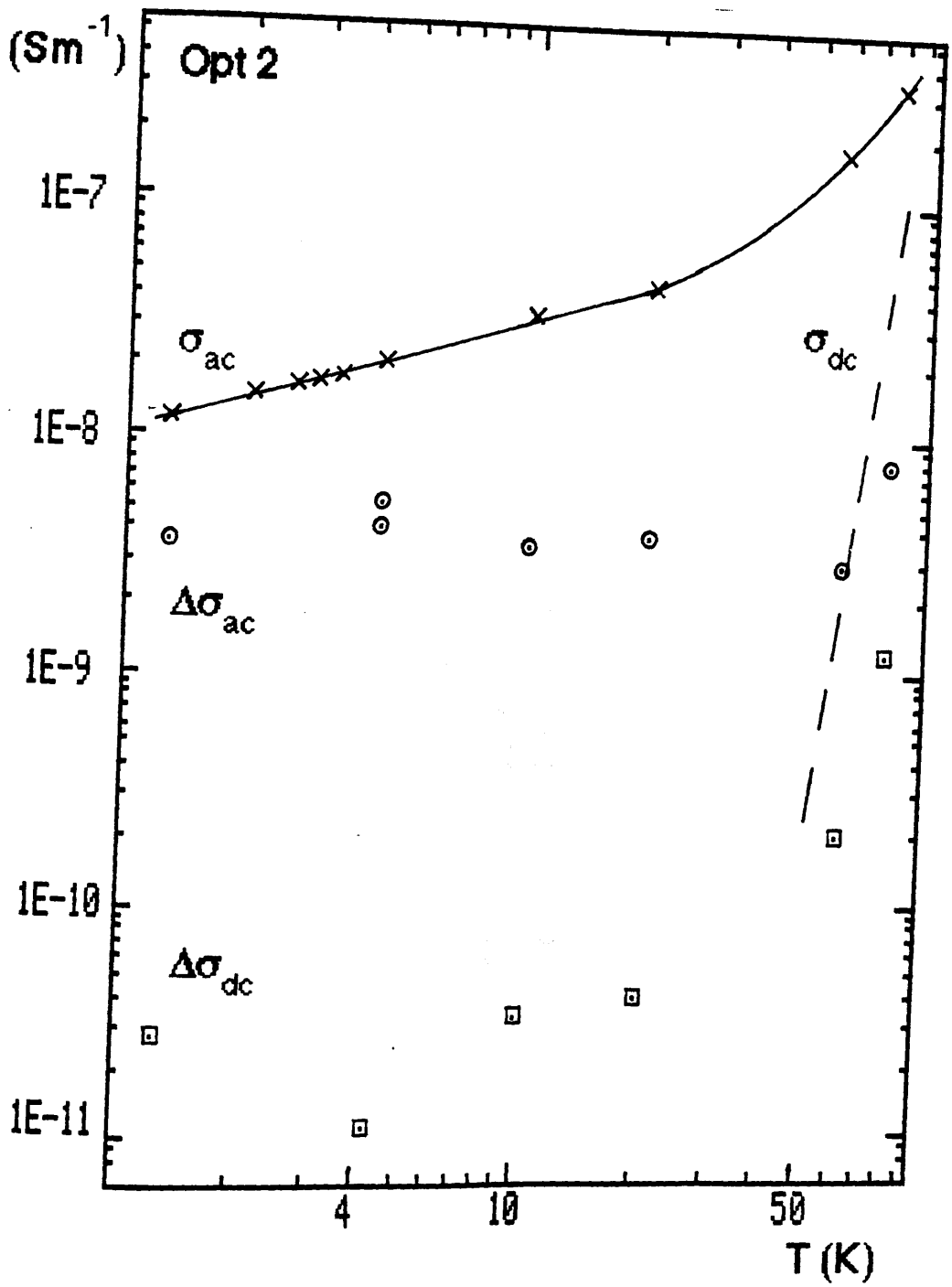

Figure 6.37 : Temperature dependence of light-induced changes in the a.c. and d.c. conductivity of Opt 2 (a-Ge:H 4:1). The temperature dependence of the dark a.c. and d.c. conductivity is also shown for comparison. I_o = 3900nWcm^{-2} (a.c. conductivity measured at 3kHz).

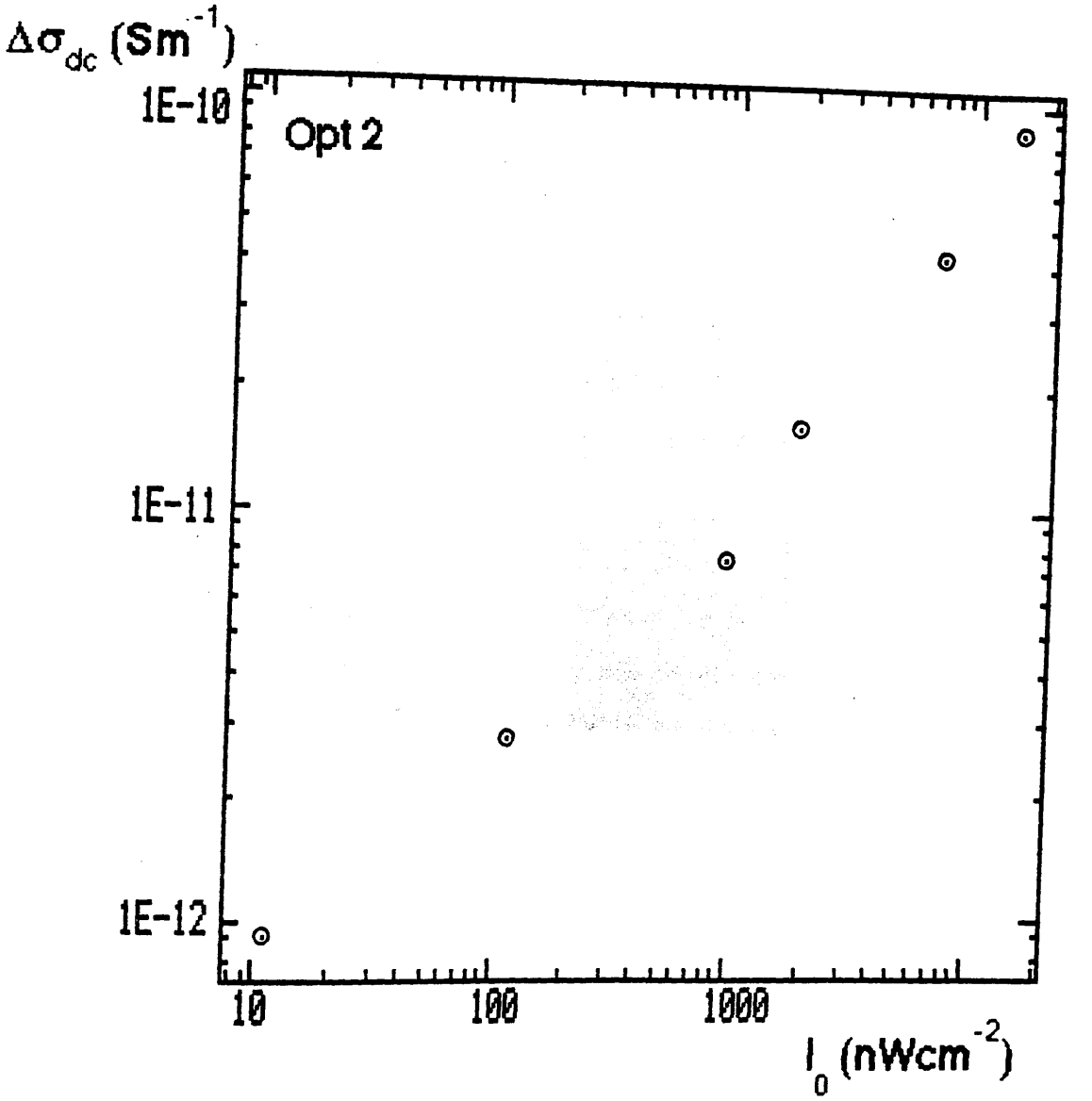

Figure 6.38 : Intensity dependence of the d.c. photoconductivity for Opt 2 at 4.2K.

CHAPTER 7 : Analysis of the Optically Induced Loss

7.1 : The General Mechanism

The permittivity and a.c. conductivity changes reported in the previous chapter occurred at illumination intensities of 1000nWcm^{-2} or less, three orders of magnitude less than intensities used to induce additional gap states in the Staebler-Wronski effect in a-Si:H. The magnitude of the loss changes ($\Delta\varepsilon_1$ or $\Delta\sigma_{ac}$) were approximately equal in pure a-Si and pure a-Ge; heavily hydrogenated material showed a slightly reduced response.

The change in permittivity is not a thermal effect because :- (i) The highest light intensities used would only register an increase in the Ge thermometer reading at 1.3K, such an increase would be typically 0.03K. The semiconductor junction would have to be locally heated by 2K to simulate the loss increases. As the samples and the Ge thermometer are in good thermal contact, it is unlikely that such a temperature change would not be detected. (ii) 25cm^3 of Helium gas was allowed into the insert can whilst the sample was at 4K. The helium would condense to form a thin layer of high thermal conductivity on all objects within the can so reducing any localized heating effects. The response was no different from that when the experiment was performed in vacuum. (iii) The power densities introduced into the sample by light (=1.4nW for I=3500nWcm^{-2}) are similar to those produced electrically by the measuring a.c. signal from the frequency generator (=8nW for 10mV a.c. signal). The latter

does not produce any long term changes in loss. (iv) The response is non-linear in intensity, whereas for a small temperature displacement a linear response would be expected.

The main features of the measurement that any model of the low temperature induced loss has to explain are :- (i) The long time constants associated with the response. The recovery to the dark state varies inversely with time at long times. (ii) The non-linear response. At low intensities the response varies as $I^{1/2}$ but a "saturation" occurs at higher intensities with increases approximately proportional to $I^{1/4}$. (iii) The temperature dependence. At high intensities this is very weak. In the $I^{1/2}$ region there can be a significant temperature dependence, although the uncertainty with which the dark state capacitance is known leads to large error bars at low intensities and hence the exact temperature dependence is difficult to deduce.

The general mechanism we propose for optically induced loss is shown in fig. 7.1. The incident photons generate free carriers, (A). The electrons (and holes) are rapidly trapped by deep, clustered defects, (B). The defects are able to relax at the frequency of the externally applied a.c. field (typically 3kHz). The trapped electrons (or holes) respond to the applied field and hence contribute an additional a.c. loss (C). The only escape from the defects at these low temperatures is by tunnelling to a neighbouring excess hole. This process occurs at a much slower rate than 1/3kHz.

If this model is correct then the additional dielectric loss is due to processes similar to those occurring in the low temperature regime of dark loss (§2.8), whereas the decay is similar to the processes found in the high temperature regime,

albeit at a lower temperature.

7.2 : The Rate Equation

In the following section, the nature of the deep state recombination processes which govern the response is analysed and simple rate equations appropriate for the $I^{1/2}$ region are formulated.

It is assumed that equal numbers of hole-like and electron-like defects are created by the light (i.e. that n=p where n is the number of excited electron-like defects per unit volume, not the number of free electrons. p is the corresponding figure for hole-like defects.) Recombination is assumed to be by simple tunnelling at a rate:

$$\tau^{-1} \sim \tau_0^{-1} \exp(-2\alpha R) \qquad (7.1)$$

where α^{-1} is the decay length of the wavefunction and R is the separation of the electron and hole defects.

If there is a uniform random distribution of excited holes around each electron the nearest-neighbour probability function is:

$$P(R) = 4\pi p R^2 \exp\left(-\frac{4}{3}\pi p R^3\right) \qquad (7.2)$$

It is possible to calculate a mean value of recombination rate by averaging over this distribution of excited hole defects giving

$$\overline{\tau^{-1}} = \int_0^\infty \tau_0^{-1} \exp(-2\alpha R) 4\pi p R^2 \exp\left(-\frac{4}{3}\pi p R^3\right) dR = \frac{\pi p}{\tau_0 \alpha^3} = \frac{\pi n}{\tau_0 \alpha^3} \qquad (7.3)$$

In order to compute the integration it has been assumed that the density of defects is low (i.e. $\alpha^{-1} << p^{-1/3}$).

The rate equation for electrons is :

$$\frac{dn}{dt} = g_0 - n\overline{\tau^{-1}} = g_0 - An^2 \quad \text{where } A = \frac{\pi}{\tau_0 \alpha^3} \tag{7.4}$$

where g_o is the generation rate due to optical excitation given by I/Ed, E being the photon energy and d the sample thickness. The quantum efficiency is taken to be unity, i.e. all the excited electrons and holes are assumed to be trapped and to contribute to the loss. Also, it is assumed that any geminate thermal recombination or luminescence is negligible.

Finally, an implicit assumption in the above analysis is that the excited defects are unrelated to the background defects and the photo-induced loss can be considered independently from the background loss. This is seen to be a reasonable assumption in §7.6.

7.3 : Applications of the Rate Equation

When an equilibrium value of loss is attained at a particular illumination intensity then dn/dt=0 and

$$n = \left(\frac{g_0}{A}\right)^{1/2} \tag{7.5}$$

Once the light is extinguished and the free decay to dark equilibrium begins then g_o=0 and the rate equation can be solved to give

$$n = (At)^{-1} \tag{7.6}$$

There is an assumption here that the excited state distribution remains uniform during the decay, i.e. the proportion of closely spaced pairs to the more distant pairs remains constant throughout the decay. We shall see that although this simplification is a reasonable approximation

for the early part of the decay (t<10ks), a more sophisticated model has to be used to explain the form of the decay over the whole period of measurement (§7.11).

We suppose that the change in permittivity is directly proportional to the number of excited electrons :

$$\Delta\varepsilon_1 = Kn \qquad (7.7)$$

Eqns. 7.6 and 7.7 lead to

$$\Delta\varepsilon_1 = \frac{1}{t}\frac{K}{A} \qquad (7.8)$$

The ratio K/A can now be calculated from free decay data. Eqn. 7.8 predicts the relationship between $\Delta\varepsilon_1$ and time, observed at times of less than 10ks.

Eqns. 7.5 and 7.7 give

$$\Delta\varepsilon_1 = \left(\frac{K^2}{A}\frac{I}{Ed}\right)^{1/2} \qquad (7.9)$$

The dependence of $\Delta\varepsilon_1$ on the square root of intensity is exactly what is seen experimentally at low intensities. The value of K can be estimated from the $I^{1/2}$ region of the permittivity versus intensity plots.

The value of K for Opt 3 at 4K is estimated to be $8\times10^{-20}cm^3$ (±30%) which implies the excited electron density at the top of the $I^{1/2}$ region is $7\times10^{17}cm^{-3}$, which is an acceptable value when compared to the expected spin density in films of this type of $5\times10^{19}cm^{-3}$. From the value of A, $7\times10^{-22}cm^3s^{-1}$ a estimate of τ_0 can be made. Taking α^{-1} from the EPA fit to the a.c. conductivity in the high temperature regime as 12Å then τ_0 = 8s. The high temperature fit gives $\tau_0 = 8\times10^{-20}s$ assuming that the excited defects are distributed over 0.1eV around the fermi level. The difference of 20 orders of magnitude between these two figures is remarkable. It is possible that the electrons are strongly trapped at the defect sites,

probably by lattice distortion. We will see in a later development of the model (§7.12) that self-trapping does play an important part in optically induced loss.

Other values of K and A for Opt 3 and the rest of the optical samples are given in table 7.1. The excited electron density values, n, at the top of the $I^{1/2}$ region and estimates of τ_0 are also shown.

It has been noted in §6.1 that the rise-time, t_r, to the equilibrium value of capacitance decreases with intensity. A simple theoretical estimate of t_r would be the time taken to fill the defects of the sample with electrons. The rise-time is therefore the number of excited defects divided by the generation rate.

$$t_r = \frac{n}{g_0} = \frac{1}{\sqrt{Ag_0}} = \left(\frac{h\nu d}{A}\right)^{1/2} I^{-1/2} \qquad (7.10)$$

For Opt 3, at a temperature of 4K, the rise-time to the top of the $I^{1/2}$ region is 3200s (see fig 6.1). Equation 7.10 gives the much faster value of 350s for the same intensity (I_o=0.72nWcm^{-2}).

A note on intensity values : The intensities used to calculate the K and A values and in other calculations in this section are average intensities :

$$I = I_0\left(\frac{1-\exp(-\alpha d)}{\alpha d}\right) \qquad (7.11)$$

where I_o is the light intensity entering the semiconductor thin film (i.e. after reflection from the surface has been taken into account), d is the thin film thickness and α is the absorption coefficient of the semiconductor (see Appendix 3). The ratio of I/I_o varies between .16 and .54 depending on sample thickness and the wavelength of light used.

7.4 : The Active Defects

In order to investigate the nature of the defects responsible for optically induced loss a model for the relaxation process has to be used. As the response is a low temperature effect, a version of the "atomic" tunnelling model appropriate for single-phonon transitions would probably be suitable (see §2.5). The tunnelling relaxation time in this case is :

$$\tau \sim \frac{B}{\Delta} \exp(2\lambda) \tanh\left(\frac{\Delta}{2kT}\right) \qquad (7.12)$$

where B is a constant and Δ is the energy difference between the two different orientations of the defect, which ranges from 0 to Δ_0. The tunnelling parameter, λ, is taken to be randomly distributed over a range $0 < \lambda < \lambda_0$ to allow for a distribution of barrier heights and widths.

The computation of the mean polarizability (see §2.5) leads to an expression for the permittivity contribution :

$$\Delta\varepsilon_1 = \frac{1}{3} \frac{\eta}{\varepsilon_0 \Delta_0} \frac{Np^2}{\lambda_0} \ln\left(\frac{kT}{\omega B}\right) \qquad (7.13)$$

for $\omega B >> kT$. Here η is the mean field factor, N is the number of states per unit volume and p is the dipole moment of the defect. There are many unknowns associated with the parameters in eqn. 7.13. As this is an order of magnitude calculation the following simplifications are made :

$$\eta \sim 1 \qquad \Delta_0 \sim 0.1\text{eV} \qquad \frac{\ln\left(\frac{kT}{\omega B}\right)}{\lambda_0} \sim 1$$

Eqn. 7.13 then reduces to

$$K \sim \frac{p^2}{\varepsilon_0 \Delta_0} \qquad (7.14)$$

For Opt 3, at a temperature of 4K, $K = 8 \times 10^{-20} cm^3$

which gives a dipole moment of 1×10^{-28}Cm or an electronic charge x 7Å. This result is strong evidence that the defect responsible for the additional loss in Opt 3 is electronic and is around 7Å in extent. The size of the active defect is in good agreement with the estimate made from the a.c. field effect data for loss in the low temperature regime; for Opt 3 at 4K the latter procedure gave the defect size = 8Å (see table 5.1).

The defect size changes little for the other samples (table 7.1); Opt 5, the heavily hydrogenated a-Si sample has a slightly smaller active defect when compared to pure material. The size of the defects is consistent with the idea that loss in sputtered material at helium temperatures is caused by states on the internal surface of voids of about 10Å in extent (see §2.8).

7.5 : The Reduced Sensitivity at High Intensities

The model presented so far gives a reasonable account of the intensity dependence of the response at low intensities. In all samples, at high intensities, $\Delta\varepsilon_1$ no longer increases as $I^{1/2}$ but less rapidly.

The loss changes in the $I^{1/2}$ region are associated with strongly self-trapped electrons. The reduced response at higher intensities suggests faster recombination and less strong self-trapping. At low intensities, light fills up states close to the Fermi level (in mid-gap) where self-trapping is strong. At higher light intensities, the states closer to the band edges begin to fill. Here α^{-1} is

larger and self-trapping is likely to be weaker; these states will therefore have shorter recombination times.

At the highest intensities the states contributing excess loss will have a broad distribution of recombination times. The shallow excited electron states will exhibit rapid recombination whereas in the deep states the recombination process will be much slower. Thus, in eqn. 7.4, the constant A will not now be a constant but will increase with n. Hence the rate of change of n with g_o under high optical excitation will decrease, as is observed.

7.6 : The Relationship to the Background Loss

So far there has been an implicit assumption that it is the optically induced changes, above the background or dark loss, that should be analysed. The background loss has been ignored and the induced loss has been treated as independent of background.

In order to justify the above it is useful to to suppose the opposite to be true; that the optical generation introduces a perturbation in a background population of excited defects which result in loss. The total number of states contributing to the loss is the sum of the background of excited defects, n_b, and the light induced excited defects, n_i.

$$n = n_b + n_i \tag{7.15}$$

The appropriate rate equation is :

$$\frac{dn}{dt} = g_0 + g_{th} - An^2 \tag{7.16}$$

where g_{th} is the thermal generation rate and g_o is the optical generation rate.

If the induced loss is a small fraction of the

background then $n_i \ll n_b$ and eqn. 7.16 can be linearized as follows :

$$\frac{dn_i}{dt} = g_0 + g_{th} - An_b^2 - 2An_b n_i \qquad (7.17)$$

For dark equilibrium, $g_{th} = An_b^2$ therefore

$$\frac{dn_i}{dt} = g_0 - 2An_b n_i \qquad (7.18)$$

Eqn. 7.18 predicts : (i) A linear intensity dependence ($n_i = g_0/2An_b$ for constant illumination). (ii) An exponential decay to equilibrium when the light is extinguished ($n_i \sim \exp(-t.2An_b)$). The experimentally observed induced loss certainly does not conform to this pattern.

Before any final conclusion is drawn, the possibility that the limit $n_i \ll n_b$ is not satisfied should be examined. Even at low temperatures and high intensities the change in the a.c. conductivity rarely excedes 10% of the background a.c. conductivity. As the temperature increases the dependence of $\Delta\sigma_{ac}$ on T is weak compared to that of σ_{ac} so the limit is met in all cases.

It is evident, therefore, that the optically induced loss involves a different population of states from the background loss. This could mean that the loss is associated with electrodes or with the sample surfaces. However, the model presented in the following section will show that the independence of the induced loss arises naturally from the characteristics of the active defects.

7.7 : A Model for the Active Defects

The e.s.r. signal from a-Si and a-Ge is usually associated with dangling bonds on the surfaces of small voids, of about 10Å in extent, within these films. The low temperature, background a.c. losses are linked with electron hopping between states on the internal surfaces of the voids (see §2.8). In §7.4 it was shown that the optically induced loss occurs at defects of 10Å in extent. It is likely that the same defects are responsible for all three of the above phenomena.

The sites of a particular void will be in close proximity so the possibility of intersite correlations must be considered. The occupation of one site by an electron will reduced the probability of occupation of a second, nearby site, by coulombic repulsion. Based on the above information, we formulate a simple model which it is postulated that the low temperature light induced loss in amorphous tetrahedrals is derived from a population of correlated pairs of dangling bond states. In reality, the electronic structure of individual voids will be more complicated.

The energy diagram for the correlated pair model is shown in fig 7.2. Separate bands are included for first (D^o states) and second (D^- states) electrons occupying each site. There is a positive correlation energy, U, within individual sites . The second site states are raised in energy with respect to the first by the intersite correlation energy, E_{12}. There will be some overlap of the electronic wavefunctions between the first and the second site, hence the coulomb repulsion energy will be lowered and $E_{12} < U$.

The bandwidth of the defect sites is Δ_0; it is assumed that $\Delta_0 >= U$. The bandwidth is taken to be mainly determined by long range potential fluctuations so the energies of each state in the pair are close to one another. If $\Delta_0 < U-E_{12}$ then each site of the pair will be filled with one electron. However, if $\Delta_0 > U-E_{12}$ there will be some overlap between the first and second sites for different pairs. Some low energy pairs will be occupied by three electrons and some by one electron. Such $1e^-$ and $3e^-$ pairs will contribute strongly to the low temperature loss, due to the processes $(1,0)<=>(0,1)$ and $(2,1)<=>(1,2)$ respectively. The loss will be largely temperature independent except for some residual effect on the transition rate.

When light is used to excite extra mobile carriers, these carriers will condense into defect pairs, resulting in additional loss. For example, an electron trapped at *(i)* creates a new $3e^-$ pair. However, this is partially compensated by an electron trapped at *(ii)* which converts a $1e^-$ pair to an two electron pair (a $2e^-$ pair contributes nothing to the a.c. loss). The process which is central to optically induced loss is the trapping of an electron at *(iii)* creating new $3e^-$ pairs. There is no process to counterbalance the extra active a.c. loss pairs; an electron trapped at energy *(iii)* unambiguously contributes to an increase in loss. The same arguments can be applied to the capture of holes at energy *(iv)* creating $1e^-$ pairs.

The experimental evidence strongly suggests that the background loss and the induced loss are independent. The electrons trapped at *(iii)* and holes at *(iv)* constitute a population of states that is completely independent of the background

$3e^-$ and $1e^-$ pairs.

The value of Δ_0 and the shape of the defect bands governs the magnitude of the photo-induced loss. If Δ_0 is large and the defect bands are flat then the states created at energy *(ii)* will exactly compensate those at energy *(i)* and the induced loss will be small. If the bands are relatively narrow and non-uniform, as in fig. 7.2, the compensation will be less and the photo-induced response will be greater. If $\Delta_0 <$ U-E_{12}, although there are no dark $1e^-$ or $3e^-$ states, these can be generated by photo-excitation and trapping. Hence a film which shows a very small a.c. loss at low temperatures may still exhibit significant photo-induced loss.

At high temperatures some pairs will be in the $3e^-$ and $1e^-$ configuration on thermal grounds. When the temperature is reduced these states will relax by tunnelling. The light induced loss results show that the relaxation process takes a long period of time so it is not surprising that samples take many hours to reach a stable dark equilibrium after cooling from 77K to 4K (see §6.7).

7.8 : Distributed Trapping

In order to compare the magnitude of the induced loss in different samples and at different wavelengths of light it is necessary to take account for the absorption of light as it passes through a semiconductor thin film. The intensity at a depth, x, is given by

$$I = I_0 \exp(-\alpha x) \qquad (7.19)$$

where α is the absorption coefficient, d is the film thickness and I_0 is the surface intensity. The generation rate at x is :

$$g(x) = -\frac{dI}{dx} = \alpha I_0 \exp(-\alpha x) \qquad (7.20)$$

Using eqns. 7.5 and 7.9 the permittivity change, at depth x, can be calculated.

$$\Delta\varepsilon(x) = K\left(\frac{g(x)}{A}\right)^{1/2} = K\left(\frac{\alpha I_0}{A}\right)^{1/2} \exp(-\alpha x/2) \qquad (7.21)$$

The total capacitance (the dark value plus the photo-induced capacitance) is as follows :

$$\frac{1}{C} = \int_0^d \frac{dx}{(\varepsilon_b + \Delta\varepsilon_0 \exp(-\alpha x))A} \qquad \text{where } \Delta\varepsilon_0 = K\left(\frac{\alpha I_0}{A}\right)^{1/2} \qquad (7.22)$$

$$= \frac{d}{\varepsilon_b A} - \frac{\Delta\varepsilon_0}{\varepsilon_b^2 \alpha A}\left(1 - \exp(-\alpha d/2)\right)$$

where $\frac{d}{\varepsilon_b A} = C_b$, the dark value of the capacitance.

$$\frac{\Delta C}{C_b} = \frac{\Delta\varepsilon}{\varepsilon_b} = \frac{\Delta\varepsilon_0}{\varepsilon_b}\left(\frac{1 - \exp(-\alpha d/2)}{\alpha d/2}\right) \qquad (7.23)$$

The measured change in permittivity is

$$\Delta\varepsilon = \Delta\varepsilon_0\left(\frac{1 - \exp(-\alpha d/2)}{\alpha d/2}\right) \qquad (7.24)$$

The parameter, $\Delta\varepsilon_0$, is independent of sample thickness and of the absorption coefficient. A plot of $\Delta\varepsilon_0$ against intensity for the results taken using three different wavelengths of light on Opt 6 is shown in fig. 7.3. The data now plots around a common line. It is clear that, in the energy range 1.55eV to 2.48eV, the choice of wavelength makes little difference to the magnitude of the response. Any radiation of energy greater than the band gap will liberate free carriers which lead to increased loss. Subbandgap radiation, however, is expected to promote recombination and

quench the induced loss (see §7.12).

Using the distributed trapping model on the data taken on the 7320Å and 4000Å films of Opt 6 produces an unexpected result (fig. 7.4). If the induced loss is a bulk effect then the magnitude of the response should be equal for both films. In fact, it is the 7320Å film which shows a 25% greater value of $\Delta\varepsilon_0$ than the 4000Å film, in the $I^{1/2}$ region. It is the raw values of $\Delta\varepsilon_1$ that are of equal magnitude for the thin and thick films (see fig. 6.35). From this limited set of data, it appears that the induced loss does have a component associated with the surface regions, at least for this sample.

The method used here and in the next section applies, in principle, only to the low intensity region because of the assumption of $I^{1/2}$ behaviour made in eqn. 7.21. There is an error of approximately a 10% increase above the correct value of $\Delta\varepsilon_0$ in the high intensity region. The effect is the same, within experimental error, on each sample.

7.9 : Magnitude of the Response in Different Materials

Fig 7.5 compares the magnitude of $\Delta\varepsilon_0$ for the six samples investigated in this work at 4K. The induced loss in pure a-Ge and pure a-Si is approximately the same magnitude at high intensities; no data is available at low intensities for the a-Ge samples. The differences between Opt 6 (magnetron sputtered a-Si) and Opt 3 (conventional sputtered a-Si) were easily within experimental error. The hydrogenated material, Opt 2 (a-Ge:H 4:1) and Opt 4 (a-Si:H 20:1) show an

equal response which is about half that of pure material at high intensities. At low intensities the induced loss in Opt 4 is only slightly less than that in pure a-Si.

The data of fig 7.5 has been calculated from raw values of $\Delta\varepsilon_1$ using the distributed trapping theory. The untreated data is presented in fig 7.6 for comparsion. It can be seen that the equality of the response in pure material and between a-Si:H (20:1) and a-Ge:H (4:1) is not as clear in the raw data.

A similar pattern in the $\Delta\varepsilon_0$ data is seen at 10K (fig 7.7) except that at this temperature the response in Opt 6 is twice that in Opt 3. The induced loss decreases as the temperature rises for the orthodox sample but remains unchanged in the magnetron sample. The heavily hydrogenated Opt 5 (10:1) shows the lowest response of all the samples at high intensities although the same sample gives a greater response than either Opt 3 or Opt 4 at low intensities.

By introducing hydrogen in a-Si and a-Ge films it is possible to reduced the magnitude of the hopping conductivity and of the ESR signal (Stuke, 1977). The incorporation of hydrogen can saturate dangling bonds and lead to a reduced density of states. There is evidence from the high temperature loss measurements to suggest that the energy scale of the self-trapping increases with hydrogen content.

In §7.5 the $I^{1/2}$ region was associated with strongly self-trapped electrons. It would be expected that the response in this region will be greater in heavily hydrogenated films and this result is seen experimentally (Opt 5 at T=10K, fig 7.7). As the light intensity increases, states further from mid-gap will be filled and the transition

to $I^{1/4}$ behaviour will occur. A consequence of the reduced number of dangling bond states in hydrogenated material is that the mid-gap states will be saturated at a lower intensity of light than in pure material and the transition to the $I^{1/4}$ region will occur at a lower intensity. This effect is particularly apparent in fig 7.7 when comparing the data for Opt 3, Opt 4 and Opt 5.

In summary, the incorporation of hydrogen into the semiconductor film leads to i) a reduced response in the high intensity region because of the reduced number of active defects ii) a greater response in the $I^{1/2}$ region because of the enhanced self-trapping in such films.

The only material to be tested for optically induced loss besides a-Si and a-Ge was sputtered arsenic selenide. Intensities of up to 100μWcm^{-2} of 633nm light were applied to one sample but no change in the capacitance or conductivity could be detected. It is possible that the loss measured at low temperatures in the arsenic selenide sample was due to deep defects caused by gold diffusion (see §5.5). Such centres would considerably enhance the recombination rate of trapped carriers and so quench the light induced loss (M. J. Anderson, unpublished). Gold diffusion may also have occurred in the a-Si and a-Ge samples. Shimakawa et al. (1987) observed the effect of gold diffusion on the dark a.c. conductivity in glow discharge a-Si. Any effect of the diffusion is likely to be negated in our samples because of the dominating effect of the high defect density found naturally in sputtered tetrahedral material.

7.10 : The Recombination Time

In order to compare the recombination times at different temperatures it is useful to plot the permittivity change against log(time) for the decay back to equilibrium after light out. Fig 7.8 shows that for Opt 3 this form of the final decay is linear for the duration of the experiment. The decays for Opt 6 show a similar linear relationship over an even longer time scale (fig 7.9). The form of the decays suggest that the simple analysis of the rate equation (§7.3) is not adequate. In the next section the assumptions made in §7.3 are examined and the theory is developed to account for the shape of the decays over the whole period of measurement.

Figs 7.8 and 7.9 show that the recombination times are temperature independent. This result is expected because at low temperatures activation from the polaron wells is by zero point energy and the hopping rate is temperature independent (Mott & Davis, Ch3). Hence the recombination rate will be temperature independent.

If the hypothesis about hydrogen contributing to the trapping of electrons in deep states introduced by Long et al. (1982) (see §2.7) is correct then hydrogenated films will need a greater energy to release electrons from their defect states, and hence would be expected to show a much enhanced recombination time for the decay of the induced loss. This premise is confirmed experimentally. Figs 7.10 and 7.11 are the final decays from the silicon samples at 4K and 10K respectively. The permittivity change in Opt 5 recovers at a rate four times slower than that for the pure a-Si samples at 10K. Opt 4 (a-Si:H 20:1) returns to equilibrium at a rate

that is intermediate between the pure samples and Opt 5. The orthodox pure a-Si sample has the most rapid decay.

7.11 : Analysis of the Decay to Equilibrium

Figs 7.8 to 7.11 show that the free decay to equilibrium is more fully descibed by expression $\Delta\varepsilon_1 \propto \ln(t)$ than by $\Delta\varepsilon_1 \propto 1/t$. The latter expression is only adequate for a limited time range (between t=1000s and t=10000s for Opt3, see fig 6.26). The analysis of §7.3 is satisfactory as applied to the equilibrium behaviour because, with carriers being continually trapped and then recombining, a random distribution of excited states is maintained. However once the light is extinguished, it is the closely spaced electron-hole pairs that will recombine first leaving a distribution of states that is bias towards more distant pairs. The average separation of pairs in the distribution will increase as the decay proceeds. Hence solving the rate equation :

$$\frac{dn}{dt} = g_0 - n\overline{\tau^{-1}} = g_0 - An^2 \qquad \text{where } A = \frac{\pi}{\tau_0 \alpha^3}$$

is not adequate because the random distribution is not preserved.

A better approximation is to write n(t) as the number of nearest neighbour pairs with recombination time τ >t. First we assume a random distribution at t=0 and that $n_o = p_o$ where n_o is the number of electron-like excited states at t=0 and p_o is the corresponding number for hole-like states. The nearest neighbour probability function

(eqn. 7.2) can be simplified by assuming a cut-off in R, the separation of the electron and hole defects, where

$$R_{max} = (3/4\pi n_0)^{1/3} \tag{7.25}$$

hence :

$$P(R) = 4\pi n_0 R^2 \qquad R < R_{max} \tag{7.26}$$

$$P(R) = 0 \qquad R > R_{max}$$

where n_0 is the number of excited states at t=0. Assuming recombination is by simple tunnelling and using eqn. 7.1 gives

$$P(\tau) = P(R)\frac{dR}{d\tau} = \frac{4\pi n_0 R^2}{2\alpha\tau} = \frac{4\pi n_0}{(2\alpha)^3\tau}\left[\ln\left(\frac{\tau}{\tau_0}\right)\right]^2 \tag{7.27}$$

The number of excited nearest neighbour pairs at time t is then calculated

$$n(t) = n_0\int_t^{\tau_{max}} P(\tau)d\tau = \frac{\pi n_0^2}{2\alpha^3}\int_t^{\tau_{max}}\left[\ln\left(\frac{\tau}{\tau_0}\right)\right]^2\frac{d\tau}{\tau} \tag{7.28}$$

$$= \frac{\pi n_0^2}{6\alpha^3}\left\{\left[\ln\left(\frac{\tau_{max}}{\tau_0}\right)\right]^3 - \left[\ln\left(\frac{t}{\tau_0}\right)\right]^3\right\} \tag{7.29}$$

Differentiating this expression with respect to ln(t) gives

$$\frac{dn_1}{d\ln(t)} = -\frac{\pi n_0}{2\alpha^3}\left[\ln\left(\frac{t}{\tau_0}\right)\right]^2 \tag{7.30}$$

Using eqn. 7.7, which supposes the change in permittivity is directly proportional to the number of excited pairs, we can estimate the gradient of the $\Delta\varepsilon_1$ versus ln(t) plot :

$$\frac{d\varepsilon_1}{d\ln(t)} = -\frac{\pi([\Delta\varepsilon_1]_0)^2}{2K\alpha^3}\left[\ln\left(\frac{t}{\tau_0}\right)\right]^2 \tag{7.31}$$

where $[\Delta\varepsilon_1]_0$ is the change in permittivity at t=0, before the light is extinguished. This is approximately constant provided that $t >> \tau_0$, giving the linear dependence of $\Delta\varepsilon_1$ on ln(t) observed.

For Opt 6 at T=10K, $[\Delta\varepsilon_1]_0$ = 0.14 and from fig 7.11

$d\varepsilon_1/d\ln(t) = 0.011$. From table 7.1 an estimate of K^2/A can be taken (K^2/A depends on the equilibrium response (see eqn. 7.9) hence is still applicable) :

$$\frac{K^2}{A} = 2.4\times10^{-17}\,cm^3s \Rightarrow \quad K^2\tau_0 = \frac{\pi.2.4\times10^{-17}}{\alpha^3} = 4.3\times10^{-38}\,cm^6s \qquad (7.32)$$

taking $\alpha^{-1} = 8A$ from the high temperature EPA fit (table 5.1). Using eqn. 7.31 leads to

$$\frac{K}{\left[\ln\left(\frac{t}{\tau_0}\right)\right]^2} = \frac{\pi}{2}\frac{[\Delta\varepsilon_1]_0}{\frac{d\varepsilon_1}{d\ln(t)}\alpha^3} = 1.7\times10^{-21}\,cm^3 \qquad (7.33)$$

Combining eqns. 7.32 and 7.33 gives

$$\tau_0\left[\ln\left(\frac{t}{\tau_0}\right)\right]^4 = 1.6\times10^4\,s \qquad (7.34)$$

which can be solved using iterative techniques to give $K = 7.4\times10^{-20}cm^{-3}$ and $\tau_0 = 8s$ for $t = 6000s$. The values given by the analysis of §7.3 which assumed a random distribution of states during the decay are $K = 1.9\times10^{-19}cm^{-3}$ and $\tau_0 = 1s$. The similarity between the two sets of results confirms that the simplified analysis of §7.3 is valid within a limited time range.

The values of K and τ_0 calculated using the above analysis at other temperatures and for other samples are given in table 7.2. The figures are comparable within an order of magnitude to those calculated using the former simplified analysis of §7.3. The values of n at the top of the $I^{1/2}$ region and the defect sizes have be estimated from the new values of K.

7.12 : An Model to Resolve the τ_0 Inconsistency

The values of τ_0 given in table 7.2 range from 0.02s to 10s, the discrepancy between these values and the high temperature fit estimate of τ_0 is still as large as in §7.3. We now introduce a new model and examine the range of R, the distance between the electron and hole defects. A maximum value of R has already been defined by eqn. 7.25. R_{max} is associated with a maximum recombination time, τ_{max} by eqn. 7.1. Following the idea that loss in sputtered material at helium temperatures is due to states on the internal surfaces of voids (see §2.8), we now define a minimum value of R, R_{min}, which reflects that voids of finite size cannot be infinately close. R_{min} is associated with a minimum recombination time, τ_{min}.

Defining the parameter R_{min} has an effect on the mean value of the recombination rate, $\overline{\tau_0^{-1}}$, and hence on the defining equation for the equilibrium behaviour and the constant A. From eqns. 7.3 and 7.26 :

$$\overline{\tau_0^{-1}} = \int_{R_{min}}^{R_{max}} \tau_0^{-1} \exp(-2\alpha R)\, 4\pi R^2 n_0\, dR \qquad (7.38)$$

$$= \frac{\pi n_0}{\alpha^3 \tau_{min}} \left(1 - \frac{\tau_{min}}{\tau_{max}}\right) \sim \frac{\pi n_0}{\alpha^3 \tau_{min}}$$

The results quoted for the 1/t fit in table 7.1 therefore still apply for τ_{min}=1s.

The value of n(t) at $t = \tau_{min}$ is now estimated using eqn. 7.29 :

$$n(\tau_{min}) = \frac{\pi n_0^2}{6\alpha^3} \left\{ \left[\ln\left(\frac{\tau_{max}}{\tau_0}\right) \right]^3 - \left[\ln\left(\frac{\tau_{min}}{\tau_0}\right) \right]^3 \right\} \qquad (7.36)$$

Note that

$$\frac{4}{3}\pi(R_{max}^3 - R_{min}^3) = n_0 \tag{7.37}$$

From eqn. 7.1 :

$$n_0 = n(\tau_{min}) = \frac{\pi}{6\alpha^3}\left\{\left[\ln\left(\frac{\tau_{max}}{\tau_0}\right)\right]^3 - \left[\ln\left(\frac{\tau_{min}}{\tau_0}\right)\right]^3\right\} \tag{7.38}$$

Combining eqns. 7.36 and 7.38 confirms that $n(\tau_{min}) = n_\infty$.

The next stage is to fit the above theory to some experimental data. From eqns. 7.29 and 7.36 as follows :

$$\frac{n(t)}{n_0} = \frac{\left\{\left[\ln\left(\frac{\tau_{max}}{\tau_0}\right)\right]^3 - \left[\ln\left(\frac{t}{\tau_0}\right)\right]^3\right\}}{\left\{\left[\ln\left(\frac{\tau_{max}}{\tau_0}\right)\right]^3 - \left[\ln\left(\frac{\tau_{min}}{\tau_0}\right)\right]^3\right\}} = \frac{\Delta\varepsilon_1}{[\Delta\varepsilon_1]_0} \tag{7.39}$$

The parameter, $\Delta\varepsilon_1/[\Delta\varepsilon_1]_0$ is plotted for Opt 5 and Opt 6 at 10K in fig 7.13. The solid curves represent the theoretical prediction (eqn. 7.39) for τ_{min} =1s, τ_{max} =340ks (chosen to fit the Opt 5 data) and τ_0 varying between 1s and 10^{-17}s. The form of the experimental data is best fitted with $\tau_0 = 10^{-17}$s which is in agreement with the high temperature fit value of τ_0. In principal it appears that the data could be fitted by a pure tunnelling model. However, by estimating values of R_{min} and R_{max}, we shall see that pure tunnelling does not fit the data in all temperature ranges.

From eqn. 7.1 R_{min} is given by

$$R_{min} = \frac{1}{2\alpha}\ln\left(\frac{\tau_{min}}{\tau_0}\right) \tag{7.40}$$

For $\tau_0 = 10^{-17}$s, τ_{min} = 1s and α^{-1} = 8Å then R_{min} = 175Å.

However, from eqn. 7.36

$$R_{max} = \left(\frac{3}{4\pi n_0}\right)^{1/3} \tag{7.41}$$

For $n_\infty = 5\times10^{17}cm^{-3}$ (from table 7.2) then R_{max} = 78Å.

Using different values of τ_0 and α^{-1} does not resolve this

paradox. This is strong evidence for carrier self-trapping at defect sites as postulated in §7.3.

7.13 : Comparison with other Light Induced Effects

Of the light induced effects reported in the literature, the one that stands out as being related to optically induced loss is the work on LESR by Street & Biegelsen (1982) and by Carius & Fuhs (1984) (see § 3.3). There are several points at which the two effects can be compared.

(i) The magnitude of the effect. Street et al. estimated that 10^{16} spins per cm^{-3} were induced by an incident light intensity (1.9eV) of $50nWcm^{-2}$ in a glow discharge a-Si:H film (T=30K). For Opt 4 (a-Si:H 20:1) the same light intensity produced $2x10^{17}$ induced states per cm^{-3} which responded to a 3kHz a.c. field (T=10K). The equilibrium dangling bond density of both films is estimated at approximately 10^{16} spins per cm^{-3}.

(ii) The intensity dependence. For $5 > I_o > 5x10^{3}nWcm^{-2}$ the number of induced spins in the glow discharge sample was proportional to $I^{1/3}$. This compares to $I^{1/4}$ in the intensity range $10 > I_o > 1000nWcm^{-2}$ for Opt 4. The sublinear response implies that the recombination process is not monomolecular.

(iii) For both experiments the time required for 90% of the induced response to decay away is approximately an hour. The LESR decay is linear in log t (see fig 3.6), the photo-induced loss decays show the same linear relationship.

(iv) The LESR lifetimes decrease with increasing

excitation intensity; this is a trait of bimolecular recombination. The characteristic decay time of the optically induced loss increases as the exciting intensity falls. For Opt 2 a characteristic decay time of 120s at I_o=11nWcm^{-2} rises to 900s for I_o=0.1nWcm^{-2}. As the number of light induced states increases, the distance between the states falls and recombination becomes more rapid.

(v) The work of Carius and Fuhs showed that the long-time decay of the metastable trap population measured by LESR was independent of temperature below 80K. The decay of the optically induced loss is independent of temperature at helium temperatures.

(vi) Street and Biegelsen used 647nm and 750nm light. Little difference was seen in the number of light induced spins once the different absorption coefficients at the two wavelengths had been accounted for. The same lack of dependence on exciting light wavelength, within the visible range, was seen for light induced loss.

Street suggests that the LESR is dominated by the more distant pairs of states which have long decay times. Under illumination, the distant pair population rises and is eventually limited by bimolecular recombination. The closer, more rapidly recombining pairs follow a geminate, radiative process and are the source of luminescence. It is the long-lived, distant pairs that will contribute to the optically induced loss.

The LESR measures the fraction of states which become paramagnetic on exposure to light. The signal records D^o states and band tail carriers; it does not represent the total occupation of the states. The induced loss signal will

not describe exactly the same set of states as the LESR. The active defects will be those pairs that can relax at the frequency of the applied field and that have the appropriate occupancy ($3e^-$ or $1e^-$ pairs).

Carius & Fuhs found that the electron and neutral dangling bond resonance of the LESR decayed more rapidly than the hole resonance. They noted that the hole signal was more stongly quenched by IR light and by annealing above 50K. These observations are consistent with the hypothesis that light causes electrons to transfer rapidly to the dangling bond states creating D^o and D^- and that the time limiting step for recombination is tunnelling of band tail holes to the D^o and D^- states. It is likely that the induced loss at long times is due to the low mobility of holes rather than electrons. This could be tested by taking measurements on doped samples. The induced loss in p-type samples should decay less rapidly than in n-type samples.

The quenching of LESR by subbandgap radiation accompanied by photocurrent and photoluminescence transients is strong evidence that the IR radiation promotes recombination between trapped carriers. It would be surprising if the additional a.c. loss could not be quenched in the same way.

The induced loss at liquid nitrogen temperatures is likely to be a photostructural change rather than an electronic phenomena. This is because of the long rise times and decay times measured and the lack of any instantaneous response to excitation at these temperatures. The response may be related to the Staebler-Wronski effect. However the differences between the S-W effect and the light induced loss

at 77K are many. The induced loss does not attain a metastable state, the excess loss decays slowly away when the light is extinguished. The intensities of light used for an S-W experiment are typically 100mWcm^{-2}; the intensities for the induced loss experiment are five orders of magnitude less. Hydrogen is thought to play an important role in the S-W effect whereas the value of $\Delta\varepsilon_1/\varepsilon_1$ decreases from 10^{-2} (Opt 6) to 10^{-3} (Opt 5) as the hydrogen content of the film is increased from zero to 10%. The origins of a photostructural change at 77K appear to be different from the models suggested for the S-W effect.

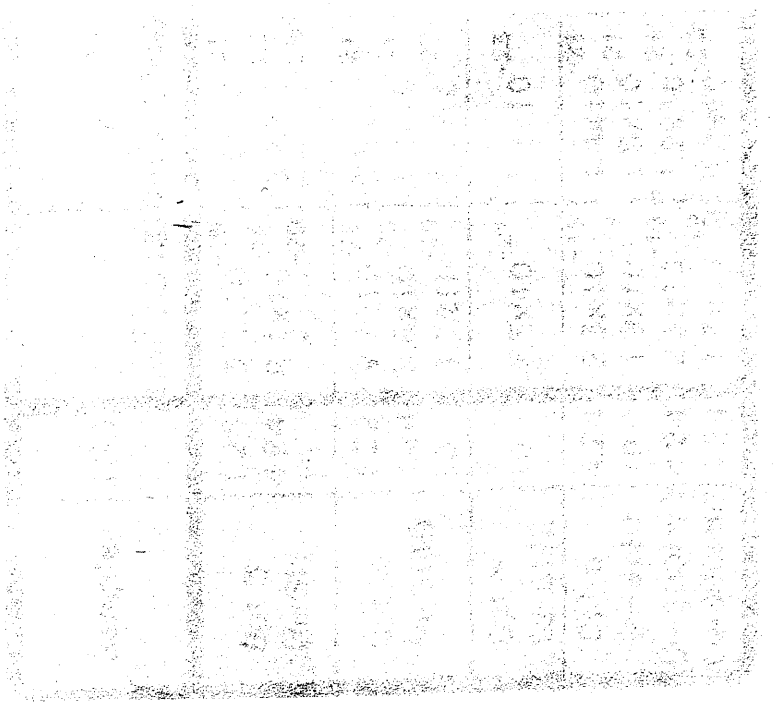

Sample	T(K)	K ($cm^3 \pm 30\%$)	A ($cm^3 s^{-1} \pm 30\%$)	n, excited carrier density at $I^{1/4}/I^{1/2}$ transition ($cm^{-3} \pm 40\%$)	τ_0 ($s \pm 30\%$)	Defect Size ($Å \pm 30\%$)
Opt 3 (a-Si)	1.26	3.4×10^{-19}	1.8×10^{-21}	1.5×10^{17}	3.0	14
	4.24	8.1×10^{-20}	6.9×10^{-22}	6.8×10^{17}	7.9	7
	10	1.6×10^{-20}	5.7×10^{-22}	3.1×10^{18}	9.5	3
Opt 4 (a-Si:H)	1.22	9.7×10^{-20}	5.5×10^{-21}	2.1×10^{17}	0.6	7
	4.24	5.6×10^{-20}	1.2×10^{-21}	3.4×10^{17}	2.9	6
	10	1.7×10^{-20}	6.0×10^{-22}	1.2×10^{18}	5.7	3
Opt 5 (a-Si:H)	10	7.5×10^{-21}	6.2×10^{-23}	1.5×10^{18}	——	2
Opt 6 (a-Si:H)	4.24	2.3×10^{-19}	1.4×10^{-21}	1.5×10^{17}	1.3	11
	10	1.9×10^{-19}	1.5×10^{-21}	1.9×10^{18}	1.2	10
(λ=500nm)	4.24	2.2×10^{-19}	1.2×10^{-21}	1.7×10^{17}	1.5	11
(λ=800nm)	4.24	1.7×10^{-19}	8.2×10^{-22}	1.9×10^{17}	2.2	10

Table 7.1

Sample	T(K)	K ($cm^3 \pm 30\%$)	A ($cm^3 s^{-1} \pm 30\%$)	n, excited carrier density at $I^{1/4}/I^{1/2}$ transition ($cm^{-3} \pm 40\%$)	τ_0 ($s \pm 30\%$)	Defect Size ($Å \pm 30\%$)
Opt 3 (a-Si)	1.28	1.6×10^{-18}	1.8×10^{-21}	3.2×10^{16}	0.1	29
	4.24	1.3×10^{-18}	6.9×10^{-22}	4.2×10^{16}	0.03	27
	10	3.7×10^{-19}	5.7×10^{-22}	1.4×10^{17}	0.02	14
Opt 4 (a-Si:H)	1.22	1.0×10^{-19}	5.5×10^{-21}	2.0×10^{17}	0.5	7
	4.24	1.7×10^{-19}	1.2×10^{-21}	1.1×10^{17}	0.3	10
	10	1.2×10^{-19}	6.0×10^{-22}	1.7×10^{17}	0.1	8
Opt 5 (a-Si:H)	10	5.8×10^{-20}	6.2×10^{-23}	1.9×10^{17}	0.4	6
Opt 6 (a-Si:H)	4.24	8.2×10^{-20}	1.4×10^{-21}	4.1×10^{17}	10	7
	10	7.4×10^{-20}	1.5×10^{-21}	4.9×10^{17}	8	6

Table 7.2

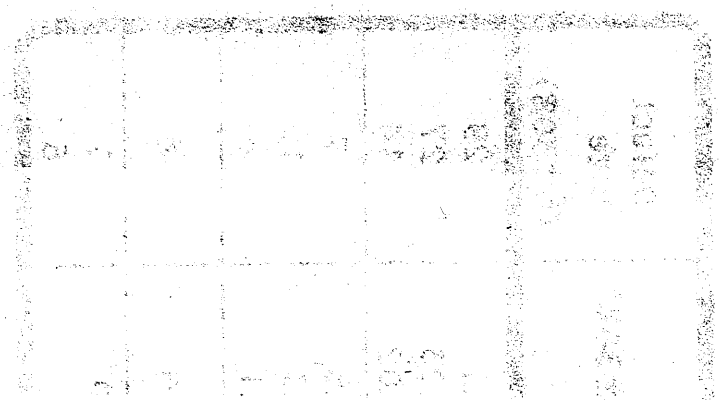

Figure 7.2 : Energy diagram for the correlated pair model.

The energy diagram represents a correlated pair of dangling bond states. Separate bands are included for first (D^0 states) and second (D^- states) electrons occupying each site. There is a positive correlation energy, U, within individual sites. The second site is raised in energy with respect to the first by the intersite correlation energy, E_{12}. Both U and E_{12} are assumed to be the same for every pair of sites. The bandwidth of the defect energy levels is Δ_0. Some low energy pairs will be occupied by three electrons (the '$3e^-$' pairs); hence the first site will be a doublely occupied D^- state and the second site will be a singlely occupied D^0 state. Some high energy pairs will be occupied by one electron, (the '$1e^-$' pairs); the first site will be a D^0 state and the second will be empty. Such $1e^-$ and $3e^-$ pairs will contribute strongly to the dark low temperature loss, due to the processes (1,0)<=>(0,1) and (2,1)<=>(1,2) respectively.

When light is used to excite extra mobile carriers, these carriers will condense into defect pairs, resulting in additional loss. For example, an electron trapped at (i) creates a new $3e^-$ pair. However, this is partially compensated by an electron trapped at (ii) which converts a $1e^-$ pair into a $2e^-$ pair (i.e. two D^0 states which can contribute nothing to the loss). The process which is central to the optically induced loss is the trapping of an electron at (iii) creating new $3e^-$ pairs. There is no process to counterbalance these extra active a.c. loss pairs; an electron trapped at energy (iii) unambiguously contributes to an increase in loss. The same arguments apply to the capture of a hole at energy (iv) creating $1e^-$ pairs.

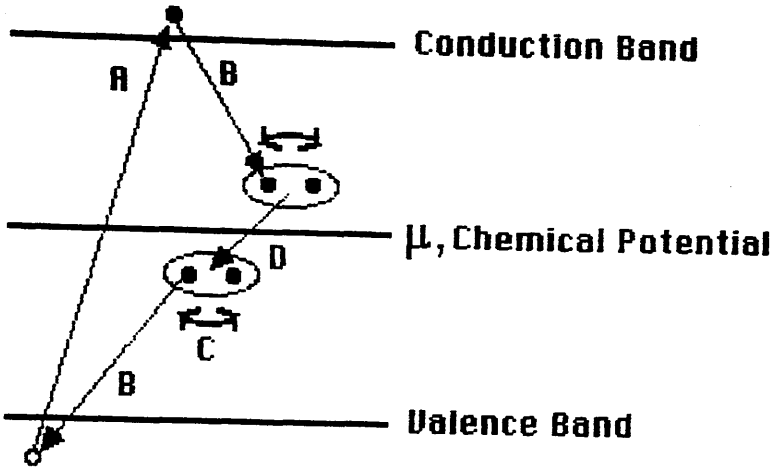

Figure 7.1 : Mechanism of optically-induced loss (see text for details).

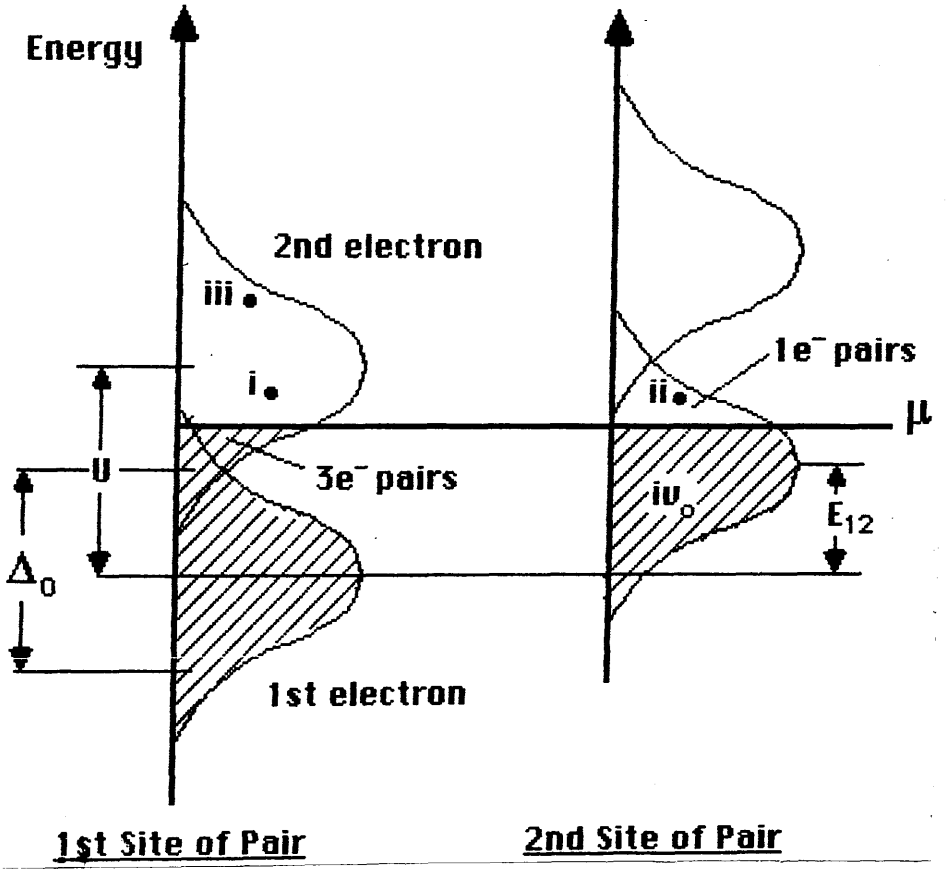

Figure 7.2 : Energy diagram for the correlated pair model.

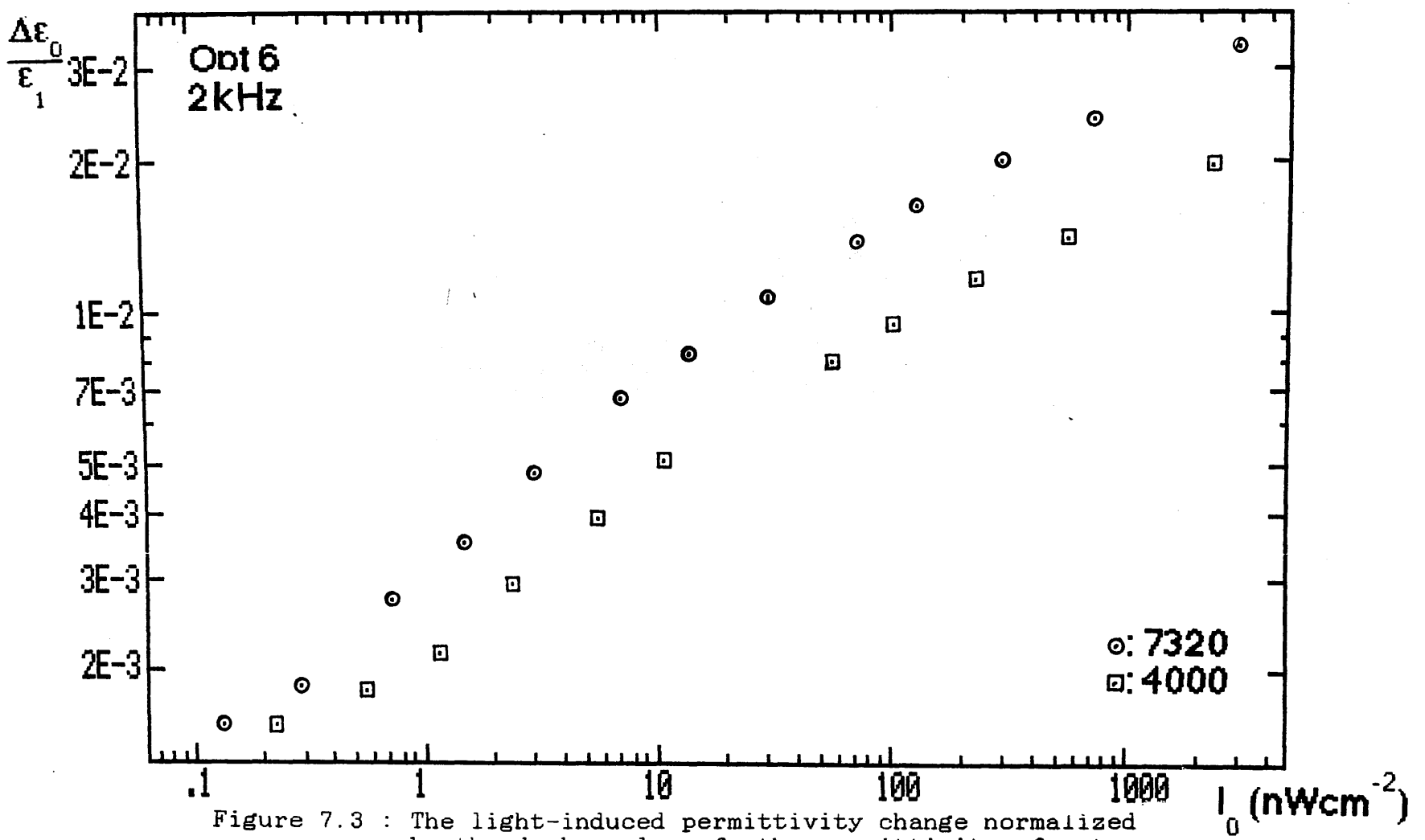

Figure 7.3 : The light-induced permittivity change normalized by the dark value of the permittivity for two film thicknesses for Opt 6 at 4.2K. The permittivity change has been modified by the distributed trapping model to take into account the absorption of light as it passes through the semiconductor film.

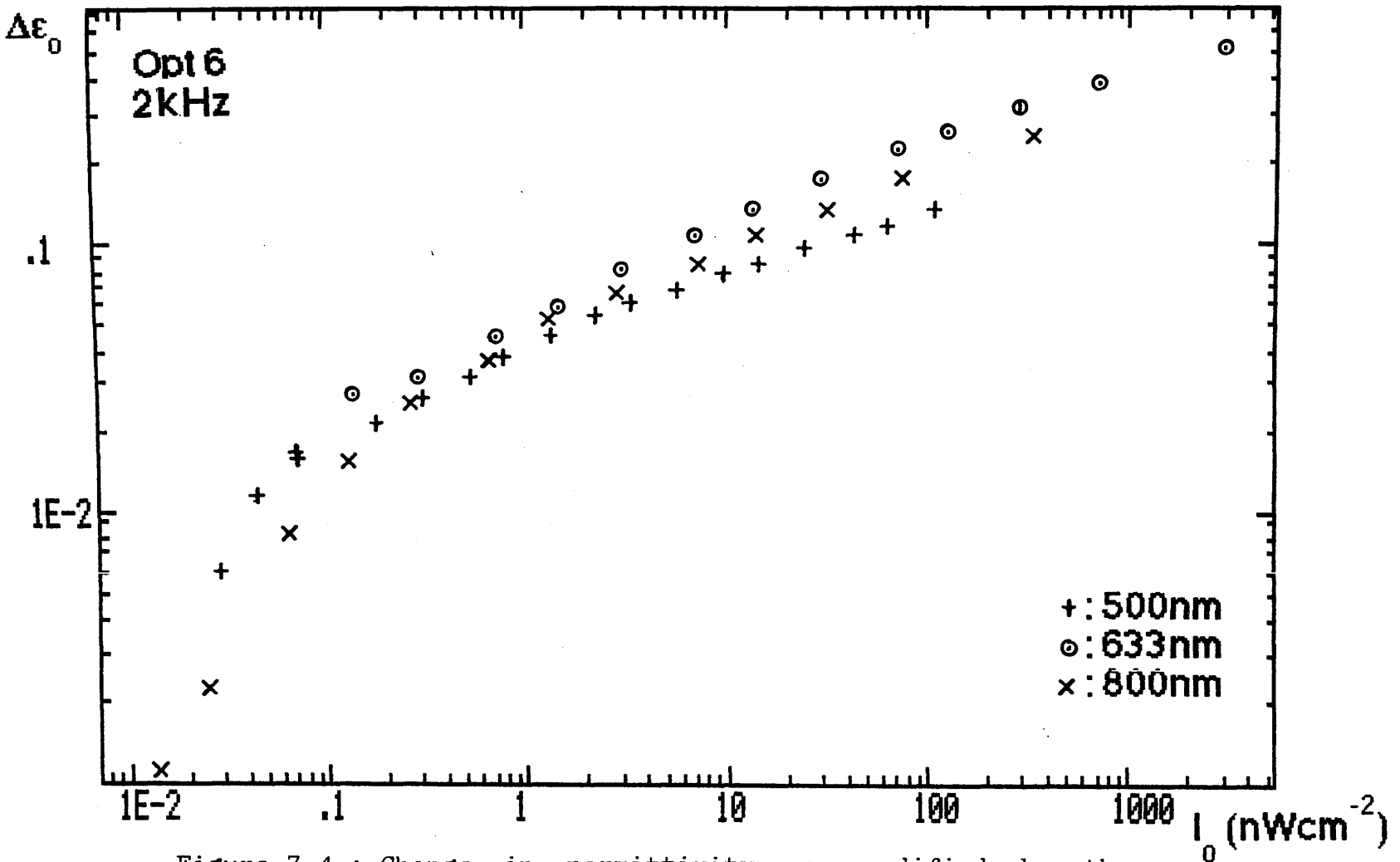

Figure 7.4 : Change in permittivity, as modified by the distributed trapping model, for excitation by light of wavelengths 500nm, 633nm and 800nm for Opt 6 at 4.2K.

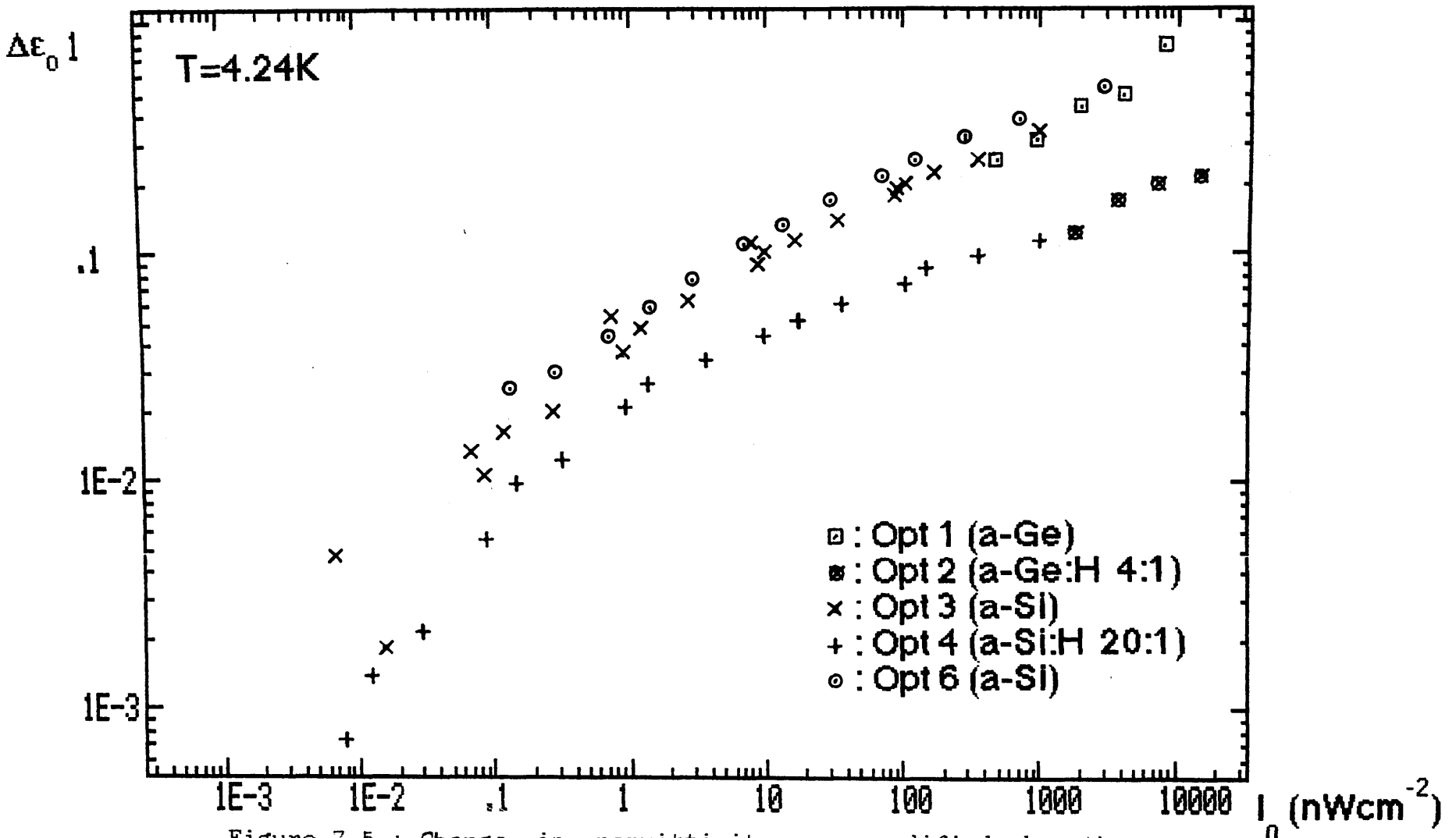

Figure 7.5 : Change in permittivity, as modified by the distributed trapping model, under d.c. illumination for several samples at 4.2K.

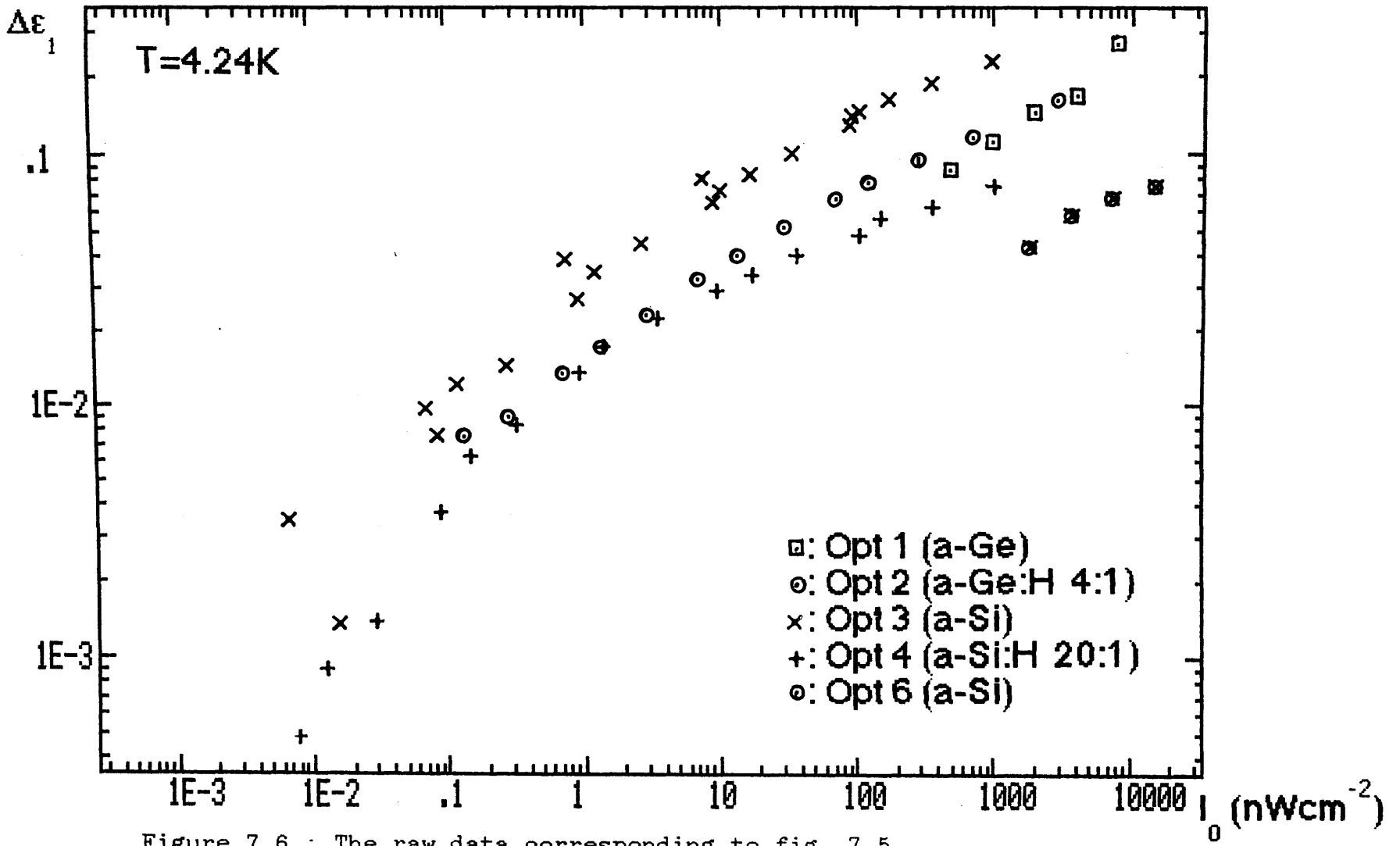

Figure 7.6 : The raw data corresponding to fig. 7.5.

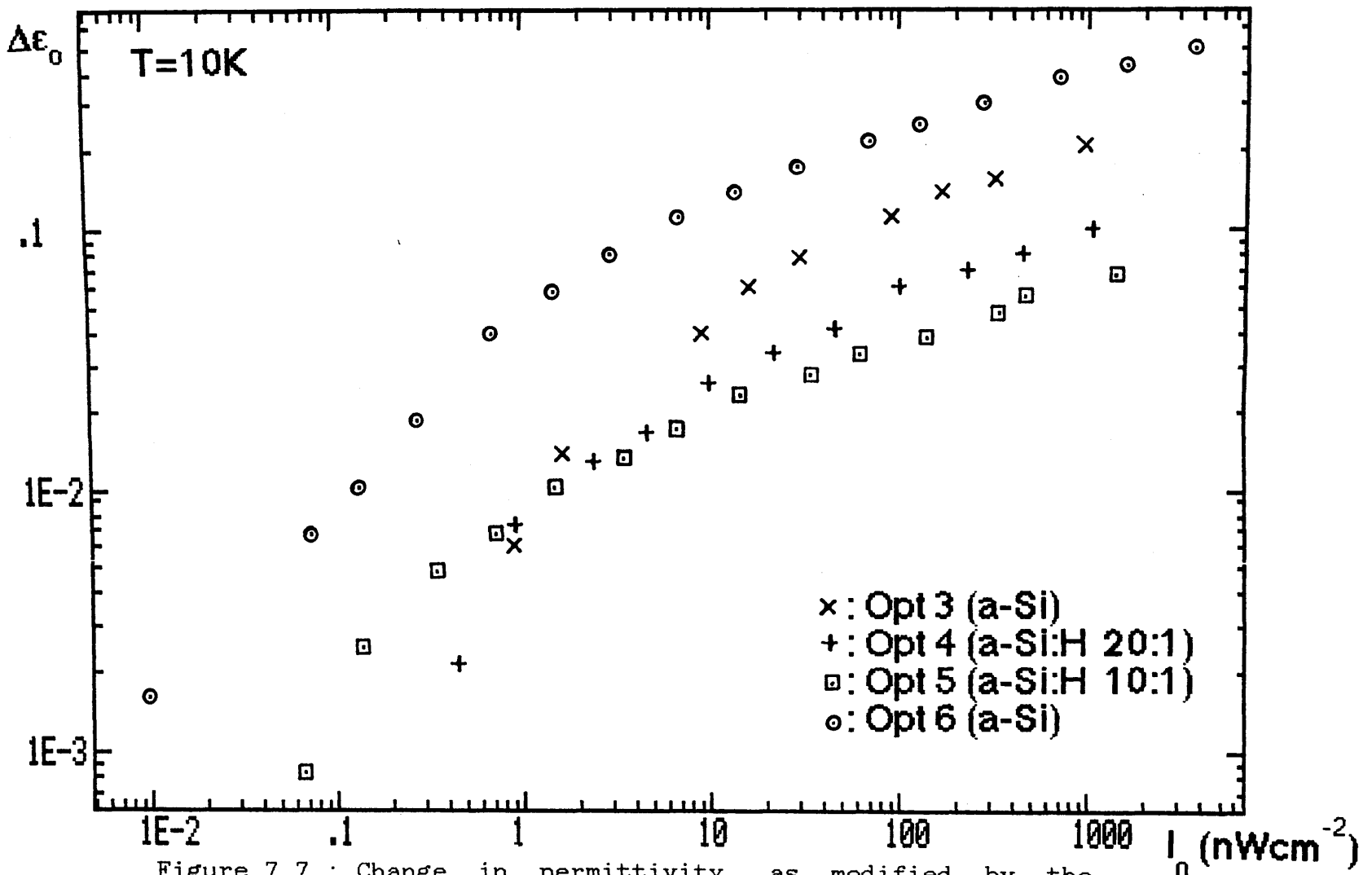

Figure 7.7 : Change in permittivity, as modified by the distributed trapping model, under d.c. illumination for several samples at 10K.

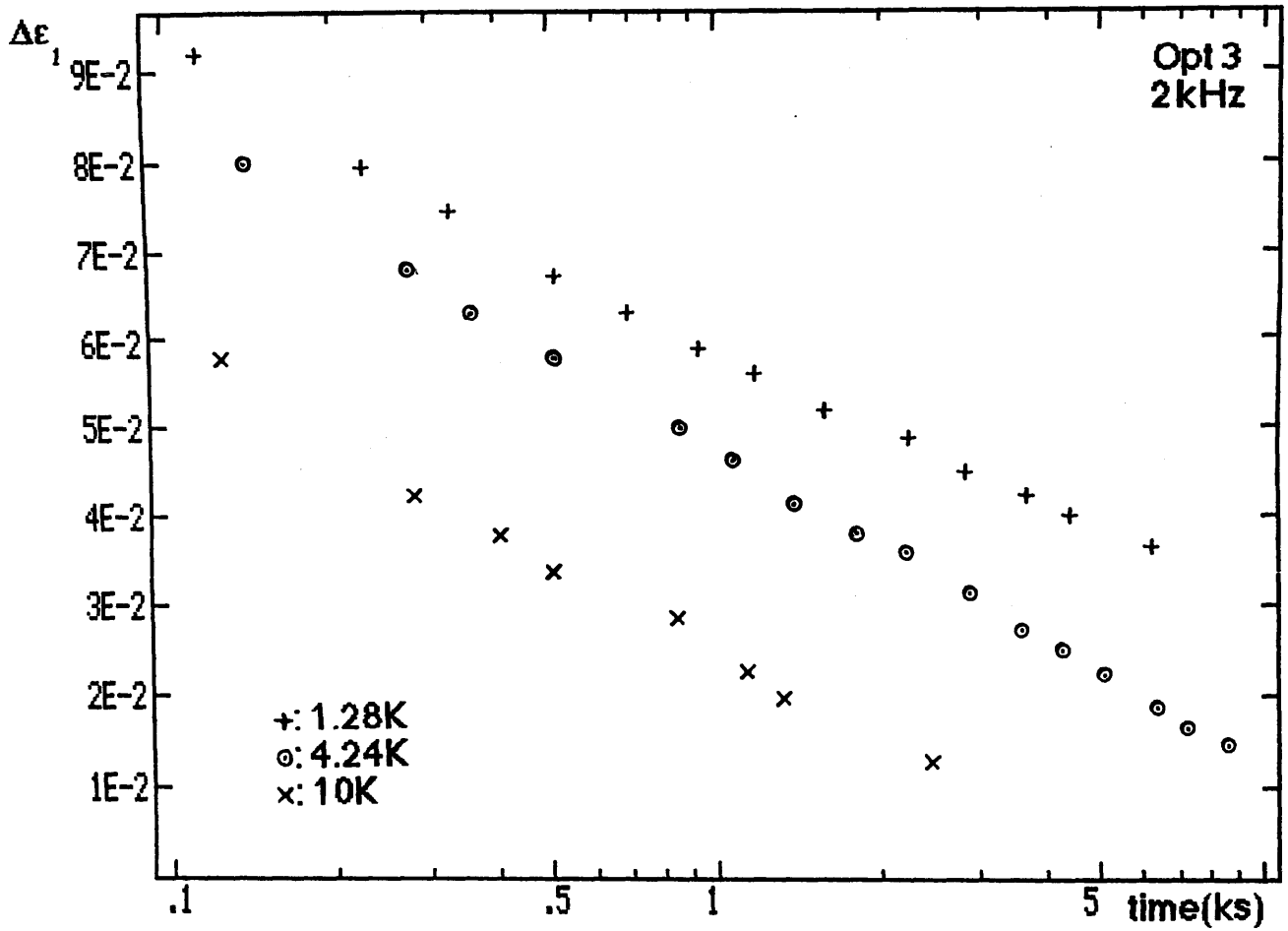

Figure 7.8 : Decay of the permittivity change in the dark for Opt 3 at 1.3K, 4.2K and 10K versus log(time). Data from fig. 6.25.

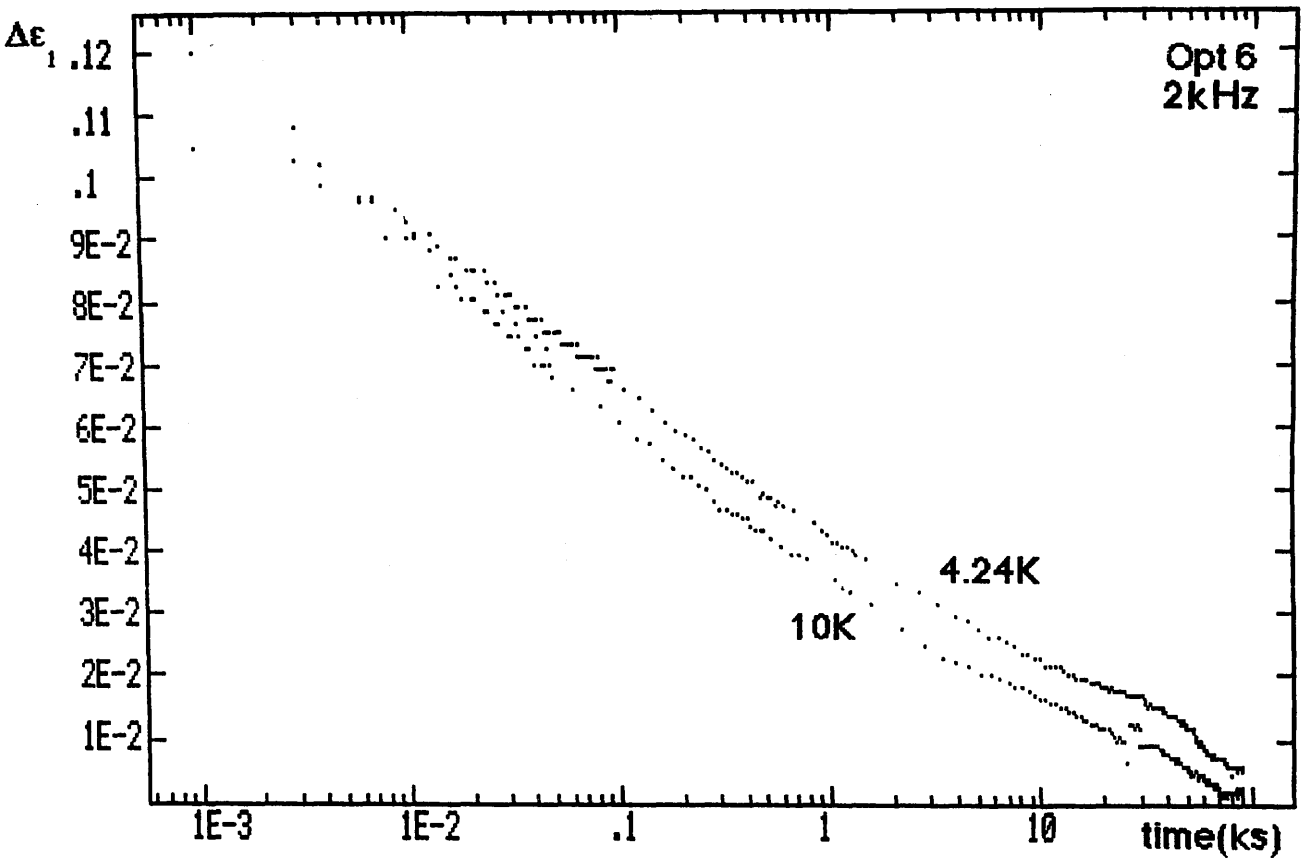

Figure 7.9 : Decay of the permittivity change in the dark for Opt 6 at 4.2K and 10K versus log(time). Data from fig. 6.23.

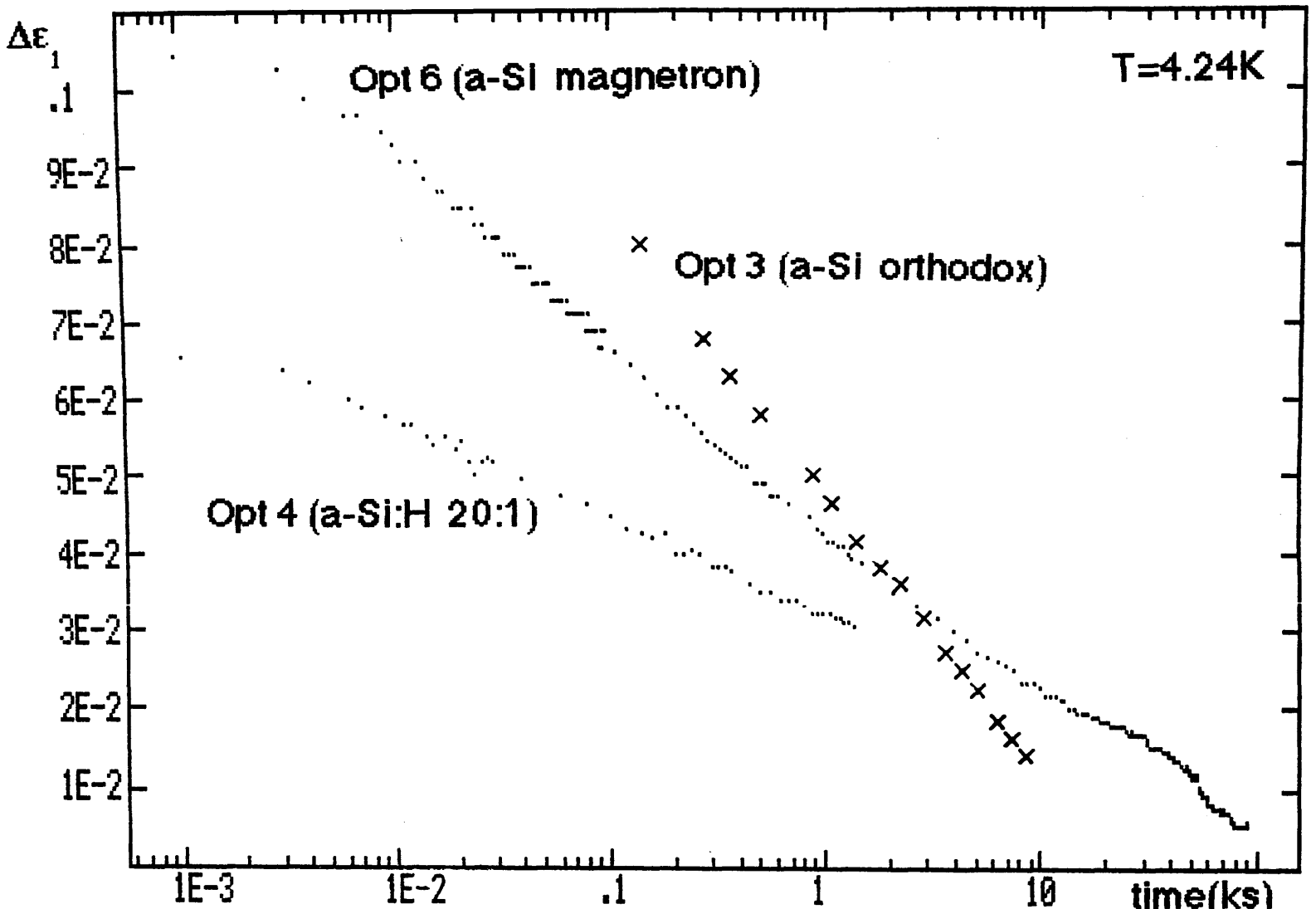

Figure 7.10 : Decay of the permittivity change in the dark for several samples at 4.2K versus log(time).

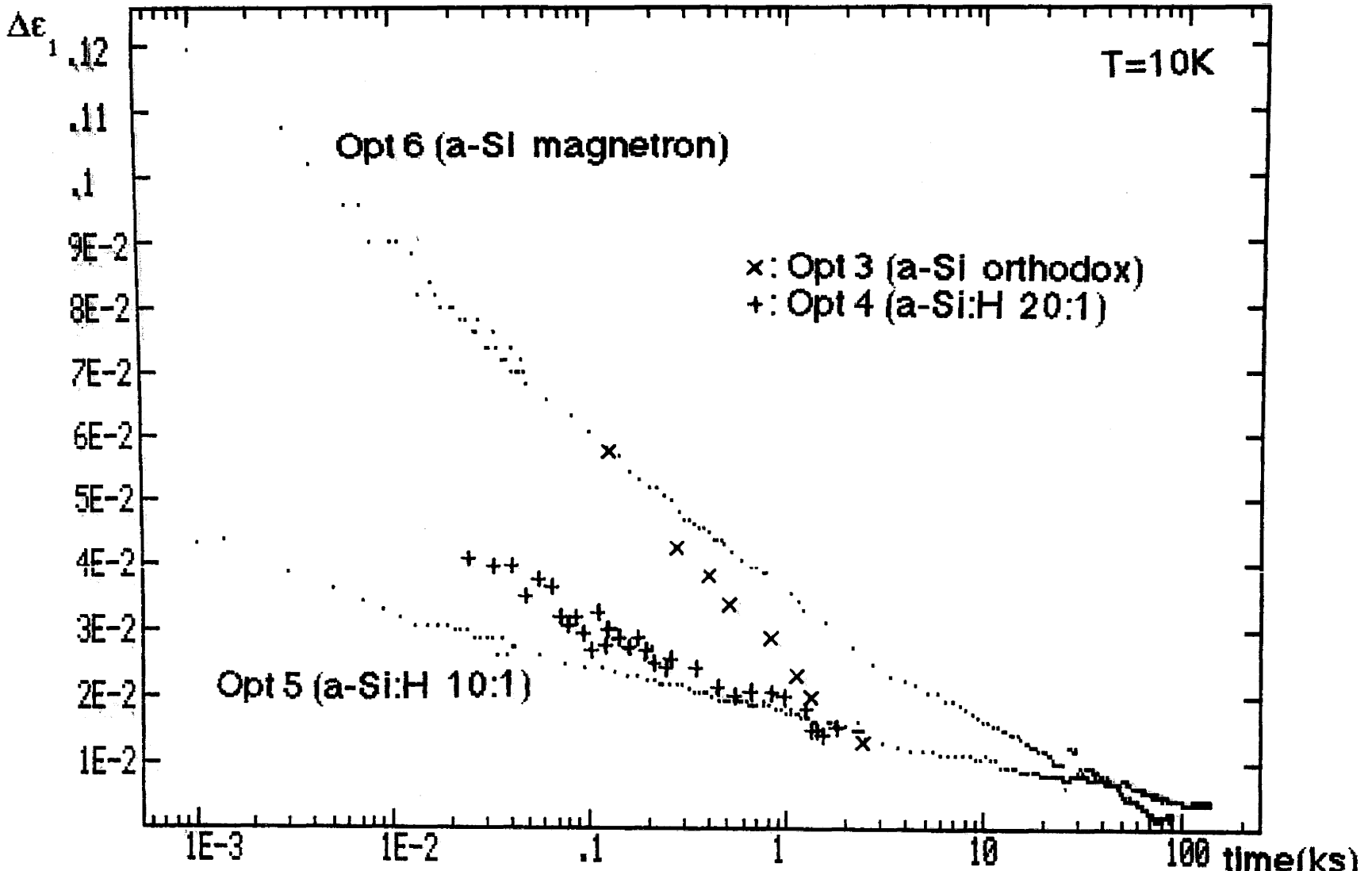

Figure 7.11 : Decay of the permittivity change in the dark for several samples at 10K versus log(time).

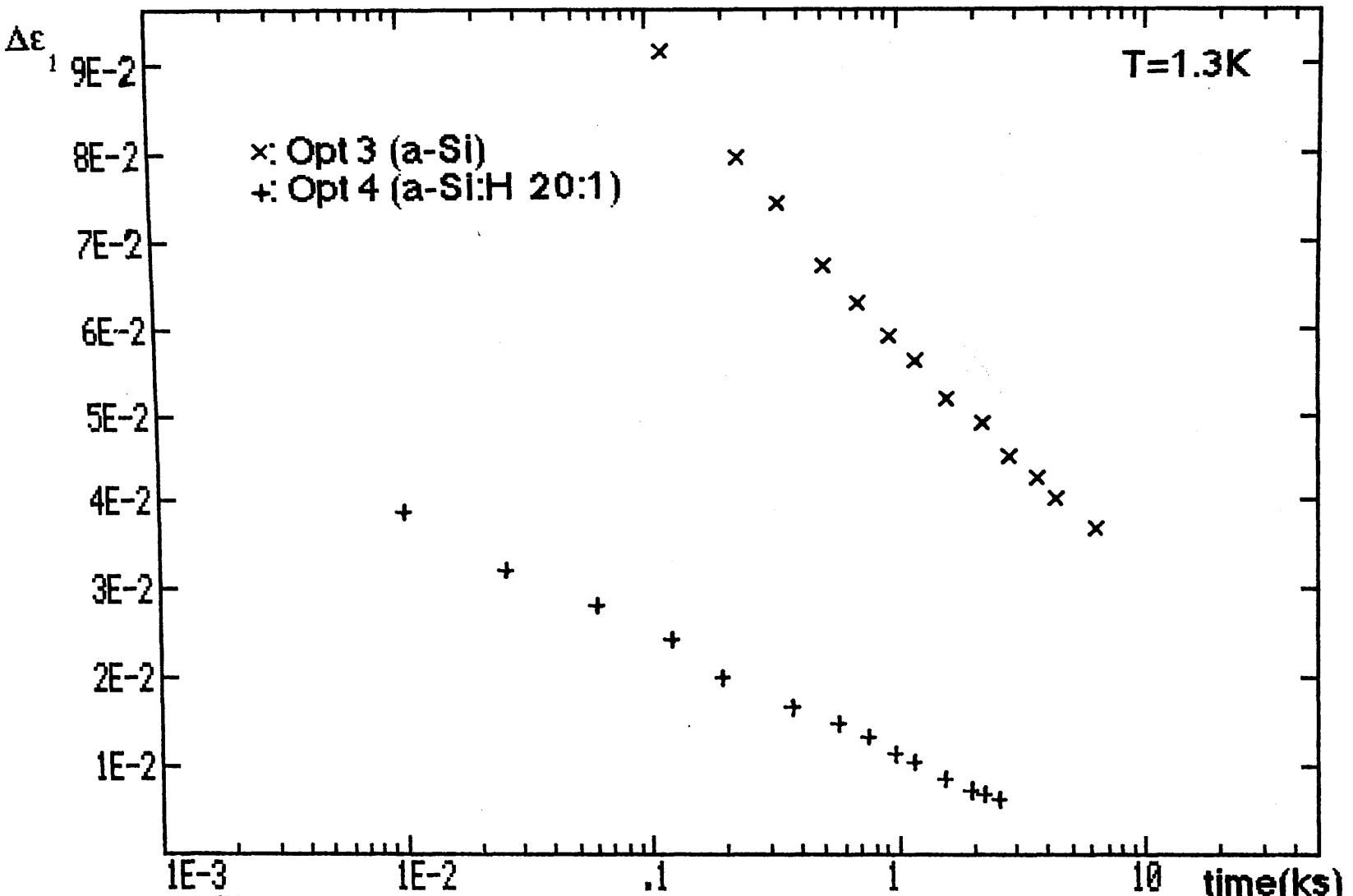

Figure 7.12 : Decay of the permittivity change in the dark for several samples at 1.3K versus log(time).

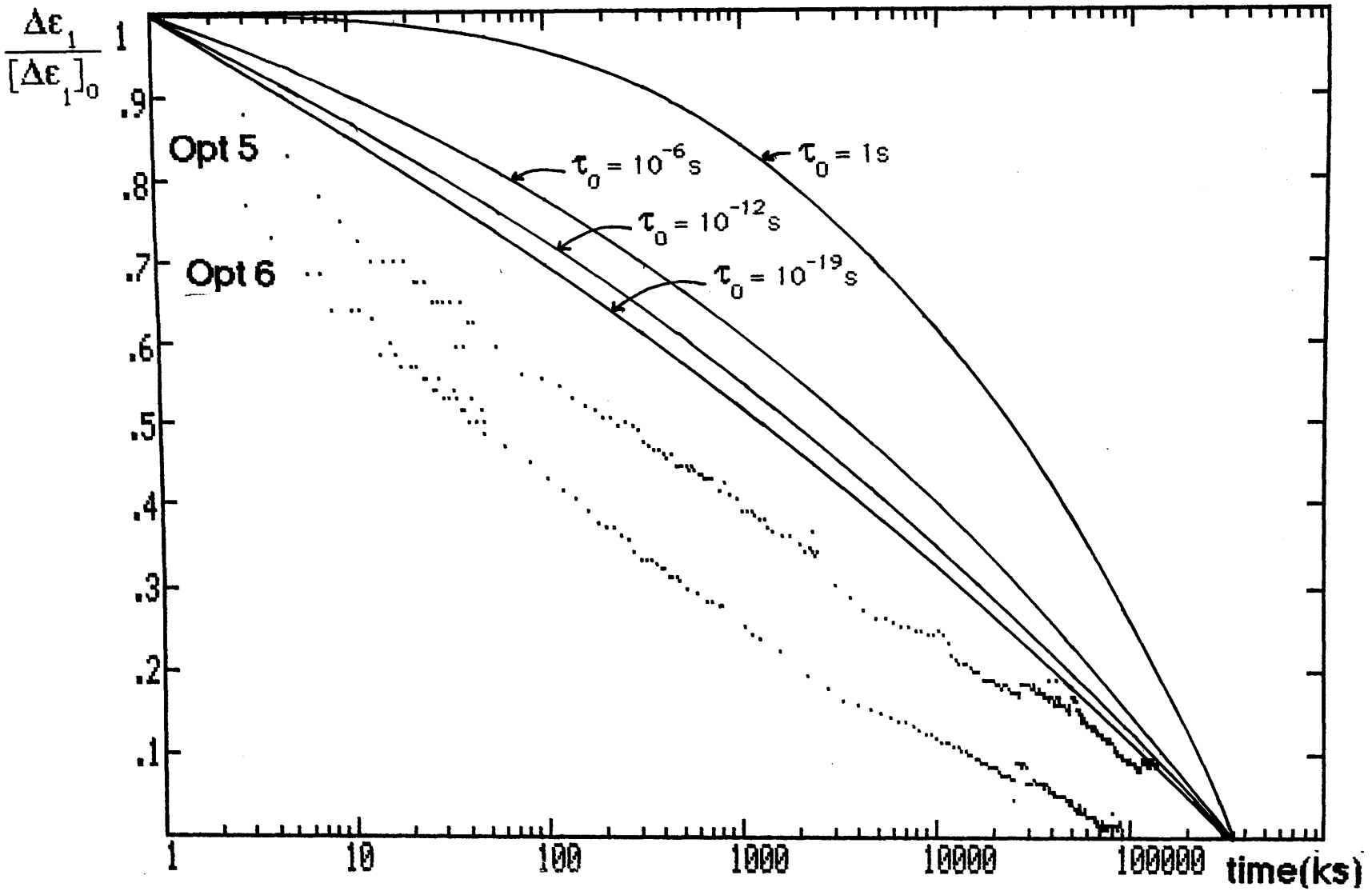

Figure 7.13 : Change in permittivity normalized by the saturation value of the permittivity change for Opt 5 and Opt 6 at 10K. The full lines are the theoretical prediction of eqn. 7.39 for τ_{min}=1s, τ_{max}=340ks and τ_0 as indicated.

CHAPTER 8 : Summary and Conclusions

The aim of this research program was firstly, to repeat the measurements of dark a.c. loss previously performed by other members of the group and then to investigate the effect of light on the a.c. loss. The dark a.c. and d.c. characteristics of the a-Ge and a-Si optical samples, which had gold top electrodes, did not differ from those measured on earlier samples with aluminium top electrodes (Long et al., 1982, 1985). The effects of gold diffusion were not seen.

After light induced loss was seen on the first germanium sample and the basic features of the effect had been established, it was felt necessary to develop two new experimental systems to facilitate the measurement of the effect. The first was the computer-controlled system for automatically recording the conductivity, capacitance and temperature of the samples. The accuracy of this system was compared to that of the more familiar manual bridges and was found to be satisfactory. The second system was the long-term low temperature insert. This insert was designed to maintain the samples at stable helium temperatures over many days and successfully performed a number of experiments of up to 12 days duration with a temperature variation of less than $\pm$0.1K.

The optical response at helium temperatures was found to be non-linear. At high intensities the permittivity increased as $I^{1/4}$ but at low intensities the response was closer to $I^{1/2}$. The temperature dependence of the response was small up to 20K. The dependence of the response on the frequency of

the exciting a.c. signal was no different from that of the dark loss. When 500nm and 800nm light was used, no difference in response could be seen after the different absorption factors of the semiconductor film at these wavelengths had been accounted for. There is limited evidence (from one sample) that the induced loss has a component associated with the surface of the film.

The magnitude of the response in the $I^{1/4}$ region is similar in pure a-Si and pure a-Ge but decreases as the hydrogen content of films increases. In the $I^{1/2}$ region heavily hydrogenated material shows a greater response than pure material.

The model used to explain the induced loss is that optically excited carriers are rapidly trapped by deep, clustered defects. The trapped electrons respond to the applied a.c. field and contribute an additional loss until they recombine by tunnelling to a neighbouring excess hole. A simple analysis of the appropriate rate equation, assuming that the excited state distribution remains random throughout the experiment, predicts the $I^{1/2}$ behaviour at low intensities and that the induced loss should be inversely proportional to time during the free decay to equilibrium. The latter is only seen over a limited time range. The experimental evidence indicates that the induced loss is, in fact, approximately proportional to -log(time) throughout the decay to the dark state.

The recombination time of an excited pair will decrease as the distance between the two states of the pair decreases. When light is continually exciting carriers into defects an equilibrium will be established in the distribution of pair

separations. Hence the intensity dependence of the effect is satisfactorily explained by the simple analysis. However during the free decay in the dark the average pair separation will increase with time. Once this has been included in the analysis, the form of the free decay can be explained, at least to a first approximation. The defect density estimated from the model compares well to the e.s.r. signal in sputtered material. The defect size is estimated to be of the order of 10Å, in agreement with the analysis of the dark low temperature loss (Long et al., 1985).

A minimum recombination time is postulated corresponding to a minimum pair separation. The maximum pair separation is estimated from the excited pair density. However this model fails in that the predicted maximum pair separation is less than the minimum pair separation. If no minimum separation is included the disagreement is even more marked. This can only be explained by postulating strong carrier self-trapping at the defect site.

Previous results suggest that self-trapping is stronger in hydrogenated material and this is consistent with the greater response of that material compared to pure material at low intensities. The reduced response at higher intensities is ascribed to reduced self-trapping for states excited fər from the fermi level. Because of the smaller density of states at the fermi level in hydrogenated material the transition from $I^{1/2}$ to $I^{1/4}$ behaviour occurs at a lower intensity than in pure materials.
The increased self-trapping in hydrogenated samples is also reflected in a slower free decay to equilibrium.

If the states responsible for additional loss were a

perturbation of the background loss then a linear intensity dependence and an exponential decay to equilibrium would be seen. As this is inconsistent with the experimental results, the excited states must be independent of the background loss. A simple model is suggested in which light induced loss is derived from correlated pairs of dangling bond states which exist on the internal surfaces of voids. The pairs of dangling bond defects that are occupied by three electrons or one electron will respond to an applied a.c. field. Extra $3e^-$ and $1e^-$ states will be created on illumination and these contribute the additional loss. These extra pairs constitute a population that is independent of the background $3e^-$ and $1e^-$ states.

The results reported here bear some resemblance to the low temperature light induced electron spin resonance work reported in the literature, although the population of states detected by the two techniques is not exactly the same.

Appendix A : "LCR" Programme

```
100 DIM T(2000),A(2000),B(2000),temp(500),temptime(500)
105 REMark dimensions for time,C,R,temperature and temp. time
110 norm=0 : tempsize=0 : temptake=0 : date1=0 :tablecall=0 :
    freqname$='none' : freqfilenum=1 : newtime=0 : high=0
115 REMark "norm" controls no. of pts/s taken; tempsize =
    total no of temp. pts so far; "temptake" is the flag
    which activates the taking of temp. data; "date1" is the
    most recently displayed time; "tablecall"=1 changes the
    screen format to eliminate prompts; "freqname$" &
    "freqfilenum" concern the no. and name of the file used
    to contain frequency sweep data; "newtime"=1 means prog.
    just started, =0 means time already running; "high"=1
    means F5 is one pt/300s, =0 means F5 is one pt/600s
120 OPEN #8,ieee_8
130 OPEN #17,ieee_17
135 REMark open channels to lcr meter (#17) and DVM for temp.
    reading (#8)
140 lcrsetup : REMark set up screen
145 REMark ************************************************
150 REPeat LOOP
160 IF KEYROW(1)=8 THEN PRINT #17,'T1' : EXIT LOOP
165 REMark if ESC is pressed start data taking on lcr
    internal trig. and exit loop
170 END REPeat LOOP
175 REMark ************************************************
180 SDATE 1961,1,1,0,0,0 : newtime=1 : REMark initialize
    clock
190 start
200 DEFine PROCedure start
210 IF newtime=0 THEN lcrsetup: tempsize=0:ELSE newtime=0
212 REMark if prog. already been running then setup screens
215 n1=1
220 FOR N=n1 TO 7000
225 REMark ************************************************
230 REPeat LOOP
235 REMark this loop continuously checks what time it is and
    which keys are pressed
240 DAT$=DATE$ : REMark DATE$ is time as "hours-mins-secs"
250 dat3=DAT$(16)+DAT$(17) : REMark dat3 = minutes
260 dat12=DAT$(19 TO 20) : REMark dat12 = seconds
270 IF KEYROW(0)= 32 THEN IF NOT norm=6 THEN PRINT ' One
    Pt/';6-3*high;'00s' : norm=6 : PRINT #17,'T3'
275 REMark if F5 is pressed then; set flag norm =6 in order
    to take one pt/600s (or one pt/300s if high=1) when the
    time check loop is left; tell lcr meter to stop taking
    data
280 IF KEYROW(0)=1 THEN IF NOT norm=3 THEN PRINT ' One
    Pt/180s' : norm=3 : PRINT #17,'T3'
290 IF KEYROW(0)=16 THEN IF NOT norm=2 THEN PRINT ' One
    Pt/60s' :norm=2 : PRINT #17,'T3'
300 IF KEYROW(0)=8 THEN IF NOT norm=1 THEN PRINT ' One
    Pt/20s' :norm=1 : PRINT #17,'T3'
310 IF KEYROW(1)=8 AND DATE>3 AND N>3 THEN GO TO 910
315 REMark if ESC is pressed and not just beginning a run
    then stop run
320 IF DAT$(17 TO 20)='0:00' THEN temptake=1
325 REMark set temptake flag=1 every ten minutes
```

```
330 IF NOT DATE=date1 THEN PRINT #6,DATE :date1=DATE
335 REMark if the time does not equal the displayed time then
    print the new time in the appropriate window
340 IF KEYROW(0)=2 OR norm=0  THEN
350 IF NOT  norm=0  THEN PRINT  #17,'T1' : PRINT  ' One Pt/s'
    :T(N)=7.77 : A(N)=0 : B(N)=0 : N=N+1 : norm=0
355 REMark if just  starting to  take one  pt/s then  put lcr
    meter on internal  trigger; put  7.77 in  time dimension,
    zero  in other dimensions, this 7.77 acts as an indicator
    of  the beginning of one pt/s data  and so of a change of
    light intensity
360 EXIT LOOP :  REMark i.e.  exit time  check loop  to begin
    recording one pt/s data
370 END IF
380 IF  (dat12=16 OR dat12=  36 OR dat12=56)  AND norm=1 THEN
    EXIT LOOP
385 REMark if time in secs is =16 or 36 or 56 and appropriate
    flag is set then exit loop and record data; these timings
    mean the average time of data is 20,40 and 60s
390 IF  dat12=53 AND norm=2 THEN EXIT  LOOP : REMark as above
    for one pt/60s
400 IF  (dat3=3 OR dat3=6  OR dat3=9 OR  dat3=12) AND dat12=0
    AND norm=3 THEN EXIT LOOP  :  REMark  as  above  for  one
    pt/180s
410 IF (DAT$(17  TO 20)='0:00'  OR (DAT$(17  TO 20)='5:00'AND
    high)) AND  norm=6 THEN EXIT  LOOP : REMark  as above for
    one pt/600s or one pt/300s
420 IF KEYROW(6)=64 THEN EXIT LOOP
425 REMark   if T is pressed then take data immediately using
    averaging according to the current value of "norm"
430 END REPeat LOOP
440 REMark **************************************************
450 IF norm=0 THEN
460 LET T(N)=DATE : record time
470 INPUT #17,a$
475 REMark a$ contains all the data from the lcr meter in the
    form
480 LET A(N)=a$(6 TO 17)
490 B(N)=a$(21 TO 32)
500 REMark   extract values of C & G from a$ and record these
    values
510 ELSE
515 PRINT #17,'T1' : REMark put lcr meter on internal trig.
520 PAUSE 75 : REMark wait a second
540 t_ave=0 : a_ave=0 : b_ave=0
550 FOR qn=1 TO 5*norm
555 REMark this is the lcr data averaging for/next loop
560 IF NOT  DATE=date1 THEN PRINT #6,DATE :date1=DATE :REMark
    update time display
570 DAT$=DATE$
580 IF DAT$(17 TO 20)='0:00' THEN temptake=1
585 REMark set temptake flag =1 every ten minutes
590 LET t_ave=t_ave+DATE : REMark record total time
600 INPUT #17,a$
610 a_ave=a_ave+a$(6 TO 17) : REMark record total capacitance
620 b_ave = b_ave +  a$(21  TO  32)  :  REMark  record  total
    conductance
630 IF NOT KEYROW(0)=0 OR  KEYROW(1)=8  THEN  N=N-1  :  PRINT
    #17,'T3' : GO TO 900
```

```
635 REMark  if  F1 to F5 or ESC are pressed then abandon this
    average data pt and go back to time check loop
640 END FOR qn
650 PRINT #17,'T3' : REMark stop lcr meter taking data
660 T(N)=t_ave/5/norm
670 A(N)=a_ave/5/norm
680 B(N)=b_ave/5/norm
685 REMark average and record time,C,G
690 END IF
695 REMark ************************************************
700 IF temptake=1 THEN
710 temp_ave=0 : temptime_ave=0
720 FOR qn=1 TO 10
725 REMark this  is the  temperature data  averaging for/next
    loop
730 IF  NOT DATE=date1 THEN PRINT #6,DATE :date1=DATE :REMark
    update time display
740 INPUT #8,atemp$
745 REMark atemps$ contains all data from DVM in the form
750 temp_ave=atemp$(1 TO 9)+temp_ave
760 temptime_ave=DATE+temptime_ave
770 IF NOT KEYROW(0)=0 OR KEYROW(1)=8 THEN GO TO 900
780 END FOR qn
790 tempsize=tempsize+1
800 temp(tempsize)=temp_ave/10
810 temptime(tempsize)=temptime_ave/10
820 END IF
860 time$=T(N)  : REMark allows time data  to be limited to 6
    digits for display
870 PRINT TO 1;N;TO 8;time$(1 TO 6);TO 19;A(N);TO 36;B(N)
875 REMark display lcr data in appropriate columns
890 IF  temptake  =  1  THEN  PRINT  #2,  TO  1;  tempsize;TO
    8;temptime(tempsize);TO 18;temp(tempsize) : temptake=0
895 REMark  display temp. data,  if  taken,  and reset temptake
    flag
897 REMark ************************************************
900 END FOR N
910 PRINT #17,"T3" : REMark stop lcr meter taking data
920 LET T(N)=9.99 : REMark put 9.99 in time dimension as flag
    to indicate last data point of lcr data
930 write : REMark write data to disc procedure
935 REMark ************************************************
940 PRINT \"Continue the experiment?    F1=Yes/F2=No"
950 REPeat LOOP
960 IF KEYROW(0)=8 THEN EXIT LOOP
970 IF KEYROW(0) = 2 THEN start : REMark i.e. goto time check
    loop
980 END REPeat LOOP
990 WINDOW 252,200,258,1 :CLS
1000 CLOSE  #17  : CLOSE  #8 :  CLOSE #6  : REMark  close lcr
     meter, DVM, and time display channels respectively
1010 END DEFine start
1020 STOP
1025 REMark ***********************************************
1030 DEFine PROCedure setup
1035 REMark this procedure sets up original QL screens
1040 PAPER #2,1 : PAPER 0
1050 INK #2,6 : INK 6 : INK #0,6
1060 WINDOW 512,256,0,0 : CLS
```

```
1070 WINDOW 512,1,0,0 :PAPER 255 : CLS
1080 WINDOW 512,1,0,201 : CLS
1090 WINDOW 2,201,0,0 : CLS
1100 WINDOW 4,201,254,0 : CLS
1110 WINDOW 2,201,510,0 : CLS
1120 WINDOW 252,200,258,1 : PAPER 1 : CLS
1130 WINDOW #2,252,200,2,1
1140 WINDOW #0,512,50,0,205
1150 CLS #2 : CLS #0 :CLS
1160 END DEFine
1165 REMark ***********************************************
1170 DEFine PROCedure write
1175 REMark this writes data  to disc, the lcr data is stored
     first followed by the temp. data
1180 INPUT\'Enter mdv & filename',name$
1190 OPEN_NEW #5  ,  name$  :  REMark  open  a  new  file  on
     appropriate disc
1200 FOR k=1 TO 7000
1210 PRINT #5,T(k)\A(k)\B(k)
1240 IF T(k) =  9.99  THEN  EXIT k  : REMark  if 'end  of lcr
     data' flag is found then start storing temp. data
1250 END FOR k
1260 FOR k=1 TO tempsize
1270 PRINT #5,temptime(k)\temp(k)
1290 END FOR k
1300 CLOSE #5
1310 END DEFine
1315 REMark ***********************************************
1320 DEFine PROCedure table
1325 REMark this procedure  displays  data  currently  in  QL
     memory on the screen
1330 PRINT \\'F1=Capacitance\Conductance'\'F2=Temperature'
1340 tablecall=1 :  REMark this  eliminates on  screen prompts
     and allows more data to be seen
1350 REPeat LOOP
1360 IF KEYROW(0)=8 THEN GO TO 1460
1370 IF KEYROW(0)=2 THEN EXIT LOOP
1380 END REPeat LOOP
1390 lcrsetup : REMark set up new screen
1400 FOR k= 1 TO N-1
1410 IF T(k)=9.99 THEN EXIT k
1420 time$=T(k)
1430 PRINT TO 1;k;TO 8;time$(1 TO 6);TO 19;A(k);TO 36;B(k)
1440 END FOR k
1450 RETurn
1460 lcrsetup
1470 FOR k=1 TO tempsize
1480 PRINT #2,TO 1;k;TO 8;temptime(k);TO 18;temp(k)
1490 END FOR k
1500 END DEFine
1505 REMark ***********************************************
1510 DEFine PROCedure lcrsetup
1515 REMark this procedure sets up the data taking screen
1520 PAPER #2,1 : PAPER 0
1530 INK #2,6 : INK 6 : INK #0,6
1540 WINDOW 512,256,0,0 : CLS : REMark clear all screen
1545 REMark next few lines draw window borders
1550 WINDOW 512,1,0,0 :PAPER 255 : CLS
1560 WINDOW 512,1,0,11 : CLS
```

```
1570 WINDOW 512,1,0,192 : CLS
1580 WINDOW 512,1,0,233 : CLS
1590 WINDOW 2,233,0,0 : CLS
1600 WINDOW 2,233,510,0 : CLS
1610 WINDOW 508,10,2,1 : PAPER 0 : REMark set up column title
     window
1620 AT 0,1 :PRINT 'No.':AT 0,8:PRINT 'Time':AT 0,19:PRINT
     'Display A':AT 0,36:PRINT'Display B':AT 0,52:PRINT
     'No.':AT 0,59: PRINT 'Time':AT 0,69:PRINT 'Temperature'
1625 REMark next few lines divide up columns
1630 WINDOW 2,11,41,0 : PAPER 255 : CLS
1640 WINDOW 2,11,95,0 :CLS
1650 WINDOW 2,11,197,0 :CLS
1660 WINDOW 4,192,305,0 :CLS
1670 WINDOW 2,11,346,0 :CLS
1680 WINDOW 2,11,400,0 :CLS
1690 WINDOW #0, 512,20,0,236 : REMark set up #0
1700 IF tablecall=1 THEN
1705 REMark if table requested i.e. not data taking screen
     then extend data columns to bottom of screen
1710 tablecall=0
1720 WINDOW 4,233,305,0 :CLS
1730 PAPER 0:WINDOW 303,221,2,12 : CLS
1740 WINDOW #2,201,221,309,12 : CLS #2
1750 RETurn
1760 END IF
1765 REMark if data taking screen then print prompts to
     screen
1770 WINDOW 2,40,190,192 :CLS
1780 WINDOW 2,40,262,192 :CLS
1790 WINDOW 189,40,2,193 : PAPER 0 :CLS
1800 AT 0,1 : PRINT 'ESC=Stop/Start':AT 1,1:PRINT'F1=One
     Pt/s':AT 2,1:PRINT'F2=One Pt/20s':AT 3,1:PRINT'F3=One
     Pt/60s':AT 1,16:PRINT'F4=One Pt/180s':AT
     2,16:PRINT'F5=One Pt/600s': AT 3,16:PRINT'T=Take a
     Point'
1805 REMark open time display screen as #6
1810 WINDOW 71,40,193,193
1820 AT 0,0:PRINT "Time So Far"
1830 OPEN #6,scr_42x10a205x209:INK #6,6
1835 REMark print more prompts
1840 WINDOW 246,40,264,193
1850 AT 0,0:PRINT'Type : SETUP for original QL screens'
1860 AT 1,7:PRINT'WRITE/TABLE to output/review data'
1870 AT 2,7:PRINT'START/ENTER to restart at n=1/n=n'
1880 AT 3,7:PRINT'FREQSWEEP for frequency sweep'
1890 WINDOW 303,180,2,12
1900 WINDOW #2,201,180,309,12
1910 END DEFine
1915 REMark ************************************************
1920 DEFine PROCedure enter
1925 REMark this procedure restarts data taking at next point
     i.e. without going back to start of data dimensions
1930 PRINT #17,'T3E' : INPUT #17,a$ :n1=N : GO TO 220
1935 REMark this line clears #17 of false data, sets n1 to
     current point number and enters for/next data recording
     loop
1940 END DEFine
1945 REMark ************************************************
```

```
1950 DEFine PROCedure freqsweep
1955 REMark this procedure takes a frequency sweep and stores
     the results on disc and on a printer
1960 const=0 : num=20
1965 REMark  "const" =1 means  all data taken  for f=2kHz, =0
     means  freq. varies from  100Hz to 100kHz;  "num" is the
     no.  of pts averaged over to get the recorded value of C
     & G
1970 DIM Afreq(12),Bfreq(12),Ffreq(12)
1980 REMark dimensions to store C,G and freq. respectively
2000 RESTORE
2010 PRINT #17,"T1" : REMark  set  lcr  meter  onto  internal
     trigger
2020 INPUT #17,a$
2025 REMark **********************************************
2030 FOR c=1 TO 12
2035 REMark this is the frequency change for/next loop
2040 cap=0:cond=0
2050 READ freq$
2060 IF const=1 THEN LET freq$="F162000"
2065 REMark if "const"=1 then keep frequency = 2kHz
2070 PRINT #17,freq$(1 TO 3)
2075 REMark send  the appropriate  code to  the lcr  meter to
     change the measuring freq. to the required value
2080 PAUSE 100 : REMark wait 1.5 seconds
2090 FOR d=1 TO num
2095 REMark this is the lcr data averaging for/next loop
2100 IF KEYROW(0)=2 THEN GO TO 2200 : REMark if F1 is pressed
     abandon freqsweep
2110 INPUT #17,a$
2120 cap=a$(6 TO 17)+cap : REMark calculate total capacitance
2130 cond=a$(21 TO 32)+cond : REMark calc. total conductance
2140 NEXT d
2150 Afreq(c)=cond/num  :  Bfreq(c)=cap/num  :  REMark  calc.
     averaged C & G
2170 Ffreq(c)=freq$(4 TO)
2180 DATA "F11100", "F12120", "F13200", "F14400",  "F151000",
     "F162000", "F223000", "F174000", "F1810000", "F1920000",
     "F2040000", "F21100000"
2185 REMark  codes for frequencies for  lcr meter followed by
     the freq. values
2190 NEXT c
2192 REMark end of freq. change for/next loop
2195 REMark **********************************************
2200 PRINT #17,"T3" : REMark stop data taking of lcr meter
2210 IF  freqname$='none'  THEN INPUT  "Enter Drive  number &
     filename ";freqname$
2215 REMark  if  this  is  first  freqsweep  then  a  name  &
     destination is requested
2220 nam$=freqname$ & freqfilenum : freqfilenum=freqfilenum+1
2225 REMark the freq. sweep  is  given  generic  name  and  a
     no.=freqfilenum
2230 OPEN_NEW #5,nam$
2240 PRINT #5,num
2250 FOR c=1 TO 12
2260 PRINT #5,Afreq(c)\Bfreq(c)\Ffreq(c)
2270 END FOR c
2280 CLOSE #5
2290 PRINT 'Frequency Sweep stored on ';nam$
```

```
2295 REMark storing of data is confirmed on screen
2297 REMark the next  few lines  print the  data on  the line
     printer
2300 OPEN #3,ser1
2310 PRINT  #3,   CHR$(27);   CHR$(68);   CHR$(1);  CHR$(10);
     CHR$(25); CHR$(0)
2320 PRINT #3,nam$;'  averaged over ';num
2330 PRINT #3,"Freq       Input Cond      Capacitance"
2340 PRINT #3,"(Hz)        (Siemens)        (Farads)  "
2350 FOR c=1 TO 12
2360 IF Afreq(c)=0  AND Bfreq(c)=0 THEN EXIT c
2370 PRINT #3, CHR$(9); Ffreq(c); CHR$(9); Afreq(c); CHR$(9);
     Bfreq(c)
2380 END FOR c
2390 CLOSE #3
2395 PRINT #17 ,'F16'
2397 REMark the lcr meter  is  requested  to  go  back  to  a
     measuring freq. of  2kHz,  this  is  in  preparation  of
     return to the main programme  and  the  taking  of  time
     dependent data at f= 2kHz
2400 END DEFine
```

Appendix B : "Lcrgraph" Programme

```
100 S : REMark setup original QL screens
110 dimsize=2500 : REMark dimension size variable
120 IF dimsize= 2500 THEN DIM x(2500),y(2500)
130 REMark dimensions for capacitance/conductance/temperature
    and time
140 PRINT \"Type : 'F'ilefind to directory discs"
150 PRINT  "       'R'eview to review files"
160 PRINT  "       'ST'art to review graph"
170 PRINT  "       'S'etup for original QL screens"
180 PRINT  "       'RE'ader to read data from disc"
190 INPUT \'Enter mdv_filename & No. of Files'\name$,files
200 REMark filename can be entered as 'flp1_data 3' in
    which case files data1,data2 &data3 are read;
    alternatively if a directory has been carried out the no.
    of the required file can be entered
210 filenum=2 : REMark see data input routine
220 logscalex=0 : logscaley=0
230 REMark these variables are used in the scales subroutine
    and are always =0 for this prog.
240 IF CODE(name$(1))>48 AND CODE(name$(1))<58 THEN
    name$=dev$&filenames$(name$)
250 REMark i.e. if the first symbol of name$ is a number
    assume a directory has been carried out and make name$=
    the device name and the appropriate filename$
260 S
270 lenfilename=LEN(name$)
280 PRINT \'F1 = Capacitance vs. Time'\'F2 = Conductance vs.
    Time'\'F3 = Temperature vs. Time'
290 REMark ************************************************
300 REPeat LOOP
310 IF KEYROW(0)=2 THEN
320 PRINT \'Capacitance Plot'
330 cond=0
340 REMark cond=0 for cap. plot, cond=1 for cond. plot,
    cond=2 for temp. plot
350 capcondinput
360 GO TO 1170
370 REMark i.e. start plotting graph
380 END IF
390 IF KEYROW(0)=8 THEN
400 PRINT \'Conductance Plot'
410 cond=1
420 INPUT\ 'Enter : Frequency (Hz) '\' Series R
    (Ohms)'\' D.C. Conductance (S)'\FREQ,RO,GDC
430 PRINT\ ' Frequency = ';FREQ;' Hz'\' Series R
    = ';RO;' Ohms'\'D.C. Conductance = ';GDC;' S'
440 REMark these lines input the values of series R and d.c.
    conductivity to correct the conductance values
450 capcondinput
460 GO TO 1170
470 END IF
480 IF KEYROW(0)=16 THEN
490 cond=2
500 tempinput
510 GO TO 1170
520 END IF
530 END REPeat LOOP
```

```
540 REMark ************************************************
550 DEFine PROCedure tempinput
560 OPEN_IN #5,name$
570 jumpdata
580 REMark   the 'jumpdata' procedure jumps over the cap/cond
    data  to get to the temp. data; the data is stored in the
    form   cap/cond/time  ending  where  time=9.99,  this  is
    followed by the temp./time data
590 FOR N=1 TO 600
600 IF EOF(#5) THEN
610 REMark i.e. if the current file has finished
620 IF filenum-1=files THEN END DEFine tempinput
630 REMark i.e. if the current file is the last file then end
    data input
640 name$=name$(1 TO lenfilename) & filenum
650 REMark make name$  the next  file; the  next file  is the
    name of the  previous file  with the  last symbol  of the
    name (which  is a  number) increased  by one;  e.g. data3
    becomes data4
660 CLOSE #5
670 OPEN_IN #5,name$
680 REMark open to the discs under the new filename
690 filenum=filenum+1
700 jumpdata
710 REMark jump the cap./cond. data of the new file
720 GO TO 840
730 REMark start inputing temp. data again
740 END IF
750 DEFine PROCedure jumpdata
760 REMark  this procedure inputs cap/cond/time data until it
    finds  the time=9.99, this is the signal for the start of
    the temp/time data
770 FOR ntt=1 TO 7000
780 INPUT #5,dummy1\dummy2\dummy2
790 IF dummy1=9.99 THEN EXIT ntt
800 END FOR ntt
810 END DEFine jumpdata
820 INPUT #5,y(N)\x(N)
830 REMark input the temperature/time data
840 END FOR N
850 END DEFine tempinput
860 REMark ************************************************
870 DEFine PROCedure capcondinput
880 OPEN_IN #5,name$
890 FOR N=1 TO dimsize
900 INPUT #5,y(N)
910 IF y(N)=9.99 THEN
920 REMark i.e. if the end of the cap/cond data for this file
    has been reached
930 IF filenum-1=files THEN EXIT N
940 REMark if no more files then stop data input
950 LET name$=name$(1 TO lenfilename) & filenum
960 REMark let name$= next file name
970 CLOSE #5
980 OPEN_IN #5,name$
990 filenum=filenum+1
1000 INPUT #5,y(N) : REMark input time
1010 END IF
1020 IF cond=1 THEN
```

```
1030 REMark the next few  lines  input  the  conductance  and
     correct it for d.c. and series R
1040 INPUT #5,cap
1050 INPUT #5,x(N)
1060 LET x(N)=x(N)-GDC/(1+RO*GDC)-RO*(6.283185*FREQ*cap)^2
1070 ELSE
1080 REMark the next line inputs the capacitance
1090 INPUT #5,x(N)
1100 INPUT #5,const
1110 END IF
1120 IF ABS(y(N))>1E7 OR ABS(x(N))>2E15  THEN y(N)=-6.66
1130 REMark  if the cap.  or cond. have  strange values label
     the time=-6.66
1140 END FOR N
1150 END DEFine capcondinput
1160 REMark ************************************************
1170 size=N-1 :  REMark this is  the number of  points of the
     graph
1180 CLOSE #5
1190 bigx=1E-20 : littlex=1E20
1200 REMark littlex &  bigx  are  the  smallest  and  biggest
     values of cap./cond. and will be chosen next
1210 FOR N=1 TO 7000
1220 IF N=size THEN EXIT N
1230 IF y(N)=7.77 OR y(N)=-6.66 THEN GO TO 1280
1240 REMark  if  'change light  intensity' label  or 'strange
     value' label found then ignore values of cap./cond.
1250 IF x(N)<littlex THEN littlex=x(N)
1260 IF x(N)>bigx THEN bigx=x(N)
1270 REMark choose smallest/largest values
1280 END FOR N
1290 st
1300 REMark start plotting graph
1310 REMark ************************************************
1320 DEFine PROCedure st
1330 graphprint=0
1340 REMark graphprint=1 means graph being dumped to printer
1350 INPUT \'Enter Timescale',timescale
1360 REMark  timescale is the maximum time value of the first
     graph
1370 power=1&"E"&INT(LOG10(timescale))
1380 REMark power is the power of ten of timescale
1390 IF timescale/power<2.1 THEN power=power/10
1400 REMark if there are two divisions or less per graph then
     multiply no. of divisions by ten
1410 ndiv=INT(timescale/power)
1420 REMark  ndiv is the no. of  divisions for the time scale
     of each graph
1430 WINDOW 512,256,0,0 : CLS
1440 REMark clear whole of screen
1450 WINDOW 15,256,498,0 : CLS : INK 6
1460 PRINT '    F1= Next  F2=Print  F3= Stop  F4= Review'
1470 REMark write prompts in column on right of screen
1480 WINDOW 481,253,16,0
1490 REMark set up screen dump window
1500 scales bigx,littlex,140
1510 REMark draw the cap./cond scale
1520 ysc=1
1530 REMark ysc=no. of first pt of this section of graph; no.
```

```
    of first pt of first section is obviously=1
1540 REMark ************************************************
1550 REMark the 'k' loop produces each new section of graph
1560 FOR k=1 TO 50
1570 IF N>size THEN EXIT k
1580 REMark if end of data then stop plotting
1590 LINE 0,0 TO 0,100
1600 REMark draw line for time axis
1610 IF k=1 THEN LINE 0,100 TO 140,100
1620 REMark draw line for cap./cond. axis if first section of
     graph
1630 FOR div=1 TO ndiv+1
1640 REMark loop for no. of divisions on time axis
1650 delimy=power*(div-1)*100/timescale
1660 REMark delimy is where the division line should be drawn
     on the time axis
1670 LINE 0,delimy TO 1,delimy
1680 REMark draw division
1690 IF div=ndiv+1 THEN EXIT div
1700 REMark don't print time for last division
1710 CURSOR 1,INT((timescale-power*(div-1))/timescale*252-10)
1720 REMark  put the cursor at a position near to the current
     division
1730 PRINT timescale*k-power*(div-1)
1740 REMark  print at this position the value of the time the
     division represents
1750 END FOR div
1760 REMark ************************************************
1770 FOR N=ysc TO size
1780 REMark  for N = beginning of this section of graph until
     end of data
1790 IF y(N)>k*timescale THEN ysc=N :EXIT N
1800 REMark  if the  time value  of the  data is  beyond this
     section of graph  then let ysc  be the no.  of the first
     pt. of the next section of graph and then stop plotting
1810 IF y(N)=-6.66 THEN GO TO 2070
1820  REMark  if the 'strange data' label is found ignore the
     data
1830 IF y(N)=7.77 THEN
1840 REMark  if the 'light intensity division' label is found
     then
1850 ycoord=100-(y(N+1)-timescale*(k-1))/timescale*100
1860 REMark  let y coordinate (time) of the marker be for the
     time  of the next pt. (usually only one second different
     from where the interval marker should be)
1870 xcoord=(x(N-1)-littlex)/(bigx-littlex)*140
1880 xcoord1=xcoord-7
1890 xcoord2=xcoord+7
1900 REMark  xcoord1 & xcoord2 are +/-7 from the x coordinate
     (cap. or cond.) of the data pt. just before the marker
1910 FOR nintdel=1 TO 9
1920 IF xcoord1<0 THEN xcoord1=xcoord1+1
1930 IF xcoord2>140 THEN xcoord2=xcoord2-1
1940 END FOR nintdel
1950 REMark  this loop reduces the length of the marker so it
     doesn't go off the graph
1960 LINE xcoord1,ycoord TO xcoord2,ycoord
1970 REMark draw the intensity marker
1980 ELSE
```

```
1990 REMark i.e. if this just an ordinary point
2000 xcoord=(x(N)-littlex)/(bigx-littlex)*140
2010 ycoord=100-(y(N)-timescale*(k-1))/timescale*100
2020 POINT xcoord,ycoord
2030 REMark choose the x & y coordinates and print point
2040 IF xcoord<1 THEN CIRCLE xcoord,ycoord,1
2050 REMark if point is on edge of graph then circle it
2060 END IF
2070 END FOR N
2080 REMark ************************************************
2090 REPeat LOOP
2100 REMark F1 to F4 menu loop
2110 IF KEYROW(0)=2 THEN EXIT LOOP
2120 REMark if F1 then plot next section of graph
2130 IF KEYROW(0)=16 THEN S:STOP
2140 REMark if F3 then stop
2150 IF KEYROW(0)=1 THEN st
2160 REMark if F4 then go back to beginning of graph and give
     an opportunity to change the time scale
2170 IF KEYROW(0)=8 OR graphprint=1 THEN
2180 REMark if F2 or graphprint=1 then dump this graph to the
     printer
2190 IF k=1 THEN
2200 REMark if this is the first section of the graph then
2210 OPEN #7,ser1 :PRINT #7,CHR$(27);'@'
2220 REMark send the 'clear' signal to the printer
2230 PRINT #7,'Data Filename = ';name$(6 TO lenfilename),
2240 PRINT #7,'Base = ',littlex
2250 IF cond=1 THEN  PRINT  #7,  'A.C.  Conductance  Plot'\\'
     Frequency = ';FREQ;'  Hz'\'          Series  R  =  ';RO;'
     Ohms'\'D.C. Conductance = ';GDC;' S'\\
2260 IF cond =0 THEN PRINT #7,'Capacitance Plot'\\
2270 IF cond=2 THEN PRINT #7,'Temperature Plot'\\
2280 REMark  print out the source file and title of the graph
     plus various other parameters
2290 CLOSE #7
2300 END IF
2310 EXEC_W flp1_dumpf
2320 REMark load and use the screen dump
2330 OPEN #7,ser1 :PRINT #7,CHR$(27);'@'; : CLOSE #7
2340 graphprint=1
2350 REMark   set graphprint=1 so that subsequent sections of
     graph will be sent to the printer
2360 IF N>size THEN st
2370  REMark if no more data  give opportunity to change time
     scale
2380 EXIT LOOP
2390 REMark if there is  more  data  then  exit  loop,  clear
     screen and start on next section of graph
2400 END IF
2410 END REPeat LOOP
2420 REMark ************************************************
2430 CLS
2440 END FOR k
2450 graphprint=0
2460 END DEFine st
2470 REMark ************************************************
2480 DEFine PROCedure S
2490 REMark set up of original QL screens
```

```
2500 WINDOW 512,256,0,0 : PAPER 0 :CLS
2510 WINDOW 512,1,0,0 : PAPER 255 : CLS
2520 WINDOW 512,1,0,201 :CLS
2530 WINDOW 2,201,0,0 :CLS
2540 WINDOW 4,201,254,0 : CLS
2550 WINDOW 2,201,510,0 : CLS
2560 WINDOW 252,200,258,1 : PAPER 1 : INK 6
2570 WINDOW #2,252,200,2,1 : PAPER #2,1 :INK #2,6
2580 WINDOW #0,512,52,0,204
2590 CLS : CLS #0 : CLS #2 : INK #0,6
2600 END DEFine
2610 REMark ************************************************
2620 DEFine PROCedure F
2630 REMark  this procedure  directorys a  disc and  puts the
     filenames  in  a  dimension  called  'filenames$',  very
     imaginative name that
2640 CLS
2650 INPUT \'Enter Device for Directory',dev$
2660 REMark e.g. :'dev$'= 'flp1_' for floppy1
2670 DIM filenames$(200,25)
2680 OPEN_NEW #5,dev$&'filenames'
2690 REMark  open channel 5 to a file called 'filenames' on a
     disc
2700 DIR #5,dev$
2710 REMark directory to this file
2720 CLOSE #5
2730 OPEN_IN #5,dev$&'filenames'
2740 REMark   the following loop gets to the beginning of the
     filenames, see remark line 2245
2750 REPeat LOOP
2760 INPUT #5,dummy$
2770 IF dummy$='' THEN GO TO 2760
2780 REMark if found a blank space input next string
2790 IF   CODE(dummy$(1))>48 AND CODE(dummy$(1))<58 THEN EXIT
     LOOP
2800 REMark  if the first symbol of  the inputted string is a
     number then  next input will be  the first filename, the
     directory  command produces discname then no. of sectors
     free and then immediately afterwards, the filenames
2810 END REPeat LOOP
2820 REMark the  following  loop  reads  the  filenames  from
     floppy disc into the dimension 'filenames$'
2830 FOR N=1 TO 200
2840 IF EOF(#5) THEN EXIT N
2850 INPUT #5,filenames$(N)
2860 IF filenames$(N)='filenames' THEN N=N-1
2870 REMark the file='filenames' will  be  on  the  disc  and
     should be ignored
2880 END FOR N
2890 CLOSE #5
2900 DELETE dev$&'filenames'
2910 REMark the temporary  file='filenames'  has  served  its
     purpose and is deleted
2920 number=N-1
2930 REMark and  the number  of files  = 'number'  is reduced
     accordingly
2940 r
2950 END DEFine F
2960 REMark ************************************************
```

```
2970 DEFine PROCedure r
2980 REMark this procedure prints the no. of file and
     filename to screen in four columns
2990 WINDOW 512,236,0,0 : PAPER 0:CLS : WINDOW
     #0,512,20,0,236 : CLS #0
3000 REMark clear the whole screen and make #0 the bottom two
     lines
3010 row=0 : col=0
3020 STRIP 0 : INK 7 : OVER 0
3030 REMark i.e. print over what is already on screen; this
     is necessary if no. of files is so great that they begin
     printing over the first screen of names
3040 spaces$='                    '
3050 FOR k=1 TO number
3060 st$=k&' '&filenames$(k)
3070 IF LEN(st$)<20 THEN st$=st$&spaces$(LEN(st$) TO 19)
3080 REMark the previous two lines make the string st$ = the
     file no. and file name and extend st$ with spaces to
     make it 20 characters long
3090 AT row,col :PRINT st$
3100 REMark print st$ at appropriate row & column
3110 IF KEYROW(1)=64 THEN PAUSE
3120 REMark if space bar pressed then stop printing files
3130 row=row+1 : IF row=23 THEN col=col+20 : row=0 : IF
     col=80 THEN col=0
3140 REMark change row & column so as to fill columns
     vertically and from left
3150 END FOR k
3160 WINDOW 512,20,0,236 : CLS
3170 REMark make channel 1 the bottom two lines of screen
3180 Re
3190 END DEFine
3200 REMark ************************************************
3210 DEFine PROCedure Re
3220 REMark this procedure goes to part of main programme
     which asks for filename from which data should be read
3230 GO TO 190
3240 END DEFine
3250 REMark ************************************************
3260 DEFine PROCedure scales ( big,little,maxscale)
3270 REMark this procedure draws the divisions and labels of
     a scale between 'big' & 'little'; maxscale=140 for x
     scale, maxscale=100 for y scale
3280 fast=0 : prevpos=0 : prevbas$=''
3290 logscale=0 :IF (logscalex AND maxscale=140) OR
     (logscaley AND maxscale=100) THEN logscale=1
3300 REMark logscale=1 if this is a log scale
3310 REMark ************************************************
3320 DEFine PROCedure base_add_find
3330 REMark this procedure works out the appropriate base and
     step increase for the scale
3340 basedelim$=little
3350 minus=0 :IF basedelim$<0 THEN minus=1
3360 nk=INT(LOG10(ABS(big)))-INT(LOG10(ABS(big-little)))
3370 REMark : Next line means that if little and big are
     close then nk increases, in this case 'basedelim$' must
     contain more significant figures of 'little'
3380 IF nk<1 THEN nk=1
3390 REMark this line makes sure 'nk' is at least=1, 'nk' is
```

```
     the no. of characters of 'little' that will make up
     'basedelim$'
3400 REMark : Next two lines increase 'nk' to take account of
     -ve nos. and '.'
3410 nk=nk+minus
3420 FOR g=1 TO nk :IF basedelim$(g)="." THEN nk=nk+1
3430 REMark      : Next two lines make ak into 2.3 if
     basedelim$=23000 or 2.3456E-7 : Not 'nk+1' because this
     causes probs if base=37 and add=20
3440 ak=basedelim$(1 TO nk)
3450 REMark 'ak'=truncated 'little'
3460 ak=ak/(1&"E"&INT(LOG10(ABS(ak))))
3470 REMark this line makes 'ak' between 1 & 9.99
3480 IF     ak=0     THEN    ak=1E-15     : IF basedelim$=0 THEN
     basedelim$=1E-15
3490 REMark  this line  makes sure  that if  the base  of the
     scale  is truly = zero then  the computer error does not
     obscure this
3500 LET basedelim=ak&"E"&INT(LOG10(ABS(basedelim$)))
3510 REMark  this line puts  back the power  of 'little' onto
     the truncated base
3520 REMark  so   far  the  object  has  been  to  round  off
     basedelim$ so the base=2.3E-7 rather than 2.3456E-7
3530 adddelim=ABS(big-little)/15
3540 REMark this line  estimates  an  interval  between  each
     division of the scale, this must now be rounded off
3550 power_add = INT  (LOG10  (adddelim  +  5&'E'&INT  (LOG10
     (adddelim))))
3560 REMark   power_add represents the power of the estimated
     division, see next comment
3570 adddelim=1&"E"&power_add
3580 REMark this line makes  adddelim  =  the  power  of  the
     estimated  interval as follows:if  est. interval=51 then
     adddelim=100, if est. interval=49 then adddelim=10
3590 REMark       the  following  loop  multiplies  the  base
     (basedelim)  if it is not the same order of magnitude as
     the interval (adddelim), this avoids the situation where
     base=.5 & adding interval=10
3600 REPeat LOOP
3610 IF INT(LOG10(ABS(basedelim)))>=power_add THEN EXIT LOOP
3620 basedelim=basedelim*10
3630 END REPeat LOOP
3640 REMark the following loop subtracts from basedelim until
     it  is one interval less than  little, makes sure base <
     little
3650 REPeat LOOP
3660 IF basedelim<little THEN EXIT LOOP
3670 basedelim=basedelim-adddelim
3680 END REPeat LOOP
3690 END DEFine base_add_find
3700 REMark ************************************************
3710 IF NOT logscale THEN
3720 base_add_find
3730 ELSE
3740 REMark if logscale required then
3750 power_base_log=1&'E'&INT(LOG10(EXP(little)))
3760 REMark  choose the power of 'little'  as the base of the
     log scale
3770 IF EXP(big)/EXP(little)<10 THEN
```

```
3780 REMark if the range of the log scale is small then treat
     it  as a linear scale for the purpose of finding a scale
     base and adding interval
3790 little=EXP(little) : big=EXP(big)
3800 base_add_find
3810 little=LN(little) : big=LN(big)
3820 END IF
3830 END IF
3840 REMark ************************************************
3850 REMark the following loop is the scale drawing loop
3860 FOR N=1 TO 1600
3870 print_cur=0 : add=0
3880 IF NOT logscale THEN li=little : bi=big :nonlogproc : GO
     TO 3900
3890 IF    EXP(big)/EXP(little)  <10  THEN  li=EXP(little)  :
     bi=EXP(big) :nonlogproc : ELSE logproc
3900 REMark          above    two    lines make  sure expression
     exp(big)/exp(little) is not attempted if not logscale
3910 REMark ************************************************
3920 DEFine PROCedure nonlogproc
3930 REMark  this  procedure draws  a linear  scale or  a log
     scale over a small range
3940 basadd=basedelim+adddelim*(N-1)
3950 REMark 'basadd' is the value of the current division
3960 IF basadd<li-adddelim/2 THEN N=N+1 : fast=1 : GO TO 3940
3970 IF fast THEN  fast=0
3980 REMark  these two lines move quickly to the beginning of
     the scale if 'basedelim' is much less than 'little'
3990 IF ABS(basadd)<1E-8 AND adddelim>.1 THEN basadd=0
4000 REMark  this line stops zero  becoming equal to computer
     error
4010 bas$=basadd
4020 IF li+adddelim*11>bi THEN  print_cur=1  :  ELSE  IF  NOT
     print_cur THEN div_check
4030 REMark  this  line  says  print  a  label  next  to  all
     divisions if  there are < 10  divisions, otherwise go to
     div_check  to  decide  whether   to   print   a   label;
     print_cur=1 means print a label, =0 means don't print
4040 IF    logscale  THEN calcbas=LN(basadd) : ELSE calcbas =
     basadd
4050 REMark  'calcbas' is the value to be printed next to the
     division marker if print_cur=1
4060 END DEFine nonlogproc
4070 REMark ************************************************
4080 DEFine PROCedure logproc
4090 REMark this procedure draws a logarithmic scale
4100 basadd=power_base_log*(N-10*INT((N-1)/10))
4110 REMark   'basadd' is the value  of the current division,
     basadd = the base of the scale + 0.1*the base
4120 IF basadd<EXP(little)/5 THEN N=N+1 :fast=1 : GO TO 4100
4130 IF fast THEN fast=0
4140 REMark  these two lines move quickly to the beginning of
     the scale if 'power_base_log' is much less than 'little'
4150 IF  basadd  =  power_base_log*10  THEN  power_base_log  =
     power_base_log*10 :print_cur=1
4160 REMark every 10 divisions print_cur is set = 1 so that a
     label is printed
4170 bas$=basadd
4180 IF EXP(big)/EXP(little)<30 THEN print_cur=1
```

```
4190 REMark if there are < 3 divisions label all divisions
4200 calcbas=LN(basadd)
4210 REMark  'calcbas' is the value to be printed next to the
     division marker if print_cur=1
4220 REMark ***********************************************
4230 END DEFine logproc
4240 DEFine PROCedure div_check
4250 REMark  this procedure decides whether a label should be
     printed or not, it differentiates between important
     divisions (7.8) and less significant divisions
     (7.81,7.82 etc.)
4260 IF basadd=0 THEN power_diff=0 : ELSE power_diff =
     INT(LOG10(ABS(basadd)))-power_add
4270 REMark  'power_diff' if the difference between the power
     of the adding interval (adddelim) and the value of the
     current division (basadd), if basadd=7.81 & adddelim=.1
     then power_diff=1
4280 eee=0 : minus=0
4290 IF basadd<0 THEN minus=1
4300 pos=power_diff+2+minus
4310 REMark  'pos' represents the no. of characters of bas$
     (basadd) which are
4320 bas$=basadd
4330 decpt='.' INSTR bas$
4340 IF decpt>pos OR decpt=0 THEN pos=pos-1
4350 REMark pos is changed to take account of a decimal pt in
     the character string 'bas$'
4360 IF pos<1 THEN pos=1
4370 eee='E' INSTR bas$(1 TO pos)
4380 IF eee THEN print_cur=1
4390 REMark 'eee'=1 if the power sign 'E' is found within the
     relevant part of the bas$ string, if so a label will be
     printed as the division is an important one
4400 nextpos_ch  = 0 :IF pos+1 <= LEN(bas$) THEN IF CODE(bas$
     (pos+1)) < 49 AND CODE(bas$(pos+1))>57 THEN nextpos_ch=1
4410 IF pos<=LEN(bas$) THEN IF bas$(pos)='0' AND nextpos_ch=0
     THEN print_cur=1
4420 REMark  these two lines take account of the situation
     were adddelim=100 and bas$=156000; here pos=5 but pos
     would not be > len(bas$) hence no label. The first line
     checks to see if the (pos+1)th character (in this case
     the 6th) is a number in which case 'nextpos_ch'=0. The
     second line sets print_cur=1 if the (pos)th character
     is=0 & nextpos_ch=0 hence a label is printed for the
     above example
4430 IF pos>LEN(bas$) THEN print_cur=1
4440 REMark  the first two cases of setting print_cur=1 are
     exceptions, usually this test is sufficient
4450 REMark  example: if basadd=7.823 and adddelim=.001 then
     pos=5 and pos is not > len(bas$) so no label; however if
     basadd=7.82 then pos (=5) is > len(bas$) so a label
     appears
4460 END DEFine
4470 REMark ***********************************************
4480 ak=(calcbas-little)/ABS(big-little)*maxscale
4490 REMark  ak is the right value of graphics coordinate to
     represent each division
4500 IF ak<0 THEN GO TO 4910
4510 REMark if ak is below the graph then next division
```

```
4520 IF ak>maxscale THEN EXIT N
4530 REMark if ak is above the graph then stop printing scale
4540 IF maxscale=140 THEN
4550 REMark x scale printing
4560 LINE ak,100 TO ak,99
4570 REMark print less significant divisions
4580 IF print_cur THEN
4590 LINE ak,100 TO ak,98
4600 REMark print more significant divisions (longer line)
4610 IF 481-INT(ak/140*481+1)<LEN(bas$)*6+2 THEN GO TO 4730
4620 REMark  this line means the last label of the x scale is
     not printed if it is going to overshoot the graph
4630 IF ak<5 THEN add=8
4640 REMark this line is to prevent no. collisions at origin
4650 newpos=INT(ak/140*478+3)+add
4660 REMark  calculation  of  cursor  position  for  division
     label, decrease 478 to pull down higher nos., increase 3
     to push up low nos.
4670 IF prevpos +6*LEN(prevbas$)>=newpos AND NOT ak<3 THEN GO
     TO 4730
4680 CURSOR newpos,3
4690 REMark this line makes sure labels on the x scale do not
     collide
4700 PRINT basadd
4710 prevpos=newpos : prevbas$=bas$
4720 REMark  'prevpos' is the position of the last label, the
     label itself is prevbas$
4730 END IF
4740 ELSE
4750 REMark drawing of y scale
4760 LINE 0,ak TO 1,ak
4770 LINE 140,ak TO 139,ak
4780 REMark print less significant divisions
4790 IF print_cur THEN
4800 LINE 0,ak TO 2,ak
4810 LINE 140,ak TO 138,ak
4820 REMark print more significant divisions (longer line)
4830 IF INT(ak/100*252+1)>242 THEN GO TO 4890
4840 REMark  if   the label is off the top of the scale don't
     try to print it
4850 IF ak<6 THEN add=2
4860 REMark 'add' prevents collisions of labels at the origin
4870 CURSOR 3,242-INT(ABS(ak)/100*251+2)-add
4880 PRINT basadd
4890 END IF
4900 END IF
4910 END FOR N
4920 END DEFine scales
```

Sample	λ nm	Semiconductor Thin Film				Electrode	Position Factor ±5%
		T ±3%	R ±3%	Absorption ±3%	Absorption Coefficient cm^{-1} ±10%	T ±3%	
Opt 1 (Ge)	633	0.0020	0.55	0.44	2.3×10^{5}	0.56	0.30
Opt2 (Ge)	633	0.0022	0.53	0.47	3.2×10^{5}	0.60	0.81
Opt3 (Si)	633	0.13	0.51	0.47	1.6×10^{5}	0.37	0.61
Opt 4 (Si)	500	0.0039	0.41	0.58	2.2×10^{5}	0.69	0.82
	633	0.11	0.37	0.53	8.0×10^{4}	0.62	
	800	0.35	0.53	0.13	1.4×10^{4}	0.46	
Opt 5 (Si)	500	0.0011	0.21	0.79	1.7×10^{5}	0.69	0.22
	633	0.16	0.13	0.71	4.4×10^{4}	0.58	
	800	0.64	0.11	0.25	8.5×10^{3}	0.25	
Opt6 (Si) (7320Å)	500	0.00038	0.48	0.52	9.8×10^{4}	0.69	0.37
	633	0.0011	0.43	0.57	8.6×10^{4}	0.56	
	800	0.12	0.45	0.44	2.1×10^{4}	0.38	
(4000Å)	500	0.00071	0.46	0.54	1.7×10^{5}		0.29
	633	0.014	0.43	0.56	9.3×10^{4}		
	800	0.24	0.30	0.47	2.7×10^{4}		

Appendix C

REFERENCES

Apsley, N., Hughes, H.P. (1974) Phil. Mag. 30, 963; (1975) Phil. Mag. 31, 1327.

Apsley, N., Davis, E.A., Troup. A.P. and Yoffe, A.D. (1977) Proc. ICALS 7, Edinburgh.

Austin, I.G. and Mott, N.F. (1969) Adv. Phys. 18, 41.

Balkan, N., Butcher, P.N., Hogg, W.R., Long, A.R. and Summerfield, S. (1985) Phil. Mag. B 51, L7.

Bottger, H. and Bryksin, V.V. (1976) Phys. Stat. Sol.(b) 78, 415.

Boulitrop, F. (1984) AIP Conf. Proc. 120, 178

Butcher, P.N., and Hayden, K.J. (1977) Phil. Mag. 36, 657 : Proc. ICALS 7, Edinburgh.

Carius, R. and Fuhs, W. (1984) AIP Conference Proc. 120, 125; (1985) J. Non-cryst. Solids 77 & 78, 659, Proc. ICALS 12, Rome.

Carius, R., Fuhs, W. and Hoheisel, M. (1984) J. Non-Cryst. Solids 66, 151.

Carlson, D.E. and Magee, C.W.(1979) Appl. Phys. Lett. 39, 81.

Chopra, K.L. and Bahl, S.K. (1970) Phys. Rev. B 1, 2545.

Dersch, H., Schweitzer, L. and Stuke, J. (1982) Phys. Rev. B 28 4678.

Dersch, H., Stuke, J. and Beichler, J. (1981) Appl. Phys. Lett. 38, 456.

Efros, A.L. (1981) Phil. Mag. B 43, 829.

Elliott, S.R. (1977) Phil. Mag. 36, 1291; (1979) Phil. Mag. 29, 349.; (1983) "Physics of Amorphous Materials" (London : Longman).

Emin, D. (1974) Phys. Rev. Lett. 32, 303.

Emin, D. and Holstein, T. (1969) Ann. Phys. 53, 439.

Fritzsche, H. (1973) "Electronic and Structural Properties of Amorphous Semiconductors" ed. : P.G. Le Comber and J. Mort.

Frossati, G., Maynard, R., Rammal, R. and Thoulouze, D. (1977) J. Phys. Lett., Paris, 38, L-153.

Fuhs, W. (1985) J. non-Cryst. Solids 77 & 78, 593, Proc. ICALS 12, Rome.

Fuhs, W., Melville, M. and Stuke, J. (1979) Phys. Status Solidi B 89, 4839.

Gilbert, M.H. and Adkins, C.J. (1976) Phil. Mag. 34, 143.

Hallerdt, M., Solomon. I. and Tran-Quoc, H. (1985) 77 & 78, 679, Proc. ICALS 11, Rome.

Hauser, J.J. and Staudinger, A. (1973) Phys. Rev. B 8, 607.

Hoheisel, M., Carius, R. and Fuhs, W. (1984) J. Non-Cryst. Solids 63, 313.

Holstein, T. (1959) Ann. Phys. 8, 325.

Hunklinger, S., and von Shickfus, M. (1981) Amorphous Solids, Low Temperature Properties, edited by W.A. Phillips (Berlin : Springer-Verlag), p. 81.

Le Cleac'h, X. (1979) J. Phys., Paris, 40, 417.

Lindgren, B.W. and McElrath, G.W. (1964) "Probability and Statistics", p.96, (New York : McMillan).

Long. A.R. (1982) Adv. Phys. 31, 553.

Long, A.R., and Balkan, N. (1980) Phil. Mag. B 41, 287.

Long, A.R., Balkan, N., Hogg, W.R. and Ferrier, R.P. (1982) Phil. Mag. B 45, 497.

Long, A.R. and Hogg, W.R. (1983) J. Non-Cryst. Solids 59 & 60, 1095.

Long, A.R., Hogg, W.R. and Balkan, N. (1983) Phil. Mag. B 48, L55.

Long, A.R., Hogg, W.R., Holland, M.C., Balkan, N. and Ferrier, R.P. (1985) Phil. Mag. B, 51, 39.

Loveland, R.J., Spear, W.E. and Al-Sharbaty (1974) J. Non-Cryst. Solids 13, 55.

Meyer, W. and Neldel, H. (1937) Z. Tech. Phys. 12, 588.

Miller, A. and Abrahams, E. (1960) Phys. Rev. 120, 745.

Mott, N.F. (1969) Phil. Mag. 19, 835; (1972) J. Non-Cryst. Solids 13, 989.

Mott, N.F. and Davis, E.A. (1979) "Electronic Process in Non-Crystalline Materials" (Oxford : Clarendon Press).

Movaghar, B., Pohlman, B. and Schirmacher, W. (1980) Phil. Mag. B 41, 49.

Movaghar, B. and Schirmacher, W. (1981) J. Phys. C : Solid State Physics 14, 589.

Patterson, A.M., Long, A.R., Craven, A.J. and Chapman, J.N. (1983) J. Non-Cryst. Sols. 59 & 60, 225.

Pankove, J.L. and Berkeyheiser, J.E. (1980) Appl. Phys. Lett. 37, 705.

Phillips, W.A. (1976) Phil. Mag. 34, 983; (1981) "Amorphous Solids, Low Temperature Properties" (Berlin : Springer-Verlag).

Pike, G.E. (1972) Phys. Rev. B 6, 1572.

Pollak, M. (1964) Phys. Rev. 133A, 564; (1971) Phil. Mag. 23, 519; (1975) Proc. ICALS 6, Leningrad.

Pollak, M. and Geballe, T.H. (1961) Phys. Rev. 122, 1742.

Pollak, M. and Pike, G.E. (1972) Phys. Rev. Lett. 28, 1449.

Pollak, M. and Reiss, I. (1976) J. Phys. C 9, 2339

Rose, A. (1960) "Concepts in Photoconductivity and Allied Problems." Wiley (Interscience), New York.

Shimakawa, K., Long, A.R., Anderson, M.J. and Imagawa, O. (1987) Proc. ICALS 12, Prague, to be published.

Staebler and Wronski (1977) Appl. Phys. Lett. 31, 292; (1980) Appl. Phys. Lett. 51, 3262.

Street, R.A. (1981) Adv. Phys. 30, 593.

Street, R.A. and Biegelsen, D.K. (1982) Solid State Comm. 44, 501.

Stuke, J. (1977) Proc. ICALS 7, Edinburgh, 406.

Summerfield, S. (1985) Phil. Mag. B 52, 9.

Summerfield, S. and Butcher, P.N. (1982) J. Phys. C : Solid State Physics 15, 7003; (1983) J. Phys. C : Solid State Physics 16, 295; (1984) Phil. Mag B 49, L65.

Tanielian, M., Goodman, N.B. and Frizche, H. (1981) J. Phys. Colloq. Orsay. Fr. 42, Suppl. 10, C4-375.

Vanier, D.E. and Griffith, R.W. (1982) J. Appl. Phys. 53, 3098.

Varmazis, C., Hirsch, M.D. and Vanier, P.E. (1984) AIP Conf. Proc. 120, 133.

Wautelet, M., Laude, L.D. and Failly-Lovoto, M. (1981) Solid State Comm. 39, 979.

Wronski, C.R. and Daniel, R. (1980) Phys. Rev. B 23, 794.